

Copyright
by
Imran Tayyab
2020

**The Thesis Committee for Imran Tayyab
Certifies that this is the approved version of the following Thesis:**

**Gas Well Deliquification:
Critical Rate Analysis and Artificial Lift
Design & Review Workflow**

**APPROVED BY
SUPERVISING COMMITTEE:**

Kamy Sepehrnoori, Supervisor

Paul M. Bommer, Co-Supervisor

**Gas Well Deliquification:
Critical Rate Analysis and Artificial Lift
Design & Review Workflow**

by

Imran Tayyab

Thesis

Presented to the Faculty of the Graduate School of
The University of Texas at Austin
in Partial Fulfillment
of the Requirements
for the Degree of

Master of Science in Engineering

The University of Texas at Austin

May 2020

Acknowledgements

This work is a result of dedication, sincerity and perseverance. However, it would not have been possible without the unweathering support of a lot of people. Many have guided me, supported me and motivated me to reach to this point, fighting all the ups and downs. I would like to extend my profound gratitude and appreciation to the following:

First and Foremost, to my Almighty Allah, for the wisdom, for bestowing clarity and direction when all seemed lost, and most importantly, for providing the strength to complete what was started.

To my parents, my mother, because of whom I have never doubted my abilities. For she is the reason, the motivation and the force that have pushed me through thick and thin. This is because of them, in all the literal and philosophical sense.

To my wife, whose love and prayers have stood by me at every step. Her patience, which has no boundaries, allowed me to work on this research, sacrificing a lot of the time I owed to her and sharing all the stresses that came along this journey.

To Dr. Paul M Bommer, for the many meetings, long discussions, comments and critique on this work. For supporting me during the low times, suggesting solutions to every roadblock and ensuring this work is completed. His expertise on artificial lift is unfathomable and without him, this project was not possible.

To Dr Kamy Sepehrnoori, for his overarching role and support during the completion of this work, and my time at UT Austin. For his multiple reviews, suggestions and feedback to improve the quality of this work. For supporting me to balance the academic and personal responsibilities and helping me manage both as best as possible.

To my employer, UEP and specially my manager, Fauzan Iqbal, who agreed to bring this project to life by providing the invaluable data. For believing in the idea of this project and supporting it until completion. His wisdom and guidance are an indispensable part of this work.

Lastly, to my brothers, Abbas and Sajid, for believing in my quest towards higher education and providing the means to make it a reality.

Abstract

Gas Well Deliquification: Critical Rate Analysis and Artificial Lift Design & Review Workflow

Imran Tayyab, M.S.E.

The University of Texas at Austin, 2020

Supervisor: Kamy Sepehrnoori

Co-Supervisor: Paul M. Bommer

Liquid loading is an inevitable phenomenon for most gas wells. Liquid loading occurs when fluids accumulate in the wellbore instead of producing to the surface. This causes additional hydrostatic pressure that lowers formation drawdown and reduces production. The process of de-watering gas wells is commonly known as gas well deliquification. This involves quantifying if liquid production is the source of un-optimization in the well and selecting an appropriate artificial lift system to offload the well. This study presents a gas well deliquification workflow, that quantifies the extent of liquid loading through production analysis, critical unloading rate, and nodal analysis. Once liquid loading is confirmed, a design & review workflow is suggested that compares different artificial lifts to select the most effective choice.

Production analysis includes; (a) evaluating decline trend of rate and estimated bottom hole pressure, (b) Nodal analysis, to create a calibrated baseline model that is used as a reference during artificial lift design, (c) VLP Stability, and Flow-point analysis to qualitatively understand unstable flow in the wellbore. A new critical rate calculation workflow is developed to quantitatively confirm liquid loading. This workflow utilizes published critical gas rate correlations and wellhead pressure as a weighing criterion to estimate a weighted average critical rate. A separate data-driven model, where machine learning is used to estimate critical rate for a target well given its well

parameters is also formulated. Both workflows are shown to better predict critical gas rate than most published models. If liquid loading is confirmed, applicable lift systems are designed, and their production impact is gauged through nodal analysis. With a direct comparison of all applicable systems, most suitable system is selected that maximizes incremental production.

Design & Review workflow is applied to a field in Lower Indus Basin, Pakistan. Several wells are evaluated to check if liquid loading is a problem and artificial lift can improve production. S-field is the largest field in this dataset, where 10 wells are evaluated. Among the technologies suggested for these wells are Gas lift, Coiled Tubing Gas Lift, and Plunger Assisted Gas lifts. Beam lift and velocity strings are found to be less effective in the specific case of S-field.

Several artificial lift selection workflows are published that focus on selecting lifts for oil wells. Most only focus on the lift selection and do not include any production analysis to ascertain if liquid loading is the cause of low production. Further, many critical rate correlations are published however most are applicable for specific ranges of well parameters. This study attempts to provide a thorough gas well deliquification workflow. It includes production analysis to quantify root cause, new critical rate calculation that is universally applicable on most wells, and artificial lift selection process, specific to gas well deliquification, to select the most suitable lift system.

Table of Contents

<i>Objectives of Study</i>	<i>1</i>
<i>Chapter-1: Artificial Lift for Gas Well Deliquification – Design & Review Workflow</i>	<i>2</i>
Introduction of Artificial Lifts	2
Gas Lift	2
Plunger Lift	4
Velocity String/Tubing Size.....	11
Nodal Analysis	12
VLP Stability	13
Flow-point Analysis.....	14
Artificial Lift Selection	15
Expert Systems.....	16
Selection through Machine Learning Models	19
Gas well Artificial Lift System Selection.....	21
Design & Review Workflow for Gas Well Deliquification	23
<i>Chapter-2: Critical Unloading Rate</i>	<i>26</i>
Weighted Average Critical Rate	26
Turner (1969) Drop Model.....	26
Coleman (1991) Model	27
Nosseir (2000) Model	28
Li et al. (2001) Model	29
Luan and He (2012) Model.....	30
Weighted Average Critical Rate Formulation.....	30
Machine Learning Model to Estimate Critical Gas Rate	37
Dataset for Model.....	38
Model Variables (Feature Engineering)	39
Prediction Model.....	45
Final Model Test	48
Model Improvement for Low Critical Gas Rate Wells	50
<i>Chapter-3: Gas Well Deliquification – S-field Case Study</i>	<i>53</i>
Lower Indus Basin Fields	53
S-Field Executive Summary	54

Well S-5.....	57
Well S-10.....	74
Well S-11.....	92
<i>Chapter-4: Summary, Conclusions and Recommendations for Future Work.....</i>	<i>105</i>
Summary	105
Conclusions	105
Recommendations for Future Work.....	106
<i>Appendices.....</i>	<i>107</i>
Appendix-A: S-field non selected wells.....	108
Well S-1	109
Well S-2	119
Well S-4	128
Well S-8	137
Well S-13	148
Well S-14.....	158
Well S-15	168
Appendix-B: Machine Learning Python Code.....	182
<i>References</i>	<i>193</i>

List of Tables

Table 1 - Parameters required in artificial lift design and selection – Ounsakul et al., 2019	20
Table 2 - Average WHP in published datasets	31
Table 3 - Statistics of dataset used in this study	38
Table 4 - Significance test results - Linearity	40
Table 5 - Executive summary of S-Field wells.....	54
Table 6 - S-field artificial lift summary	56
Table 7 - Well S-5 Plunger lift design	67
Table 8 - Well S-5 PAGL design with current 4-1/2" tubing.....	68
Table 9 - Well S-5 PAGL design with 2-7/8" tubing	70
Table 10 - Well S-5 PAGL design with in-house model.....	71
Table 11 - Well S-5 hyperbolic and exponential DCA results	72
Table 12 - Well S-5 incremental recovery from gas lift	73
Table 13 - Well S-10 PAGL design with current 5-1/2" tubing.....	88
Table 14 - Well S-10 PAGL design with 2-7/8" tubing	90
Table 15 - Well S-10 hyperbolic and exponential DCA results	91
Table 16 - Well S-10 incremental recovery from gas lift.....	91
Table 17 - Well S-11 PAGL design with current 4-1/2" tubing.....	101
Table 18 - Well S-11 PAGL design using 2-7/8" tubing.....	102
Table 19 - Well S-1 PAGL design with current 4-1/2" tubing.....	117
Table 20 - Well S-2 PAGL design with current 5-1/2" x 4-1/2" tubing.....	125
Table 21 - Well S-13 PAGL design with current 4-1/2" tubing.....	156
Table 22 - Well S-15 PAGL design using 2-7/8" tubing.....	178

List of Figures

Figure 1 - Components of gas lift system (Lea et al., 2008).....	3
Figure 2 - Feasibility chart for gas lift (Lea et al., 2008).....	4
Figure 3 - Typical plunger lift setup (Lea et al., 2008).....	5
Figure 4 - Plunger lift feasibility chart (Lea et al., 2008)	6
Figure 5 - PAGL components (Lea et al. 2008).....	8
Figure 6 - Typical beam lift setup (courtesy Harbison Fischer)	10
Figure 7 - Beam lift feasibility chart (Lea et al., 2008)	10
Figure 8- Mud anchor (Lea et al., 2008).....	11
Figure 9 - Different tubing size comparison (Lea et al. 2008).....	12
Figure 10 - Nodal analysis plot (Lea et al., 2008)	13
Figure 11 - Components of pressure loss in tubing (Lea et al., 2008).....	14
Figure 12 – Flow-point analysis plot (Lea et al., 2008).....	15
Figure 13 - SEDLA program flow (Espin 1994)	17
Figure 14 – OPUS artificial lift selection workflow – Valentin et al. 1988	19
Figure 15- Normalized cost vs production - Ounsakul et al., 2019	21
Figure 16 - Lift selection matrix for wells with little or no solids (Oyewole and Lea 2008).....	22
Figure 17 - Lift Selection matrix for wells with solids (Oyewole and Lea, 2008).....	22
Figure 18 - Artificial lift selection workflow for gas well deliquification suggested in this study	25
Figure 19 - Results from WACR using Turner's (1969) dataset.....	34
Figure 20 - Results from WACR using Coleman's (1991) dataset	34
Figure 21 - Results from WACR using Awolusi's (2005) dataset	35
Figure 22 - Pearson correlation coefficient.....	41
Figure 23 - Partial Correlation Coefficient	42
Figure 24 - Feature Importance using random forest.....	42
Figure 25 - Sample Decision tree model diagram	43
Figure 26 - RFE using cross validation using SVM	45
Figure 27 - Hyperparameter Tuning Plots for Random forest and gradient boosting models.....	47
Figure 28 - Critical rate validation plot for the final model.....	49
Figure 29 - Histograms of different parameters in original data	50

Figure 30 - Log transform of response feature	51
Figure 31 - Critical Rate Plots for Final model.....	52
Figure 32- Well S-5 wellbore configuration.....	57
Figure 33 - Well S-5 FWHP plot	58
Figure 34 - Well S-5 BHP Plot	58
Figure 35 - Well S-5 System analysis - reservoir pressure sensitivity	59
Figure 36 - Well S-5 VLP Stability plot.....	60
Figure 37 - Well S-5 Flow point plot.....	60
Figure 38 - Well S-5 gradient traverse calculations.....	61
Figure 39 - Well S-5 BHP sensitivity using WGR values	62
Figure 40 - Well S-5 system analysis plot with WGR sensitivity	63
Figure 41 - Well S-5 base model using oil IPR	64
Figure 42 - Well S-5 Gas lift design oil IPR.....	64
Figure 43 - Well S-5 CTGL design using oil IPR	65
Figure 44 - Well S-5 Velocity string system analysis.....	66
Figure 45 - Well S-5 PAGL type plot.....	68
Figure 46 - Well S-5 PAGL plot with 2-7/8" tubing	69
Figure 47 - Well S-5 DCA plots	72
Figure 48 - Well S-10 wellbore configuration.....	74
Figure 49 - Well S-10 FWHP Plot.....	75
Figure 50 - Well S-10 BHP plot	75
Figure 51 - Well S-10 system analysis - reservoir pressure sensitivity	76
Figure 52 - Well S-10 VLP Stability plot.....	77
Figure 53 - Well S-10 Flow point plot.....	77
Figure 54 - Well S-10 Load-up condition.....	78
Figure 55 - Well S-10 BHP sensitivity using WGR	79
Figure 56 - Well S-10 Gas lift analysis.....	80
Figure 57 - Well S-10 system analysis using oil IPR	81
Figure 58 - Well S-10 Gas lift methods comparison	82
Figure 59 - Well S-10 Beam Lift Design.....	84
Figure 60 - Well S-10 beam lift design using long-stroke unit.....	86

Figure 61 - Well S-10 Velocity string and 2-7/8" Tubing	87
Figure 62 - Well S-10 PAGL type plot.....	88
Figure 63 - Well S-10 PAGL plot with 2-7/8" tubing	89
Figure 64 - Well S-10 DCA Plots.....	90
Figure 65 - Well S-11 wellbore profile.....	92
Figure 66 - Well S-11 FWHP plot	93
Figure 67 - Well S-11 BHP plot	93
Figure 68 - Well S-11 reservoir pressure sensitivity	94
Figure 69 - Well S-11 VLP stability plot.....	95
Figure 70 - Well S-11 flow-point analysis plot	96
Figure 71 - Well S-11 WGR sensitivity.....	97
Figure 72 - Well S-11 WGR sensitivity on system plot	98
Figure 73 - Well S-11 system plot using oil IPR.....	99
Figure 74 - Well S-11 conventional gas lift design (4-1/2" tubing)	99
Figure 75 - Well S-11 coiled tubing gas lift design.....	100
Figure 76 - Well S-11 PAGL type plot.....	101
Figure 77 - Well S-11 PAGL system plot.....	103
Figure 78 - Well S-11 velocity string design.....	104
Figure 79 - Well S-1 Wellbore profile.....	109
Figure 80 - Well S-1 FWHP Plot.....	110
Figure 81 - Well S-1 BHP plot	110
Figure 82 - Well S-1 reservoir pressure sensitivity	111
Figure 83 - Well S-1 VLP stability plot.....	112
Figure 84 - Well S-1 flow-point analysis.....	113
Figure 85 - Well S-1 WGR sensitivity.....	114
Figure 86 - Well S-1 WGR sensitivity on system plot	115
Figure 87 - Well S-1 Lower ID/Velocity string comparison	116
Figure 88 - Well S-1 PAGL type plot.....	117
Figure 89 - Well S-2 wellbore profile.....	119
Figure 90 - Well S-2 FWHP plot	120
Figure 91 - Well S-2 BHP Plot.....	120

Figure 92 - Well S-2 reservoir pressure sensitivity	121
Figure 93 - Well S-2 VLP Stability plot	122
Figure 94 - Well S-2 WGR sensitivity.....	123
Figure 95 - Well S-2 WGR Sensitivity on system plot.....	124
Figure 96 - Well S-2 PAGL type plot.....	125
Figure 97 - Well S-2 Lower ID/velocity string comparison	126
Figure 98 - Well S-4 wellbore profile.....	128
Figure 99 - Well S-4 FWHP plot	129
Figure 100 - Well S-4 BHP Plot	129
Figure 101 - Well S-4 reservoir pressure sensitivity	130
Figure 102 - Well S-4 VLP stability plot.....	131
Figure 103 - Well S-4 flow-point analysis plot	132
Figure 104 - Well S-4 WGR Sensitivity	133
Figure 105 - Well S-4 WGR sensitivity on system plot	134
Figure 106 - Well S-4 PAGL type plot.....	134
Figure 107 - Well S-4 Lower ID/velocity string comparison.....	135
Figure 108 - Well S-8 wellbore profile.....	137
Figure 109 - Well S-8 FWHP plot	138
Figure 110 - Well S-8 BHP plot	138
Figure 111 - Well S-8 reservoir pressure sensitivity	139
Figure 112 - Well S-8 VLP stability plot.....	140
Figure 113 - Well S-8 flow-point analysis plot	140
Figure 114 - Well S-8 WGR Sensitivity	142
Figure 115 - Well S-8 WGR sensitivity on system plot	143
Figure 116 - Well S-8 Conventional gas lift design	144
Figure 117 - Well S-8 system analysis using oil IPR	144
Figure 118 - Well S-8 CT gas lift design.....	145
Figure 119 - Well S-8 Lower ID/velocity string comparison.....	146
Figure 120 - Well S-8 PAGL type plot.....	147
Figure 121 - Well S-13 wellbore profile.....	148
Figure 122 - Well S-13 FWHP plot	149

Figure 123 - Well S-13 BHP plot	149
Figure 124 - Well S-13 reservoir pressure sensitivity	150
Figure 125 - Well S-13 VLP stability plot.....	151
Figure 126 - Well S-13 flowpoint analysis plot.....	152
Figure 127 - Well S-13 WGR sensitivity.....	153
Figure 128 - Well S-13 WGR sensitivity on system plot	154
Figure 129 - Well S-13 Velocity string design	155
Figure 130 - Well S-13 PAGL type plot.....	156
Figure 131 - Well S-14 wellbore profile.....	158
Figure 132 - Well S-14 FWHP plot	159
Figure 133 - Well S-14 BHP plot	159
Figure 134 - Well S-14 reservoir pressure sensitivity	160
Figure 135 - Well S-14 VLP stability plot.....	161
Figure 136 - Well S-14 flow-point analysis plot	161
Figure 137 - Well S-14 WGR sensitivity.....	163
Figure 138 - Well S-14 WGR sensitivity on system plot	164
Figure 139 - Well S-14 conventional gas lift design	165
Figure 140 - Well S-14 system plot using oil IPR	165
Figure 141 - Well S-14 coiled tubing gas lift design	166
Figure 142 - Well S-14 PAGL type plot.....	166
Figure 143 - Well S-14 velocity string design	167
Figure 144 - Well S-15 wellbore profile.....	168
Figure 145 - Well S-15 FWHP plot	169
Figure 146 - Well S-15 BHP plot	169
Figure 147 - Well S-15 reservoir pressure sensitivity	170
Figure 148 - Well S-15 flow-point analysis plot	171
Figure 149 - Well S-15 VLP Stability plot.....	171
Figure 150 - Well S-15 WGR sensitivity.....	173
Figure 151 - Well S-15 WGR sensitivity on system plot	174
Figure 152 - Well S-15 system plot using oil IPR	175
Figure 153 - Well S-15 coiled tubing gas lift design	176

Figure 154 - Well S-15 conventional gas lift design	176
Figure 155 - Well S-15 CTGL abandonment pressure sensitivity	177
Figure 156 - Well S-15 PAGL type plot.....	178
Figure 157 - Well S-15 PAGL system plot.....	180
Figure 158 - Well S-15 velocity string design	180

Objectives of Study

This work is conducted in two main phases. The first phase consists of details about artificial lift techniques, literature review regarding published artificial lift selection workflows, and a brief overview of critical unloading rates. The outcome of the first phase is a workflow that can be used to select and design artificial lift systems for gas wells for deliquification.

The second phase of this study implements the suggested workflow to evaluate the optimum artificial lift system for a field in the lower Indus Basin in Pakistan. Complete evaluation consisting of production analysis, artificial lift design, production benefit, and final recommendation based on comparison is conducted. This demonstrates the applicability of workflow developed in phase-I on real wells while also aids the operator of these wells in their field development plans.

Salient outcomes from this work are:

- Predict the onset of liquid loading through critical rate calculation
 - Estimate critical rate through weighted average technique
 - Cross-check critical rate through machine learning methods
- Develop artificial lift design & review workflow to select lift systems for deliquification purposes
- Recommend artificial lift systems for field in the Lower Indus Basin using developed workflow

Chapter-1: Artificial Lift for Gas Well Deliquification – Design & Review Workflow

Introduction of Artificial Lifts

When the gas production is high, gas velocity carries fluid to the surface. As velocity in the wellbore decreases due to lower gas influx from the reservoir, its ability to carry liquid droplets to the surface diminishes. This results in liquid accumulation in the wellbore, which hinders gas production and can ultimately halt it completely. This phenomenon is known as liquid loading.

Artificial lifts can be used to remove water from the wellbore to reinstate and improve production from gas wells. The approach towards selection of artificial lift varies slightly in the case of deliquification applications, as produced fluid is generally of no economic value (unless loading is due to condensate, which is uncommon). Therefore, the economics of the project is based on incremental or lost gas reserves unlocked by deliquification.

All artificial lift systems and technologies can be used for dewatering gas wells. For this study, based on the field data used to test the deliquification workflow, select artificial lifts systems are considered, given prior field experience and infrastructure availability in the region. Note that this is not an exhaustive list of technologies that are used for deliquification, but only relevant to the case study used in this work. For example, Electrical Submersible Pumps (ESP) have many successful dewatering applications. However, their application in the field data used for this study is inappropriate; therefore, they are not included.

Gas Lift

Gas lift is an artificial lift method that requires the injection of external gas into the wellbore from the surface. Injected gas is often procured from nearby wells; however, in-situ gas could also be used with a wellhead compressor. The addition of gas into wellbore lowers the density of production stream, which lowers the flowing bottom hole pressure. This results in lower hydrostatic pressure of the accumulated fluid (which is easier to carry out by gas stream) and more gas influx from the reservoir. For dewatering applications, the injected gas volume is often designed to make the total gas velocity in wellbore higher than the critical velocity.

Gas lift has been the artificial lift of choice around the world due to its versatility in application. It mimics the phenomenon of natural production and is one of the few lift systems where no mechanical parts are installed in the flow conduit (except for gas lift valves in tubing). It is also an excellent choice for application in gas wells where the Gas-Liquid Ratio (GLR) is high. Most conventional pumping systems typically become inefficient when GLR exceeds ~500 SCF/BBL (Lea et al. 2008). However, gas lifts can be applied to high GLR wells where the higher formation gas instead aids the system by lowering the requirement for injected gas. Moreover, gas lifts are also applicable in wells with significant solid production or deviation. As no mechanical equipment is installed in the production conduit, gas lift is relatively unaffected by these parameters. Figure 1 shows a schematic of different components of a gas lift system.

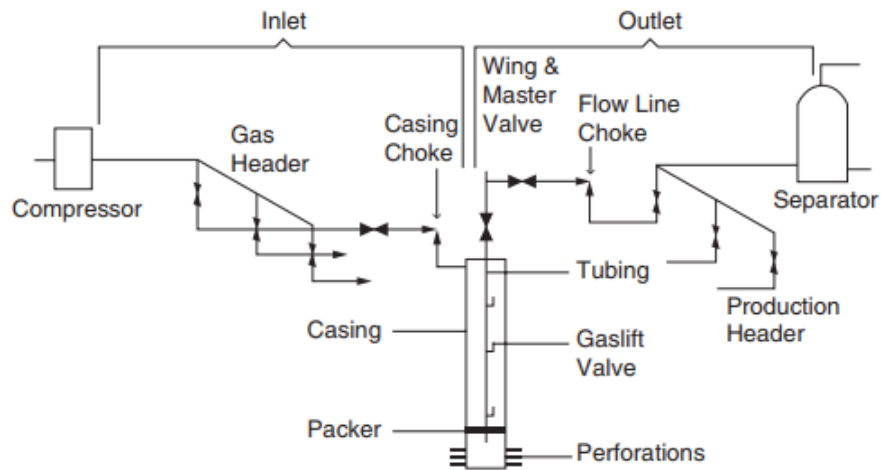


Figure 1 - Components of gas lift system (Lea et al., 2008)

Gas lift is operated in two ways, continuous or intermittent injection. In this study, only continuous gas lift is considered. When gas is injected outside the tubing (often in production annulus), it is called conventional gas lift. Conventional gas lift is applicable at any depth and wellbore profile (as long as injection pressure is available). It is also efficient at a wide range of liquid volume only limited by the injection pressure and tubing size. Figure 2 plots the feasibility chart for conventional gas lifts. In low production wells or wells where gas lift valves cannot be placed in tubing due to mechanical constraints, gas can be injected at the optimum depth using coiled tubing. This application is commonly known as Coiled Tubing Gas Lift (CTGL). When gas is injected through coiled tubing placed inside the production tubing, coiled tubing not only delivers the gas

at the bottom of the well but also acts as a velocity string, increasing the velocities of gas and fluid. The downside of CTGL compared to conventional gas lift is higher frictional losses.

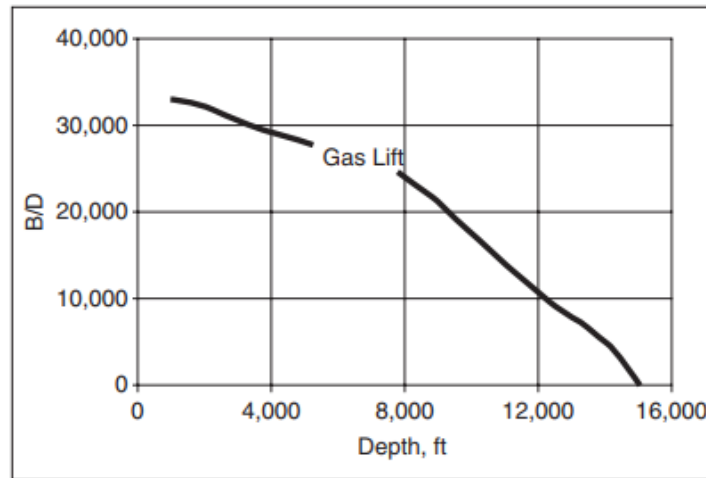


Figure 2 - Feasibility chart for gas lift (Lea et al., 2008)

Plunger Lift

Plunger lift is an artificial lift system that relies on the reservoir energy to operate. It employs the use of a free travelling piston called a plunger, that travels in the production tubing carrying the fluid load. The plunger depends on reservoir pressure to rise towards the surface, and gravity to fall back. This makes it a cyclic system that has four main stages; pressure build-up, plunger rise, gas production (including blowdown time), and plunger fallback. Figure 3 shows a typical conventional plunger lift setup.

Plunger lift is an intermittent artificial lift method, as the well is shut-in in every cycle to allow for pressure build-up. It is vital to have enough reservoir energy that can lift the weight of the fluid column and the plunger to the surface for this system to work. Often a high permeability reservoir is also required to ensure build-up time (well shut-in time) is minimum, and maximum cycles per day are achieved. In the deliquification application, once the plunger has lifted the static fluid column, it is held at the surface (in the lubricator), and gas is allowed to produce until rates fall below the critical rate. This is when liquid starts to reaccumulate in the tubing. This production stage is part of the blowdown time in gas wells and is a function of liquid production rate. As the produced liquid by the plunger is often of no economic value in deliquification applications (unlike oil well applications), cycle count is not the only criterion for optimizing plunger lift.

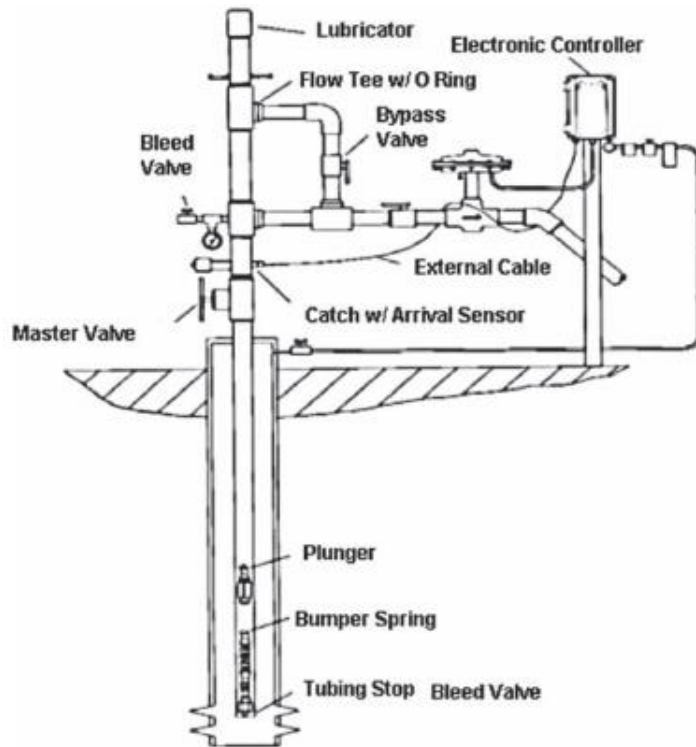


Figure 3 - Typical plunger lift setup (Lea et al., 2008)

Candidate selection criteria for plunger lift is more rigorous in comparison to other deliquification techniques as it relies solely on reservoir energy to operate. Firstly, the well must have a GLR higher than ~400 SCF/BBL for every 1000ft of lift (Lea et al. 2008). This ensures the reservoir can provide enough gas to lift the slug and plunger to surface. Secondly, due to the energy constraints, there is a maximum limit to the total volume that plungers can lift. Although this maximum limit varies with depth and tubing size, it is still in the ranges of 200-300 bbl/day and significantly lower than other lift systems. Plungers also have a limitation in terms of well geometry. As plunger falls due to gravity, fall speed starts to decrease in deviated sections negatively effecting the cycle time and total liquid production. Figure 4 shows the feasibility chart for conventional plunger lifts.

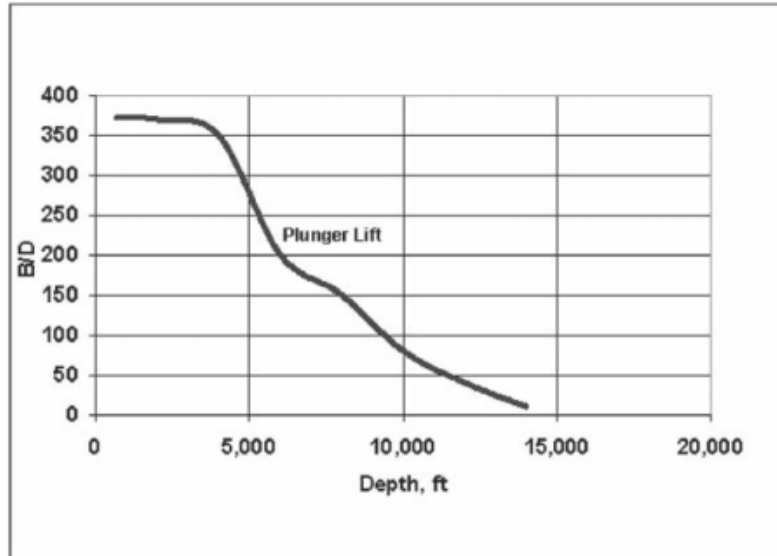


Figure 4 - Plunger lift feasibility chart (Lea et al., 2008)

Plunger Assisted Gas Lift

Plunger Assisted Gas Lift (PAGL) is a hybrid of two artificial lift systems; gas lift and plunger lift. A plunger is used as a separator between the fluid column and injected gas, which reduces the slippage of fluid in the wellbore. Moreover, the applicability of the plunger lift is extended as the system no longer relies on reservoir energy to produce. The energy required to propel the fluid column and plunger to the surface is provided by surface gas injection. Therefore, PAGL can work in any well regardless of reservoir pressure until well can flow liquids above the plunger, and adequate surface injection pressure is available. However, as well shut-in is often required as part of the PAGL cycle, it may not be very productive in high producing wells.

PAGL can be operated continuously or intermittently (similar to its constituent plunger lift). Several publications refer to the intermittent PAGL as Gas Assisted Plunger Lift (GAPL). However, in this study, both modes are referred to as PAGL (Burns 2018). In continuous PAGL, gas is continuously injected into the flow stream even when the plunger has retrieved the fluid load and is held at the surface in the lubricator. A bypass port plunger is used in such applications that allows flow through the plunger body.

On the contrary, conventional plungers are used in intermittent PAGL, where gas is only injected to lift the plunger and fluid column to surface. Once the plunger is held in the lubricator, gas injection is halted until the cycle repeats. For continuous PAGL, injection gas pressure is limited

by the Flowing Bottom Hole Pressure (FBHP) of the well, as the reservoir has to produce against the injection pressure. This often adds a bottleneck in the design for total liquid removal. In either mode, a one-way check valve is used in the wellbore to ensure injected gas is not injected into the reservoir. Figure 5 shows the different components in a PAGL system.

PAGL cycle consists of three main stages, similar to conventional plunger lift. The cycles include:

- Rise: The fluid column has accumulated on top of plunger, and gas injection can be initiated through the tubing gas lift valve to lift column and plunger to surface.
- Production/blowdown: The plunger is held at the surface in a lubricator while the well is flowing. As gas rates decline, the liquid will start to accumulate in wellbore over the plunger Bottom Hole Assembly (BHA). In continuous PAGL, gas is continuously injected into the wellbore in this stage while it is halted in intermittent PAGL as soon as the plunger reaches the lubricator.
- Fall: Based on a preset timer, or gas production rate, the plunger is released from the lubricator. For continuous PAGL, plunger falls across the production stream. For intermittent PAGL, well is shut-in to allow the plunger to fall to the bottom. The plunger falls through any accumulated fluid and sits on the bumper spring in the BHA. The cycle is then repeated.

Feasibility plots are used for each well to ascertain the applicability of PAGL. The critical gas unloading rate and a cut-off of 10 ft/s velocity are used to determine the type of PAGL. Moreover, Burns et al. (Burns 2018) suggested the use of Gas-Liquid Ratio (GLR) cut-offs as a guiding parameter in the selection between gas lift, plunger lift, and PAGL. For wells with GLR greater than 10 Mscf/STB, a conventional plunger lift is recommended. For GLR between ~3 and ~10 Mscf/STB, PAGL is the suitable lift choice, while a gas lift is recommended for wells with GLR less than 3 Mscf/STB. These guidelines, coupled with type plot, are used to determine the PAGL type for each well.

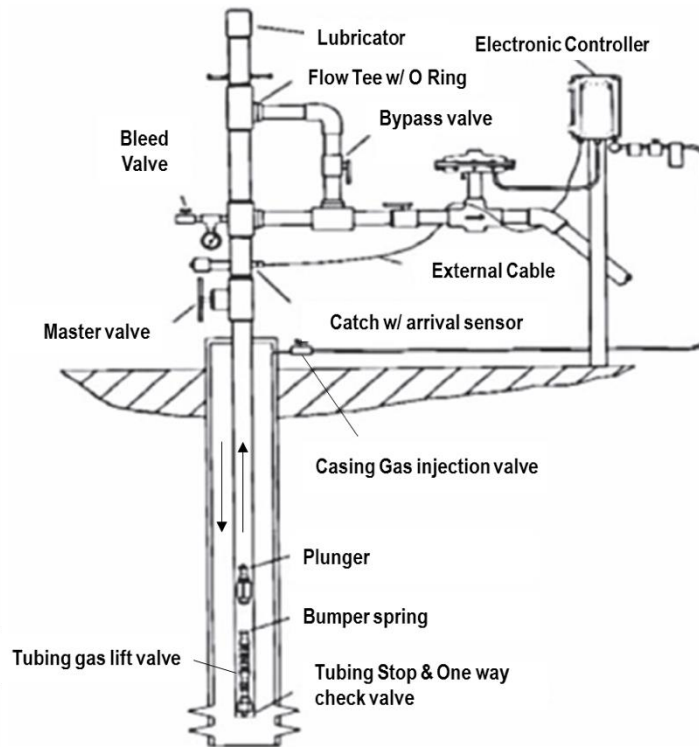


Figure 5 - PAGL components (Lea et al. 2008)

Based on the critical rate and velocities inside the wellbore, continuous or intermittent PAGL is selected. The design process for PAGL is similar to conventional plunger lift, except that a pressure calculation is made and fine-tuned based on available injection pressure and flowing bottom hole pressure in case of continuous PAGL. The following details are used in the design workflow for PAGL.

- A Small-port generic bypass plunger is used for continuous plunger lift. Rise velocity is 700 ft/min and fall velocity in gas and liquid is 800 and 400 ft/min, respectively. This rise and fall rates are approximations that should be verified in practice using a fluid level sounder.
- A Generic plunger is used for conventional plunger lift. Rise velocity is 750 ft/min and fall velocity is 250 ft/min, this rise and fall rates are approximations that should be verified in practice using a fluid level sounder.
- Based on the average total cycle time for continuous plungers of ~20-40 min, total cycles per day are limited to 60. This is used as a boundary condition in design.

- The maximum available injection pressure in the region is ~1000 psi that is used as a boundary condition in design.
- Downhole injection pressure is limited to 90% of flowing bottom hole pressure in wells where continuous PAGL is suitable. This is to ensure that reservoir fluid can flow into the wellbore against injection pressure.
- Iterative calculations are made to maximize liquid production while ensuring boundary conditions of max casing pressure (injection pressure) and max cycles are met.

A Microsoft Excel based design model is used for conventional plunger lift, which is updated for the PAGL design. Moreover, commercial software is also used to conduct the plunger lift design. One well is used to calibrate both techniques. Once an agreement between the two techniques is achieved, only commercial software is used for all other wells for what is believed to be better accuracy.

Beam Lift

Wide availability, reliable infrastructure, and ease of operation have made beam lift possibly the most common method to produce liquids from gas wells. Beam lifts consist of a prime mover that moves the pumping unit (converting rotary motion to reciprocating motion). Connected to the pumping unit are sucker rods that have a downhole pump. Beam lift can operate at any reservoir pressure until the fluid level can reach the pump. Figure 6 shows a typical beam lift installation. Despite the high upfront cost, beam lifts can be an excellent option for deliquification because it has no lower limit for production (several liquid producing gas wells are ultra-low producers), unlike other pumping systems like ESPs. Nevertheless, similar to other pumping systems, the presence of gas does deteriorate the pump's efficiency. This is countered to an extent by using gas separators or designing the wellbore profile to ensure gas does not enter the pump. Figure 7 shows the applicability range of beam lift.

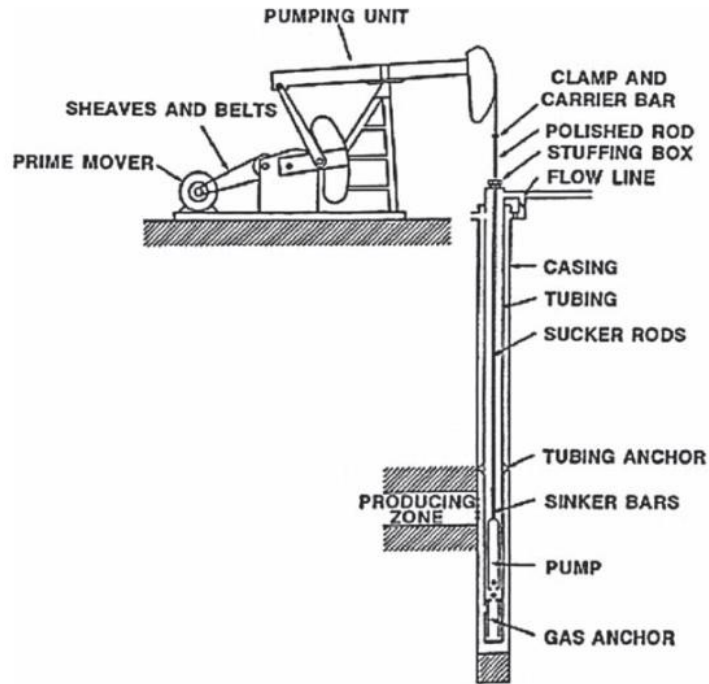


Figure 6 - Typical beam lift setup (courtesy Harbison Fischer)

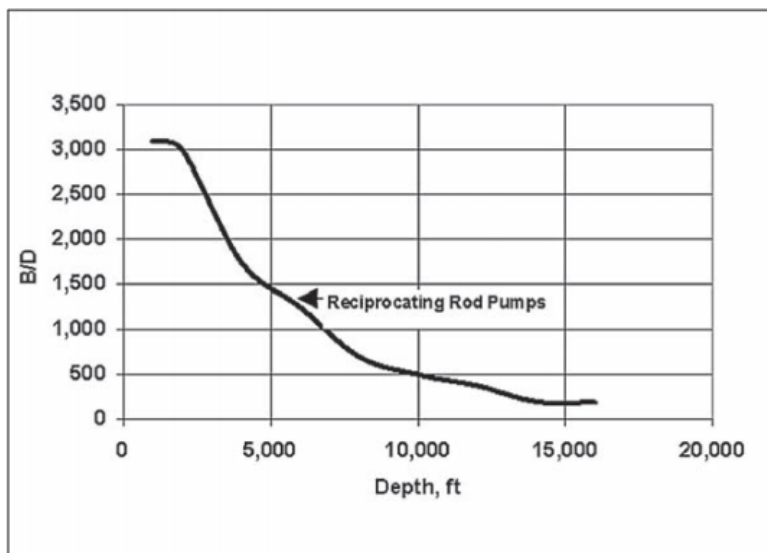


Figure 7 - Beam lift feasibility chart (Lea et al., 2008)

In most deliquification applications, due to the low volume of liquid production from reservoir in comparison to the pump rate of beam lift, the level of fluid falls below the pump depth. The pump at this point is said to be "pumped-off". Gas from the reservoir then enters the pump causing several

problems, including gas locking and mechanical damage. Several remedies are possible to avoid being in a pumped-off scenario. Automated controllers that predict pump-off conditions based on design rate or surface dynamometer are one possible solution to mitigate fluid pound conditions.

Other techniques to minimize gas interference is placing the pump below perforations. Due to higher density, liquid tends to fall inside wellbore while gas migrates upwards in the production annulus. This liquid is then produced through the pump into the tubing. Often wellbore construction does not provide enough rat-hole to place pump below perforations; therefore, gas separators are required. Mud anchors, a kind of gas separator, forced the fluid to travel downwards to enter the pump. The fluid downwards velocity should be less than 0.5 ft/sec to ensure it does not carry gas bubbles into the pump. This allows for gas fluid separation, similar to placing the pump below perforations. Figure 8 depicts a mud anchor-based gas

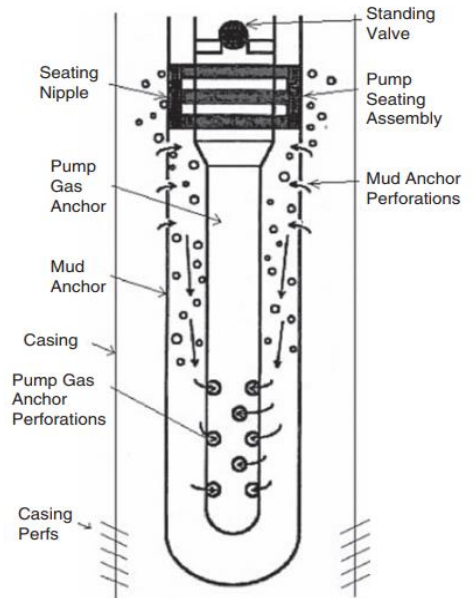


Figure 8- Mud anchor (Lea et al., 2008)

separator. Beam lifts are also not suitable for installation in deviated sections. As the downhole pump is mechanically connected with the surface unit through sucker rods, placing downhole pump in the deviated section creates excessive drag forces on sucker rods in deviated sections, causing the "hack-saw" effect. This dramatically reduces the working life of the equipment. Dip-tubes are used as an alternative to placing the pump in the deviated section, where the pump is located in vertical section, while an extended dip-tube is placed in the deviated section to produce liquids.

Velocity String/Tubing Size

The cross-sectional area available for flow in tubing determines how long and optimized the well will flow, as it influences the velocity of the fluid. Selection of tubing size is a trade-off between excessive friction pressure, that is minimized by selecting a larger tubing, and ensuring high flow velocity so liquid loading will not occur, which is maximized in a smaller tubing. Finally, it is also desired that the tubing can reasonably adjust to changes in reservoir performance like depletion without the need to conduct frequent workovers.

Velocity string is a small diameter string that is typically installed inside the current larger tubing to lower the available flow area. Generally, these strings are closed from bottom-end, so the production of fluids is from the annulus of tubing and velocity string. As velocity strings can be run without a workover, similar effects as a smaller tubing can be achieved. Closed-end coiled tubing is commonly used as velocity strings due to their rapid installation, retrieval, and easy availability. Permanent Downhole Gauge (PDG) for continuous pressure and temperature measurements can also be installed on a coiled tubing used as a velocity string. Although velocity string is an excellent remedy for liquid loading, its overall performance is often inferior to re-completion with smaller size tubing with equivalent flow area. This is owing to higher friction pressures in velocity strings due to the presence of two concentric tubing.

Tubing design is optimized using nodal analysis. Reservoir performance is quantified through Inflow Performance Relationship (IPR) that models flowing bottom hole pressure with production rate. Flow in the tubing is quantified using Vertical Lift Performance (VLP) that also models flowing bottom hole pressure with the production rate in the wellbore. Using multiple VLPs (each for different tubing sizes) and single IPR, most optimum tubing size can be determined. It is paramount to ensure flow through selected tubing is stable (in the mist flow region), and the total production rate is higher than the critical unloading rate for that tubing size to ensure effecting unloading of fluids. Figure 9 shows a nodal analysis plot where different tubing sizes are compared, giving different solution flowrates.

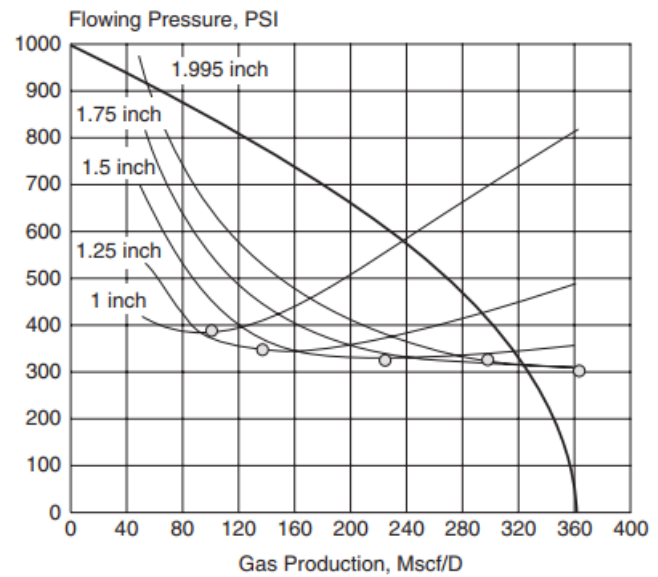


Figure 9 - Different tubing size comparison (Lea et al. 2008)

Nodal Analysis

Gas flows through several restrictions on its way from the reservoir matrix to surface. Nodal analysis is a technique to quantify the flow (pressure drop, rates) at a determined node. This node is conventionally set at the sand face; however, many applications require calculation at the

wellhead (such as flow-point analysis). The inflow from the reservoir on the node is explained by Inflow Performance Relationship (IPR), which is a correlation of bottom hole pressure with production. It is also described as the reservoir deliverability equation. Several IPR correlations are used to model different wells in this study. The most common model is Gas Well Backpressure equation that plots IPR based on measured well test data. Other IPR models used include Jones and Productivity Index when modelling gas reservoir as oil using equivalent Gas Oil Ratio (GOR).

Going outwards from the node is the flow in tubing till wellhead (wellbore flow), which is described by Vertical Lift Performance (VLP) correlations. These equations measure the pressure drop due to frictional, hydrostatic, and acceleration components while oil/gas travels through the wellbore. There are several multiphase VLP correlations published that model the effects of different fluids flowing in the wellbore. As this is a gas study, Gray 1978 correlation, which is widely used to model gas wells, is used in this work.

When IPR and VLP curves are constructed on the same plot, their intersection is the operating point of the well. Often the VLP curve will intersect IPR at two points. The selection of operating point among these two intersections is based on the stability of flow in the wellbore. Figure 10 shows a schematic of nodal analysis plot.

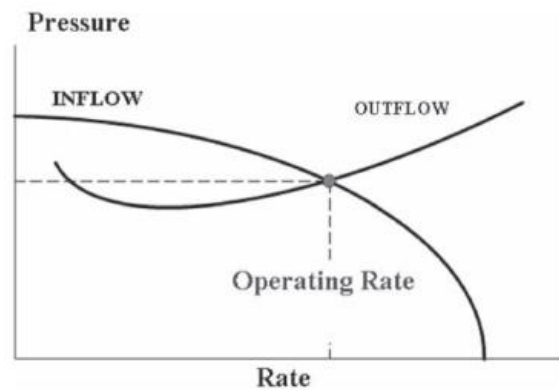


Figure 10 - Nodal analysis plot (Lea et al., 2008)

VLP Stability

VLP correlations are used to model pressure drop across tubing. Among three components that add to total pressure drop, frictional losses, and hydrostatic head are the dominating factors. Hydrostatic pressure component is derived from the pressure of the fluid column that is accumulated in the wellbore. Specific to gas wells, at high production rates, all liquid produced in the wellbore is carried by the gas to the surface in mist form. In this scenario, frictional losses make the primary component of pressure loss. As production rates decline, flow patterns change to bubble flow where liquid is held-up in wellbore, and gas flows through this liquid in the form of bubbles. In this scenario, hydrostatic pressure is the dominating factor. Figure 11 shows two

dotted lines depicting these two phenomena. The combination of these is plotted in the solid line. This combined effect forces the curve through a minimum, which is generally considered the limit of stability.

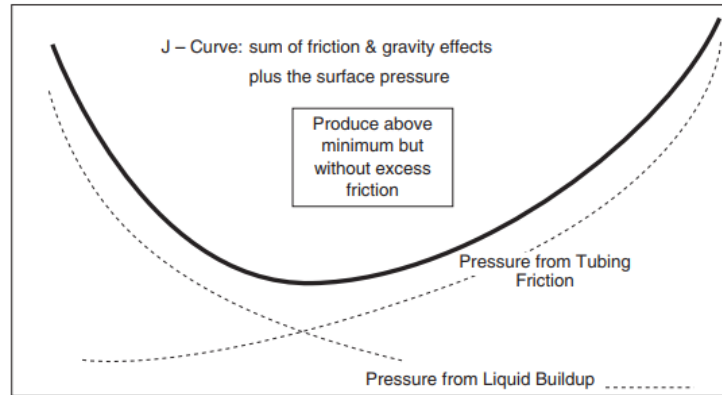


Figure 11 - Components of pressure loss in tubing (Lea et al., 2008)

In practice, the VLP curve alone can be used to predict the onset of liquid loading. The far-right of minimum on the VLP curve is considered stable region, predicting mist flow. Under these conditions, most produced liquid is carried to the surface by the gas stream. As production nears the minimum, it enters a slug region where chunks of liquids are produced by gas pockets. This behaviour is a precursor to liquid loading. The left side of the VLP curve minimum is considered an unstable region, and produced water is expected to accumulate in the wellbore. When production is near, on or at the left of VLP minimum, a remedy is required to bring production back in the stable (far right) region. Although this is a qualitative approach, it can be used as a first step tool to check for liquid loading.

Flow-point Analysis

Flow-point is the apex of the outflow curve when the node is set to the wellhead. This VLP curve (estimated at the wellhead) is plotted with IPR to conduct the flow-point analysis. The difference between the two curves is the difference between wellhead pressure and flowing bottom hole pressure. Similar to VLP stability, production on the right of the apex (flow-point) is stable while production near or left of the apex is unstable. Although the root cause of instability is the same (liquid loading), the mechanism of instability is not the same as VLP stability, where the instability is due to lower velocities that are insufficient to carry fluid to surface. For the flow-point curve,

every change in wellhead pressure translates to a similar change in bottom hole pressure. Often production rate is not available from the reservoir that corresponds to this bottom hole pressure value. This results in an unstable flow condition. As there cannot be two pressure values at the same point, the system readjusts by moving the flowrate to a compatible value (that is to the right of flow-point), or if such a point is not possible, the instability kills the well (Greene 1983). Figure 12 shows a flow-point analysis plot schematic highlighting unstable region with dotted lines.

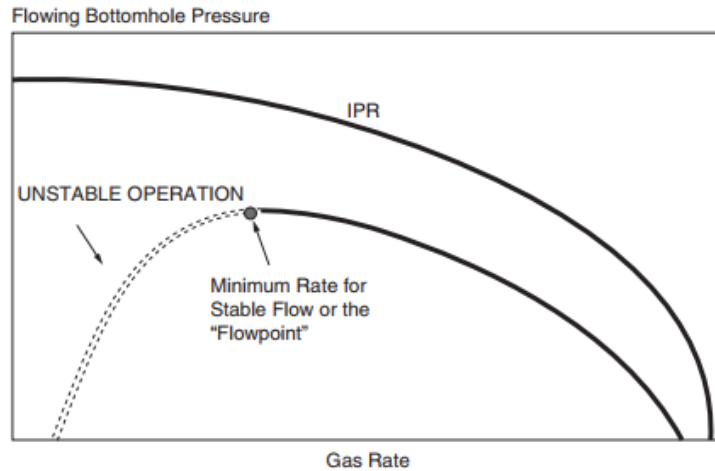


Figure 12 – Flow-point analysis plot (Lea et al., 2008)

VLP stability, in conjunction with flow-point and nodal analysis, can be used to supplement investigation for stable flow in the wellbore. Critical rate with production plots can further be used with these tools to qualitatively and quantitatively ascertain liquid loading in gas wells before investing in artificial lifts to remedy the problem.

Artificial Lift Selection

Several workflows that aid in the selection of artificial lifts have been published. The primary goal of these workflows is to guide design engineers in selecting the most suitable artificial lift based on multiple factors that include well parameters, reservoir properties and operating ranges of artificial lifts. As selection and design is a complex process, therefore these workflows are used to systematically compare the artificial lifts and select the most appropriate option.

Selection workflows are mainly categorized as Expert Systems, Machine Learning, or design & review models. Although these programs are only as good as their knowledge base and training dataset, they provide a new paradigm to the classical methods of selection. Arguably, there is no right approach to select an artificial lift system, which should vary with the case as much as the artificial lift itself.

Expert Systems

Expert systems are computer programs that are designed to make decisions based on the fulfilment of certain criteria. In a nutshell, expert systems are a collection of *what-if* statements that execute based on the initial input data.

All expert systems have a knowledge base, where the results of several decisions to common problems are stored. This is the most vital element of any expert system, and the system is as good as its data bank. It is also critical that the knowledge base is not intrinsically biased, which will force the entire system to make flawed decisions. The databank is created by data from experts in the respective field (hence the name), through direct input or by completing carefully designed surveys. Two widely popular expert systems for artificial lift selection are SEDLA and OPUS.

SEDLA Expert system (Espin et al. 1994)

This is one of the most thorough attempts in creating an expert system for artificial lift selection. The system consists of three distinct modules, each tackles a different aspect of the problem. Module-1 is the classic expert module, where an applicable artificial lift is selected based on the input data. The inputs for this module are well and reservoir data, while the output is the artificial lift type. Module-2 is based on textbook design calculations, that takes observations and user input data from Module-1 and conducts design of the selected artificial lift system. The inputs for this module are the selected artificial lift and well data, while the output is production rates. Module-3- conducts economic analysis to evaluate the financial feasibility of installing the selected artificial lift using estimated production rates from that lift. Figure 13 depicts the SEDLA program flowchart.

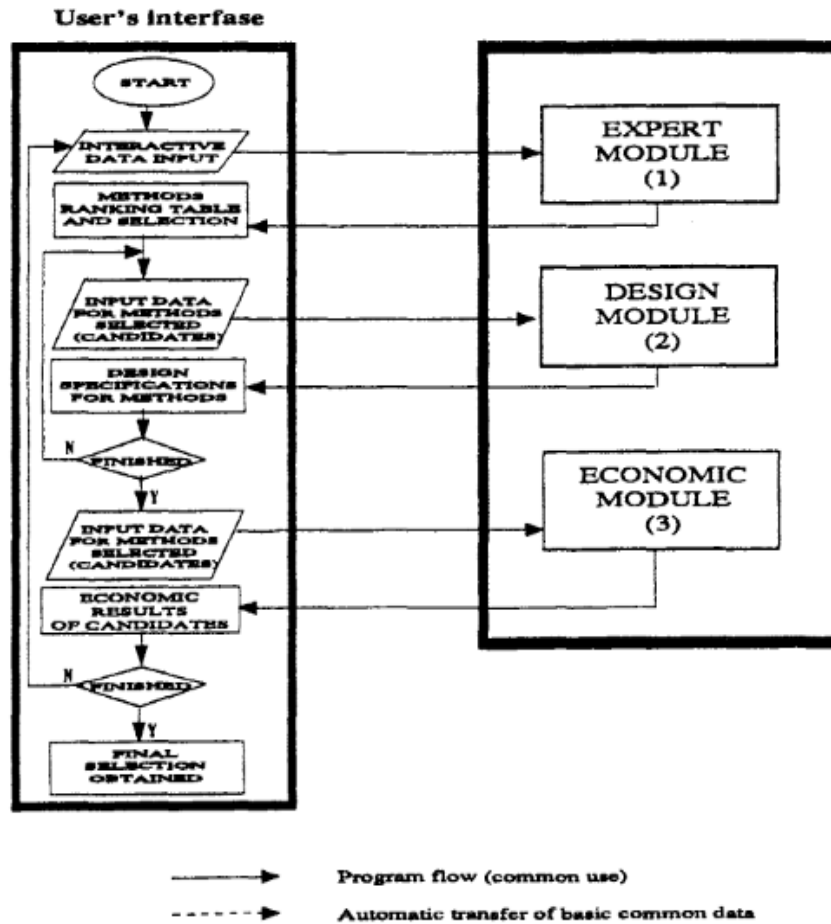


Figure 13 - SEDLA program flow (Espin 1994)

The expert system module in SEDLA uses the following logic flow to select the artificial lift method (Espin et al. 1994).

1. Input parameters provided by users are sorted as
 - a. Quantitative parameters such as well depth, reservoir pressure, et cetera.
 - b. Qualitative parameters such as well locations, availability of gas for injection, et cetera.
 - c. Production problems such as H₂S, corrosion, asphaltenes, formation scale, et cetera.
2. Using input parameters, unsuitable options are discarded.

- a. If injection gas is not available, any artificial lift requiring gas injection is ruled out immediately.
3. Remaining options are high graded based on input data by using a weighing score attributed to each parameter
 - a. *If-else* conditions are used for each parameter to assign a weighing score to each artificial lift system. For example: if the depth is greater than 10,000ft, PCP will get a negative score as its applicability is limited to depths shallower than 10,000ft. Similarly, if a well has sand production, PCP will receive higher positive scores for this parameter.
 - b. The system with the highest cumulative score gets ranked highest and is selected as the lift system of choice by the expert system

Despite being one of the most thorough expert systems published for artificial lift selection, SEDLA falls short of automating the entire process. Some of the shortfalls include:

- The knowledge base does not account for local limitations that may significantly skew the selection of lift system.
- Use of global averages for operating expenses for different lift systems that may vary significantly with geographical location.
- As this is a feed-forward system (information flows from module 1 to 3), there is no effect of economics results on the outcome of Module-1. Consequently, Module-1 might select an artificial lift system based on the expert review, however, it may not be the most economical lift type. This is a major drawback of this system.

The overall workflow of OPUS is very similar to SEDLA. Instead of directly using a weighted scoring method to high-grade and select artificial lift systems, it uses an elimination methodology. Further, its knowledge base consists of several rules that are used by the inference engine to make a decision. An example of such a rule is: *If Oil API < 20, ESP = not suitable*. The sets of rules are divided between two levels, where the rejection of any level-1 rule results in instant elimination. Similarly, the inference engine checks all the user input parameters against the knowledge base and eliminates a lift system if the rules are not satisfied. The user is left with the most applicable lift system and a range of other systems that are not a perfect match but were not eliminated as they did not reject any level-1 rule in the knowledge base. A design and economics module similar to SEDLA is then used to size the lift system and predict economic parameters. Figure 14 shows the hierarchal structure of OPUS.

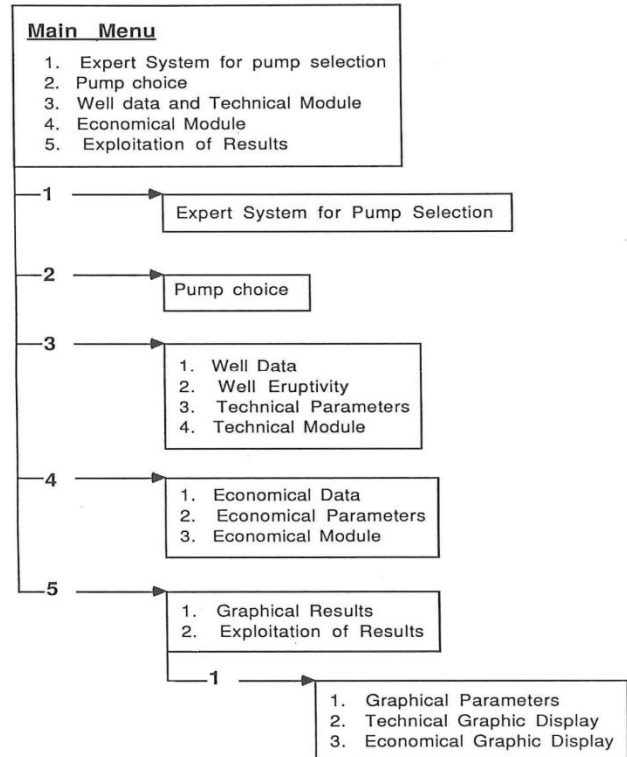


Figure 14 – OPUS artificial lift selection workflow – Valentin et al. 1988

Although significant work has been done on expert systems for artificial lifts, this approach has not picked up mainstream popularity between operators and producers due to significant bias of each system towards their knowledge base. This shortfall coupled with advances in artificial intelligence led to the development of machine learning models, that could be trained with local data and be applicable in more scenarios than the *static* knowledge held in expert systems.

Selection through Machine Learning Models

Supervised machine learning is a great alternative to expert systems for selection of artificial lifts. Database of wells installed with artificial lifts can be used to train machines such as decision tree

models and artificial neural networks to correlate different well and reservoir parameters with successful artificial lift implementation.

Machine learning has two obvious benefits to expert systems. First, the model can be trained using a local dataset, wells in similar area/field that have already been tested with different forms of artificial lift and have positive or negative results. Therefore, the model has local experience rather than global knowledge or set of rules. Second, as machine learning is a constant process, every successful or failed installation is another data point for the model to improve its correlation. Lastly, the design module of the program can use expected production profiles versus realized production to improve the correlation between the reservoir and the design parameters.

Artificial lift selection problem consists of a large set of properties all of which have a varying degree of influence on the final selection. A few of these properties are listed in Table 1. As this a multivariate problem, it is vital to conduct feature engineering (*lower the dimensions of the problem by selecting the most important variables*). Several techniques such as feature ranking, dimensionality reduction, etc. can be employed to ensure maximum variance is explained by a minimum number of input parameters.

Well Parameters	Production Conditions	Fluid Properties	Reservoir Parameters
Depth	Flow Rates	Density	Pressure
Tortuosity	Decline Rates	Viscosity	Temperature
Tubulars	GOR	Solid Production	DAQ requirement
	Water Cut	Scales	Productivity
Surface Facilities	Profitability Factors	Supplier Factors	HSE Considerations
Power grid	Service Life	Availability	Noise Level
Gas Availability	CAPEX	Ease of Maintenance	CO ₂ Emission
Pipeline	OPEX	Access to Spare Parts	Well Integrity
Capacity constraints	Production Deferment	Staff Experience	Staff Competency

Table 1 - Parameters required in artificial lift design and selection – Ounsakul et al., 2019

Ounsakul (Ounsakul et al. 2019) developed an artificial lift selection workflow using neural networks. They use a database of 30,000 wells to train this machine. Each artificial lift installation is characterized on a quantifiable scale for the machine to interpret the success of lift installation. The artificial lifts used in the sample set included Gas Lift, Beam pump, ESP and PCP. The

database is split into train-validate-test sets, where the model is trained on the train set, fine-tuned on the validate set and tested for accuracy on the test set.

This model was used to select artificial lifts for 9 new wells. They used normalized lifting cost per barrel versus normalized production to check if selected artificial lift resulted in lower cost and higher production. Figure 15 cross-plots normalized cost and production of the sample set wells (black dots) and the new 9 wells (yellow dots). As seen, the machine learning model selected a lift system that resulted in low lifting cost and relatively high production for most of the 9 new wells.

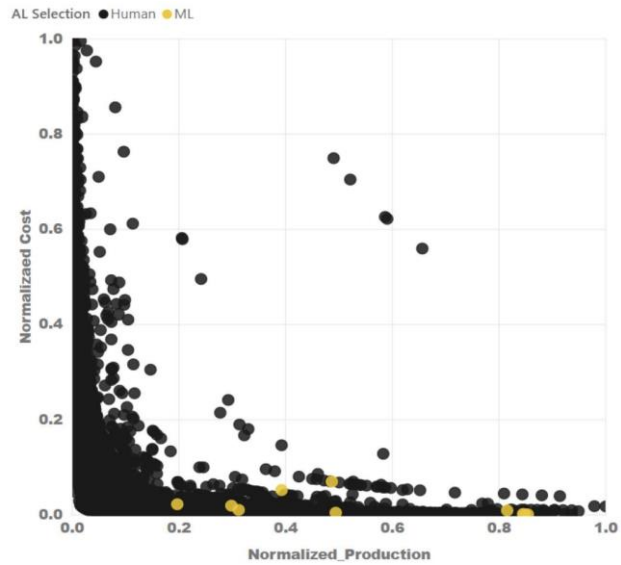


Figure 15- Normalized cost vs production - Ounsakul et al., 2019

Gas well Artificial Lift System Selection

Artificial lift installation for dewatering gas wells, pose additional challenges in selecting an optimum system. Most types of pumps (electric, hydraulic, etc.) significantly loose efficiency when operated with large amounts of gas. Despite state-of-the-art gas separation modifications (like Advanced Gas Handlers, Poseidon- Schlumberger, and Gas Master-Centrilift for electrical submersible pumps, Vortex separators for beam lifts, etc.) efficiency and run life is not comparable to installations done in low gas conditions. Therefore, using selection workflows designed for oil wells will yield incorrect results in deliquification applications.

Oyewole and Lea, 2008 suggested workflow for selecting lift system using bottom hole pressure. They compared several lift types in different wellbore constructions (vertical, horizontal, S-shaped, etc.) and suggested to use the lift system that produced the lowest bottom hole pressure estimated through nodal analysis. Their review and selection process is based on the gas well field test in North San Juan basin. Despite using a design and review approach to compare and select the optimum lift system, their workflow lacks completeness as production profiling is not part of the algorithm. Figure 16 and Figure 17 depicts selection criteria.

Well Conditions	Vertical	Horizontal*	HST	S Shaped
<20 bpd LS	(1) BP (2) RDPCP (hi end) (3) GL (lo end)	(1) GL (2)ESP gas separation	(1)BP, (2)GL (3) RDPCP SA	(1)BP co-rod (2)GL
20–100 bpd LS	(1) BP (2) RDPCP (hi end) (3) GL (lo end)	(1) GL (2)ESP gas separation	(1)BP, (2)GL (3) RDPCP SA	(1)BP co-rod (2)GL
100–Qmax bpd LS	(1) BP (2) RDPCP (hi end) (3) GL (lo end)	(1) GL (2)ESP gas separation	(1)BP, (2)ESP (3) RDPCP SA	(1)BP co-rod (2)GL
>Qmax LS	(1) BP (2) RDPCP (hi end) (3) GL (lo end)	(1) GL (2)ESP gas separation	(1)BP, (2)ESP (3) RDPCP SA	(1)BP co-rod (2)GL
400 scf/bbl–1000', <20 bpd, P _{csq} > 1.5 LP<35psi, LS	PLUNGER	PLUNGER	PLUNGER	PLUNGER
SS = Severe Solids LS = Low Solids	BP = Beam Pump with CoRod	ESPCP = elec sub PCP - TTC implied RD PCP = Rod Driven Progressive Cavity Pmp	GL = Unconventional Gaslift (see chapter)	Qmax ≈ 300-350 bpd SA = Special Application * Horizontal poor for pmps

Figure 16 - Lift selection matrix for wells with little or no solids (Oyewole and Lea 2008)

Well Conditions	Vertical	Horizontal*	HST	S Shaped
<20 bpd SS (~<setling velocity)	(1)GL (2) RDPCP SA	(1)GL	(1)GL (2) BP SA (3) RDPCP SA	(1)GL (2) BP co-rod
20–100 bpd SS (~<setling velocity)	(1) GL (2) RDPCP SA	(1) GL	(1) GL (2) RDPCP SA (3) BP SA	(1)GL (2) BP co-rod
100– Qmax bpd SS	(1) GL (2) RDPCP depth dependent	(1) GL (2) ESPCP depth dependent	(1) RDPCP (2) GL	(1)GL (2) BP co-rod
>Qmax SS	(1) GL (2) RDPCP depth dependent	(1) GL (2) ESPCP depth dependent	(1) RDPCP (2) GL	(1)GL (2) BP co-rod
400 scf/bbl–1000', <30 bpd, P _{csq} > 1.5 LP<35psi, LS	PLUNGER NOT APPLICABLE	PLUNGER NOT APPLICABLE	PLUNGER NOT APPLICABLE	PLUNGER NOT APPLICABLE
SS = Severe Solids LS = Low Solids	BP = Beam Pump with CoRod for all cases SA=special app with annulus water, other	ESPCP = elec sub PCP - TTC implied RD PCP = Rod Driven Progressive Cavity Pmp	GL = Unconventional Gaslift (see chapter)	Qmax ≈ 300-350 bpd SA = Special Application * Horizontal poor for pmps

Figure 17 - Lift Selection matrix for wells with solids (Oyewole and Lea, 2008)

Design & Review Workflow for Gas Well Deliquification

In the absence of significant datasets (that rules out machine learning), a straightforward approach to select artificial lift for deliquification is conducting design, review and comparison of each applicable technology on a well-by-well basis. Applicable technologies can be listed by eliminating options that are not possible (such as gas lift in the absence of injection gas). A general structure is then used that directs the flow of information from one lift system to others. Results from all lift systems can be compared to select the most optimum solution.

Given the proportion of gas is significant in gas producing wells, downhole pumps have an inherent disadvantage due to lower efficiency. Nevertheless, they can be superior options for a specific case, therefore should be included in the comparison.

For the specific case of fields used in this study, based on prior experience in the region and availability of infrastructure, following lift systems are part of this workflow. However, the suggested workflow can be used with any number and type of lifts.

- Gas Lift
- Coiled Tubing Gas Lift
- Plunger Lift
- Plunger Assisted Gas Lift
- Beam Lift
- Velocity Strings / Tubing Size Optimization

Unlike most of the selection workflows published in the literature, the approach in this work suggests starting from production analysis of the target well. It is vital to quantify if liquid loading is the cause behind unoptimized production and develop a baseline understanding of the production trend. This aids in the selection of a lift system, quantification of incremental production and evaluation of production trends post-installation.

Liquid loading can be quantified by comparing the production rate with the critical unloading rate for the target well. This will suggest the onset and extent of liquid loading. Moreover, production logs and fluid level detection can also be used to estimate fluid holdup (fluid accumulation in the wellbore). System nodal analysis is used to create baseline models to estimate current bottom hole

pressure, calibrated with last known well test data. These models can then be used to compare changes in production and well parameters post artificial lift installation.

Nodal analysis in this workflow is conducted on PROSPER, a commercial system analysis tool developed by Petroleum Experts. Several Inflow Performance Relationships (IPR) models are used to create reservoir deliverability curves. For baseline models, Gray 1978 Vertical Lift Performance (VLP) model is used due to its applicability in gas wells.

Figure 18 shows a schematic of the gas well deliquification workflow developed and used in this study.

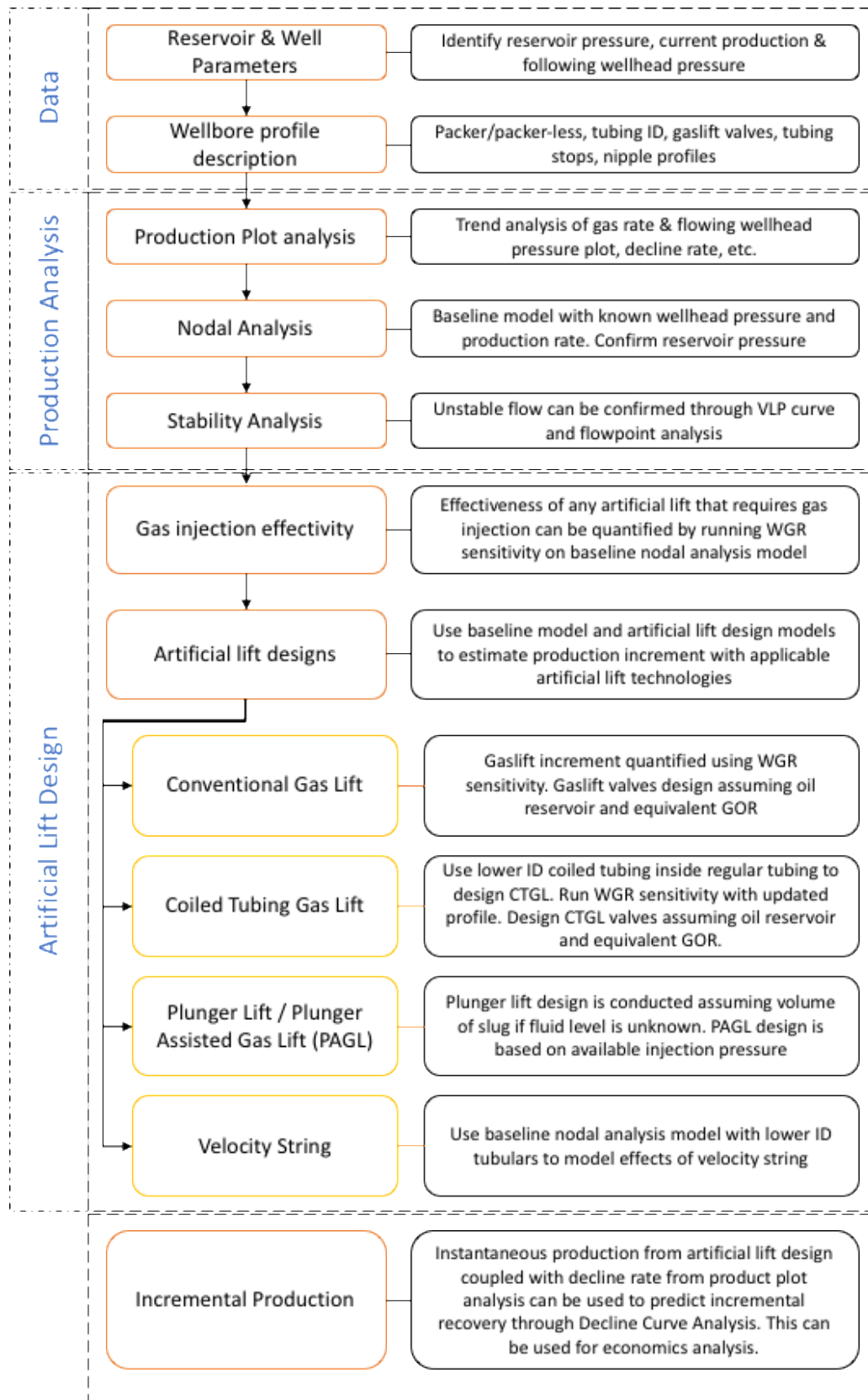


Figure 18 - Artificial lift selection workflow for gas well deliquification suggested in this study

Chapter-2: Critical Unloading Rate

Weighted Average Critical Rate

The most widely accepted technique to predict liquid loading is to estimate the critical gas rate required to produce all liquids in the wellbore to the surface. Several authors have suggested different correlations to predict the gas velocities, required to lift a known diameter of a liquid bubble in the wellbore. Despite the significant understanding of the physical phenomena of liquid flow in the core gas stream, most published models are empirical correlations that try to fit Stokes' law using empirical constants on an experimental dataset. Among the many published works, more widely used correlations include the Turner's 1969 model and Coleman's 1991 modification to Turner's model. As most of these equations are empirical, they are most applicable in situations on which they were fine-tuned. This can easily be tested by applying these correlations on different datasets – *for example, testing Turner's model on ultra-low Wellhead Pressure (WHP) wells.*

This work proposes a new weighted average critical rate calculation workflow, that utilizes published empirical correlations together with wellhead pressure as a weighing parameter to estimate critical rate. Instead of using a single model, this technique utilizes all major correlations while controlling their influence on the final critical rate through the weighting factor. The next section introduces major liquid loading models briefly, for the reader to better understand why only certain correlations are used in this study's weighted average workflow.

Turner (1969) Drop Model

Turner et al. 1969, proposed estimating critical gas rate using fluid mechanics, where they equated forces from gas flow pushing upwards to gravitational pull downwards on the liquid droplet. At the instance where the relative velocity of the drop with gas flow is negligible, liquid droplet would be motionless and flow towards the surface with the gas stream. As gravitational and drag forces are a function of the droplet size, quantifying largest drop size is critical to estimating gas velocity.

Hinze 1955, correlated the use of weber number with maximum droplet size, as it depends on the velocity, pressure and surface tension. Given the critical weber number of 30, at which most droplets shatter into smaller ones, terminal velocity equation is shown in Eq (1).

$$v_t = \frac{1.3 \sigma^{\frac{1}{4}} (\rho_L - \rho_g)^{1/4}}{C_d^{1/4} \rho_g^{1/2}} \quad (1)$$

Further, Turner et al. 1969, showed that for a typical field application, drag coefficient has a relatively constant value of 0.44, therefore the terminal velocity equation reduces to Eq (2).

$$v_t = \frac{17.6 \sigma^{\frac{1}{4}} (\rho_L - \rho_g)^{1/4}}{\rho_g^{1/2}} \quad (2)$$

Although the development of the drop model is based on force balance in fluid mechanics, there are empirical constants built into the final equation widely used in industry today. Moreover, the resultant equation associated with the Turner model has a 20% upwards adjustment to better fit the dataset they used to validate this equation. This adjustment coupled with the use of experimental weber number cutoff and constant drag coefficient embedded significant empirical roots in the final form of the Turner model as shown in Eq (3).

$$v_t = \frac{20.4 \sigma^{\frac{1}{4}} (\rho_L - \rho_g)^{1/4}}{\rho_g^{1/2}} \quad (3)$$

Coleman (1991) Model

The dataset used by Turner et al. 1969, to test their model had most wells with WHP higher than 500psi. A large chunk of these wells had WHP higher than 2500 psi, therefore, suggesting their work was tuned using a dataset of higher rate wells. Coleman et al. 1991, while reviewing the formulation and assumptions of the droplet model, applied Turner's model on low-pressure wells with WHP lower than 500 psi and found discrepancies. Their work led to a significant understanding of the droplet model.

Coleman suggested using Turner's model without the 20% upward adjustment when modelling wells with low WHP. Using field tests, they suggested condensed water as a major cause of loading in low pressure gas wells. Moreover, by carefully manipulating individual parameters in test wells, they found that variables like temperature, liquid gravity, interfacial tension, liquid rate and Liquid Gas Ratio (LGR) has minimum influence on the terminal velocity. This was a powerful decoupling of important parameters with critical rate calculation and endorsement of application Stokes' law.

Essentially, they proposed that the critical gas rate can be reasonably estimated by knowing the target well's WHP and gas specific gravity. Similar to Turner et al., Coleman's work provided field dataset with known results to test these modifications to critical gas rate correlation.

As Coleman's work is the same as Turner's, it follows the same assumptions for droplet size, shape, and drag coefficients. Coleman's terminal velocity is given in Eq (4).

$$v_t = \frac{17.6 \sigma^{\frac{1}{4}} (\rho_L - \rho_g)^{1/4}}{\rho_g^{1/2}} \quad (4)$$

Nosseir (2000) Model

Adopting Turner's liquid droplet model as a basis, Nosseir et al. 2000, critiqued inaccuracy in the empirical model suggested by Turner and Coleman as one recommended 20% upward adjustment while other argued against it. Nosseir attempted to analytically explain the requirement of the adjustment factor by investigating the drag coefficient assumption used by Turner. They worked on flow regime in the wellbore, classifying it as laminar, transient and turbulent flow.

Stokes' law was initially derived for terminal velocity of a solid particle in the laminar regime - Reynold's number (N_{Re}) < 1. However, in reality, most gas wells during high production will have Reynold's number significantly higher than 1. Moreover, the initial application of Stokes' law was on spherical solid particles while the application in this scenario is on liquid particles that are assumed to be spherical. The latter assumption is questionable given transition and turbulent flow regime in gas wells. Transition regime is classified as N_{Re} between 1 and 1000 while the turbulent regime is N_{Re} greater than 1000. To account for different flow regimes, Nosseir suggested modification to the droplet model approach by Turner.

Turner et al. 1969, assumed constant turbulent flow in gas wells, with N_{Re} between 10,000 and 200,000. This resulted in a constant drag coefficient of 0.44, that was inbuilt in the terminal velocity equation. Nosseir found, for many wells from the Turner's dataset, N_{Re} exceeded well beyond 200,000, for which drag coefficient should be adjusted to 0.2. Similarly, for lower N_{Re} wells, drag coefficient should be appropriately adjusted. Using this as a guiding principle (keeping everything else similar to Turner's approach), Nosseir suggested Eq (5) and Eq (6) for terminal velocity.

For transition flow regime (low gas flowrate wells):

$$v_t = \frac{14.6 \sigma^{0.35} (\rho_L - \rho_g)^{0.21}}{\mu^{0.134} \rho_g^{0.426}} \quad (5)$$

For highly turbulent flow regime (high gas flowrate wells):

$$v_t = \frac{21.3 \sigma^{0.25} (\rho_L - \rho_g)^{0.25}}{\rho_g^{0.5}} \quad (6)$$

This modification to the Turner model resulted in a ~3% reduction in error between observed and actual critical rate on Turner's dataset. However, the authors of this study observed that Nosseir did not use the entire dataset provided by Turner. This might create a bias in the results presented by Nosseir.

Li et al. (2001) Model

Similar to Nosseir's working, Li et al. 2001, evaluated Turner's droplet model by applying it to wells in China and found that it over-predicted critical rates in two-third of the cases. Their attempt to improve the droplet model lies in investigating the shape of the droplet as it moves in the wellbore. Turner assumed spherical droplet and used 30 as weber number cutoff when deriving their equation. Li suggested that due to the presence of pressure differential between the fore and aft sides of the drop, assumption of spherical shape is invalid. The liquid drop will most likely transform away from spherical shape to convex bean-like shape. This will increase the effective surface area for drag forces, requiring lower gas velocities to lift the droplet to the surface.

As a bean-shaped drop is considered, the effective area available to gas is almost 100%, therefore Li suggested using drag coefficient as 1, increasing it from 0.44 as assumed by Turner for highly turbulent gas wells. Incorporating these modifications - change of shape and drag coefficients - into Stokes' law and following similar derivation approach as Turner, Li's terminal velocity is given in Eq (7).

$$v_t = \frac{0.7241 [(\rho_L - \rho_g)\sigma]^{0.25}}{\rho_g^{0.426}} \quad (7)$$

A comparison of Li's model with other published model depicts significant under-prediction of critical gas rate by their model. The dataset used in their study was limited to a few wells from

China. Furthermore, the application of their model on Turner and Coleman’s dataset showed significant mispredictions. Li’s basic assumption of bean shape droplet may not be entirely accurate throughout the wellbore, as near-surface, pressures are often significantly lower than bottom hole and differential across the droplet may be insignificant to cause any shape change.

Luan and He (2012) Model

Luan and He, 2012, took an approach similar to the working in this study. They compared the critical rates estimated by Li and Turner’s correlation using a dataset of ~300 low pressure gas wells. Similar to the observation in this study, Li’s method underestimated while Turner’s method overestimated the predictions. Hypothesizing that the real unloading rate lies between these two extremes, Luan and He suggested to use the two rates as boundary conditions and defined a new empirical constant S - *loss of gas energy* - that ranges from zero to unity to estimate the real unloading rate.

The physical reason between the difference in rate estimated by Li and Turner’s model is their description of the liquid droplet and corresponding drag coefficient. Luan and He suggested, that neither is completely correct as droplets change shape while rising, coalesce, break and rollover. This is empirically captured in the constant S . Their critical velocity correlation is given in Eq (8).

$$v_t = v_{crit-L} + S \times (v_{crit-T} - v_{crit-L}) \quad (8)$$

where v_{crit-T} is Turner critical velocity and v_{crit-L} is Li critical velocity respectively. Authors used the dataset to identify the range of constant S , which was shown to be from 0.75 to 0.83. For simplification, the upper limit of loss factor S (0.83) is used for calculation of critical velocity.

Weighted Average Critical Rate Formulation

Most of the critical gas rate models discussed above relied on a dataset to fine-tune their correlations. This introduced an empirical constant to the model that limits its universal applicability. Moreover, the dataset used by most authors have wells that are similar in terms of one parameter or other. For Turner’s dataset, this was high wellhead pressure wells (most WHP > 1000 psi) while Coleman’s dataset included wells with only 2.441 inch tubing ID and most wells with WHP < 250 psi. Awolusi (Awolusi 2005) based their work on low pressure stripper gas wells with setup in a laboratory using air and water only.

This suggests none of the empirical models has been validated for application in all cases, regardless of well parameters. Furthermore, from investigating the dataset of these published models, it is evident that one of the most important parameters in selecting a particular equation is WHP. For example, if the target well wellhead pressure is high than Turner’s model is more applicable given it was calibrated using high WHP dataset.

Using wellhead pressure as a weighting criterion, instead of selecting one model, a weighted average of multiple published model is used. As will be shown later, this results in better estimation of critical rate. This largely because, by employing a weighting criterion, the appropriate critical model for that specific scenario is used for calculation.

Weighting Criteria

The dataset of all major models described above are investigated and average wellhead pressure in each of them is noted. Average WHP for each major publication is given in Table 2.

Model	Avg Pressure (psia)
Turner	2481
Coleman	149
Nossier	1540
Li et al	2380
Luan & He	149

Table 2 - Average WHP in published datasets

As Luan and He used the dataset of Coleman, their average pressure is the same. Furthermore, by using Luan and He (that uses a loss factor S to weight Li’s correlation), we do not need to consider Li’s model in our correlation. Given Coleman’s equation is exactly Turner’s model without empirical adjustment, we can also omit Coleman’s equation from our calculation. Therefore, the weighted average technique utilizes Turner, Nossier and Luan and He model with wellhead pressure as the weighting parameter for an average between these three equations.

The workflow in selecting the appropriate equation is as follows:

- If Wellhead pressure is above 2481 psi, use Turner et al. 1969 correlation

- If Wellhead pressure is below 149 psi, use Luan and He 2012 correlation
- If Wellhead pressure is between 2481 and 1540, use a weighted average of Turner 1969 and Nousseir 2000 models
- If Wellhead pressure is between 1540 and 149, use a weighted average of Nousseir 2000 and Luan and He 2012 models

Further, during the validation process of this workflow, it was found that normal loss factor S in Luan and He correlation as suggested by the authors is not between 0.7 and 0.85. Instead, this value is lower than 0.5, around between 0.2-0.3 in most cases. If we analyze Luan and He correlation, lowering this constant, forces the equation to the result near Li's model (which predicts a lower than expected critical gas rate). As we are already using Turner's model and the appropriate weighting factor for high WHP wells, it makes sense to use lower S factor to dampen the effect of Turner model when using Luan and He for low WHP wells. Alternatively, we can also remove Luan and He completely and use Li's model for lower WHP wells, however, the results achieved with this method are not as accurate. The reason for this is likely embedded in the formulation of Li's correlation, as it is stipulated assuming highly turbulent wells, where bubbles of liquid change into bean-like shape due to pressure gradient across the bubble. In low WHP wells, gas flowrate is likely on the lower side therefore bubbles might not be as elliptical throughout the wellbore as hypothesized by Li et al. 2001.

To estimate the Weight Factor (WF), the following correlations are used

- If Wellhead pressure is between 2481 and 1540 – use Eq (9) and (10):

$$WF = \frac{2481 - WHP}{941} \quad (9)$$

$$WACR = (1 - WF) \times Q_{crit_{Turner}} + (WF) \times Q_{crit_{Nousseir}} \quad (10)$$

- If Wellhead pressure is between 1540 and 149 – use Eq (11) and (12):

$$WF = \frac{1541 - WHP}{1392} \quad (11)$$

$$WACR = (1 - WF) \times Q_{crit_{Nossier}} + (WF) \times Q_{crit_{Luan\&He}} \quad (12)$$

Validation

Assessing the performance of the critical equation is key to evaluate its effectiveness in field implementation. Most publications have used cross plots (scatter plots) to validate their correlations. Test critical flowrate for each well is plotted against the calculated critical flowrate. The diagonal line on this plot divides it in unloaded and loaded-up regimes. If a well is near load-up condition, it should fall on or near the diagonal lines. To measure effectiveness, it is paramount to use data in which we know the true critical rate. This is either known by observing the flow behavior in a laboratory or by observing wellhead pressure, wellhead temperature fluctuation and production data fluctuations on the field using a chart recorder. Historically, most publications have used dataset provided by Turner et al. 1969 (high WHP wells) or Coleman et al. 1991 (low WHP wells). As the intention is to demonstrate the applicability of the weighted average critical rate over the entire spectrum of wells, both datasets are used for validation. Moreover, a study conducted by Awolusi, 2005, separately measured critical flowrates for ultra-low wellhead pressure (<50 psi) using air and water in a laboratory setup. This dataset is also used for validation of this workflow to demonstrate its universal applicability.

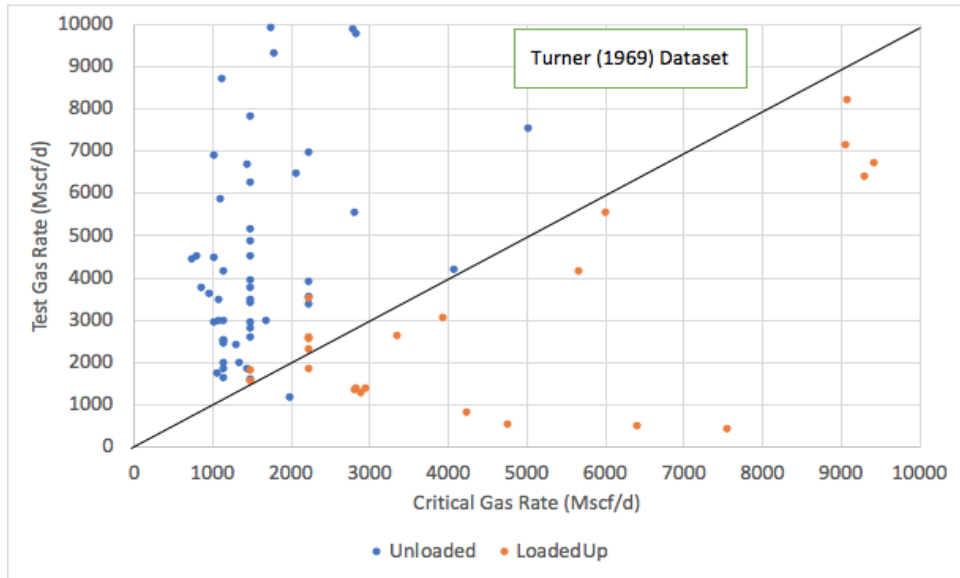


Figure 19 - Results from WACR using Turner's (1969) dataset

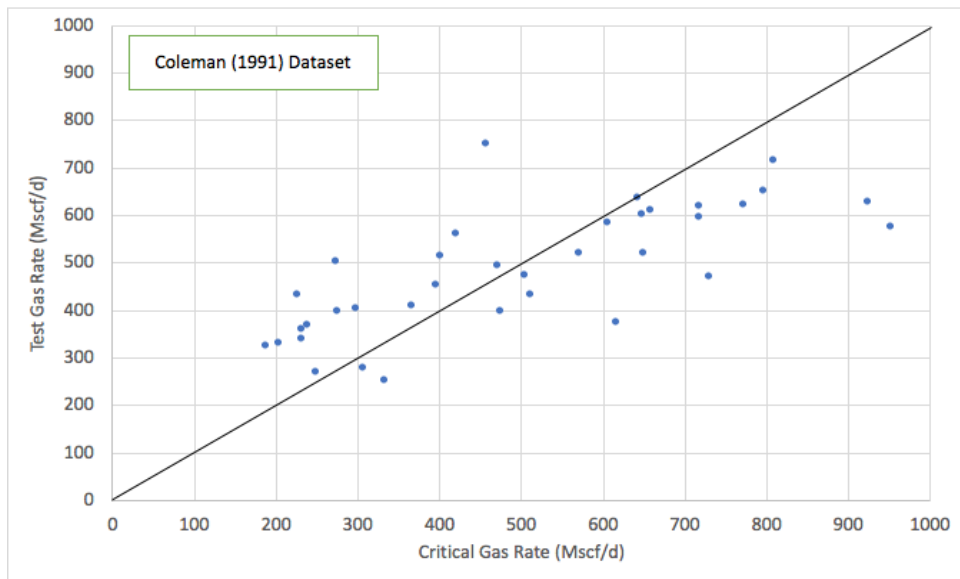


Figure 20 - Results from WACR using Coleman's (1991) dataset

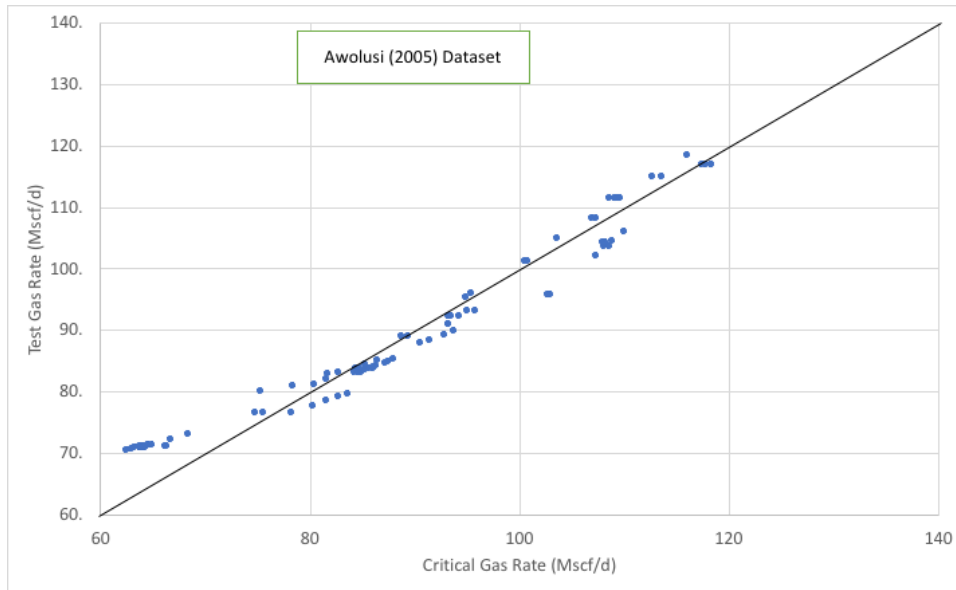


Figure 21 - Results from WACR using Awolusi's (2005) dataset

Figure 19 plots Turner et al. 1969 dataset where the critical gas rate is estimated using the weighted average technique. The plot depicts reasonable accuracy in predicting the unloaded and loaded up wells - segregation of blue points above black diagonal and orange points below diagonal. There are a couple of mispredictions of loaded-up wells that are predicted as being unloaded however overall accuracy is reasonable. The mean absolute error in Turner's dataset is ~20%.

Figure 20 plots Coleman et al. 1991 dataset where the critical gas rate is estimated using the weighted average technique. This plot differs from Turner's as Coleman's dataset only included wells that were near load-up. Therefore, we are plotting estimated critical rate with known true critical rates. As depicted by the plot, the weighted average technique produces reasonable results, as we observe that the diagonal line is the best fit line to Coleman dataset. It should be noted that the same model is used on Turner and Coleman's dataset and reasonable results are produced across the entire spectrum of wellhead pressures. The mean absolute error in Coleman's dataset is ~11%.

The applicability of this workflow to any wellhead pressure is also validated by testing it on the dataset collected by Awolusi during their experiment to measure the critical flowrate of ultra-low wellhead pressure wells (WHP < 50 psi). Figure 21 plots Awolusi's dataset where the critical gas rate is estimated using the weighted average technique. The plot type is similar to Coleman's where

the diagonal acts as a best-fit line. As depicted in the plot, the weighted average technique produces excellent match with test critical gas rate for wellhead pressures less than 50psi. This validates the applicability of this method on ultra-low flowrate gas wells.

Nomenclature

v_t = Critical velocity

σ = interfacial tension

ρ_L = Liquid density

ρ_g = Gas density

C_d = Drag coefficient

μ = viscosity

S = loss of gas energy

Machine Learning Model to Estimate Critical Gas Rate

Despite a plethora of analytical and empirical correlations to predict the onset of liquid loading, there has been minimal work done to estimate this property through data-driven methods. In developing these equations, there are often in-built principles and biases (often coming from expert knowledge) that may not be applicable in all scenarios where the equation is applied. This limits the predictive ability of correlations. One approach to counter this problem is to employ data-driven techniques in understanding the influence of individual parameters on the critical rate. Moreover, using these inferences, data can be used to train machine learning models for prediction purposes. Therefore, this section seeks to:

- Understand what parameters have the most significant influence on the critical rate.
- Use the best fit model, together with the most influential parameters, to predict the critical rate.

Approach

Similar to all machine learning workflows, the approach undertaken in this study involves data engineering and model creation/tuning. A supervised machine learning method, decision tree model, is used to estimate the critical gas rate. As supervised learning methods rely on known actual values in the training dataset to learn, the dataset available was limited to studies where authors measured the true critical rate.

Data engineering includes gathering data from different sources, estimating missing values in the dataset using interpolation/extrapolation techniques, categorizing different variables, and feature engineering. Feature engineering involves analyzing different features in dataset (for example, Depth, Wellhead Pressure, et cetera in this application) to ensure they can be compared/correlated with each other. This involves reviewing each feature in light of its distribution, spread, skewness, and how they correlate with one another. The main objective of data engineering is to ensure all features add value to the model, without introducing collinearity or redundancy. It is vital to ensure the number of features is optimized for a given data size. Higher features with small dataset does not provide adequate information to the model to learn the underlying correlations and may lead to errors.

Model creation/tuning is the process that uses the dataset prepared in the previous step to define and optimize different machine learning models that can be used for the prediction of the target variable. Machine learning models have hyper-parameters that are tuned using a training dataset so the model can fit the data. Once a reliable fit is achieved using specific hyper-parameters, they are locked, and then the final model is used for prediction.

The entire workflow for this section is made on Python. Libraries from Scikit Learn, NumPy, Matplotlib, Pandas, Scipy, and Seaborn were utilized. Complete code is given in Appendix B.

Dataset for Model

The dataset used for this study is taken from published papers from Turner et al. 1969, Coleman et al. 1991, and the thesis of Awolusi 2005. The idea is to create a dataset that represents diversity of wells with varying WHP, depth, tubing diameter, etc. Although the sample count is on the lower side, it is paramount that data used includes true critical value (measured in lab or field) as prediction models are created using supervised machine learning.

The basic statistics of the dataset utilized are shown in Table 3.

	Depth (ft)	WHP (psi)	Tubing ID (inches)	Gas SG	CGR	WGR	Test Flow MScf/D)
count	241.000000	241.000000	241.000000	241.000000	241.000000	241.000000	241.000000
mean	4717.294606	1064.187842	2.466125	0.74905	13.220332	39.505311	1870.635436
std	3819.469866	1481.053600	0.992612	0.18690	27.353230	76.379947	2479.920319
min	40.000000	0.900000	1.750000	0.58200	0.000000	0.000000	53.190000
25%	40.000000	35.000000	1.995000	0.60000	0.000000	0.000000	109.180000
50%	5934.000000	165.000000	1.995000	0.61700	2.500000	3.400000	593.000000
75%	7531.000000	2003.000000	2.441000	1.00000	10.300000	54.230000	2949.000000
max	11850.000000	8215.000000	7.386000	1.00000	130.800000	602.310000	11767.000000

Table 3 - Statistics of dataset used in this study

It is vital to have values for all features (columns) to ensure consistency in training of the machine learning model. Often datasets have missing values, such as unknown Condensate-Gas Ratio (CGR) for a well that does not produce condensate. Imputation techniques are used that rely on the mean and most frequent values of that feature to fill in the missing data.

Model Variables (Feature Engineering)

The first step towards creating a machine learning model is to understand the relationship between input variables (or features) and the target variable. The main objective is to rank all input variables in order of their influence on the target variable. In this application, these input variables are well and production parameters while the target variable is critical gas rate. Identifying the most influential parameters also enable operators to only record variables that are required to predict the onset of liquid loading. This is particularly helpful in low producers, where installing equipment like separators and flowmeters may not be economical.

It should be noted that no prior information or expert knowledge is added in this analysis based on the physical or analytical understanding of the system. Instead, conclusions derived in this section are purely based on data, and if they coincide with prior knowledge, it only endorses those beliefs.

Predictor features (or independent variables) in this case are; Depth (ft), Wellhead Pressure (WHP) (Psi), Tubing Internal Diameter (inches), Gas Specific Gravity, Condensate Gas Ratio (CGR), Water Gas Ratio (WGR). Response feature (or dependent variable) is Test Flow (true critical gas rate – Mscf/d)

Given sparse samples in the dataset, features WGR and CGR can be merged to form a single, Liquid Gas Ratio (LGR) feature. This not only lowers the dimensionality of the dataset, but makes physical sense as the concern is regarding higher density fluid, regardless of that being condensate or water or both.

Instead of relying on one method to rank predictor features, a variety of techniques are used to average out results and overcome limitations of each technique:

- Linearity
- Spearman's Product Moment Correlation
- Partial Correlation Coefficient
- Feature Importance
- Recursive Feature Elimination – *Using random forest model*

Linearity

Linearity is the property of a function that describes two or more variables, that can be represented using a straight line or space. In machine learning applications, linearity or linear relationship between variables is often a pre-requisite for many models (such as linear regression). Therefore, it is vital to confirm linearity between predictor features and response features to use many of the ranking and prediction models. This can be easily quantified using a significance test (or hypothesis test), which confirms a particular hypothesis based on its probability of being statistically significant (Joshi 2020). Significance test is conducted using a confidence interval of 95% (which suggests an error of 0.05 that the estimated result is incorrect), and the following hypothesis:

- Null Hypothesis H_0 : The population correlation coefficient is not significantly different from zero. *There is not a significant linear relationship.*
- Alternate Hypothesis H_a : The population correlation coefficient is significantly different from zero. *There is a significant linear relationship (correlation)*

If the probability value (p -value) is less than the significance level (0.05), reject the null hypothesis and accept alternate hypothesis (Dangeti 2017), suggesting linearity exists between critical gas rate and the variable under consideration.

Feature	P-value	Result
Depth	3.27E-15	<i>Reject Null Hypothesis – Linearity exists</i>
WHP	7.52E-29	<i>Reject Null Hypothesis – Linearity exists</i>
Tubing ID	6.21E-08	<i>Reject Null Hypothesis – Linearity exists</i>
Gas Specific Gravity	8.02E-22	<i>Reject Null Hypothesis – Linearity exists</i>
LGR	1.78E-05	<i>Reject Null Hypothesis – Linearity exists</i>

Table 4 - Significance test results - Linearity

Table 4 suggests that all five features in the dataset have a linear relationship with the target variable (critical gas rate). Therefore, all statistical ranking techniques can be used to quantify the influence of these parameters on the critical gas rate.

Pearson's Product-Moment Correlation

Pearson correlation is a statistical model to compare the variation between two distributions (features in this case). The value of correlation lies between -1 and 1, where -1 denotes strong inverse correlation while +1 denotes strong direct correlation. As the value approaches zero, the correlation between the two variables weakens, with zero indicating no correlation (Joshi 2020).

Pearson correlation model can be used to measure the strength of a linear relationship between different predictor features and critical gas rate. As the correlation compares two variables in one instance, results are shown in Figure 22 in the form of a correlation matrix. The coefficients are unity along the diagonal, as parameter is compared to itself and, therefore, perfectly correlates.

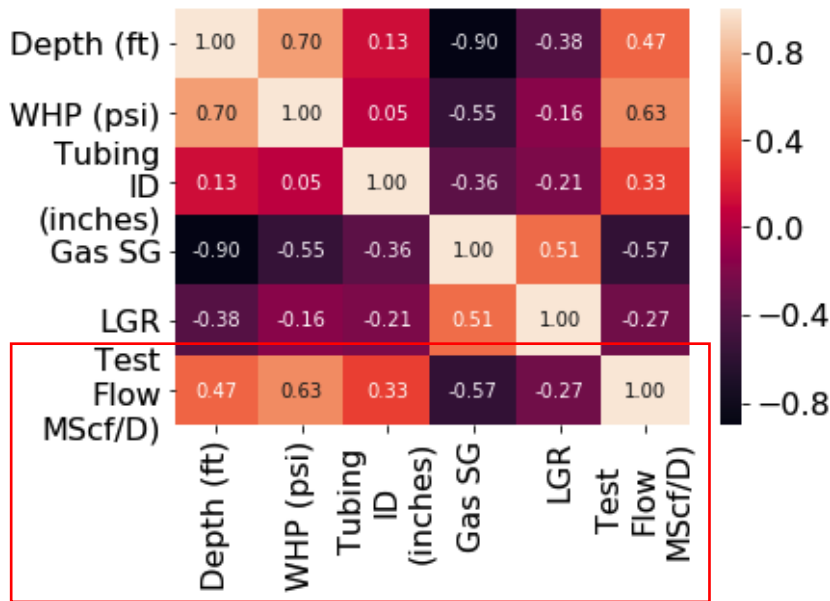


Figure 22 - Pearson correlation coefficient

Figure 22 shows a positive correlation of depth, WHP, and tubing diameter with the critical rate while negative correlation of Gas SG and LGR with the critical rate. Although an indicative trend, the Pearson correlation model assumes independence of predictor features with each other's (there is no influence of one predictor feature on other), which might not always be valid. A partial correlation coefficient is evaluated, which accounts for collinearity between predictor features to address this concern.

Partial Correlation Coefficient

The partial correlation coefficient measures the correlation between two variables in a multivariate dataset while holding all other variables constant. It is still a linear, least-squares regression. Through a series of regressions between all the variables, residual distribution of the predictor and response feature is calculated. The residuals are then used to estimate the correlation coefficient. As all other variables (except the target variable and predictor variable in question) are held constant, the effects of collinearity are addressed.

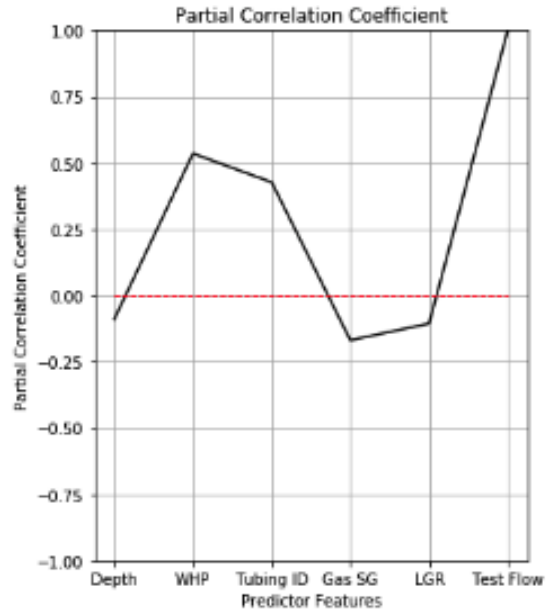


Figure 23 - Partial Correlation Coefficient

Figure 23 shows partial correlation coefficients for each variable compared to the critical gas rate (note coefficient of critical gas with critical gas rate is 1). In comparison to the coefficients predicted by Pearson’s technique, a stark drop in depth’s coefficient is observed. The coefficients of all other features are relatively similar to the previous technique. This suggests all the variance explained by depth feature can be captured other parameters. Therefore, it does not provide any additional information to predict the critical gas rate better.

Feature Importance

Feature selection can depend on statistical correlations between parameters like Pearson’s model or Partial correlation. However, it can also be quantified using machine learning models, such as random forests regressors. These are ensemble decision tree models that operate through a series of logical decision gates that terminate at a nodal value that represents the solution (critical gas rate in our scenario).

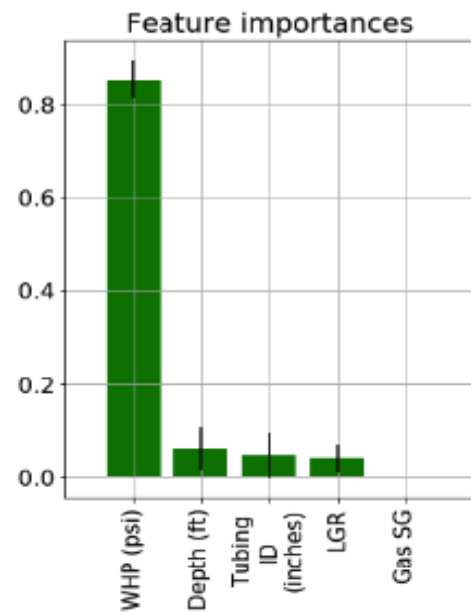


Figure 24 - Feature Importance using random forest

A decision tree model consists of a series of logic gates based on the variables present in the dataset. The lowest end of a series of tree nodes lies the leaf, which is the answer. Number of tree nodes and the branches of the tree are hyperparameters of the model that are optimized using the training data. Figure 25 shows a diagram for decision tree components.

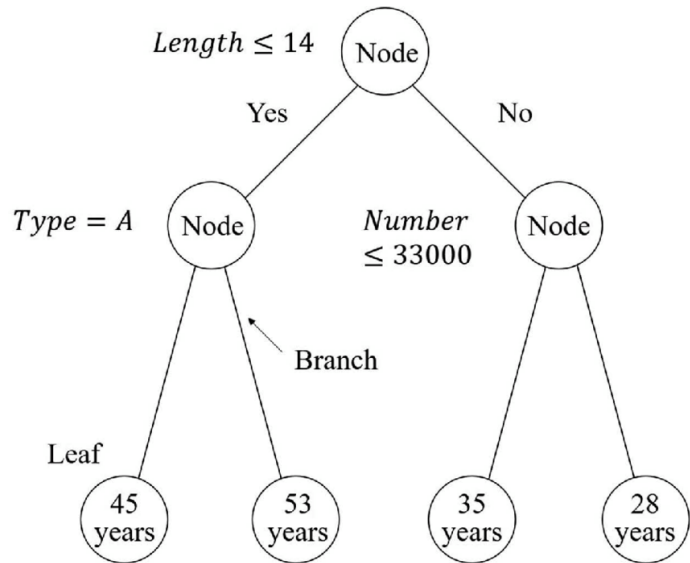


Figure 25 - Sample Decision tree model diagram

Feature importance works by evaluating which variable results in most error reduction when a split is done. As each logic

gate during training for a particular feature is made (e.g., if $WHP > 500$, critical gas rate is 500 Mscfd), it measures the effects of this permutation on model accuracy. By comparing the reduction in error brought by each feature, a rank is assigned to all features. Important features have a significant effect on error while permuting, and unimportant features have little to no effect (Albon 2017).

Using a random forest model with optimized parameters, Figure 24 shows the feature ranking. WHP and LGR are ranked as the most important features through this technique. It should be noted that collinearity between the variables is not accounted for in this technique, which may introduce errors.

Recursive Feature Elimination (RFE)

RFE is similar to feature importance as it utilizes a machine learning model to estimate the influence of each feature on the response parameter. It starkly differs from the previous technique as it removes the weakest feature in each iteration. Starting with all features and successively eliminating the least important feature, a list of features ranked in order of their influence on predictor feature is created. Through elimination, RFE attempts to minimize dependencies and collinearity in the dataset. Using linear regression following is the feature ranking based on the dataset used in this study:

1. Gas specific gravity
2. Tubing ID
3. Wellhead pressure
4. Depth
5. Liquid Gas Ratio

Feature Selection

The evaluation of Stokes' law and physical analysis conducted by Turner et al. and others suggested tubing cross-sectional area (controlled by tubing diameter), gas specific gravity, and wellhead pressure as the most influential parameters. Coleman et al., through the analysis of individual parameters in test wells, suggested that variables like temperature, liquid gravity, interfacial tension, liquid rate and LGR has minimum influence on critical gas rate.

The analysis conducted above using different techniques to rank the predictor features provides a data-driven insight into the influence of these parameters on the critical gas rate. The feature ranking, using observations from all the previous analysis, is given as:

1. Wellhead Pressure
2. Gas specific gravity
3. Tubing ID
4. Liquid Gas Ratio
5. Depth

As expected, the ranking from data-driven methods is in reasonable agreement with the physical understanding of the system. Despite the significance of each feature, developing a machine learning model with all five features is not appropriate, given the small dataset. The dataset used has only 241 samples, which do not provide adequate coverage for all dimensions. Therefore, it is vital to reduce the dimensionality (number of features) of the dataset.

Support Vector Machines (SVM), which are a set of supervised learning methods, are used to identify optimum number of features. SVM is very effective in high dimensional datasets,

specifically in cases where the number of samples is limited in comparison to the number of dimensions. SVM conducts a best fit on the dataset using all features and calculates the residual error known as score. Further, one feature is removed from the dataset after each run, and the model is re-run to estimate the new score. This is compared with the previous score (with more features) to identify the increase/decrease in error. Features are consecutively reduced, and model re-run until one feature is remaining. Optimum number of features is selected by comparing the score (Scikit-Learn-Developers 2019). Figure 26 plots the cross-validated recursive feature elimination technique using SVM that suggests four features should be used for prediction. If three features are used, a significant drop in score is observed. If five features are used, no improvement in score is observed.

Using the feature ranking conducted previously, four features used for model creation are WHP, Gas SG, Tubing ID, and LGR.

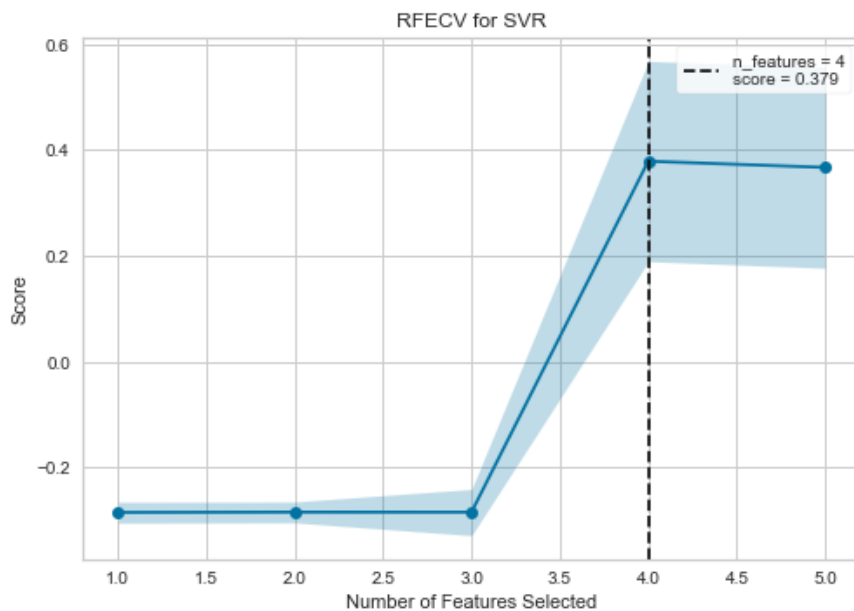


Figure 26 - RFE using cross validation using SVM

Prediction Model

Feature engineering conducted in the previous section reduced the dimensionality of the dataset. A prediction model based on supervised learning algorithms can be created using the optimized dataset. A decision tree model is the most suitable choice for this specific scenario, as an outcome

is predicted given specific values of input variables. As decision trees have a variety of variants, this work will utilize the industry-standard random forest and gradient boosting techniques.

Random forest models are a modification of decision trees that utilize several trees created at random (using a random subset of features for creation of each tree) to create a “forest” of trees. The final tree is an average of all the random trees (Sullivan 2018). By introducing randomness in selecting features for each tree, problem such as collinearity is addressed as all trees are forced to evolve differently (Koehrsen 2018). Gradient boosting is a machine learning technique that can be implemented with decision trees. Gradient boosting works by employing an ensemble of weak predictors. In the next step, residual (error) of these weak predictors with the true value is estimated, and another prediction is made on the residuals instead of base data. Finally, an additive model of many weak learners is used as the final model. A learning rate is used as a hyperparameter, that deliberately slows the learning process of this model, to ensure several weak learners are created to be added in the final additive model. This protects the gradient boosting approach from over-fitting the data (Brownlee 2016).

The dataset is split into training and testing subsets using a random splitting technique where test fraction is 10%. The training set is further split into model training and model validation subsets where validation fraction is 20%. These split percentages are based on the standard industry practice, to ensure adequate samples are available for model training. Model parameters are trained on the training subset, while model hyperparameters are tuned on the validation subset. The testing subset is used to determine the final accuracy of the model.

Model Training and Validation

Random forest and gradient boosting models are instantiated using a maximum depth of 3, number of trees as 10, and leaf nodes as 10. Similar parameters are used for both models to ensure an equal comparison. Model error is estimated by comparing the critical rate estimated by the model with true critical rate. The absolute difference between the two rates is used. For example, if the true critical rate is 500 Mscfd, while the critical rate predicted by the model is 700 Mscfd, the absolute error is 200 Mscfd. The mean of absolute error, for all samples, is used to quantify the accuracy of the model.

- Validation *Mean Absolute Error (MAE)* for the random forest model is: 629 Mscfd

- Validation *Mean Absolute Error (MAE)* for the gradient boosting model is: 1342 Mscfd

As observed, there is a significant error in prediction by the model. The gradient boosting model is off by ~1300 Mscfd. However, this can be improved using hyperparameter tuning. Initial models were constructed with 10 trees and 3 maximum depth (branches of tree). Through a sensitivity on these parameters, most optimum tree count and maximum depth can be identified.

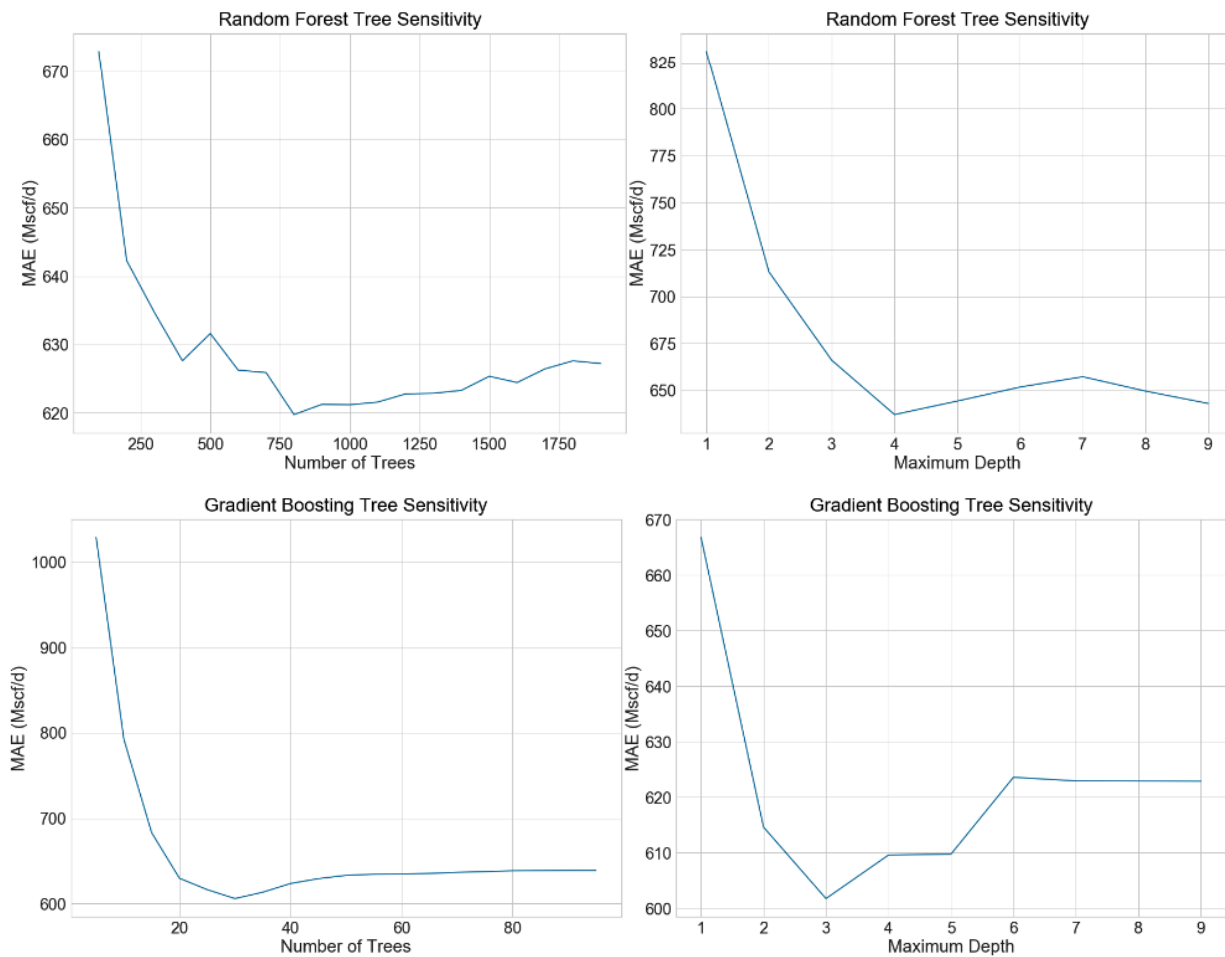


Figure 27 - Hyperparameter Tuning Plots for Random forest and gradient boosting models

Figure 27 shows the results of sensitivity analysis on number of tree and tree depth parameters of random forest and gradient boosting model. The most optimum parameter in both models would be the one where estimated MAE is relatively low, while the parameters are not very high (as

higher values tend to create complex models). Therefore, in this scenario, the following parameters produce relatively low MAE:

Random forest model: Number of trees: 250 Maximum tree depth: 4

Gradient Boosting model: Number of trees: 30 Maximum tree depth: 3

Updated hyperparameters are used to re-run the models, and error on the validation subset is estimated to check if it has reduced after the sensitivity exercise.

- Validation *Mean Absolute Error (MAE)* for the random forest model is: 482 Mscfd
- Validation *Mean Absolute Error (MAE)* for the gradient boosting model is: 422 Mscfd

As observed from the MAE, significant improvement is made, especially for the gradient boosting model where error has reduced more than 50%.

Final Model Test

The completed model can be used to predict the critical gas rate in future wells. A subset of data was withheld from the training and validation process, named test subset (10% split of the original dataset), to simulate this process. As the gradient boosting model is slightly better than the random forest (it has a lower MAE), it will be considered as the final model. Also, with the selected hyperparameters, the entire training dataset (training + validation) is used for the training of the final model. This provides more samples to train the final model.

As dataset split was done before the model was created, it has only seen 90% of the data. The remaining 10% samples act as future wells for this model, and the accuracy achieved in predicting the critical gas rate of these samples endorses the applicability of this model on future wells.

- Testing *Mean Absolute Error (MAE)* for the gradient boosting model is: 356 Mscf

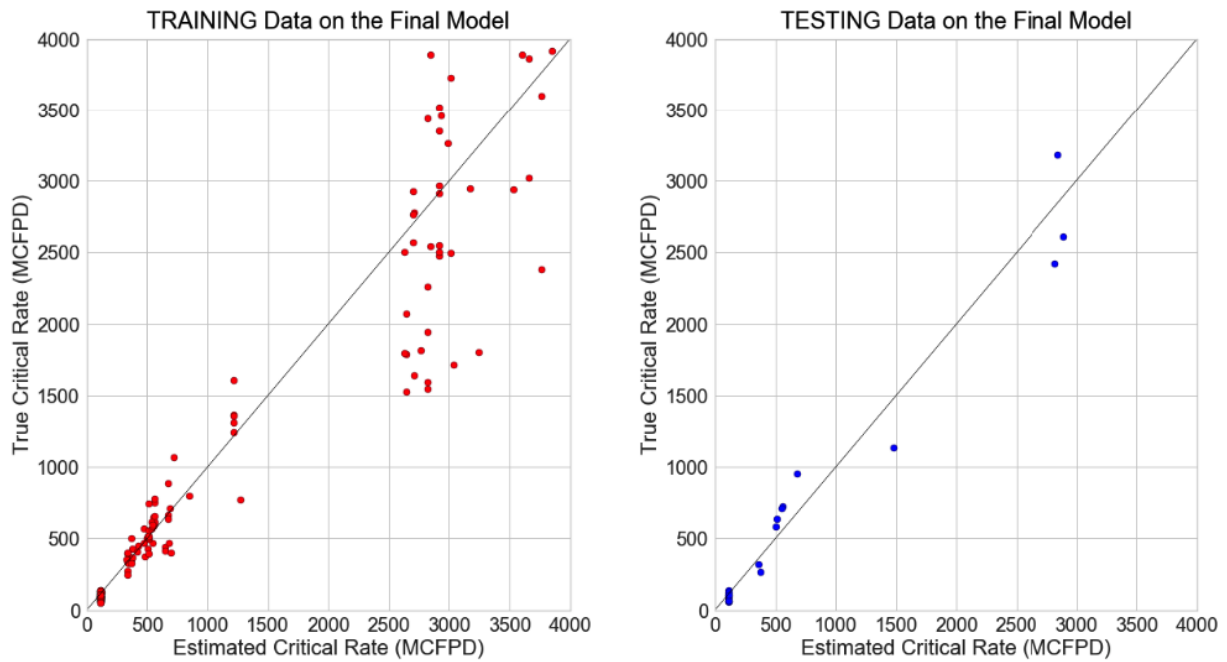


Figure 28 - Critical rate validation plot for the final model

Figure 28 shows the validation plot of the training and testing subset. It plots the true critical rate with model (estimated) critical rate. If the critical rate predicted by the model is similar to the true critical rate, they will fall on the diagonal line. Any significant deviation from the diagonal indicate mispredictions (error). The MAE on the testing subset is ~350 Mscfd. In other words, if the model predicts a critical gas rate of ~1000 Mscfd, the prediction may be off by +/- 350 Mscfd. As the error is an absolute gas rate, it will be insignificant when wells with high (expected) critical gas rate are evaluated through this workflow. For example, a well where expected critical gas rate is ~3000 MScfd, an error of ~350 Mscfd is manageable. However, for wells where the critical gas rate is expected to be ~700 Mscfd, an error of ~350 Mscfd is almost 50% and would not be a fair solution. To address the error for this subset of wells, a separate model that is fine-tuned on wells where lower critical gas rate is expected is developed in the next section.

Model Improvement for Low Critical Gas Rate Wells

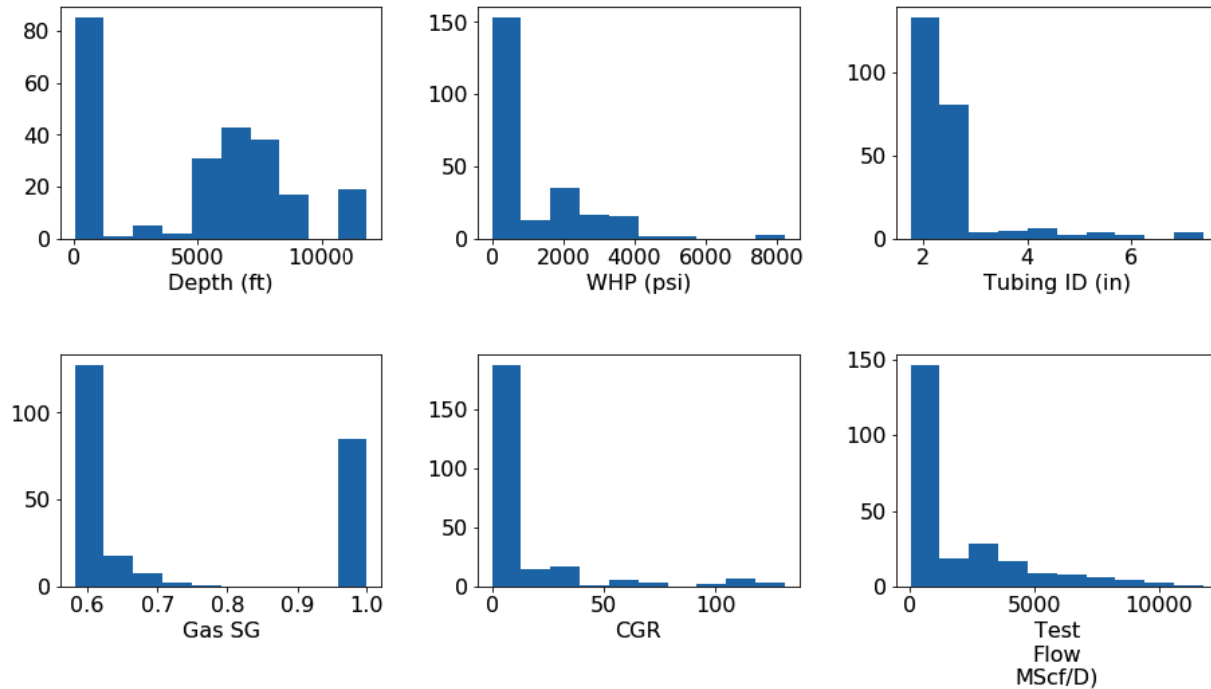


Figure 29 - Histograms of different parameters in original data

Despite achieving a significant reduction in error, it is still on the higher side, especially for low producers where critical gas rate is already a small number. This section attempts to improve the accuracy of the model by manipulating the dataset. Ocular inspection of feature histograms (Figure 29) suggests that the target feature (test critical rate) is skewed. Moreover, outliers can be observed in almost all features in the data, which is expected given sparse samples in the dataset. Nevertheless, skewness and outliers, both can negatively impact the accuracy of machine learning models (Dangeti 2017) and addressing these issues may improve the predictive ability of this workflow.

Z-tests are an effective way to find points that lie significantly away from the mean of the distribution. As it is a relationship of the data point with standard deviation, a z-score threshold of $-2.5/2.5$ can be used to detect outliers (Iglewicz and Hoaglin 1993). This would simply eliminate all samples from the dataset whose features are outliers in their respective distribution. For example, if most tubing ID are between 2-7/8" and 4-1/2" and a well has an ID of 7", this would be considered an outlier, and the entire well will be removed from the dataset.

Outlier elimination result in the removal of 14% data from the training subset. Furthermore, using the results of the previous model, poor match (deviation from the solid line) is observed in wells where the test critical rate is higher than 2500 Mscfd. The dataset is further reduced to include only wells where test critical rate is less than 2500 Mscf/d, using the previous model as a guideline. This manual shrinking of the dataset is to create a subset of original data, that focuses on low producer wells. This would, therefore, limit the applicability of this specific model on wells where high critical gas rate is expected. For such wells, the previous model is more suitable.

Lastly, to address skewness in the target feature, log transform is conducted. Using gaussian distribution in statistical tests and models is always preferred as it satisfies the assumptions of homogeneity of variances for the errors (Zheng and Casari 2018). Although the central limit theorem dictates that the addition of several features will turn target distribution to normal, it is safe to cater for skewness in our dataset, especially given its relatively small size. Figure 30 plots the log transform of the target feature.

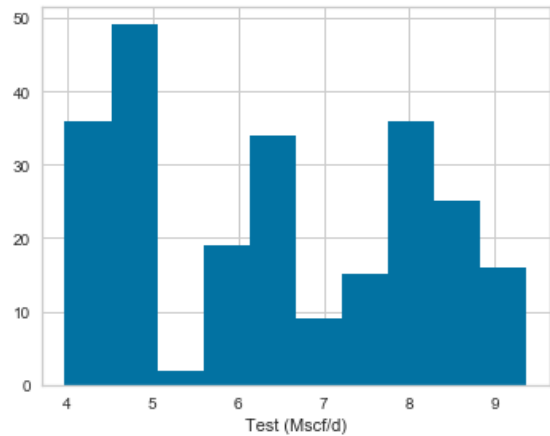


Figure 30 - Log transform of response feature

After correcting for outliers and skewness, the predictive ability of the model has significantly improved as error in the predictions has decreased by ~75%. Figure 31 shows the critical rate plots.

- Testing *Mean Absolute Error (MAE)* for improved model: 80 Mscf

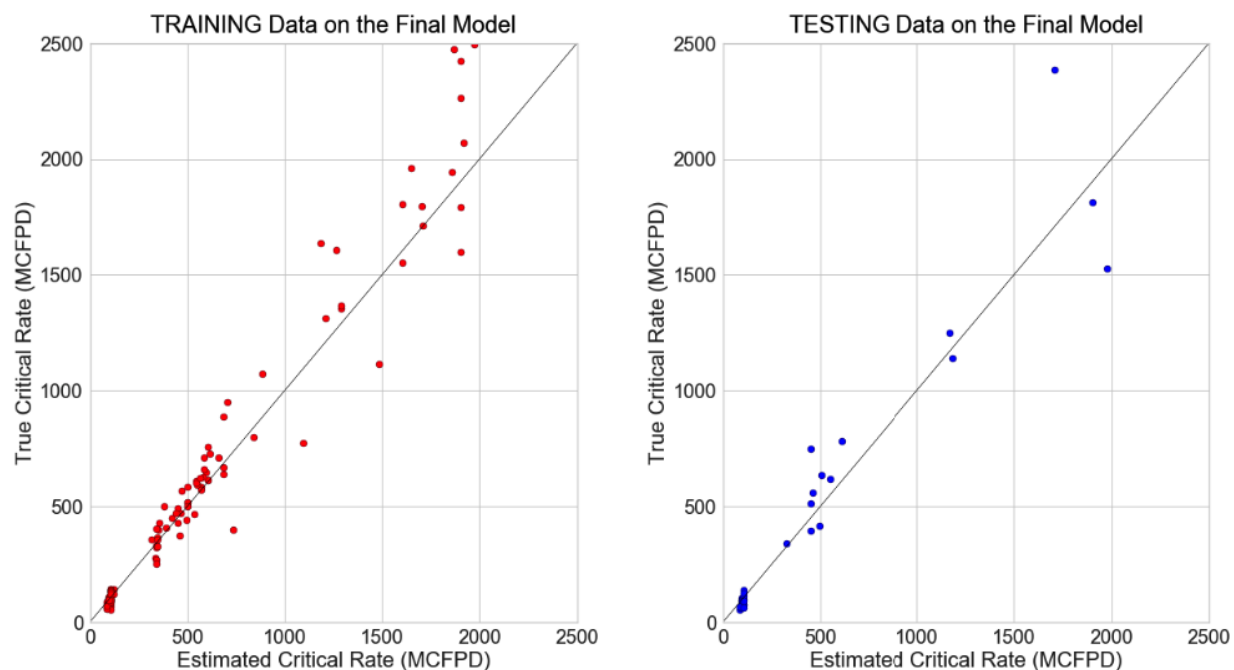


Figure 31 - Critical Rate Plots for Final model

Summary

Critical gas rate is vital to predict the onset of liquid loading. It is the most direct technique to evaluate the period in gas well's life when an artificial lift is required. Therefore, it plays a critical role in field development and lift development planning. Several empirical correlations have been published since Turner's model to predict the critical gas rate given different well and reservoir parameters. Most models have been fine-tuned with data that included wells with similar parameters, introducing bias in the model's ability to predict critical gas rate universally. This section introduces data-driven techniques in evaluating critical gas rate given wellhead pressure, tubing diameter, LGR, and gas specific gravity. Through feature engineering, these four parameters are found to have the most influence on the critical gas rate. Lastly, using the dataset of wells with known true critical gas rate, decision tree models are used to develop prediction models. Hyper-parameters of the models are optimized using the validation subset and the final model is created. Mean absolute error of the final model is found to be ~350 Mscfd. A second model, fine-tuned to low gas producers, is developed that has a mean absolute error of ~80 Mscfd. Despite reducing the error, it is worthwhile to note that this exercise is significantly reliant on the dataset and its manipulation. If that dataset is improved or deteriorated, so would the results of this working. Such is the limitation of all data-driven models.

Chapter-3: Gas Well Deliquification – S-field Case Study

Artificial lifts for fields in the Lower Indus Basin, Pakistan are selected using the workflow developed in the previous chapter. The primary underlying objective of this study was to screen the well set provided by the operator for liquid loading problems and recommend appropriate artificial lift methods. Gas well deliquification workflow and weighted average critical rate were developed to fulfill this objective. Significant fields and their wells in the Lower Indus basin are introduced, and only wells where the workflow recommends an artificial lift, are discussed in detail. Results of all the wells evaluated using the workflow are provided in the executive summary. To optimize the length of the document, only wells where significant liquid loading and optimum lift solution was identified are discussed in this chapter. All other wells, where significant benefit from the artificial lift was not realized, are documented in appendix-A with complete details.

Lower Indus Basin Fields

The Lower Indus Basin is a prolific oil and gas producer in Sindh province, Pakistan. Several fields with equivalent reserves of hundreds of Billion Cubic Feet (BCF) have produced from this basin. It is one of the most oil and gas rich areas in Pakistan and home to a few of the most significant discoveries in the country. Major formations in the basin are the B-Sand and the C-Sand. Hydrocarbon types vary from field to field. For the fields analyzed in this study, most are dry to wet gas reservoirs.

Several artificial lift methods have been tested in the basin with mixed results. Due to the vast network of wells and pipelines in the area, gas lift is the most common technique used. Several oil fields in the area are also operated with ESP. However, the runtime, maintenance cost, and reliability have been inadequate. Due to poor infrastructure, sucker rod pumps and beam lift have also had high costs that make them an unpopular choice in the region.

Nevertheless, hydraulic pumps are widely used in the basin to augment oil production. For this study, ESP and hydraulic pumps are out of consideration due to poor efficiencies and poor outcomes in gas wells. However, sucker rod pumps are part of the evaluation as they can work with very low reservoir pressures.

S-Field Executive Summary

S-field is primarily a gas field that has cumulatively produced more than half a TCF. A structural trap, significant reservoirs in the field are found at ~3300 meters TVD. The field is divided between two flanks, where the majority of the wells are on the north flank which is primarily depletion drive. The south flank has a few wells that are expected to have low bottom water drive. Therefore, water production on the southern flank is higher than its northern counterpart.

The field is normally pressured with initial reservoir pressure of ~4200 psi. Most wells have produced more than ~20 Billion Cubic Feet (BCF) and have now entered the mature production stage. Due to high initial gas production, most wells are completed with larger tubing (5-1/2" or more) to achieve higher flowrates. Lately, depletion and water production (condensed and formation) have resulted in poor wellbore hydraulics in most wells. Moreover, very few wells in the field were initially planned with artificial lift in consideration, therefore do not have gas lift valves, pump cavities or pre-requisite wellbore hardware installed. As a consequence, any artificial lift installation may require a workover that would negatively affect economics.

Eleven wells are evaluated in the S-field. The average depth of these wells is ~3000 meters while current gas production varies from ~6 to ~1 Million standard cubic feet per day (MMscfd). Design and Review workflow is applied to these eleven wells and results are summarized in Table 5.

Well Name	Reservoir Pressure (psi)	Target Depth (ft)	Current Production (MMscfd)	Wellhead Pressure (psi)	WGR	Water Rate (stb/d)	Water Salinity as NaCl (ppm)	Unstable	Best Artificial Lift	Max Optimiation	Recommended
S-1	800	3286	6.6	114	56	369.6	202	No	GasLift	0.1 MMscfd	No
S-2	700	3447	3.7	127	82	303.4	2862	No	GasLift	0.15 MMscfd	No
S-4	1400	3260	3.3	115	20	66	32000	No	GasLift	0.2 MMscfd	No
S-5	525	3288	1.9	108	108	205.2	20000	Yes	GasLift	0.8 MMscfd	Yes
S-8	680	3300	6.3	111	91	573.3	2387	No	GasLift	0.5 MMscfd	No
S-10	700	3355	1.1	97	200	220	50000	Yes	GasLift with 2-7/8"	0.5 MMscfd	Yes
S-11	650	3288	2.014	130	76	153.064	744	No	PAGL	0.6 MMscfd	Yes
S-13	600	3320	3.1	143	102	316.2	9798	No	N/A	N/A	No
S-14	650	3260	2.49	108	110	273.9	12730	No	GasLift	0.2 MMscfd	No
S-15	525	3300	2.08	98	120	249.6	338	No	GasLift	0.5 MMscfd	No

Legend: Recommend installation in future

Recommend installation in current scenario

Table 5 - Executive summary of S-Field wells

Most wells that were evaluated had incremental production from an artificial lift. However, this optimization was less than 0.5 MMscfd and unlikely to create enough revenue to justify the

artificial lift installation and operational cost. However, economics should be reviewed before they are entirely rejected as artificial lift candidates. Key technical reasons for non-selection of these wells are listed below:

- Vertical Lift Performance (VLP) and flow point analysis suggest wellbore flow is stable. This is likely due to a negligible increase in bottom hole pressure with water production
- Source of water production is condensed water that is produced shallower in the wellbore. This would suggest minimum water hold-up in the bottom of well that may cause increased sand-face pressure and decreased drawdown. A more precise prediction or measurement of where in the well the water condenses would lead to a better idea of if an artificial lift could be used to help these wells.

Table 6 summarizes the results of artificial lift design for all S-field wells. The artificial lift section in Table 6 compares the production increment expected by installing each specific lift system. As is evident, in most wells, gas lift results in positive incremental production. Velocity strings are the second-best choice with production rates being unaffected post-installation. Coil tubing gas lift (CTGL) and smaller diameter tubing mostly have a detrimental effect in the current scenario due to excessive frictional pressures post-installation.

It is vital to note that these calculations are based on the current performance of the wells. Some of the wells (S-1,8,9, etc.) are still producing higher than 5 MMscfd and its current rate is only less than 20% lower to the predicted critical gas rate. Moreover, the source of water in these wells is condensed which has a negligible impact on water holdup. Therefore, at this instance, these wells turn out to be poor candidates for any artificial lift application.

Among the list of S-field wells, S-5 and S-10 are the best choices for artificial lift installations in current scenario. Well S-5 is also an ideal trial candidate for Plunger Assisted Gas Lift (PAGL) when current production in the well drops below ~1.6 MMscfd. As current production is greater than 1.6 MMscfd, installation of PAGL at this instance will lower production rate and hence NPV. The next section describes these wells in detail.

Artificial Lift Systems										
Well	Current Gas	Critical Gas Rate %	VLP Stability	Flowpoint Stable	WGR Sensitivity Improvement	Gas Lift	CTGL	Lower ID Tubing	Velocity String	Other Lift Systems
S-10	1.1	84%	No	No	Significant	~0.8 MMscfd (2-7/8")	~0.6 MMscfd	2-7/8" - RD	RD	Beam Lift - 200 STB/day
S-5	1.98	56%	Borderline	Yes	Significant	~0.8 Mmscfd	RD	N/A	RD	
S-11	2.014	55%	Yes	Yes	Negligible	0.2 MMscfd	N/A	2-7/8" - RD	RD	PAGL - 1.6 MMscfd
S-15	2.081	53%	Yes	Yes	Significant	~0.5 MMscfd	RD	3-1/2" - RD	RD	PAGL - 1.6 MMscfd
S-14	2.59	41%	Yes	Yes	Significant	0.5 MMscfd	RD	2-7/8" - RD	Similar	
S-13	3.168	28%	Yes	Yes	Significant	Similar	N/A	N/A	RD	
S-4	3.37	26%	Yes	Yes	Negligible	0.2 MMscfd	N/A	2-7/8" - RD	RD	
S-2	3.75	24%	Yes	Yes	Negligible	0.15 MMscfd	N/A	2-7/8" - RD	Similar	
S-9	6.3	12%	Yes	Yes	Significant	~0.5 MMscfd	RD	3-1/2" - RD	RD	
S-8	6.377	8%	Yes	Yes	Significant	0.5 MMscfd	RD	2-7/8" - RD	Similar	
S-1	6.69	13%	Yes	Yes	Negligible	0.1 MMscfd	N/A	5-1/2" - RD	Similar	

Critical Gas Rate % = Current gas rate percent lower than critical gas rate. For e.g. 10% mean 10% lower than critical gas rate

RD = Rate Decrease from current production

Similar = Similar to current production

Table 6 - S-field artificial lift summary

Well S-5

S-5 is a development well drilled in S-field. Producing from a sandstone reservoir at ~3300m true vertical depth (TVD), S-5 has produced more than 43.7 BCF gas since December 2005. Initial gas production was ~24 MMscfd. Gas rates dropped with natural depletion and current gas rates are ~1.9 MMscfd. Water production started in 2013 with increasing WGR. Due to scarcity of well test data, only annual WGR was available and that was used in production and nodal analysis. Figure 32 shows the current wellbore configuration of S-5.

Reservoir Pressure	525 psi	Target Interval	3288 m
Current Production	1.9 MMscfd	Following Wellhead Pressure	108 psi

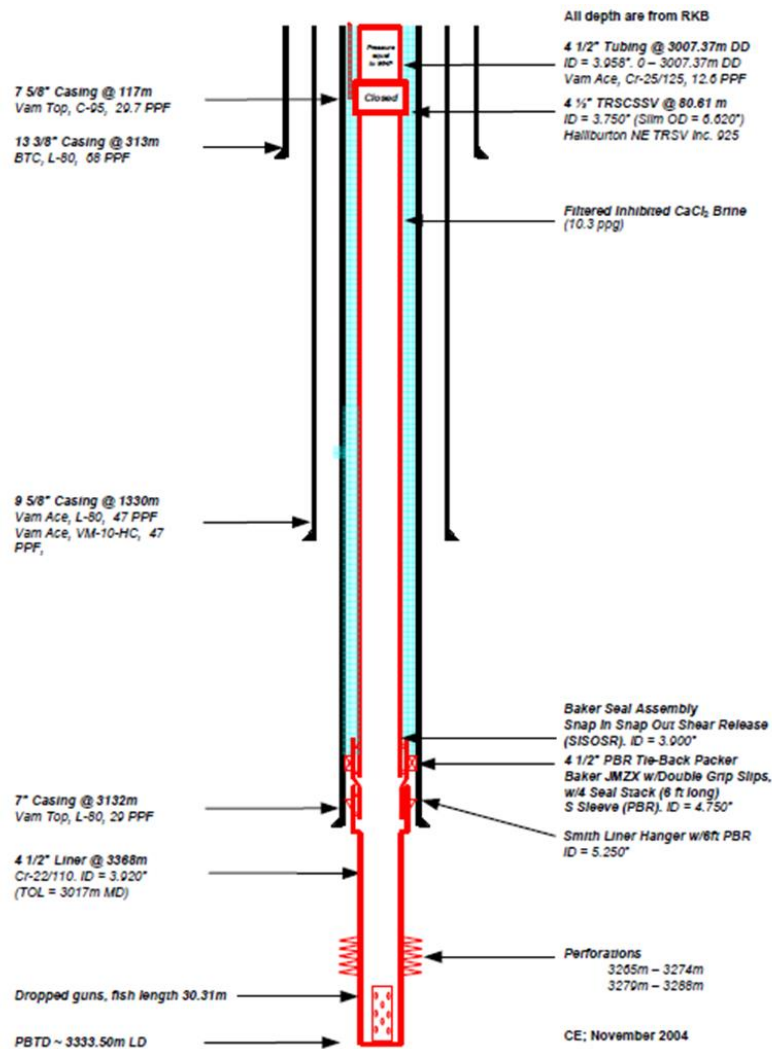


Figure 32- Well S-5 wellbore configuration

Production plot

Figure 33 shows gas production and Flowing Wellhead Pressure (FWHP) of S-5 from 2013. Using this data set, we can calculate Bottom Hole Pressure (BHP) from measured WHP using the Vertical Lift Performance (VLP) correlation. This allows the evaluation of changing sand-face pressure to observe unusual trends and anomalies that may indicate issues like liquid loading.

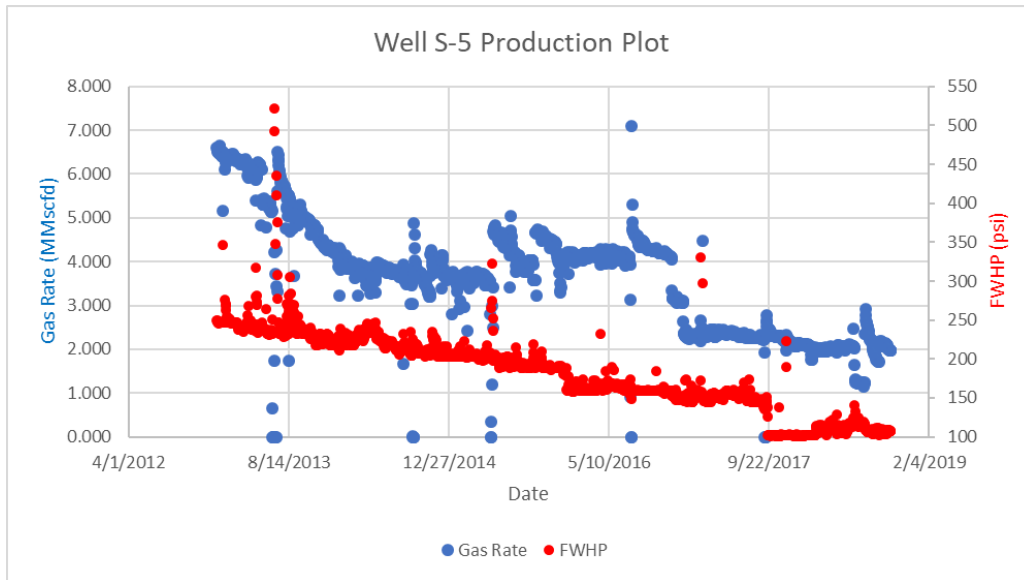


Figure 33 - Well S-5 FWHP plot

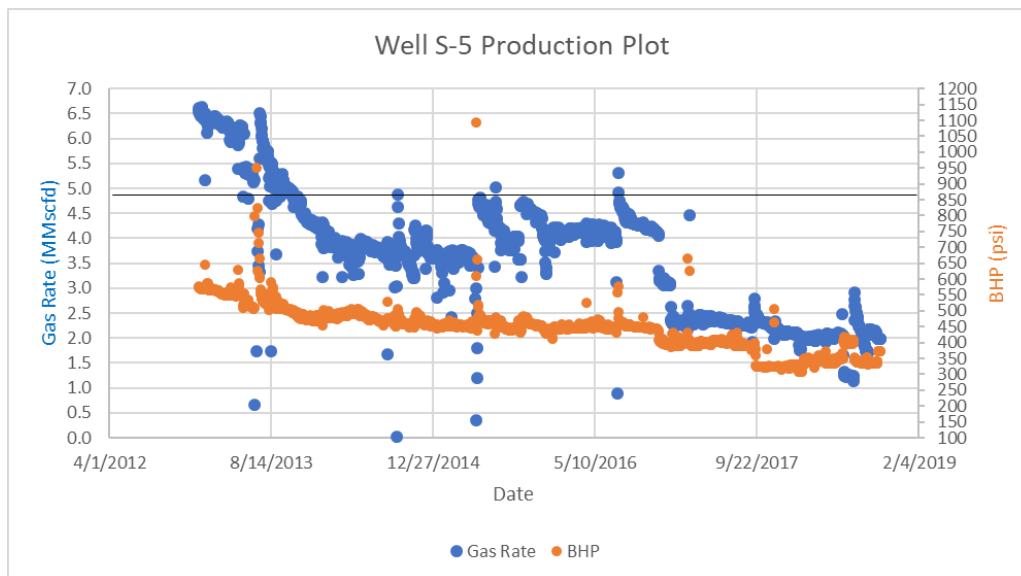


Figure 34 - Well S-5 BHP Plot

Figure 34 plots the calculated BHP with gas rates. The solid black line at gas rate ~4.6 MMscfd in Figure 34 depicts the critical gas unloading rate required to offload all fluids from the wellbore effectively. Based on the current production rate of ~1.9 MMscfd, it is ~56% lower than the required critical rate. This suggests that liquid loading is a significant issue in this well.

Well S-5 has a relatively stable BHP pressure with sharply decreasing gas rates. For conventional sandstone reservoirs, the decrease in gas rate is the result of steadily decreasing BHP. As BHP is relatively constant, this suggests, water hold-up in the wellbore is the cause behind relatively stable BHP. Moreover, WGR for this well has risen drastically from 30 in 2013 to ~108 STB/MMscfd by the end of 2018.

Nodal Analysis

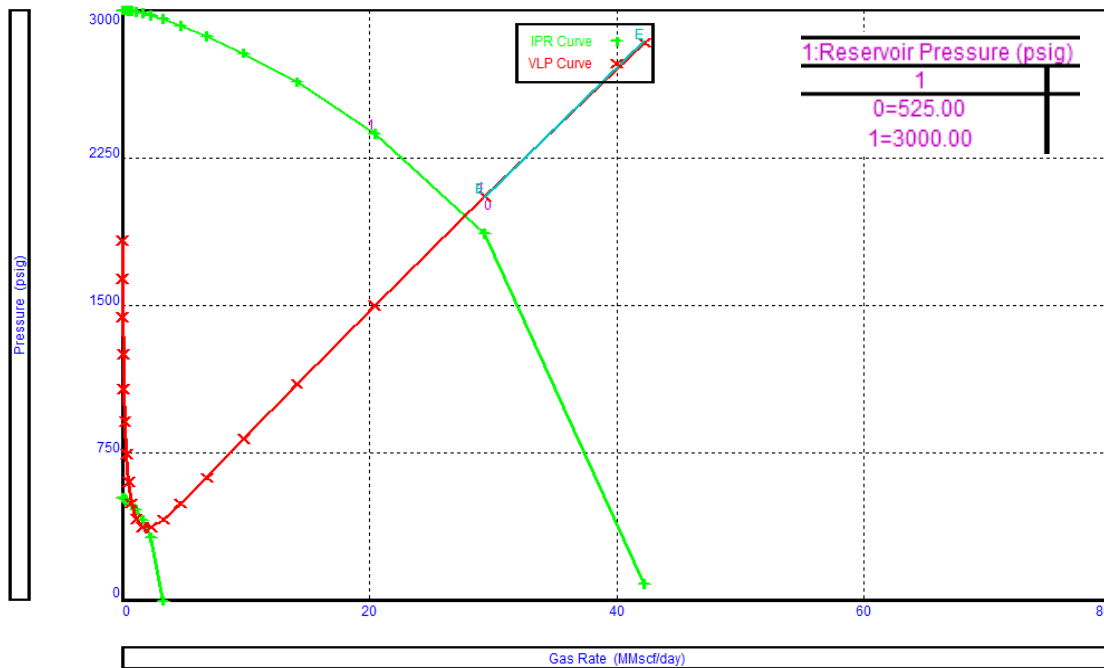


Figure 35 - Well S-5 System analysis - reservoir pressure sensitivity

Figure 35 shows the sensitivity of reservoir pressure that is used to match the current production of the well in nodal analysis. This suggests reservoir pressure has depleted from ~3000 psi (initial pressure for this well was probably depleted from virgin due to production from other wells) to ~525 psi. This is the primary reason behind the drop in production over the years.

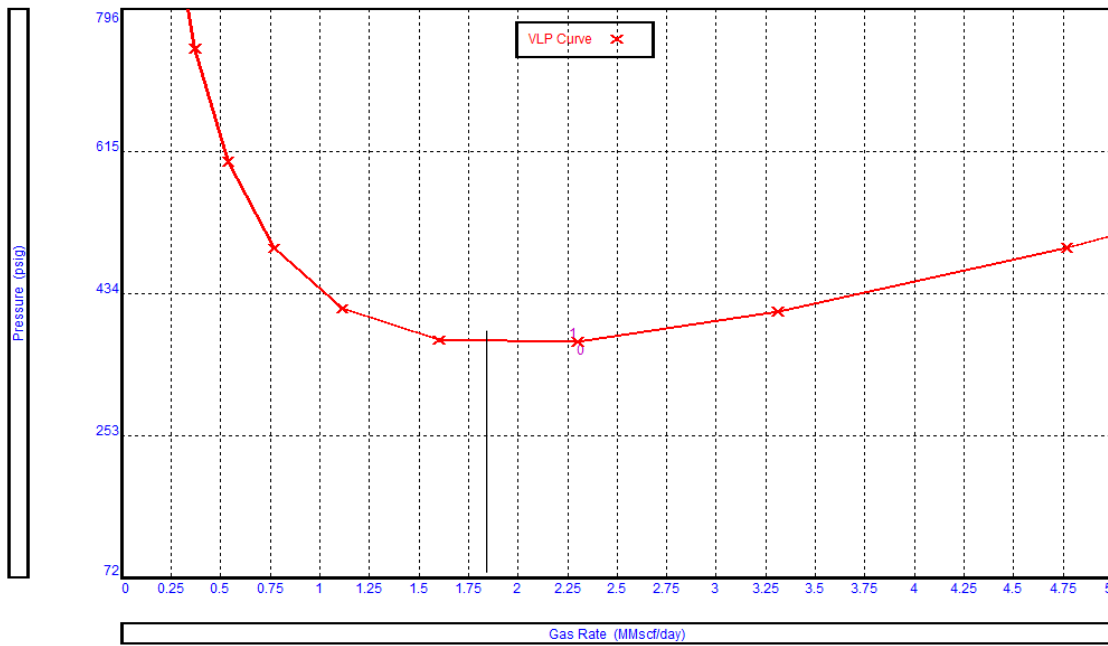


Figure 36 - Well S-5 VLP Stability plot

Stability analysis through the VLP curve suggests current production is very near to the minimum, as depicted in Figure 36. This suggests flow is critical in the wellbore, and any further decrease in gas rates may result in unoptimized flow and possibly a load-up condition.

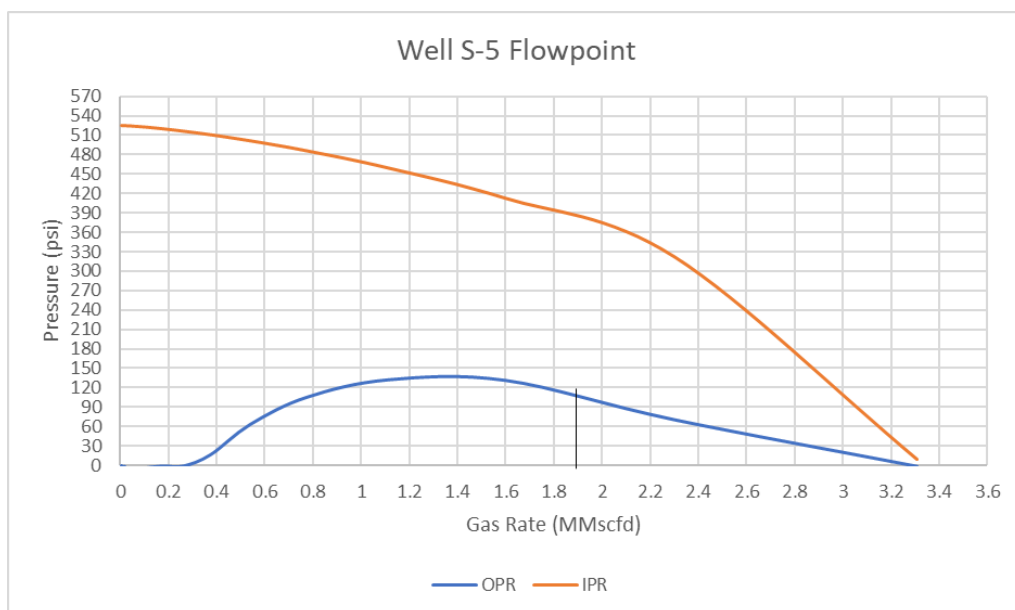


Figure 37 - Well S-5 Flow point plot

Flow-point analysis (Figure 37) suggests a pressure differential of ~300 psi between Inflow Performance Relationship (IPR) and Outflow Performance Relationship (OPR) curves. This is consistent with the trend observed in other wells where higher differences between current production and critical gas rate result in higher pressure differences between curves.

Running gradient traverse calculations in *Prosper* to estimate the flowing regime based on liquid and gas superficial velocities suggest the well is flowing in the slug regime. This is expected as VLP stability is minimum, which also suggests a slug flow regime in the wellbore. Figure 38 is a screenshot of Prosper results.

Gradient Results									
Label	Bottom Measured Depth	True Vertical Depth	Pressure	Temperature	Gradient	Holdup	Regime	Heat Transfer Coefficient	
	m	m	psig	deg F	psi/ft			BTU/h/ft ² /F	
28	1870.8	1870.8	254.13	259.00	0.032443	0.0625	Slug	8.0000	
29	1945.4	1945.4	262.07	264.70	0.03246	0.0625	Slug	8.0000	
30	2020.0	2019.9	270.02	270.40	0.032475	0.0625	Slug	8.0000	
31	2094.6	2094.5	277.97	276.09	0.032489	0.0625	Slug	8.0000	
32	2169.1	2169.1	285.92	281.77	0.032502	0.0625	Slug	8.0000	
33	2243.7	2243.7	293.88	287.43	0.032513	0.0625	Slug	8.0000	
34	2318.3	2318.3	301.84	293.08	0.032522	0.0625	Slug	8.0000	
35	2392.9	2392.9	309.80	298.69	0.03253	0.0625	Slug	8.0000	
36	2467.5	2467.5	317.76	304.27	0.032537	0.0625	Slug	8.0000	
37	2542.1	2542.1	325.73	309.80	0.032544	0.0625	Slug	8.0000	
38	2616.7	2616.7	333.69	315.25	0.03255	0.0625	Slug	8.0000	
39	2691.3	2691.3	341.66	320.60	0.032556	0.0625	Slug	8.0000	
40	2765.9	2765.9	349.63	325.81	0.032563	0.0625	Slug	8.0000	
41	2840.5	2840.4	357.60	330.82	0.032573	0.0625	Slug	8.0000	
42	2915.0	2915.0	365.57	335.57	0.032585	0.0625	Slug	8.0000	
43	2989.6	2989.6	373.55	339.95	0.032603	0.0625	Slug	8.0000	
44	3064.2	3064.2	381.54	343.82	0.032629	0.0625	Slug	8.0000	
45	3138.8	3138.8	389.53	346.98	0.032667	0.0625	Slug	8.0000	
46	3213.4	3213.4	397.54	349.17	0.032722	0.0625	Slug	8.0000	
47	3288.0	3288.0	405.57	350.00	0.032802	0.0625	Slug	8.0000	

Figure 38 - Well S-5 gradient traverse calculations

Artificial Lift Techniques

Gas Lift

A sensitivity run is made on the bottom hole pressure (BHP) with changing WGR to evaluate if the application of any artificial lift that requires gas injection (in the wellbore) will aid in improving production. For most conventional reservoirs such as S-field, reduction in BHP will generally translate to an increase in hydrocarbon production. This is used as a starting point to quantify the effectiveness of gas injected technologies for this well. Figure 39 shows the sensitivity of BHP with different WGR values.

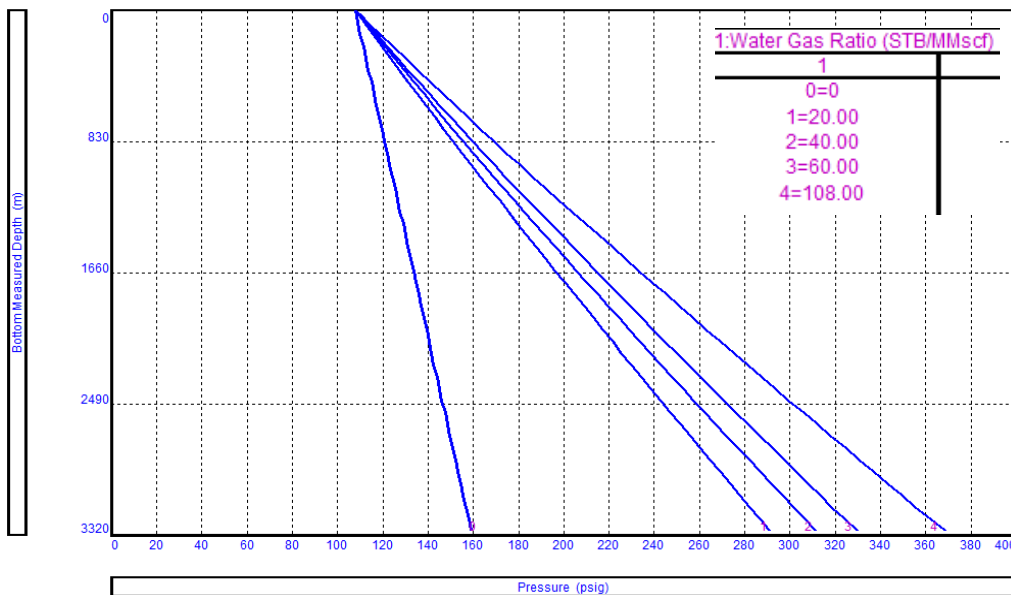


Figure 39 - Well S-5 BHP sensitivity using WGR values

The current WGR in S-5 is ~108 STB/MMscf. By lowering WGR through gas injection, significant bottom hole pressure reduction is observed. This would suggest that gas production improvement is possible through a gas lift technology, which is confirmed by WGR sensitivity on system analysis.

Figure 40 shows the effect of lowering WGR on system analysis. Significant gas improvement is observed if WGR is lowered to ~20 or less. Compared to other S-field wells, we see a definite improvement in S-5 with lowered WGR. The addition of extra gas does not increase friction

pressures, instead aids in the removal of liquids. Therefore ~0.6 MMscfd improvement in gas production is observed with a reduction in WGR.

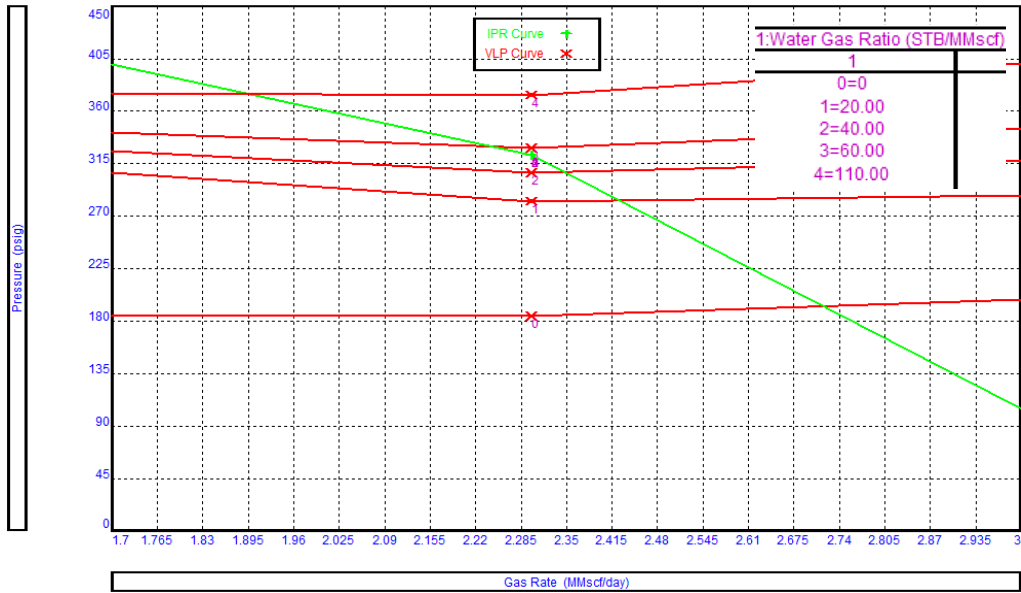


Figure 40 - Well S-5 system analysis plot with WGR sensitivity

Gas lift design is required where the effects of the gas injection are modeled to quantify the actual improvement in gas production. Most gas lift models are designed for oil reservoirs, therefore as a way around, the current performance of S-5 can be matched using an oil IPR and equivalent Gas-Liquid Ratio (GLR). Figure 41 shows the matched model with the same reservoir parameters as Gas IPR with a GLR of ~198480 SCF/STB.

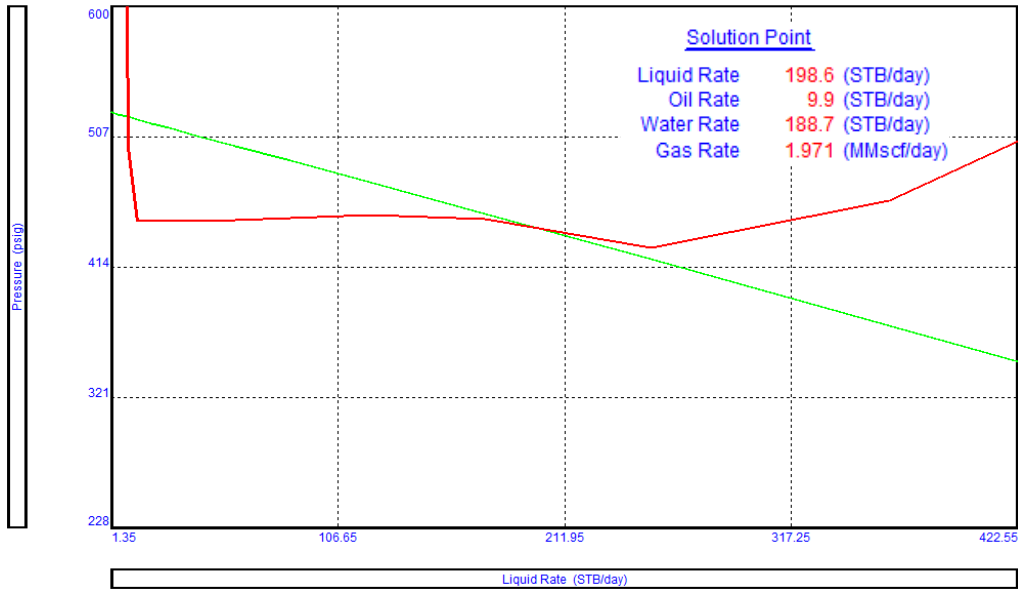


Figure 41 - Well S-5 base model using oil IPR

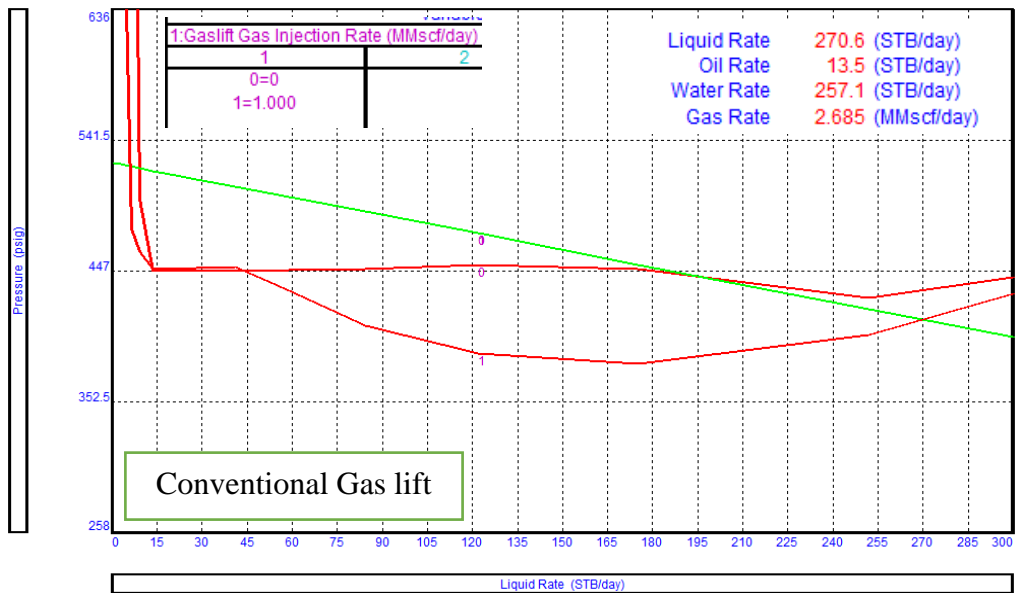


Figure 42 - Well S-5 Gas lift design oil IPR

The effects of conventional gas lift and Coiled Tubing Gas Lift (CTGL) can be modeled using oil IPR and compared. In the conventional gas lift, gas is injected down the annulus and produced

through 4-1/2” tubing, whereas in CTGL, 1.5” CT is used inside current 4-1/2” tubing where gas is injected down the CT.

Conventional gas lift results in ~0.8 MMscfd increment, while CTGL results in lower gas rates than current production. This is due to current smaller ID tubing in the well where installing CT will further increase friction pressures. Moreover, due to improved hydraulics, the gas lift can produce this well until the reservoir pressure declines below ~450 psi. However, the well will load-up in its current configuration when reservoir pressure decreases to ~500 psi. Therefore, the gas lift would not only improve the instantaneous production but also optimize the ultimate recovery of this well by reducing the abandonment pressure slightly.

Figure 42 and Figure 43 shows system analysis using oil IPR for conventional and Coiled Tubing gas lift designs respectively.

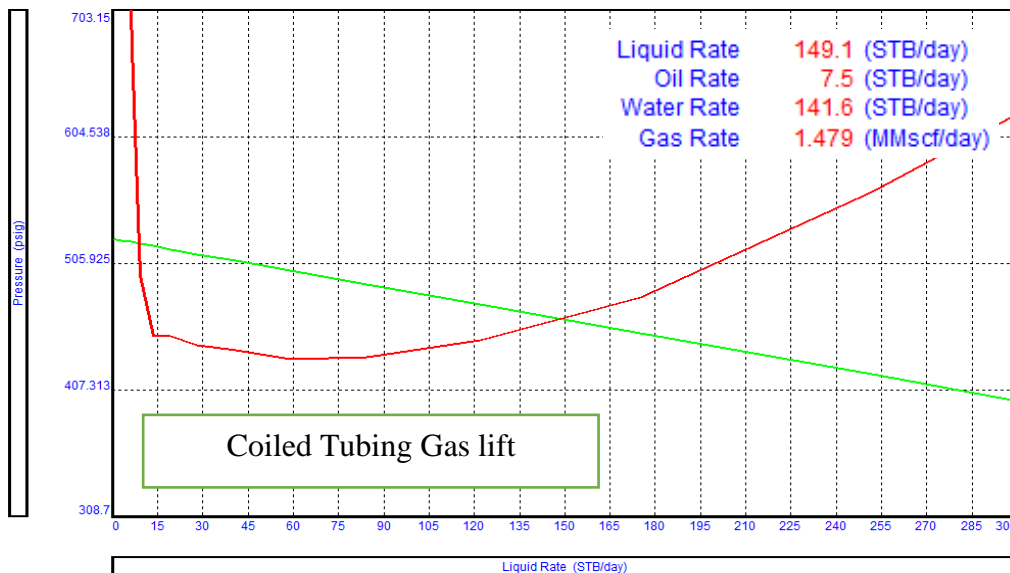


Figure 43 - Well S-5 CTGL design using oil IPR

Velocity String / Smaller ID Tubing

A velocity string can be used in well S-5 to optimize the flow velocities and improve wellbore dynamics. The sensitivities conducted for smaller flow area include:

- Current Profile: 4-1/2" Tubing.
- Velocity String: Install 1" CT in 4-1/2" Tubing.

The use of smaller ID tubing significantly deteriorates performance due to very high friction pressures, making it an unfeasible option in the current scenario. This is similar to the effect in CTGL; however, production without gas injection in CT is higher than that with gas injection. This decreased production in CTGL is expected as the additional injected gas further increases the frictional pressures. Figure 44 depicts the system analysis conducted using different sensitivities of tubing size.

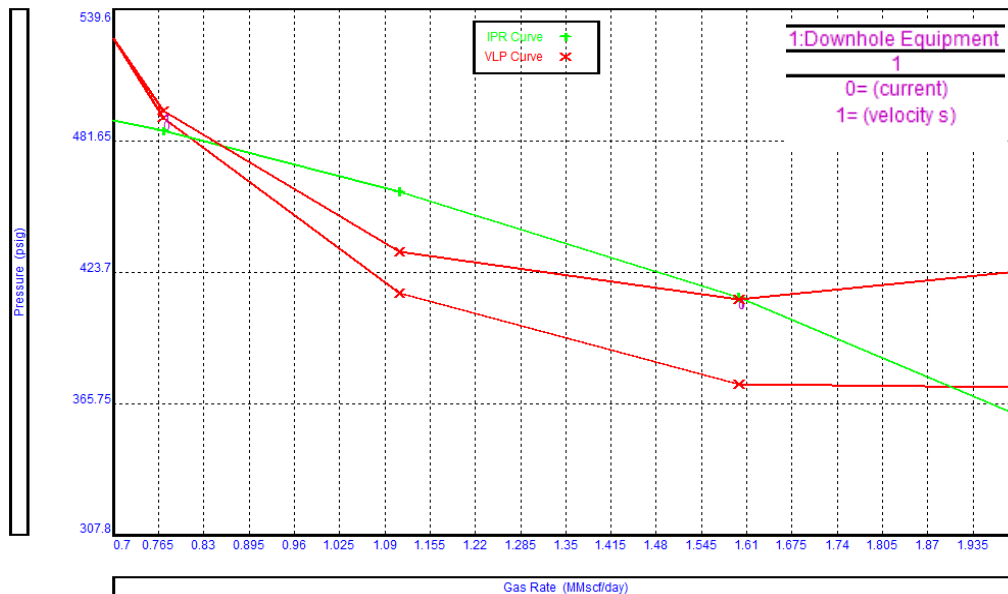


Figure 44 - Well S-5 Velocity string system analysis

Plunger Lift

Given there is significant gas production from the reservoir, the required energy to produce the liquid slug with a plunger is available. Therefore, the plunger lift can be evaluated as an artificial lift option for S-5. Table 7 depicts the input parameters and results of the plunger lift design for S-5.

Like most plunger lift designs, slug volume directly influences the design. In well S-5, this is assumed to be ~14 bbls or ~980 ft of fluid in S-5 tubing. However, in practice, slug volume can be measured using a fluid level sounder. Using ~14 bbls slug volume, total liquid production from the plunger lift is ~165 bbls per day.

In comparison with conventional gas lift, total liquid production from the plunger lift is lower. As the objective of the deliquification technique is to retrieve maximum liquid from the wellbore, conventional gas lift for this well is a better choice.

Input Window	
Tubing ID (in)	3.89
Casing ID (in)	6.184
Depth to Spring (ft)	9800
Plunger rise vel (ft/min)	750
Plunger fall vel (ft/min)	250
Tubing Exit Pressure (psi)	108
Delta T buildup (min)	30
Delta T flow (min)	15
Tubing full factor	0.1
OR Volume of Slug (bbl)	
Liq Sp. Gravity	1
Gas Sp. Gravity	0.69
Gas fraction in Liquid	0.2
Water Cut (%)	95
Surface Temp (deg F)	80
Reservoir Temp (deg F)	350

Results	
Cycles per day	11.43
Total Liquid Production per day (bbl/d)	164.68
Water Production (bbl/d)	156.44
Oil Production (bbl/d)	8.23

Table 7 - Well S-5 Plunger lift design

Plunger Assisted Gas Lift

With current 4-1/2" Tubing and 4.6 MMscfd critical rate

Figure 45 shows the flow rate vs pressure plot to select the plunger type. Based on gas velocity, a continuous plunger lift is more feasible compared to intermittent. This selection is based on the fact that the current rate is lower than the critical rate but not too low therefore pressure buildup time is minimum.

This plot only suggests feasibility regardless of design. To confirm applicability, plunger design is required.

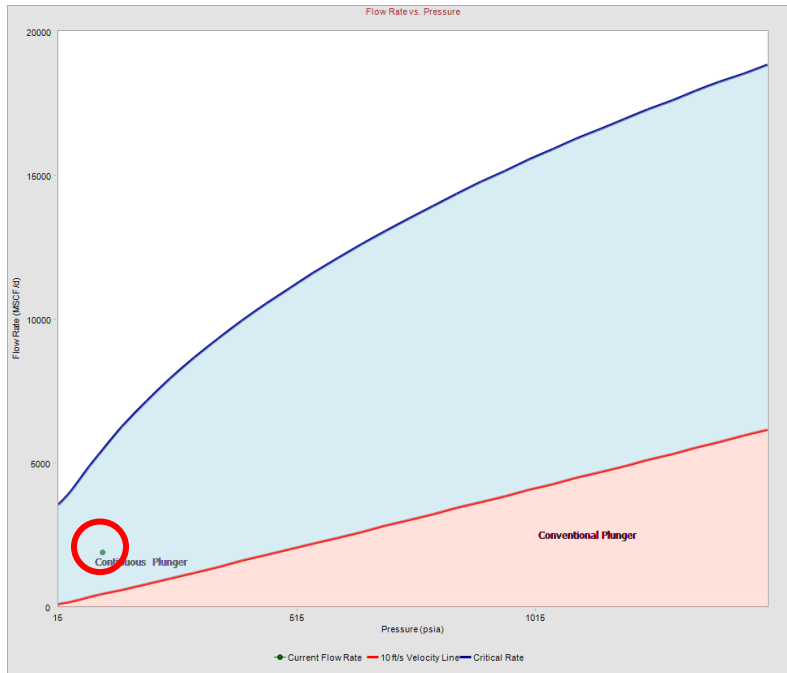


Figure 45 - Well S-5 PAGL type plot

Plunger Assisted Gas Lift Design		Results	
Well Name	S-5	Required Casing Injection Pressure (psi)	1923
PAGL Type	Continuous	Calculated WHP (psi)	1908
Target Gas Production (Mscf/d)	1900	Volume of Liquid Slug (bbl)	0.58
Target Liquid Production (STB/d)	70	Number of Cycles per day	120
Tubing ID (in)	3.985	Gas Velocity at bottom hole (ft/sec)	138
Tubing OD (in)	4.5	Minimum Gas velocity (ft/sec)	39.7
Design WHP (psi)	20	PAGL Possible?	No
Expected Flowing BHP (psi)			
Fall Rate in Gas (ft/min)	800		
Fall Rate in Liquid (ft/min)	400		
Rise Rate (ft/min)	700		

Table 8 - Well S-5 PAGL design with current 4-1/2" tubing

Table 8 depicts the design of PAGL with the current tubing. Due to a high critical rate in 4-1/2" tubing, installing a plunger requires ~1900 psi surface gas injection pressure to lift the fluid and

plunger to the surface. Also due to low slug volume in the continuous plunger, the estimated total liquid production is minimum.

Further, due to a high target liquid requirement, the plunger needs to conduct ~120 cycles per day which is also unattainable. Therefore, a plunger lift with the current tubing is not a feasible option for this well. An alternative option to install PAGL in this well is to re-complete it with 2-7/8” tubing.

With 2-7/8” Tubing and 1.35 MMscfd critical rate

Current modeled conditions are shown in the red circle in Figure 46.

If well S-5 is recompleted with 2-7/8” tubing, expected gas production will decrease to ~0.8 MMscfd from current ~1.9 MMscfd due to added friction in smaller diameter tubing. Figure 46 depicts the PAGL selection plot where current conditions are borderline for a continuous plunger installation. As continuous PAGL is the more



Figure 46 - Well S-5 PAGL plot with 2-7/8" tubing

suitable choice for well S-5, injection pressure in this well is limited to 90% of Flowing Bottom Hole Pressure (FBHP), which is ~480 psi in 2-7/8” tubing.

Plunger Assisted Gas Lift Design																					
Well Name	S-5	<table border="1"> <thead> <tr> <th colspan="2">Results</th> </tr> </thead> <tbody> <tr> <td>Required Casing Injection Pressure (psi)</td> <td>459</td> </tr> <tr> <td>Injection pressure Limited by</td> <td>FBHP</td> </tr> <tr> <td>Calculated WHP (psi)</td> <td>339</td> </tr> <tr> <td>Volume of Liquid Slug (bbl)</td> <td>1.75</td> </tr> <tr> <td>Number of Cycles per day</td> <td>57</td> </tr> <tr> <td>Gas Velocity at bottom hole (ft/sec)</td> <td>39.3</td> </tr> <tr> <td>Minimum Gas velocity (ft/sec)</td> <td>18.56</td> </tr> <tr> <td>PAGL Possible?</td> <td>Yes</td> </tr> </tbody> </table>		Results		Required Casing Injection Pressure (psi)	459	Injection pressure Limited by	FBHP	Calculated WHP (psi)	339	Volume of Liquid Slug (bbl)	1.75	Number of Cycles per day	57	Gas Velocity at bottom hole (ft/sec)	39.3	Minimum Gas velocity (ft/sec)	18.56	PAGL Possible?	Yes
Results																					
Required Casing Injection Pressure (psi)	459																				
Injection pressure Limited by	FBHP																				
Calculated WHP (psi)	339																				
Volume of Liquid Slug (bbl)	1.75																				
Number of Cycles per day	57																				
Gas Velocity at bottom hole (ft/sec)	39.3																				
Minimum Gas velocity (ft/sec)	18.56																				
PAGL Possible?	Yes																				
PAGL Type	Continuous																				
Target Gas Production (Mscf/d)	1000																				
Target Liquid Production (STB/d)	100																				
Tubing ID (in)	2.441																				
Tubing OD (in)	2.875																				
Design WHP (psi)	130																				
Expected Flowing BHP (psi)	480																				
Fall Rate in Gas (ft/min)	800																				
Fall Rate in Liquid (ft/min)	400																				
Rise Rate (ft/min)	700																				

Table 9 - Well S-5 PAGL design with 2-7/8" tubing

Given the max cycle limit of 60 per day, using a 2-7/8" continuous plunger, well can offload ~100 STB/d liquid with the limited ~450 psi injection pressure from 2-7/8" tubing (Table 9). To lift this column in every cycle, an injection pressure of ~450 psi is required that is also near the limit of maximum injection pressure.

In comparison with continuous gas lift in 4-1/2" tubing, total liquid production estimated through nodal analysis exceeds ~270 STB/day. This suggests conventional gas lift is a better alternative to PAGL in well S-5 for two main reasons:

1. Higher liquid rate is achieved by a conventional gas lift in current 4-1/2" tubing
2. To install 2-7/8" PAGL, workover will be required however gas lift in 4-1/2" tubing can be initiated using tubing puncture.

The following design is conducted using the Microsoft Excel model with similar design parameters and 2-7/8" tubing.

Input Window	
Tubing ID (in)	2.441
Casing ID (in)	6.184
Depth to Spring (ft)	9800
Plunger rise vel (ft/min)	700
Plunger fall vel (ft/min)	400
Tubing Exit Pressure (psi)	100
Delta T buildup (min)	0
Delta T flow (min)	0
Slug Volume type	(B)
(A) Tubing full factor	0.03
(B) Volume of Slug (bbl)	2
Liq Sp. Gravity	1.035
Gas Sp. Gravity	0.69
Gas fraction in Liquid	0.2
Water Cut (%)	95
Surface Temp (deg F)	80
Reservoir Temp (deg F)	350
Reservoir pressure (psi)	525
Gas density @ avg pressure (lb/ft3)	
Reservoir Temp (deg F)	350
Results	
Cycles per day	37.40
Total Liquid Production per day (bbl/d)	74.81
Max Pressure Required (psi)	469.33
Water Production (bbl/d)	71.06
Oil Production (bbl/d)	3.74

Table 10 - Well S-5 PAGL design with in-house model

Table 10 lists the input parameters and results of PAGL design with 2-7/8” tubing. Similar to previous results, total liquid production is ~75 bbl/day and maximum injection pressure required to achieve this rate is ~470 psi.

As this model is based on energy balance, friction effects have been modeled through a 1.5 multiplication factor. However, frictional pressure loss is precisely calculated in the design conducted by the commercial software. This is the reason behind slight variations between the two approaches. The maximum pressure requirement used in the Excel model is detailed in Hashmi et al. 2016.

Production Profile

Decline Curve Analysis (DCA) can be used to forecast the production of S-5 after installing the most appropriate artificial lift, which in this case, is the conventional gas lift. Although a full-scale reservoir model will result in better prediction of post-installation performance, DCA can yield reasonable estimates towards additional reserves that can be produced with artificial lift. Figure 47 depicts the match of S-5 production using hyperbolic and exponential decline.

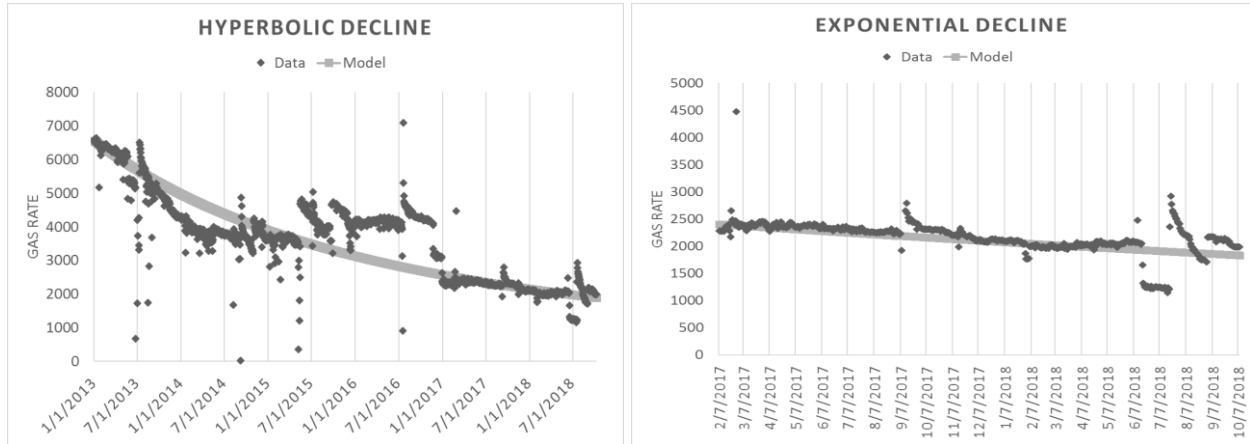


Figure 47 - Well S-5 DCA plots

Results - Hyperbolic				
Start Rate	1984		Start Date	10/9/18
End Rate	718.35316		End Date	3/13/23
Reserves (Bcf)	1.929778609		Time (days)	1616
Results - Exponential				
Start Rate	1984		Start Date	10/9/18
End Rate	708.511296		End Date	1/12/25
Reserves (Bcf)	2.83349458		Time (days)	2287

Table 11 - Well S-5 hyperbolic and exponential DCA results

Table 11 summarizes the results of DCA on well S-5. Expected reserves based on DCA for S-5 are ~1.9 to ~2.8 BCF. In the case of gas lift installation, instantaneous gas production will increase to ~2.6 MMscfd from current ~1.9 MMscfd.

End Point Estimate		End Point Estimate	
<i>Case</i>	W/o Gaslift	<i>Case</i>	W/ Gaslift
Start Rate	1984	Start Rate	2600
End Rate	707	End Rate	707
Decline	0.00045005	Decline	0.00045005
Time (days)	2292.74471	Time (days)	2893.56483
Reserves (Bcf)	2.83749038	Reserves (Bcf)	4.20624063

Table 12 - Well S-5 incremental recovery from gas lift

Table 12 shows the additional recovery expected by the gas lift. Based on the current decline and expected increment production, additional ~1 BCF gas reserves can be produced by initiating gas lift on the well. However, this is contingent on the assumptions in the gas lift model.

Well S-5 Summary

Observations drawn from the analysis conducted suggest the application of gas lift can result in improvement in well S-5. Further, using the conventional gas lift, abandonment pressure can be reduced by ~100 psi, giving additional recovery from the reservoir. This would significantly improve the economics of installing gas lift. Salinity data compared with other S-field wells suggest water produced in this well is formation water. This is supplemented by the instability depicted in VLP analysis and gradient traverse calculations.

Well S-10

S-10 is also a development well drilled in S-field. Producing from a sandstone reservoir at ~3355 m true vertical depth (TVD), it has produced more than 34.7 BCF gas since July 2007. Initial gas production was ~38 MMscfd, however with natural depletion, current gas production is ~1.1 MMscfd. Water production started in 2013 with increasing WGR. Due to scarcity of well test data, only annual WGR was available and that was used in production and nodal analysis. Figure 48 shows the current wellbore configuration of well S-10.

Reservoir Pressure	700 psi	Target Interval	3355 m
Current Production	1.1 MMscfd	Following Wellhead Pressure	97 psi

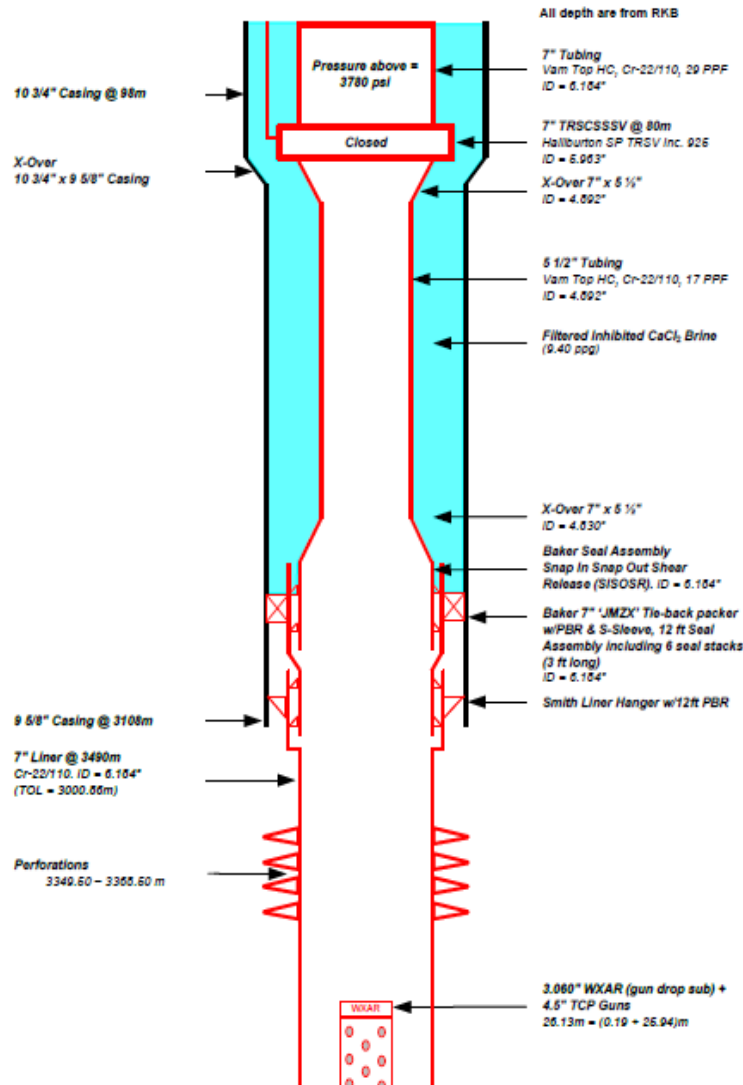


Figure 48 - Well S-10 wellbore configuration

Production plot

Figure 49 shows the gas production and Flowing Wellhead Pressure (FWHP) for S-10 from the start of production. Using this dataset, we can calculate the Bottom Hole Pressure (BHP) from measured WHP using the VLP correlation. This allows the evaluation of changing sand-face pressure to observe unusual trends and anomalies that may indicate issues like liquid loading.

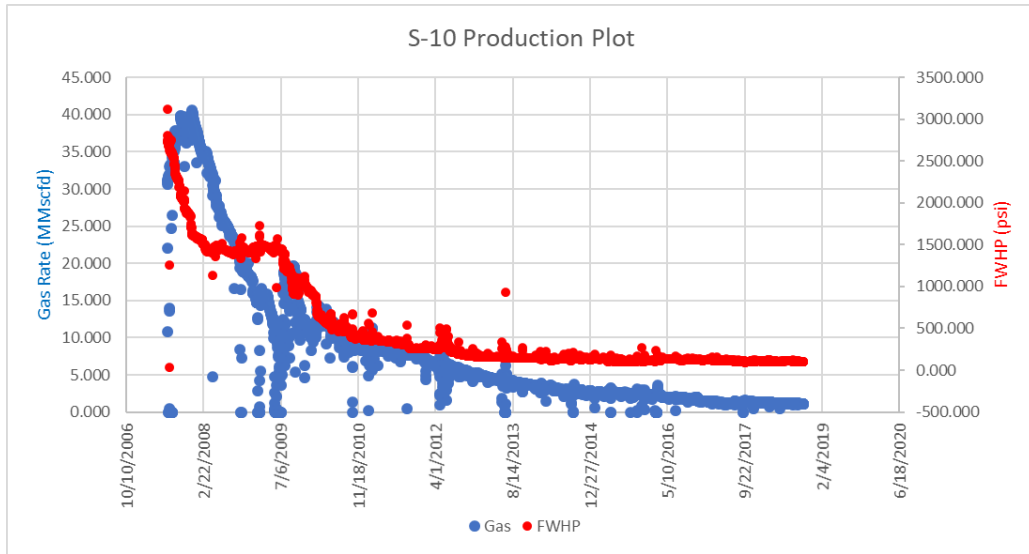


Figure 49 - Well S-10 FWHP Plot

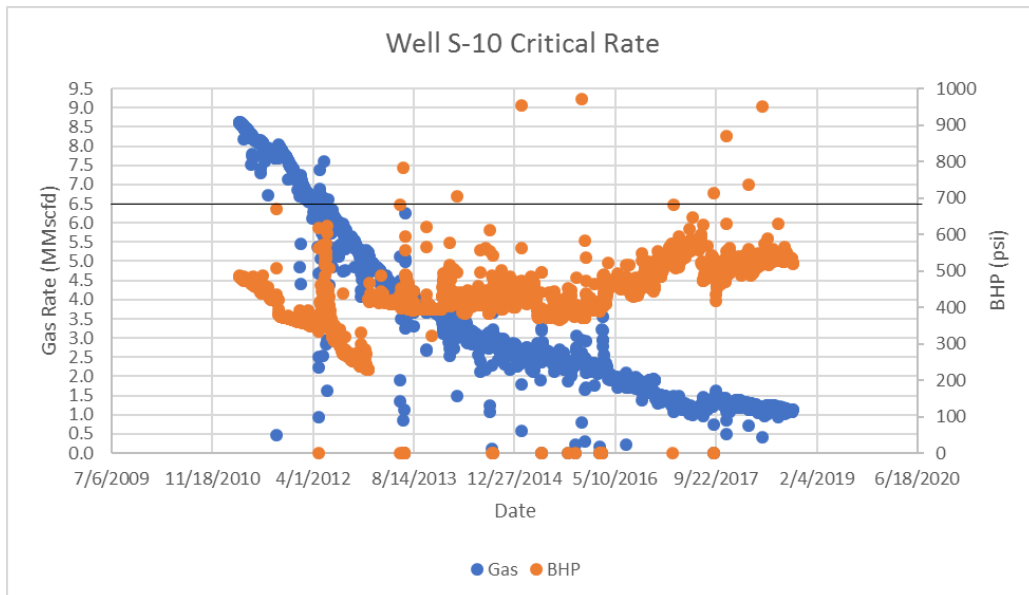


Figure 50 - Well S-10 BHP plot

Figure 50 shows the gas rates and BHP for well S-10. The solid black line at gas rate ~6.5 MMscfd depicts the critical gas unloading rate required to offload all the fluids from the wellbore effectively. Based on the current production rate of ~1.1 MMscfd, current gas rates are ~84% lower than the required critical rates. This suggests production in this well is unoptimized and well may cease to flow.

The BHP trend is increasing with annual WGR in well S-10. This is highly suggestive of increasing hydrostatic pressure in the wellbore that resulted in higher BHP. The WGR value (~200 STB/MMscf) for this well is also relatively high in comparison to other S-field wells, while the production in well S-10 is the lowest. Moreover, this well is in the southern flank of the field, which is a bottom water drive reservoir that contributes towards the high water production. Therefore, this well is an ideal candidate to evaluate the artificial lift options.

Nodal Analysis

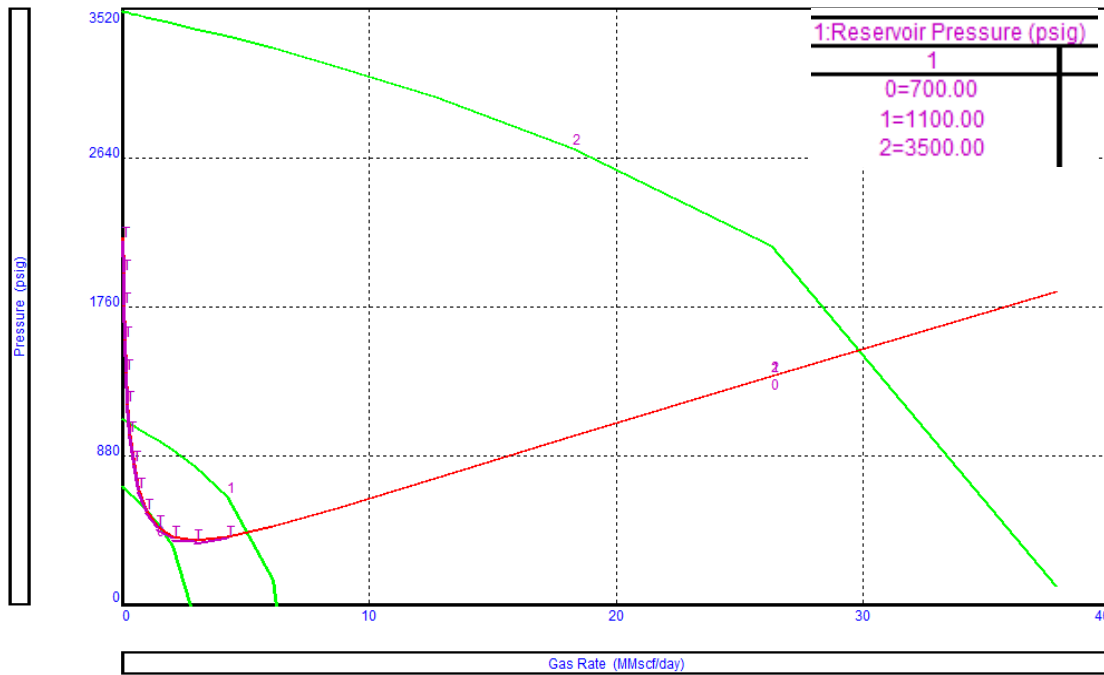


Figure 51 - Well S-10 system analysis - reservoir pressure sensitivity

Figure 51 shows the sensitivity of reservoir pressure that is used to match the current production of S-10 in the nodal analysis. This suggests that reservoir pressure has depleted from ~3500 psi

(initial pressure for this well was probably depleted from virgin due to production from other wells) to ~700 psi. This is the primary reason behind the drop in production over the years.

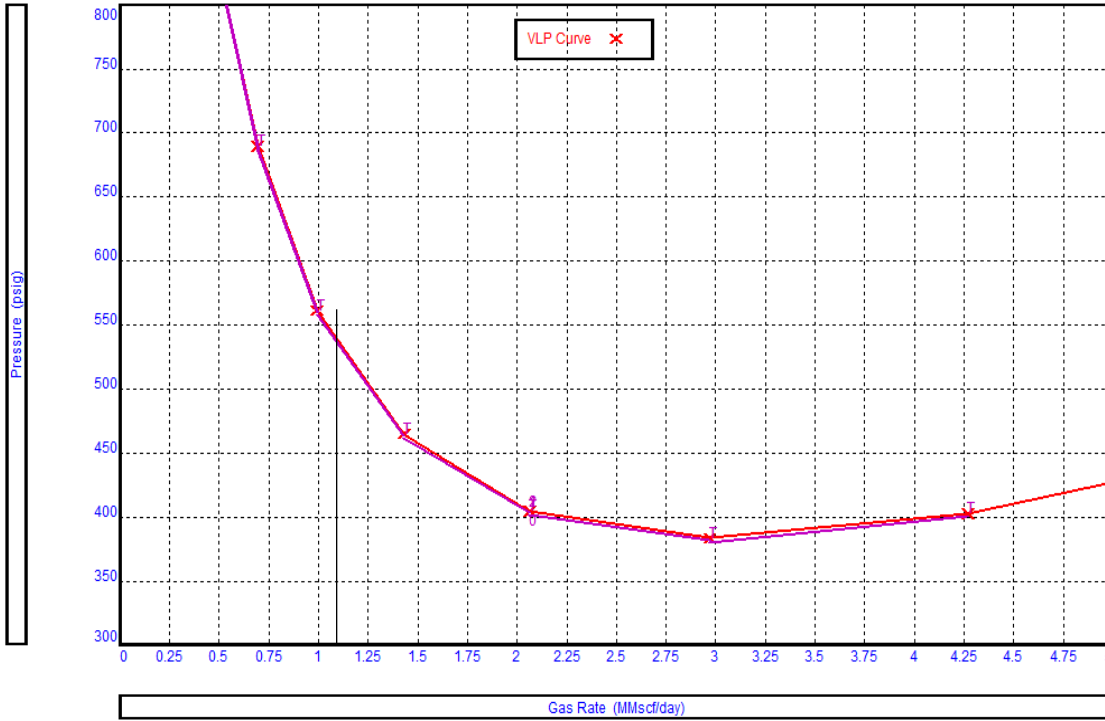


Figure 52 - Well S-10 VLP Stability plot

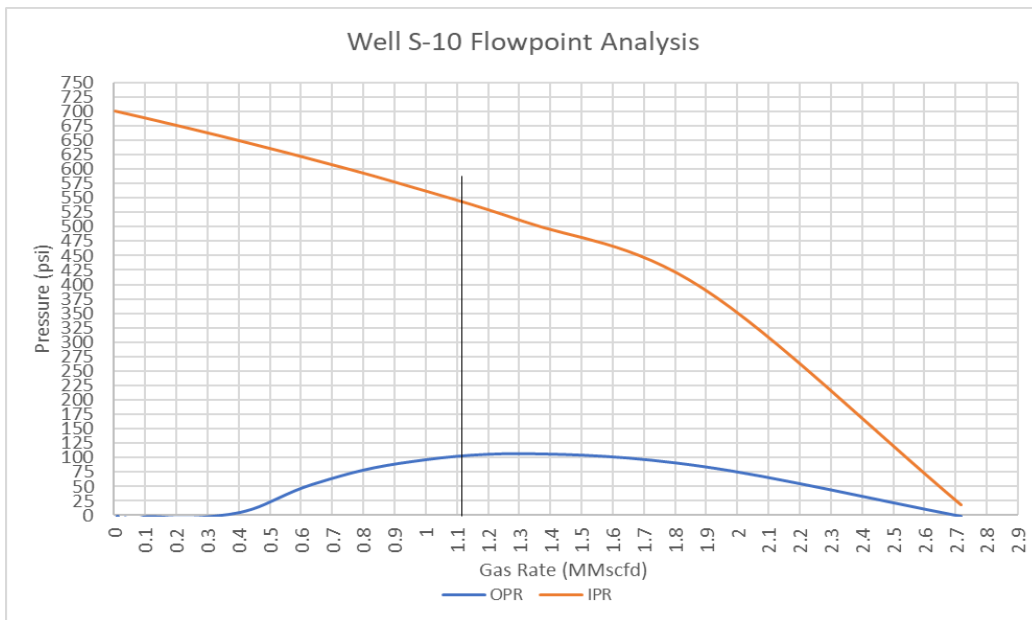


Figure 53 - Well S-10 Flow point plot

Stability analysis through the VLP curve (Figure 52) suggests that current production is in an unstable regime, which is left of the minimum. As current tubing is 7” and the production rates are well below critical, it is expected that flow dynamics are unstable in the wellbore. Further, this would require investigation on the unstable solution in the nodal analysis (left-side intersection of IPR and VLP curves).

Flow-point analysis (Figure 53) suggests a well pressure differential of ~400 psi between Inflow Performance Relationship (IPR) and Outflow Performance Relationship (OPR) curves. Moreover, the current production is in the unstable region of the OPR curve (left to the apex of the curve). Consistent with the observations in other S-field wells, a greater extent of liquid loading results in higher pressure differential between OPR and IPR curves. Given that S-10 has the lowest gas rate and greatest liquid loading extent, the pressure difference between the two curves is highest among all S-field wells.

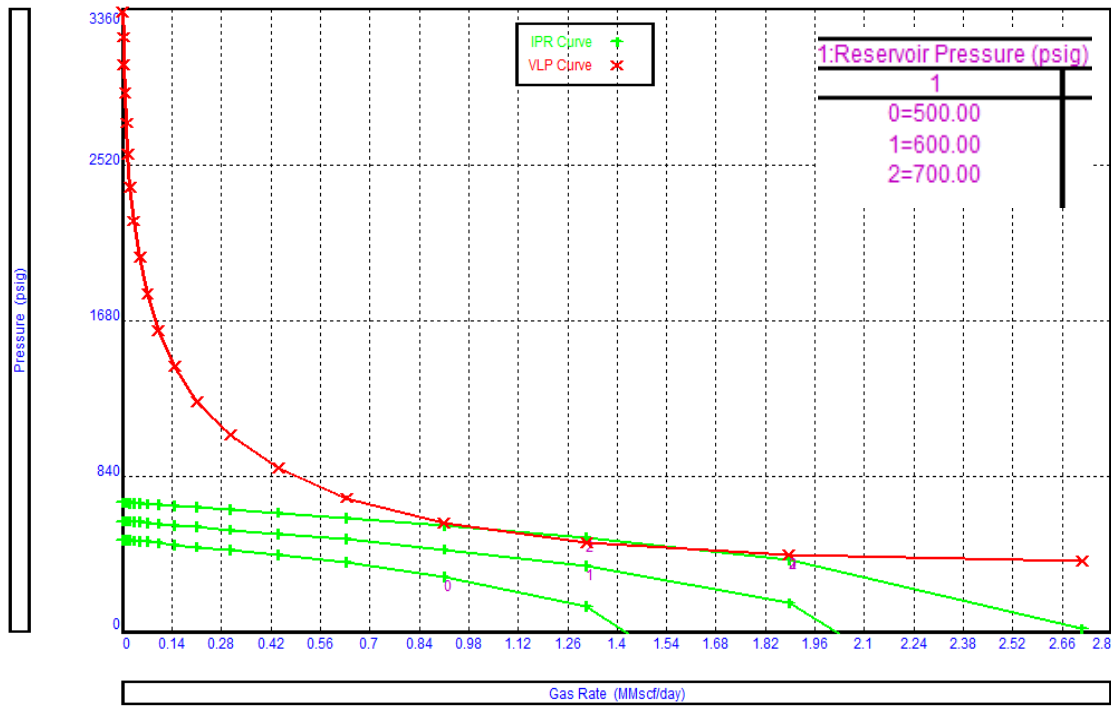


Figure 54 - Well S-10 Load-up condition

Further, system analysis to predict the load-up conditions is conducted by depleting the reservoir pressure. Figure 54 depicts that well S-10 will load up when the reservoir pressure falls below ~700 psi, assuming the IPR model used applies to this well. For S-10, nominal S-field reservoir parameters used in most wells did not result in an accurate IPR match with current production data. This is possible if reservoir stimulation was conducted on this well, which would require the use of a stimulated IPR or negative skin model. Further information regarding the well history was unavailable to ascertain these hypotheses and use an appropriate IPR model.

Artificial Lift Techniques

Gas Lift

A sensitivity run is made on the bottom hole pressure (BHP) with changing WGR to evaluate if the application of any artificial lift that requires gas injection (in the wellbore) will aid in improving production. For most conventional reservoirs such as S-field, reduction in BHP will generally translate to an increase in the hydrocarbon production. This can be used as a starting point to quantify the effectiveness of gas injected technologies for this well. Figure 55 shows the sensitivity of BHP with different WGR values.

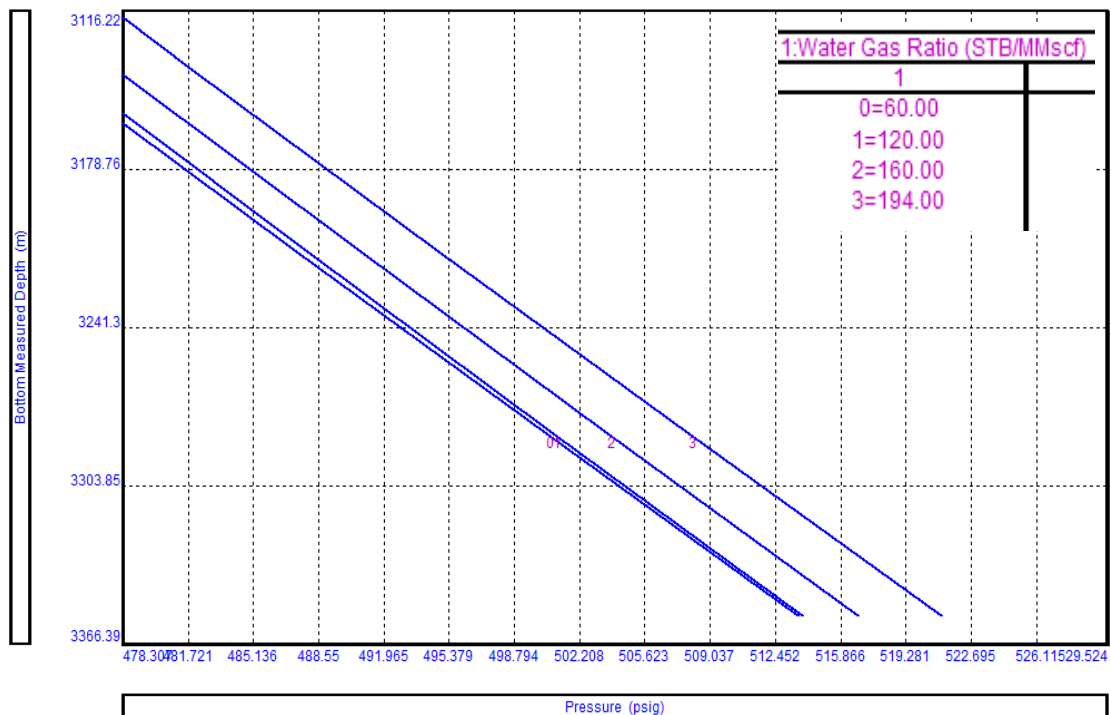


Figure 55 - Well S-10 BHP sensitivity using WGR

The current WGR in S-10 is ~200 STB/MMscf. As confirmed by the VLP stability analysis, current production is in the unstable region of flow. Therefore, a significant reduction in the WGR is required to push the current gas rates to the right of minimum on the VLP curve (without changing wellbore configuration).

Figure 56 shows the effect of lowering WGR on system analysis. Significant gas improvement is observed if the WGR is lowered to ~120 STB/MMscf or less. Compared to the other S-field wells, we see a definite improvement in S-10 by lowering WGR, due to the larger tubing (7" x 5-1/2") with which this well is completed. The addition of extra gas does not increase friction pressures; therefore, significant ~0.8 MMscfd improvement in gas production is observed.



Figure 56 - Well S-10 Gas lift analysis

Although incremental production is realized by lowering the WGR through gas injection, as evident in the VLP plot, production is still in the unstable region. This is due to the low gas inflow from the reservoir, which is unable to create the flow velocities required for effective unloading in larger 7" tubing.

Gas lift design is required where the effects of the gas injection are modeled to quantify the actual improvement in gas production. Most gas lift models are designed for oil reservoirs. Therefore, oil IPR models with equivalent Gas-Liquid Ratio (GLR) are used to match the current performance of S-10. Figure 57 shows the matched model with the same reservoir parameters as Gas IPR with a GLR of ~112783 SCF/STB

Given that the flow is not optimized when gas is injected down larger 7” tubing, conventional gas lift using current wellbore is not a feasible option. Nevertheless, the well can be re-completed with smaller diameter tubing. Thereby, a gas lift can be installed using two methods: (1) Coiled Tubing Gas Lift (CTGL) with 1.5” CT, (2) Conventional gas lift with 2-7/8” tubing.

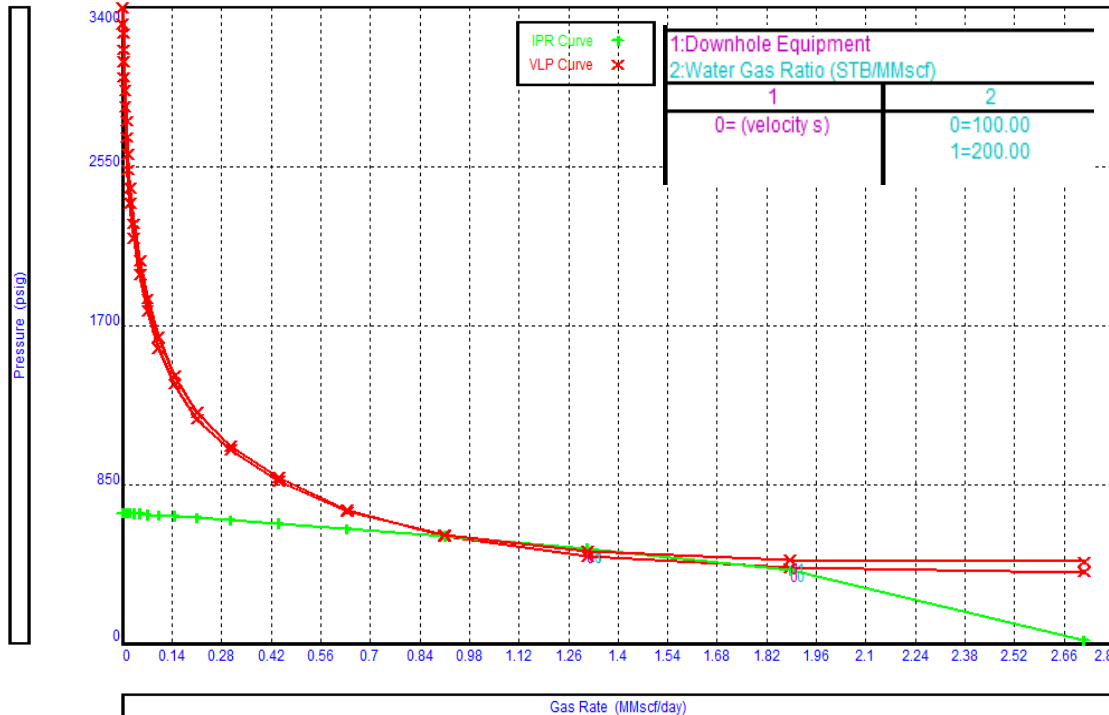


Figure 57 - Well S-10 system analysis using oil IPR

Use of CTGL with 1.5” CT deployed till 2000m and gas injection rate of ~1 MMscfd results in improvement of wellbore dynamics. Figure 58 shows that VLP has shifted in the stable regime suggesting optimized flow from this wellbore profile. Similarly, 2-7/8” tubing also shows stable flow. In both cases, significant improvement in gas production is observed due to lower WGR

(unloading water with gas injection) and better flow velocities in the wellbore. Higher production in the case of CTGL is due to lower frictional pressures. As gas is injected from CT and hydrocarbons are produced from the annulus of CT and tubing, this provides a larger flow area. Lastly, to ensure incremental recovery, it is prudent to check for the abandonment pressure with both completions. In late life scenarios, it is beneficial to select the lift system that maximizes recovery.

Figure 58 compares the use of 2-7/8" tubing conventional gas lift with 1.5" CTGL. In both the cases, gas is injected at ~1 MMscfd rate to produce the well. Although CTGL has a higher instantaneous production, it also has a higher abandonment pressure compared to 2-7/8". Therefore, despite relatively lower instantaneous production in case of 2-7/8", because it moderately increases the recovery, it would be a better choice for this well.

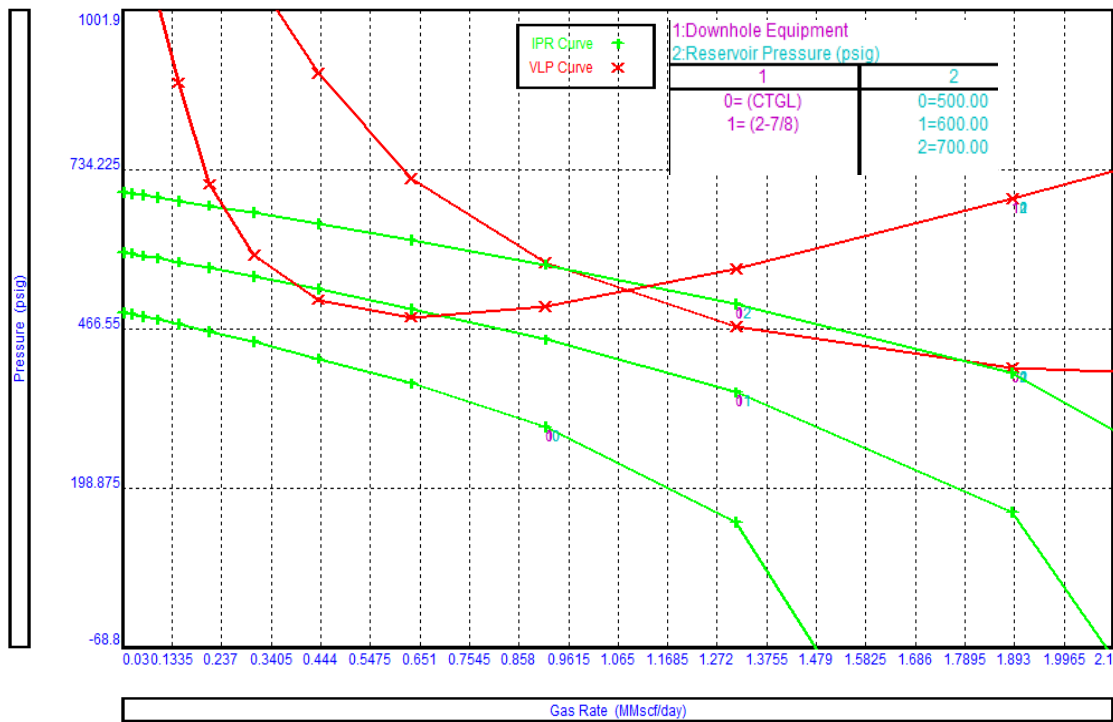


Figure 58 - Well S-10 Gas lift methods comparison

Beam Lift

Beam lift can be used to unload fluids from S-10 to lower bottom hole pressure and increase formation drawdown. As pump efficiency is significantly affected by gas, it is vital to install pump below the perforations to avoid gas intake in the pump. Fortunately, in case of S-10, there is enough rat-hole to install and anchor the pump below the perforations. The pump is set at 3377 meters and well is completed with 2-7/8" tubing inside the current 5-1/2" string. The annulus of 2-7/8" and 5-1/2" is used to produce gas while liquids are produced through the pump in 2-7/8" tubing.

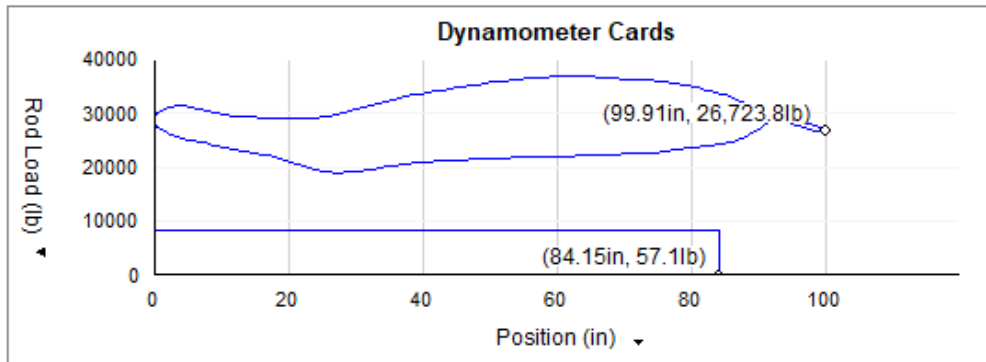
Beam lift design is based on two underlying principles, continuous production of fluids that can be produced by the reservoir (estimated through stable gas rate and WGR), and ensure minimum pumping speed for maximum pump life (as low as possible with a limit of 10 Stokes Per Minute - SPM). Design is conducted on QRod and RODSTAR, commercial software available to design beam lifts.

Figure 59 shows the beam lift design for S-10. Expected production, at 80% pump efficiency (to model gas effects) and nine strokes per minute, is ~160 STB/day. This is produced using a 456-427-100 pumping unit with 100" surface stroke length and 87-E steel sucker rods.

Due to the high depth of S-10, a large pumping unit and higher-grade sucker rods are required that would increase the cost of equipment. Apart from the cost, there are several important factors that adversely affect the overall value of beam lift in S-10. These include:

- Despite being under the 10 SPM, significant wear and tear is still expected due to relatively high speed. This would considerably reduce the operating life of equipment.
- Significant gas production from annulus would cause corrosion. Corrosion inhibition of appropriate grade tubulars/sucker rods are required to maximum life
- Due to minimum infrastructure of pumping units available locally, maintenance and upkeep of equipment can be a challenge, incurring significant logistical expenditures

Design Inputs		Results	
Unit	CWConv	Rate (100% pump volumetric eff.)	198.6 BBL/D
Pump Depth	3,377 m	Rate (80% pump volumetric eff.)	158.9 BBL/D
Surface Stroke Length	100.00 in	Rod Taper	28.2%, 71.8%
Pump Diameter (D)	1.500 in	Top Steel Rod Loading	94.0 %
Tubing Size	2.875" (6.40 lb/ft) 2.441" ID	Min API Unit Rating	456-427-100
<input checked="" type="checkbox"/> Anchored Tubing		Min NEMA D Motor Size	33.87 HP
Rods		Polished Rod Power	22.23 HP
<input checked="" type="radio"/> Steel Rods		TVLoad	32,004 lb
<input type="radio"/> Fiberglass and Steel Rods		SVLoad	23,537 lb
API Rod Number	87	Calculate from SPM or Target Rate	
API Rod Grade	E	Rate	
		<input checked="" type="radio"/> Stroke Rate	<< 9.00 >> SPM
		<input type="radio"/> Target Rate	<< 158.89 >>
		<input type="button" value="Calculate"/>	



PPRL	36,917.5 lb	MPRL	19,016.1 lb	Fo	8,466.9 lb
Pump Stroke Length	84.15 in	Static Stretch	56.86 in	Overtravel	41.01 in
Fo/Skr	0.569	Kr	149 lb/in	Kt	403 lb/in

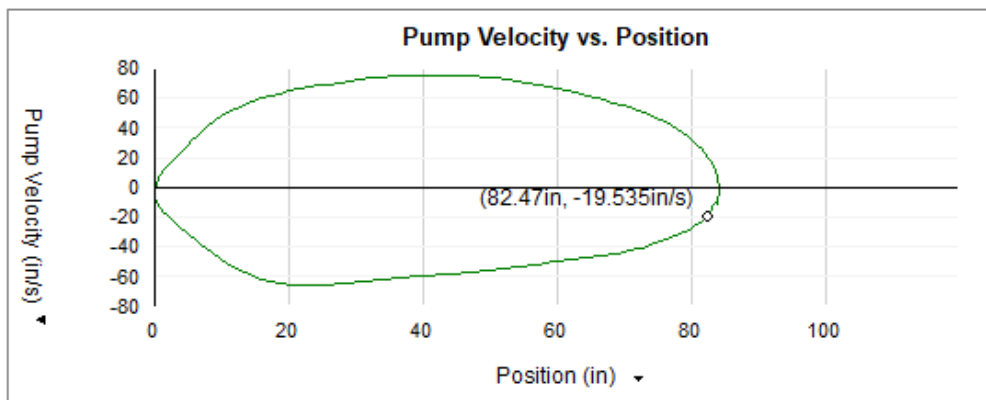


Figure 59 - Well S-10 Beam Lift Design

An alternative to maximize pump life while ensuring maximum production is to use long-stroke surface unit with larger diameter downhole pump. Due to their extended surface stroke, they can be run at significantly lower speed than their conventional counterparts. A larger downhole pump would also increase pumping capacity in each stroke. Fiber-glass rods with steel rods can be used to lower rod weight, however they negatively affect the downhole stroke length (due to elasticity) therefore are not considered. These modifications can mitigate some of the factors listed above.

Figure 60 shows a beam lift design for well S-10 using a Rotaflex long-stroke unit. 1.5” downhole pump is used with 290” surface stroke length. Expected liquid production from this setup is ~200 STB/day at only ~3.8 SPM. The reduced pumping speed translates to lower wear of equipment and significantly increased equipment life.

Despite being technically possible, using specialized equipment will considerably increase capital expenditure to install beam lift. Although it will mitigate few of the technical challenges, the logistical concerns due to infrastructure unavailability will still be of prime importance when conducting economic feasibility analysis. Nevertheless, for trial purposes, long stroke units can be a viable option for S-10 and other wells in S-field with similar characteristics.

INPUT DATA			
Target prod. (bfpd):	200	Pump int. pr. (psi):	250
Run time (hrs/day):	24.0	Fluid level	
Tubing pres. (psi):	50	(ft over pump):	543
Casing pres. (psi):	50	Stuf.box fr. (lbs):	100

Fluid properties		Motor & power meter	
Water cut:	99%	Power Meter	Detent
Water sp. gravity:	1.03	Electr. cost:	\$.06/KWH
Oil API gravity:	48.0	Type:	NEMA D
Fluid sp. gravity:	1.0276		

Pumping Unit: Rotaflex (900)	
API size:	R-320-360-288 (unit ID: R9)
Crank hole number	#1 (out of 1)
Calculated stroke length (in):	290.7
Crank Rotation with well to right:	CCW
Max. CB weight (M lbs):	Unknown

Tubing and pump information			
Tubing O.D. (ins):	2.875	Upstr. rod-tbg fr. coeff:	0.500
Tubing I.D. (ins):	2.441	Dnstr. rod-tbg fr. coeff:	0.500
Pump depth (ft):	11076	Tub.anch.depth (ft):	11076
Pump condition:	Full	Pump load adj. (lbs):	0.0
Pump type:	Insert	Pump vol. efficiency :	80%
Plunger size (ins)	1.5	Pump friction (lbs):	200.0

Rod string design (rod tapers calculated)			
Diameter (inches)	Rod Grade	Length (ft)	Min. Tensile Strength (psi)
.875	WFT EL	4376	N/A
.75	WFT EL	6525	N/A
@ 1.5	NRS PR Norloy	175	100000

CALCULATED RESULTS		
Production rate (bfpd):	205	Peak pol. rod load (lbs): 30584
Oil production (BOPD):	2	Min. pol. rod load (lbs): 14898
Strokes per minute:	3.83	MPRL/PPRL 0.487
System eff. (Motor->Pump):	48%	Unit struct. loading: 85%
Permissible load HP:	91.5	PRHP / PLHP 0.30
Fluid load on pump (lbs):	8381	Buoyant rod weight (lbs): 18650
Polished rod HP:	27.9	N/No: .17 , Fo/SKr: .251

Required prime mover size (speed var. not included)	BALANCED (Min Torq)
NEMA D motor:	40 HP
Single/double cyl. engine:	40 HP
Multicylinder engine:	40 HP

Torque analysis and electricity consumption	BALANCED (Min Torq)
Peak g'box torq. (M in-lbs):	132
Gearbox loading:	41%
Cyclic load factor:	1.1
Counterbalance weight (M lbs):	22.74
Daily electr.use (KWH/day):	612
Monthly electric bill:	\$1120
Electr.cost per bbl. fluid:	\$0.179
Electr.cost per bbl. oil:	\$17.936

Tubing, pump and plunger calculations	
Tubing stretch (ins):	.0
Prod. loss due to tubing stretch (bfpd):	0.0
Gross pump stroke (ins):	255.1
Pump spacing (in. from bottom):	51.6
Minimum pump length (ft):	37.0
Recommended plunger length (ft):	6.0

Rod string stress analysis (service factor: 0.9)				
Stress Load %	Top Maximum Stress (psi)	Top Minimum Stress (psi)	Bot. Minimum Stress (psi)	Stress Calc. Method
88%	50746	24993	12461	WFT EL
88%	48123	16239	16	WFT EL
55%	12343	9	-113	API MG

@ Stress calculations based on elevator neck of 7/8" (for 1.25" sinker bars) or 1" (for other sinker bars).
NOTE Stress calculations do not include buoyancy effects.

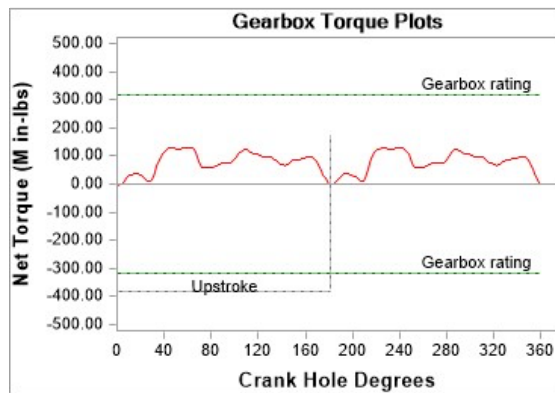
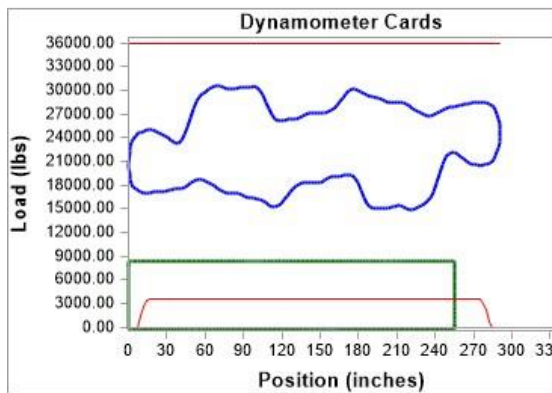


Figure 60 - Well S-10 beam lift design using long-stroke unit

Velocity String/Lower ID Tubing

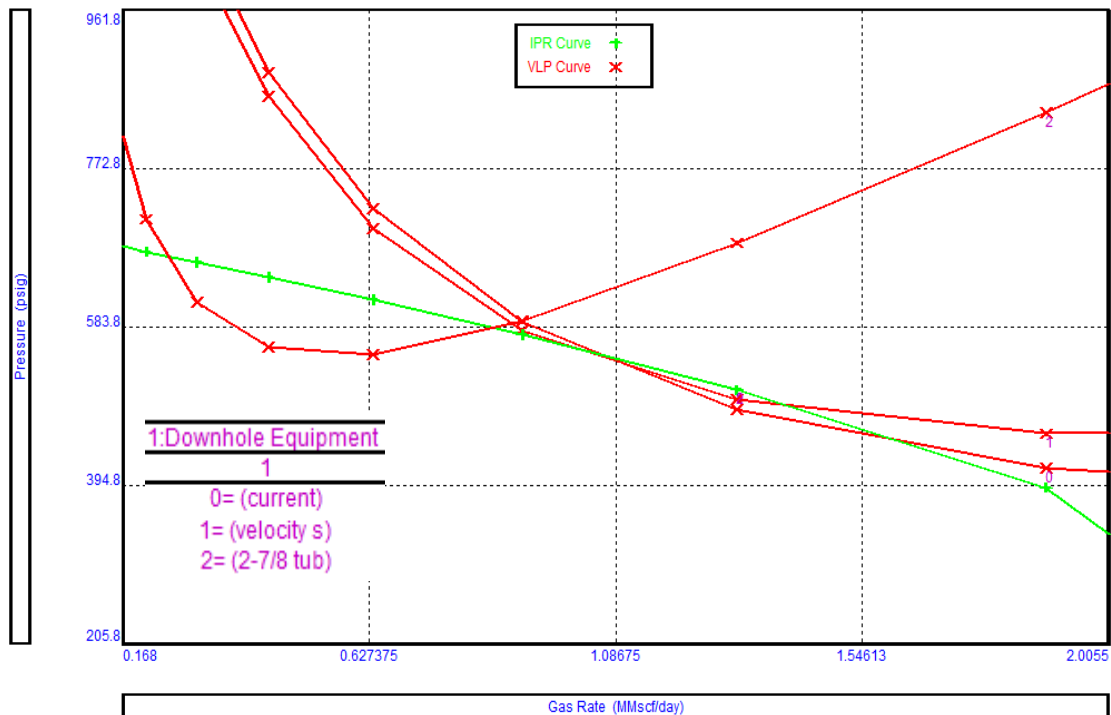


Figure 61 - Well S-10 Velocity string and 2-7/8" Tubing

Velocity string or smaller diameter tubing can be used to improve wellbore dynamics and production. Different combinations of strings are evaluated to compare performance. These sensitivities include:

- Current Profile: 7" x 5-1/2" Tubing with ~250 meters of 7" casing flow
- Velocity String: Install 1" CT in 7" x 5-1/2" Tubing
- Lower ID 2-7/8" Tubing inside 7" x 5-1/2" Tubing

As evident from Figure 61, the use of smaller diameter tubing significantly deteriorates performance due to very high friction pressures. Application of 1.5" CT as velocity string results in higher current incremental production of ~0.4 MMscfd however, due to poor VLP stability, any further decline in reservoir pressure causes the well to cease production. Moreover, while installing a smaller ID tubing or CT in the well, it is advantageous to inject gas from this conduit to realize the additional benefit in the production. Therefore, a gas lift is a better option than a velocity string in this scenario.

Plunger Assisted Gas Lift

With 5-1/2" tubing and ~6 MMscfd critical rate

Figure 62 shows the flow rate vs pressure plot to select the plunger type. Current modeled conditions are shown in the red circle in Figure 62. Based on gas velocity, current conditions fall under continuous plunger lift range however due to severe liquid loading, velocity in the wellbore is low and current conditions are near the border for a conventional plunger.



Figure 62 - Well S-10 PAGL type plot

This plot only suggests feasibility regardless of design. To confirm applicability, plunger design is required.

Plunger Assisted Gas Lift Design		Results	
Well Name	S-10	Required Casing Injection Pressure (psi)	1556
PAGL Type	Continuous	Injection pressure Limited by	Surface
Target Gas Production (Mscf/d)	1100	Calculated WHP (psi)	1541
Target Liquid Production (STB/d)	220	Volume of Liquid Slug (bbl)	0.86
Tubing ID (in)	4.895	Number of Cycles per day	255
Tubing OD (in)	5.5	Gas Velocity at bottom hole (ft/sec)	61.44
Design WHP (psi)	20	Minimum Gas velocity (ft/sec)	11.19
Expected Flowing BHP (psi)		PAGL Possible?	No
Fall Rate in Gas (ft/min)	800		
Fall Rate in Liquid (ft/min)	400		
Rise Rate (ft/min)	700		

Table 13 - Well S-10 PAGL design with current 5-1/2" tubing

Table 13 shows the design of PAGL with current tubing. Due to the high tubing critical rate, installing a plunger requires ~1600 psi surface gas injection pressure to lift fluid and plunger to the surface, which is not available. Also due to low slug volume in the continuous plunger, liquid production is minimum.

In this design, due to the high target liquid requirement, the plunger needs to conduct ~255 cycles per day, which is also unattainable. Therefore, a plunger lift with current tubing is not a feasible option. An alternative option to install PAGL in this well is to re-complete the well with 2-7/8” tubing.

With 2-7/8” Tubing and 1.35 MMscfd critical rate

If well S-10 is recompleted with 2-7/8” tubing, expected gas production is similar to the current production of ~1.1 MMscfd. Figure 63 depicts the PAGL selection plot where current conditions are suitable for a continuous plunger, denoted by the red circle. As continuous PAGL is the more suitable choice for well S-5, injection pressure in this well is limited to 90% of Flowing bottom Hole Pressure (FBHP), which is ~590 psi in 2-7/8” tubing.

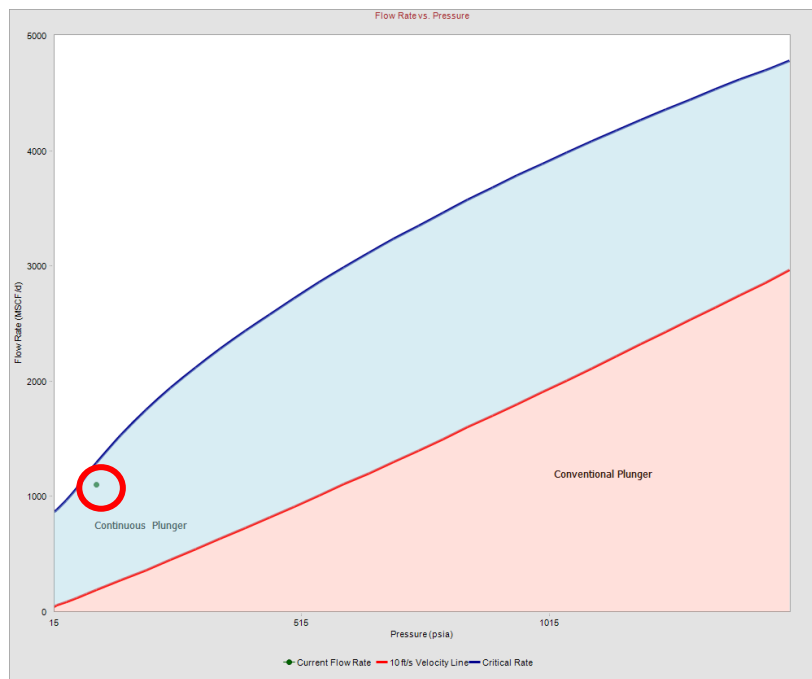


Figure 63 - Well S-10 PAGL plot with 2-7/8" tubing

Given the max cycle limit of 60 per day, using a 2-7/8” continuous plunger, well can offload ~120 STB/d liquid with the limited ~480 psi injection pressure from 2-7/8” tubing (Table 14). To lift this column in every cycle, an injection pressure of ~470 psi is required that is also near the limit of maximum injection pressure.

Plunger Assisted Gas Lift Design		Results	
Well Name	S-10	Required Casing Injection Pressure (psi)	476
PAGL Type	Continuous	Injection pressure Limited by	FBHP
Target Gas Production (Mscf/d)	1100	Calculated WHP (psi)	337
Target Liquid Production (STB/d)	220	Volume of Liquid Slug (bbl)	2
Tubing ID (in)	2.441	Number of Cycles per day	60
Tubing OD (in)	2.875		
Design WHP (psi)	150		
		Gas Velocity at bottom hole (ft/sec)	38.3
Expected Flowing BHP (psi)	470	Minimum Gas velocity (ft/sec)	17.9
Fall Rate in Gas (ft/min)	800		
Fall Rate in Liquid (ft/min)	400		
Rise Rate (ft/min)	700	PAGL Possible?	Yes

Table 14 - Well S-10 PAGL design with 2-7/8" tubing

In comparison with continuous gas lift in 2-7/8" tubing, total liquid production estimated through nodal analysis exceeds ~300 STB/day. This suggests that conventional gas lift is a slightly more productive alternative to PAGL in S-10.

Production Profile

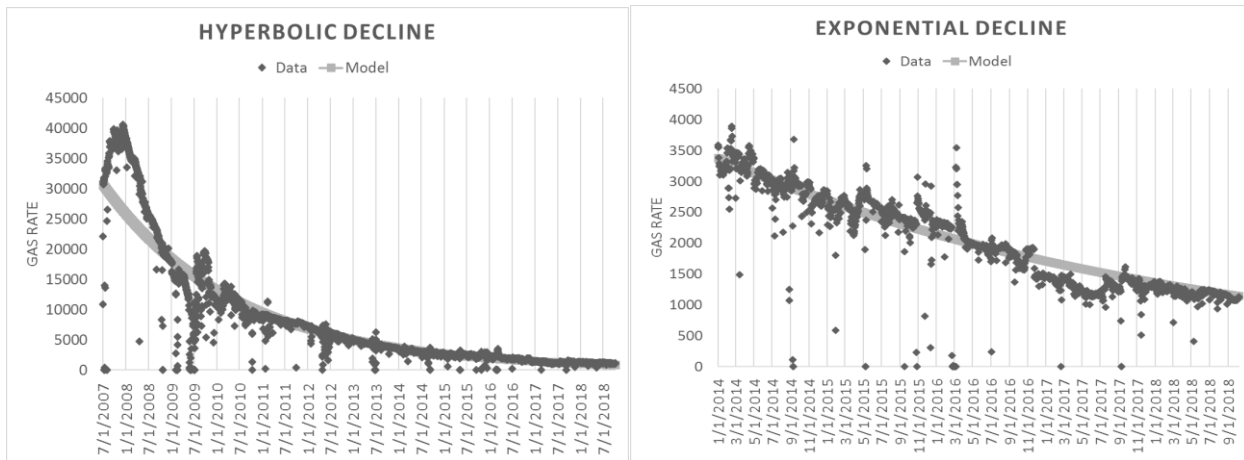


Figure 64 - Well S-10 DCA Plots

Decline Curve Analysis (DCA) is used to forecast the production of S-10 after re-completing the well with 2-7/8" tubing and installing the gas lift. Despite the requirement of a full-scale reservoir model for accurate results post-installation, DCA can yield reasonable estimates of additional reserves unlocked by artificial lift. Instantaneous production from the artificial lift is predicted by the nodal analysis. Figure 64 depicts the match of S-10 production using hyperbolic and exponential decline rates.

Results - Exponential				
Start Rate	1127		Start Date	10/9/18
End Rate	271.814891		End Date	1/12/25
Reserves (Bcf)	1.37537954		Time (days)	2287
Results - Hyperbolic				
Start Rate	1127		Start Date	10/9/18
End Rate	260.3856662		End Date	3/13/23
Reserves (Bcf)	0.947749445		Time (days)	1616

Table 15 - Well S-10 hyperbolic and exponential DCA results

Table 15 summarizes the results of DCA using hyperbolic and exponential decline respectively. The expected reserves based on DCA for S-10 are 0.94 and 1.37 BCF using the two decline methods. By re-completing the well with 2-7/8” gas lift completion, instantaneous production and ultimate recovery will improve.

End Point Estimate		End Point Estimate	
<i>Case</i>	<i>W/o Gaslift</i>	<i>Case</i>	<i>W/ Gaslift</i>
Start Rate	1127	Start Rate	1600
End Rate	300	End Rate	300
Decline	0.00062159	Decline	0.00062159
Time (days)	2129.27558	Time (days)	2693.06449
Reserves (Bcf)	1.33046337	Reserves (Bcf)	2.09141764

Table 16 - Well S-10 incremental recovery from gas

Based on the current decline rate and expected production increment, additional ~0.7 BCF gas reserves can be produced from S-10 by employing a gas lift as summarized in Table 16. This estimation is contingent on the assumptions used in the gas lift design model.

Well S-10 Summary

Observations drawn from the above analysis suggest well S-10 should be recompleted with 2-7/8” conventional gas lift technology, which will result in incremental production. Further field wise analysis and salinity data suggest water production in this well might be from the reservoir. This endorses the results of VLP and flow-point analysis, suggesting that liquid loading is a concern for this well. As Beam lift design also suggests liquid removals of ~200 STB/day, it could be an option.

Well S-11

S-11 is a development well drilled in S-field. Producing from a sandstone reservoir at ~3288 m TVD, S-11 has produced more than 31.2 BCF gas since December 2008. Initial gas production was ~22 MMscfd. Pressure depletion caused rates to decline over the years, and the current gas rate is ~2.01 MMscfd. Water production started in S-11 from 2016 with increasing WGR. Due to the scarcity of well test data, only annual WGR was used in production and nodal analysis. Figure 65 shows the current wellbore profile of S-11.

Reservoir Pressure	650 psi	Target Interval	3288 m
Current Production	2.014 MMscfd	Following Wellhead Pressure	130 psi

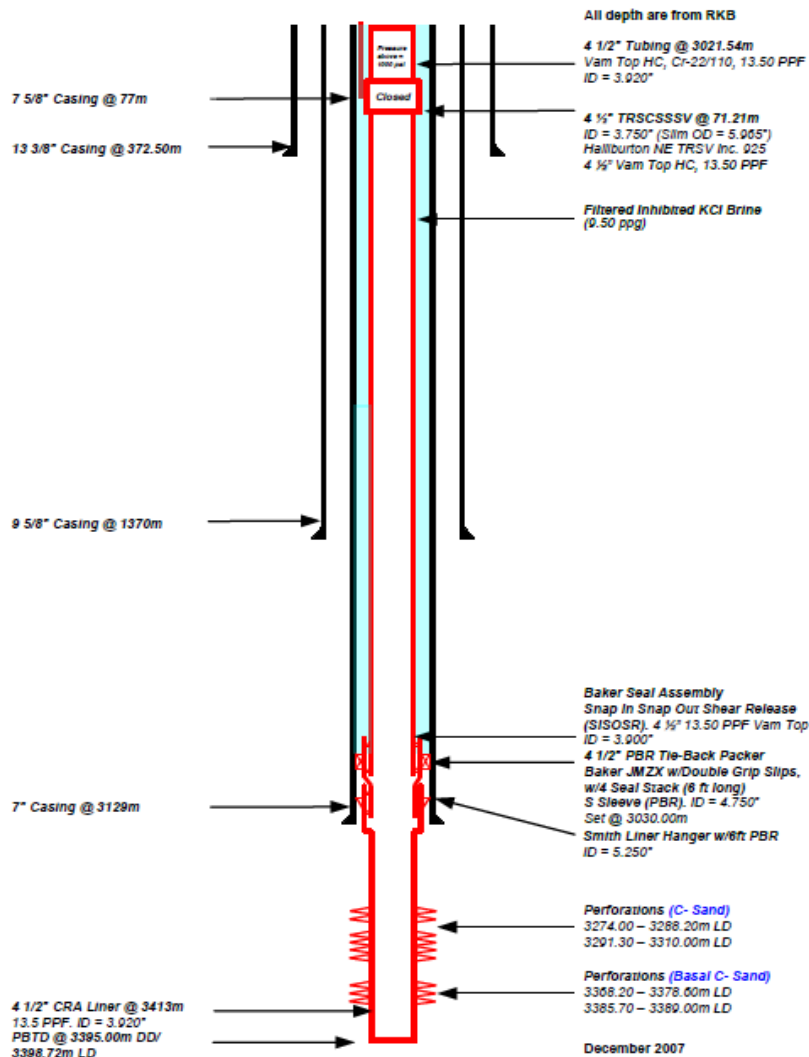


Figure 65 - Well S-11 wellbore profile

Production Plot

Figure 66 shows the gas production and Flowing Wellhead Pressure (FWHP) for S-11 from 2014. Bottomhole Pressure (BHP) can be calculated from measured WHP using the VLP correlation for this dataset. This allows the evaluation of changing sand-face pressure to observe unusual trends and anomalies that may indicate issues like liquid loading.

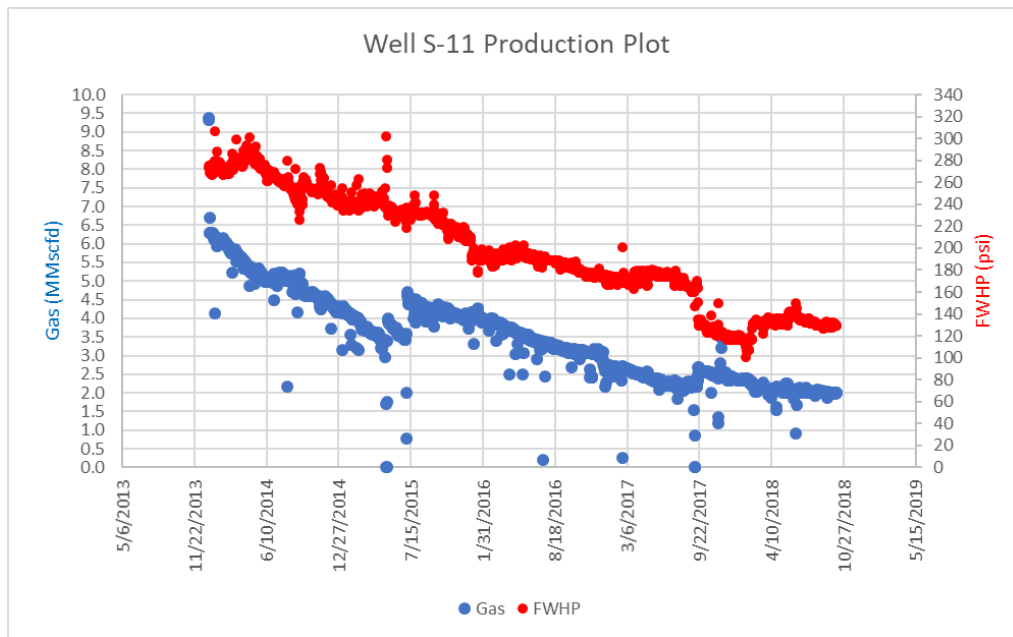


Figure 66 - Well S-11 FWHP plot

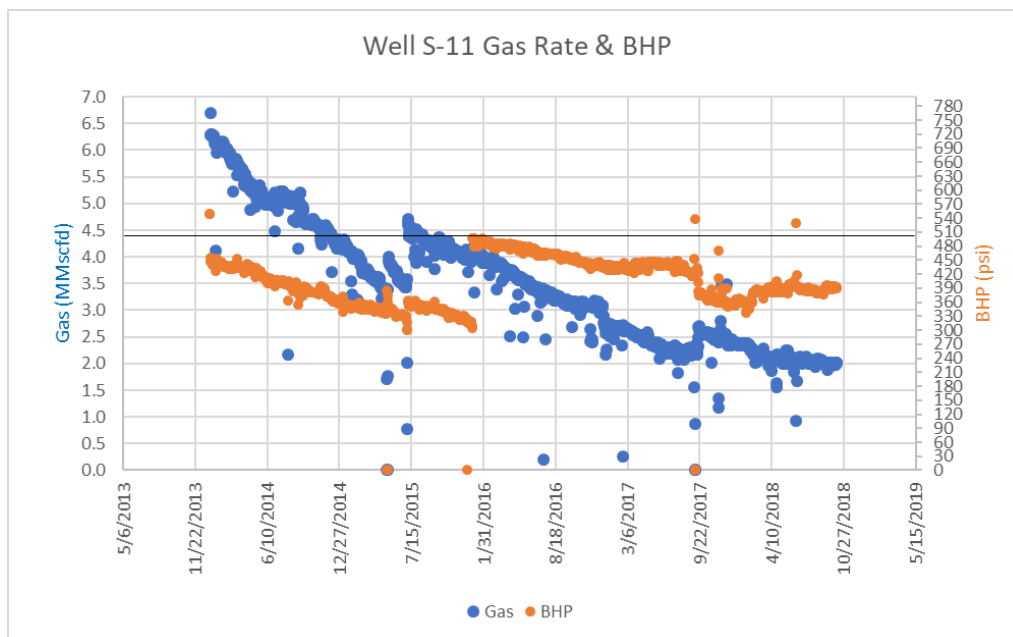


Figure 67 - Well S-11 BHP plot

Figure 67 shows the gas rates and BHP for S-11 from 2014. The solid black line at gas rate ~4.4 MMScfd in Figure 67 depicts the critical gas unloading rate required to offload all fluids from wellbore effectively. Based on the current production rate of ~2.01 MMScfd, current gas rates are ~54% lower than required critical rates. This suggests that liquid loading is a significant issue in this well.

The well S-11 has a relatively stable decline in BHP pressure that suggests a steady increase in water hold-up in the wellbore. A sharp increase in BHP is observed at the start of 2016. This is due to the onset of water production that resulted in increased hydrostatic pressure in the wellbore. For conventional sandstone reservoirs, a decrease in gas rate is a result of steadily decreasing BHP.

Nodal Analysis

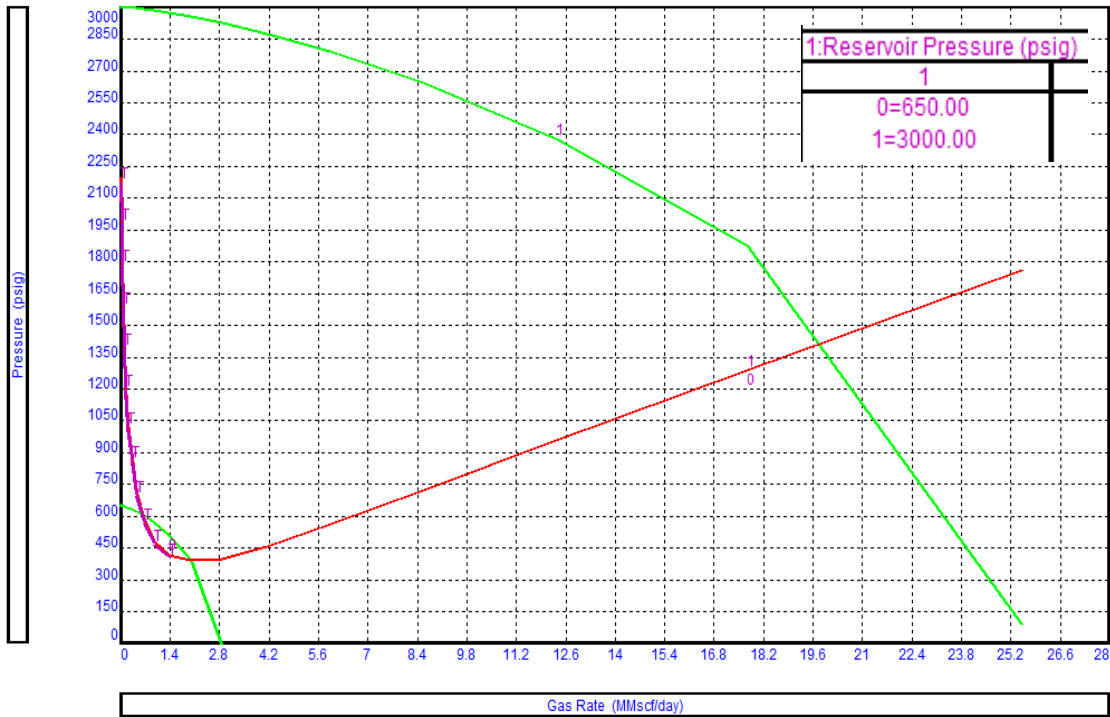


Figure 68 - Well S-11 reservoir pressure sensitivity

Figure 68 shows the sensitivity of reservoir pressure used to match the current production of the well in nodal analysis. This suggests reservoir pressure has depleted from ~3000 psi (initial pressure for this well was probably depleted from virgin due to production from other wells) to ~650 psi. This is the primary reason behind the drop in production over the years.

Stability analysis through the VLP curve (Figure 69) suggests current production is on the left of the minimum, although very near to the minimum. This suggests flow is critical in the wellbore, and any further decrease in gas rates may result in unoptimized flow and possibly a load-up condition.

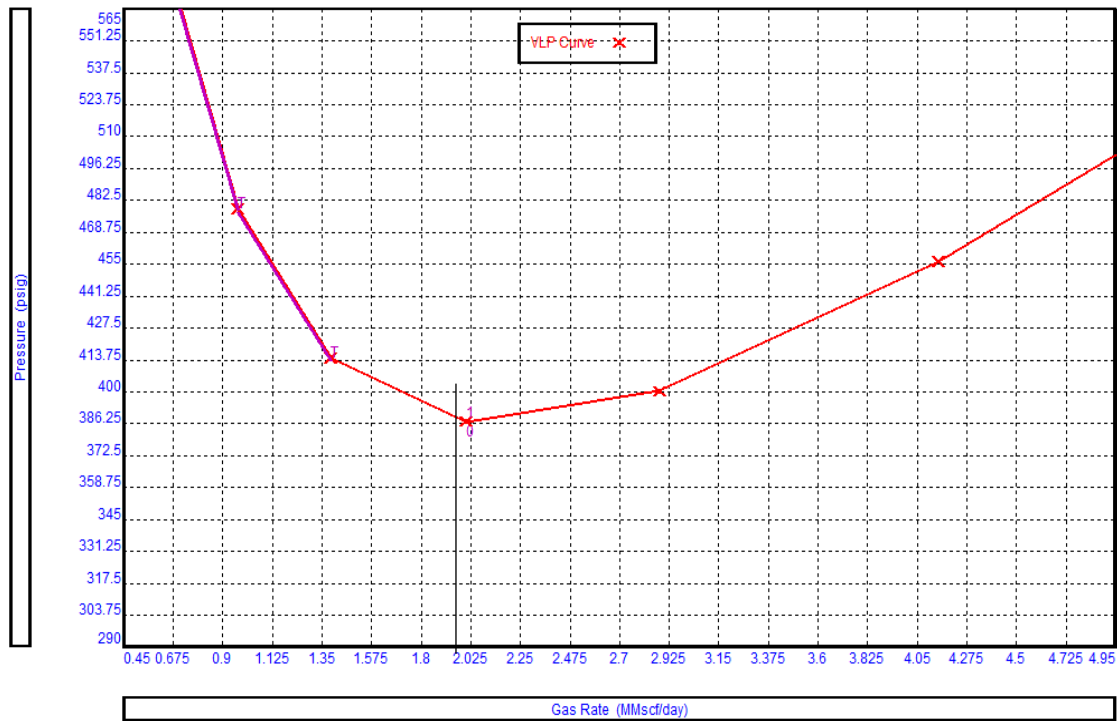


Figure 69 - Well S-11 VLP stability plot

Flow-point analysis (Figure 70) and VLP stability (Figure 69) give a contradicting view on this well. Current gas rates are on the left of the VLP curve minimum, suggesting unoptimized flow in the wellbore. However, in flow-point analysis, current gas rates are in the stable region (right to the apex of OPR curve). Nevertheless, the pressure difference between the IPR and OPR curve is ~240 psi.



Figure 70 - Well S-11 flow-point analysis plot

Salinity Analysis

Source of liquid production in the wellbore can also be used to designate the severity of liquid loading. Although any fluid – condensate, formation water and condensed water – can cause an increase in hydrostatic pressure and deteriorate well performance, often formation water is most detrimental to production. This is mainly because the liquid is introduced at sand-face from formation and in lower velocities, is not carried towards the surface. The other two sources of fluids are often near the wellbore; therefore, they have to travel a shorter distance.

In the absence of production logs, salinity data from produced water is used to classify condensed water from formation water. Commonly, chloride or sodium chloride content form the basis of salinity classification. Gorrell 1958 suggest the following brackets:

0 to 10,000 ppm NaCl – Fresh/Brackish water

10,000 to 100,000 ppm NaCl – Salty water

Over 100,000 ppm NaCl – Brine

As S-11 water has ~744 ppm salinity, based on the above categories, produced water is most likely condensed in this well and is sourced near the surface.

Artificial Lift Techniques

Gas Lift

A sensitivity run is made on bottom hole pressure with changing WGR to evaluate if the application of any artificial lift that requires gas injection (in the wellbore) will aid in improving production. For most conventional reservoirs, reduction in BHP will generally increase hydrocarbon production.

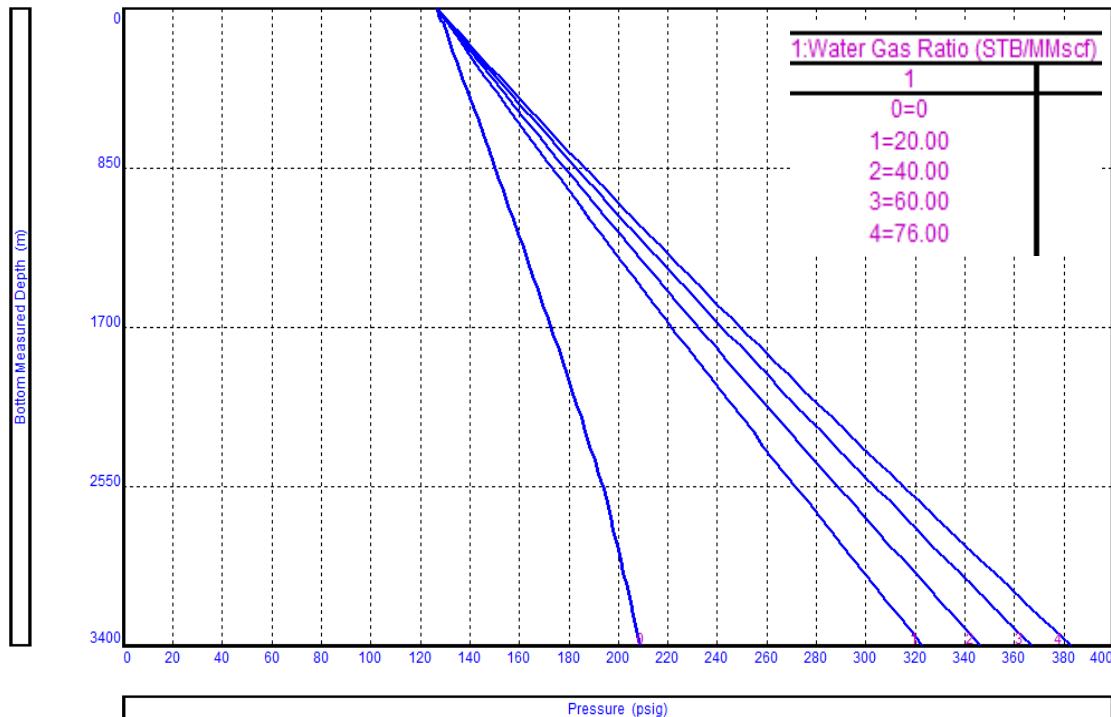


Figure 71 - Well S-11 WGR sensitivity

The current WGR in well S-11 is ~76 STB/MMscf. As evident in Figure 71, by lowering WGR through gas injection, bottom hole pressure reduction is observed. This would suggest gas increment is possible through a gas lift, which can be confirmed by WGR sensitivity on system analysis.

Figure 72 shows the effect of lowering WGR on system analysis. Gas improvement is observed if WGR is lowered to ~20 STB/MMscf or less. Compared to other S-field wells, we see a definite improvement in S-11 with lowering WGR due to poor wellbore hydraulics, as suggested by VLP stability.

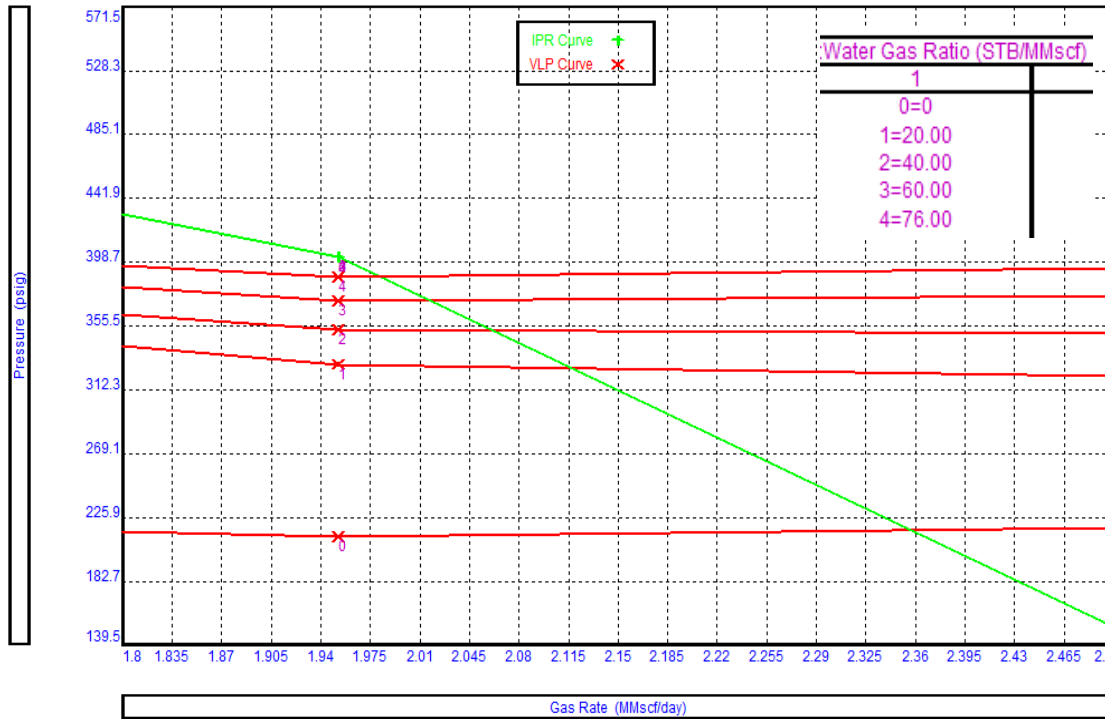


Figure 72 - Well S-11 WGR sensitivity on system plot

A gas lift design is required where the effects of the gas injection are modeled to quantify the actual improvement in gas production. Most gas lift models are designed for oil reservoirs, therefore as a way around, oil IPR using equivalent GOR is used to match the current performance of S-11. Figure 73 shows the matched model with the same reservoir parameters as Gas IPR with a GLR of ~201419 SCF/STB.

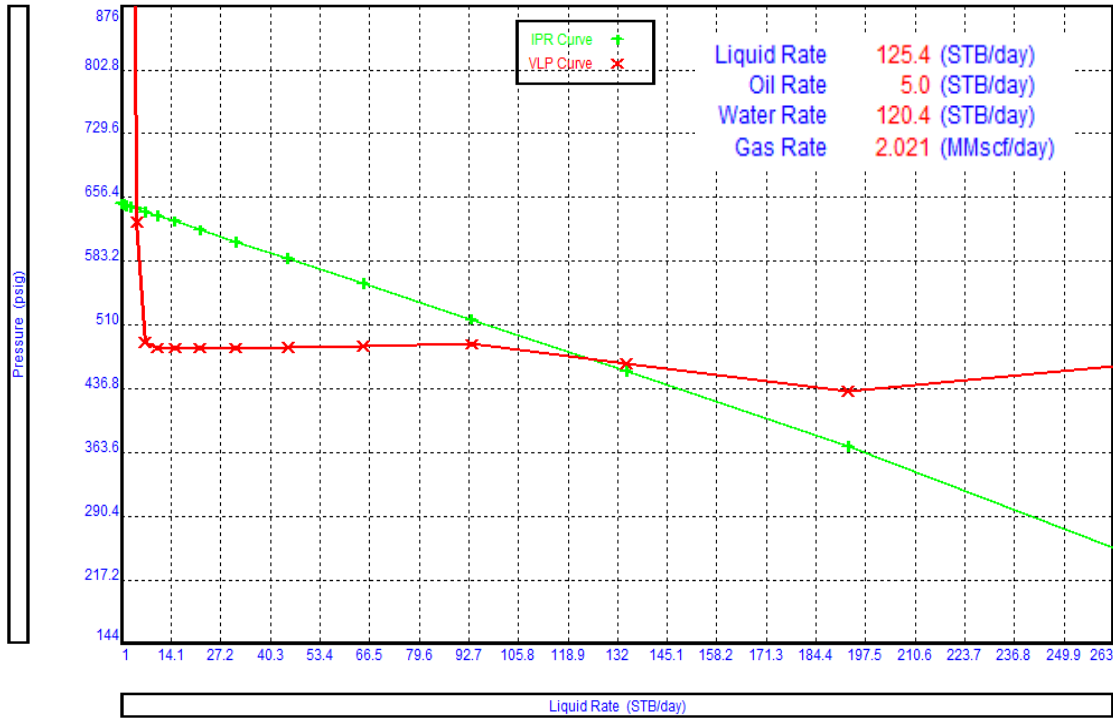


Figure 73 - Well S-11 system plot using oil IPR

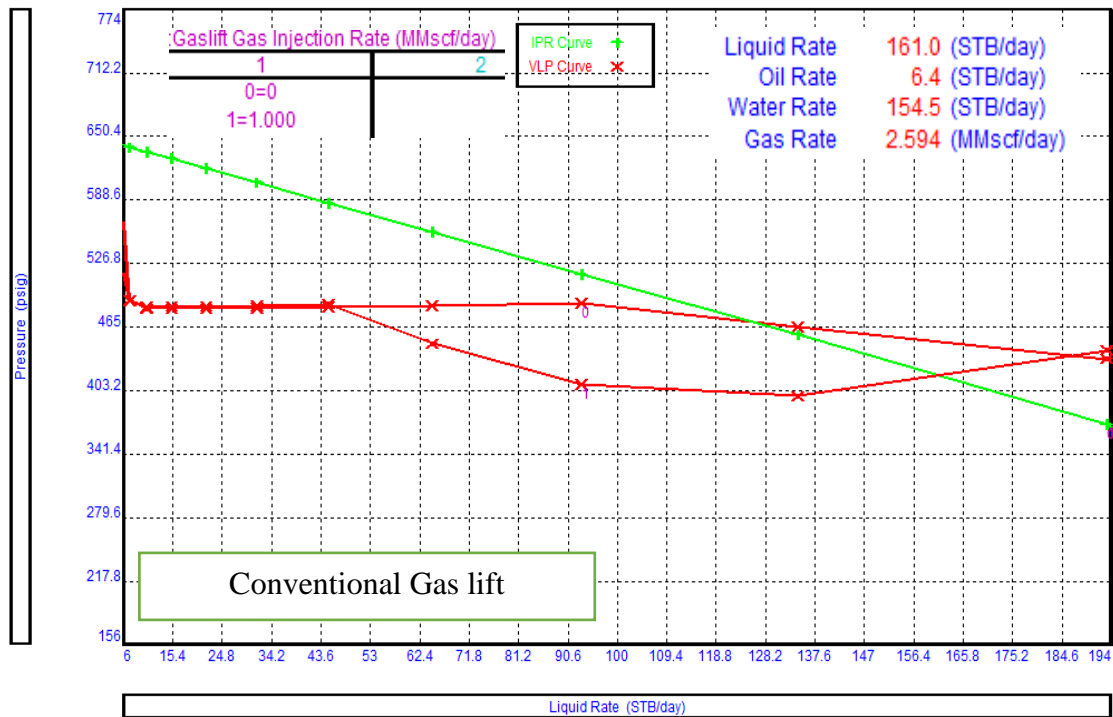


Figure 74 - Well S-11 conventional gas lift design (4-1/2" tubing)

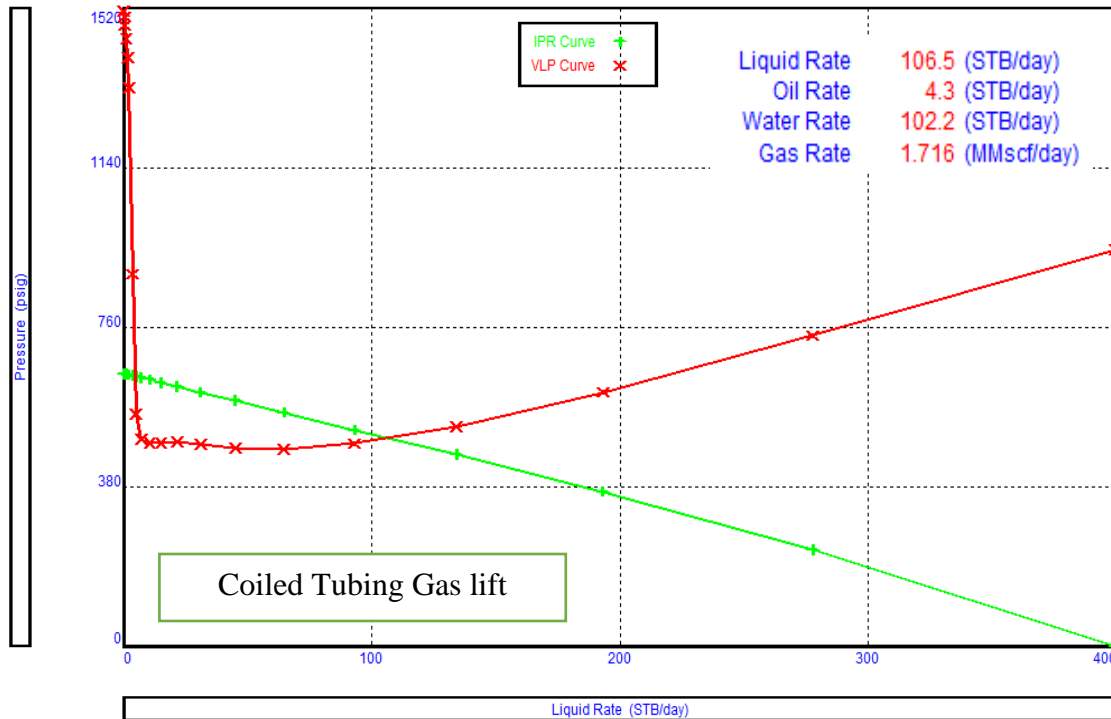


Figure 75 - Well S-11 coiled tubing gas lift design

Figure 74 shows a conventional gas lift design using 4-1/2” tubing that results in ~0.4 MMscfd increment. Further, due to improved hydraulics, the gas lift can produce well until reservoir pressure declines below ~450 psi, whereas well will load-up in the current configuration when reservoir pressure decreases to ~500 psi. Therefore, a gas lift would not only improve instantaneous production but increase ultimate recovery by reducing abandonment pressure of this well.

Gas can also be injected by deploying coiled tubing inside 4-1/2” tubing. Figure 75 depicts system analysis with 1.5” CT in wellbore till ~2500m using ~1 MMscfd gas injection. Due to a lower conduit available for flow with CT in the wellbore, friction pressures mask the positive effect of reduced liquid loading. This results in overall gas rate reduction from current gas rates. Further, there is no significant improvement in ultimate recovery by using CTGL. Therefore, it is not a viable option for this well.

Plunger Assisted Gas Lift

With 4-1/2" tubing (Plunger BHA @ 3030m)

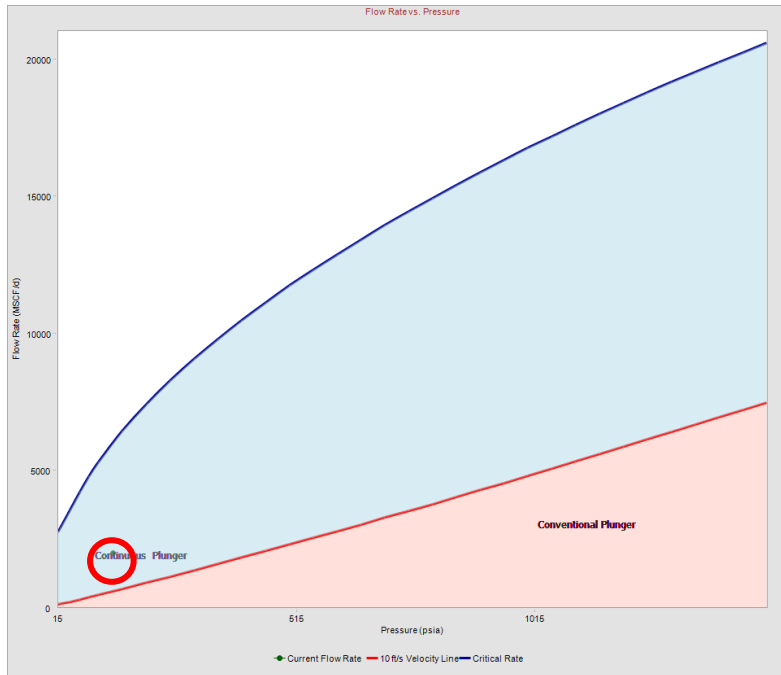


Figure 76 - Well S-11 PAGL type plot

Figure 76 shows the flow rate vs pressure plot to select the plunger type. Current model conditions are shown in the red circle in Figure 76. Based on gas velocity, current conditions fall under continuous plunger lift range however due to severe liquid loading, velocity in the wellbore is low and current conditions are near the border for a conventional plunger.

This plot only suggests feasibility regardless of design. To confirm applicability, plunger design is

required.

Plunger Assisted Gas Lift Design		Results	
Well Name	S-11	Required Casing Injection Pressure (psi)	2860
PAGL Type	Continuous	Injection pressure Limited by	Surface
Target Gas Production (Mscf/d)	2000	Calculated WHP (psi)	2815
Target Liquid Production (STB/d)	200	Volume of Liquid Slug (bbl)	1.71
Tubing ID (in)	3.92	Number of Cycles per day	116
Tubing OD (in)	4.5	Gas Velocity at bottom hole (ft/sec)	80.09
Design WHP (psi)	50	Minimum Gas velocity (ft/sec)	28.25
Expected Flowing BHP (psi)		PAGL Possible?	No
Fall Rate in Gas (ft/min)	800		
Fall Rate in Liquid (ft/min)	400		
Rise Rate (ft/min)	700		

Table 17 - Well S-11 PAGL design with current 4-1/2" tubing

Table 17 shows the design of PAGL with current tubing. Due to the high tubing critical rate, installing a plunger requires ~2800 psi surface gas injection pressure to lift fluid and plunger to the surface, which is not available. Also due to low slug volume in the continuous plunger, liquid production is minimum.

In this design, due to the high target liquid requirement, the plunger needs to conduct ~116 cycles per day, which is also unattainable. Therefore, a plunger lift with current tubing is not a feasible option.

Nevertheless, as current production is low and the WGR of this well is relatively high, continuous plunger lift may improve well performance. However, 2-7/8” tubing is required to install plunger.

Plunger Assisted Gas Lift Design		Results	
Well Name	S-11	Required Casing Injection Pressure (psi)	486
PAGL Type	Continuous	Injection pressure Limited by	FBHP
Target Gas Production (Mscf/d)	1200	Calculated WHP (psi)	347
Target Liquid Production (STB/d)	125	Volume of Liquid Slug (bbl)	2.08
Tubing ID (in)	2.441	Number of Cycles per day	60
Tubing OD (in)	2.875		
Design WHP (psi)	150	Gas Velocity at bottom hole (ft/sec)	41.9
Expected Flowing BHP (psi)	480	Minimum Gas velocity (ft/sec)	19.09
Fall Rate in Gas (ft/min)	800		
Fall Rate in Liquid (ft/min)	400	PAGL Possible?	Yes
Rise Rate (ft/min)	700		

Table 18 - Well S-11 PAGL design using 2-7/8" tubing

Gas production drops to ~1.2 MMscfd if tubing in the well S-11 is switched to 2-7/8”. Given the max cycle limit of 60 per day, using a 2-7/8” continuous plunger, well can offload ~125 STB/d liquid with the limited ~480 psi injection pressure from 2-7/8” tubing. To lift this column in every cycle, an injection pressure of ~480 psi is required that is also near the limit of maximum injection pressure.

The addition of a continuous plunger lift, that can offload additional fluid from the wellbore (compared with 2-7/8” tubing without plunger lift), results in production increase to ~1.6 MMscfd. This increment is estimated through the solution bottom hole pressure that will be achieved if ~125 STB/day fluid is produced by installing a continuous plunger lift. Table 18 shows the PAGL design using 2-7/8” for well S-11.

Figure 77 shows the system plot including sensitivity for plunger lift. The black arrow depicts incremental production that is achieved by lowering bottom hole pressure. Although incremental production, and possibly additional reserves, are unlocked with plunger lift, these are contingent to the following:

- Well is currently completed with 4-1/2” tubing; workover is required to re-complete well with 2-7/8” tubing and install plunger lift
- Increased production of ~1.6 MMscfd with plunger lift is still lower to the current production of ~2 MMscfd from 4-1/2” tubing

PAGL with 2-7/8” tubing is a feasible option to optimize production from well S-11 when current production falls below ~1.6 MMscfd or well loads up due to unoptimized flow in larger 4-1/2” tubing. Economics analysis is required to ascertain if reserves that will be produced through the plunger lift will be sufficient to make this project profitable.

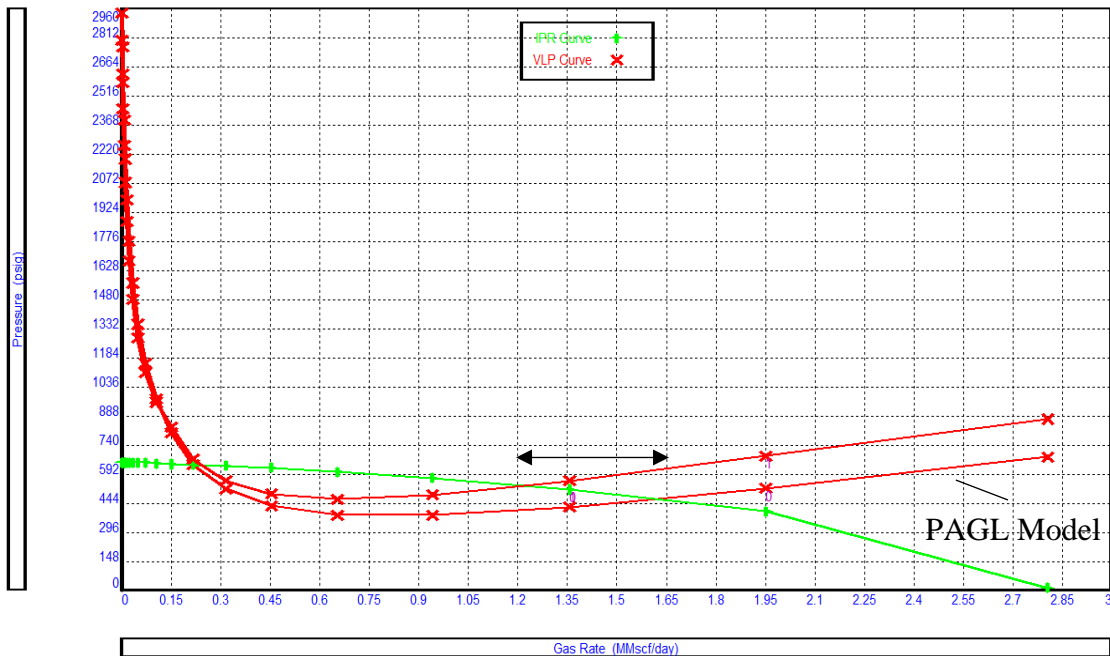


Figure 77 - Well S-11 PAGL system plot

Velocity String

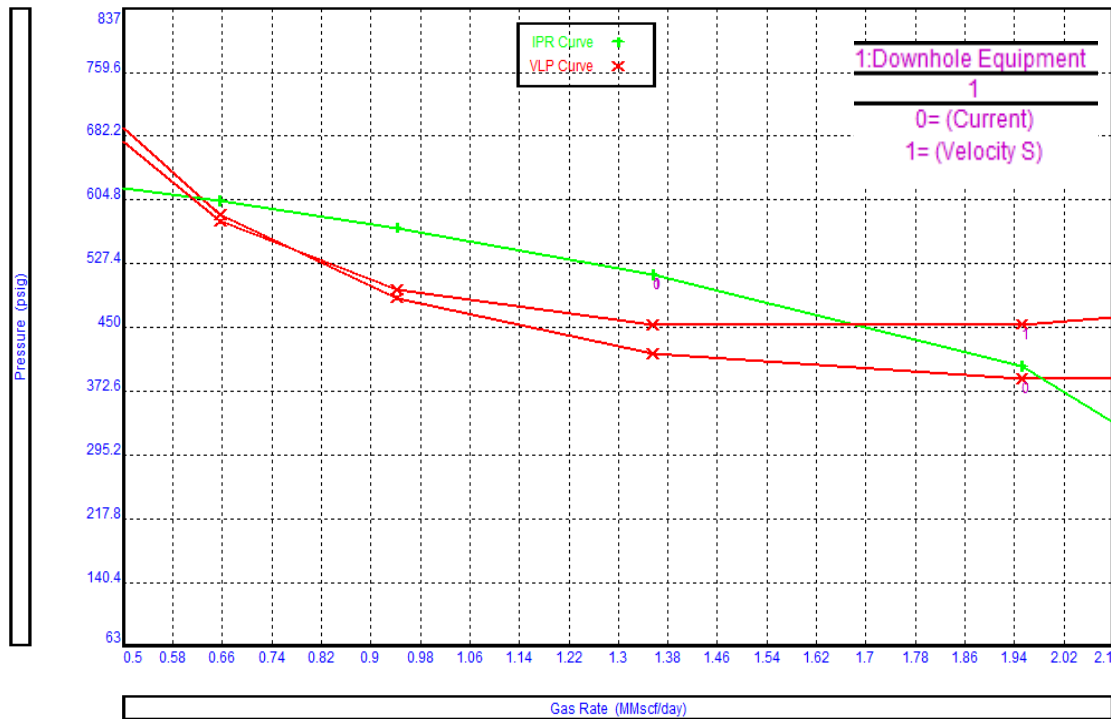


Figure 78 - Well S-11 velocity string design

Figure 78 depicts system analysis results by re-completing S-11 using 1" velocity string. Similar to the results of CTGL, using coiled tubing or velocity string increases friction pressures in wellbore resulting in higher BHP and lower gas rates. Therefore, installing a velocity string does not provide incremental production.

Well S-11 Summary

Observations drawn from the analysis conducted suggest the application of gas lift can result in improvement in well S-11. The increment realized by injecting gas in current 4-1/2" tubing is ~0.4 MMscfd. However, given salinity data of ~744 ppm (as NaCl), produced water is likely condensed water that is not extensively affecting bottom hole pressure. If fluid level in wellbore is confirmed using a fluid sounder, PAGL with 2-7/8" tubing is a feasible option to optimize production from well S-11 when current production falls below ~1.6 MMscfd or well loads up due to unoptimized flow in larger 4-1/2" tubing.

Chapter-4: Summary, Conclusions and Recommendations for Future Work

Summary

This study focuses on the selection of an artificial lift system for dewatering gas wells. A design & review workflow is suggested that can be used to compare artificial lift technologies specific to the deliquification application. This workflow includes production analysis that quantifies current production trends, decline rates, and develops a baseline nodal analysis model. Further, critical gas rate analysis is used to confirm liquid loading. Artificial lift design is conducted for all applicable lift options, and incremental production is predicted using nodal analysis software. Results are compared with the baseline model, and the most optimum lift system is recommended.

The critical gas rate is discussed in detail as a tool to predict the onset of liquid loading. Widely used correlations and their limitations are presented. Based on the drawbacks of published models, a weighted average technique is suggested to estimate the critical unloading rate for gas wells. Further, a separate discussion introduces machine learning methods that use published datasets to predict the critical gas rate. Both the weighted average and machine learning techniques are shown to agree in predicting the critical rate.

Conclusions

The weighted average critical rate technique is found to fit published datasets of several authors better than most other correlations. The error achieved with Turner's dataset is ~20%, while with Coleman's dataset is ~11%. Excellent match is also achieved with Awolusi's dataset that consists of ultra-low producers. These validations endorse the universal applicability of weighted average critical rate for most well types, regardless of their pressure, wellbore design and other parameters.

The working of weighted average critical rate and design & review workflow is tested on a field in Lower Indus Basin, Pakistan. S-field produces from a gas reservoir that has entered its late-life, with significant water production in many wells. A total of 10 wells are evaluated from which 3 are recommended for artificial lift installation based on their current performance, while rest don't require immediate intervention. However, the workflow is completed on these candidates as well to suggest why they aren't selected. Conventional gas lift is recommended for well S-5, which is

significantly loaded under current condition. Gas lift with 2-7/8” re-completion is suggested for well S-10 while Plunger Assisted Gas Lift is recommended for well S-11 when its production drops below ~1.6 MMscfd. These applications endorse the practicality of developed design & review workflow, and also aids the operator of these fields in their development plan.

Recommendations for Future Work

The outcome of this study is a new method to estimate critical gas rate that is applicable to most wells regardless of their characteristics. This critical rate is used to confirm if liquid loading is the reason behind production decline in gas wells. If such is the case, a design & review workflow is suggested that can be used to compare all applicable artificial lifts for deliquification, to select the most effective solution. To further improve the applicability and effectiveness of this study, following is recommended as future work

- Validate and improve the working of weighted average critical rate and machine learning model through a large dataset. The machine learning model is created using sample set of only 241 wells, which is on the lower side. With significantly more wells, a more robust and universally applicable model can be trained using the workflow outlined in this study.
- Design & Review workflow suggested specific artificial lifts for certain wells in S-field. A comparison of predicted and actual production should be conducted after artificial lifts are installed in these wells. This will validate the design approach used in this study and improve it for future wells if discrepancies are found.
- Economics analysis was not part of the design in the suggested workflow. NPV calculation is an essential component and may alter technical decisions if a project is found to be uneconomical, despite being technically possible. Future work can include NPV calculations based predicted production profile and estimated cost of artificial lift.

Appendices

Appendix-A: S-field non selected wells

Well S-1

S-1 is the discovery well drilled in S-field. Producing from the sandstone reservoir at ~3200 m TVD, S-1 has produced more than ~194 BCF gas since 2003. Initial gas production was ~68 MMscfd. Pressure depletion caused rates to decline over the years, and the current gas rate is ~6.6 MMscfd. Water production started in 2016 with an increasing Water-Gas Ratio (WGR). Due to the scarcity of well test data, only annual WGR was available for production and nodal analysis. Figure 79 shows the current wellbore profile of S-1.

Reservoir Pressure	800 psi	Target Interval	3286 m
Current Production	6.6 MMscfd	Following Wellhead Pressure	114 psi

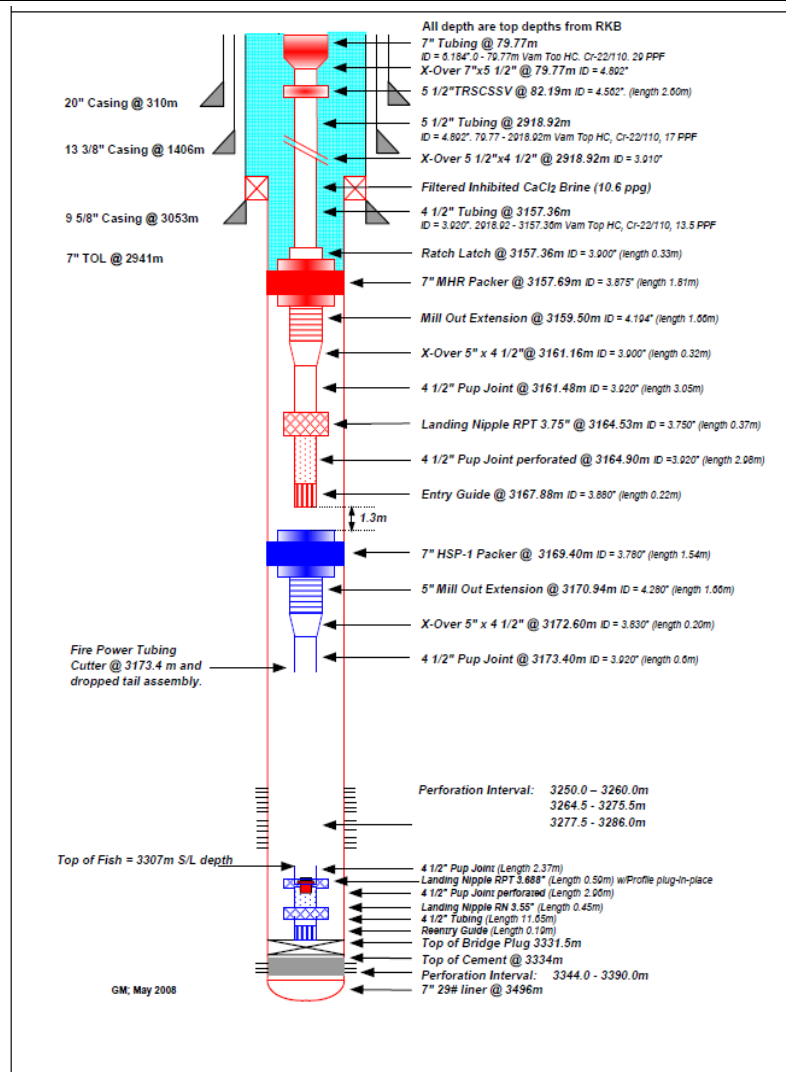


Figure 79 - Well S-1 Wellbore profile

Production Plot

Figure 80 below shows gas production and Flowing Wellhead Pressure (FWHP) for S-1 from 2012. Bottomhole Pressure (BHP) is calculated from measured WHP using the VLP correlation for this data set. This allows the evaluation of changing sand-face pressure to observe unusual trends and anomalies that indicate issues like liquid loading.

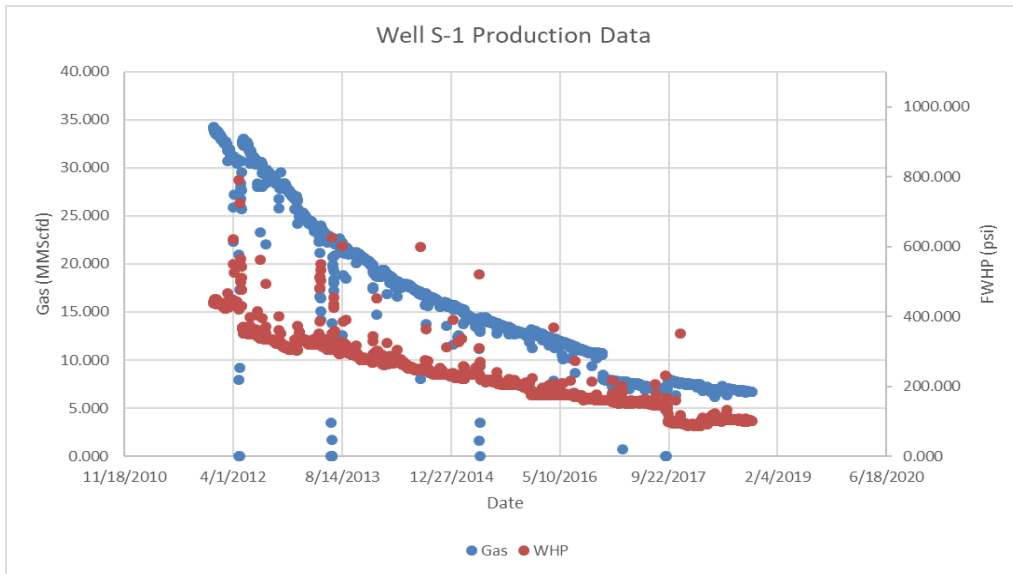


Figure 80 - Well S-1 FWHP Plot

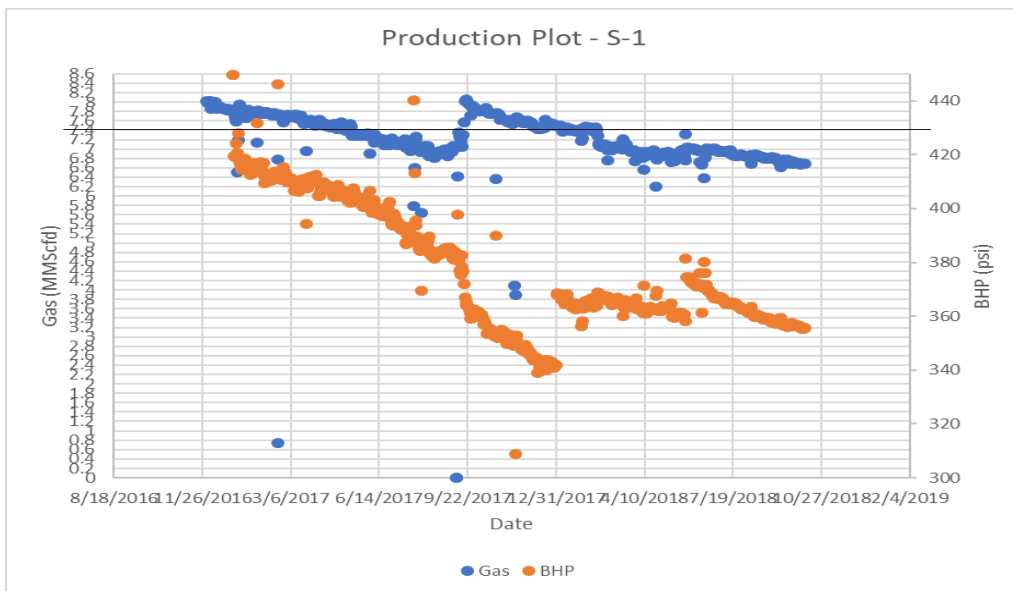


Figure 81 - Well S-1 BHP plot

Figure 81 shows the gas rates and BHP for S-1 from 2016. The solid black line at gas rate ~7.6 MMScfd in Figure 81 depicts the critical gas unloading rate required to offload all fluids from wellbore effectively. Based on the current production rate of ~6.6 MMScfd, current gas rates are only ~13% lower than required critical rates.

An apparent change in trend is observed in BHP data post December 2017. The decline in BHP has changed, which correlates well with the trend in gas rates that have fallen below the critical unloading rate. Moreover, with the loading of water in the wellbore, BHP values had decreased for similar gas rates before and after loading started. This is visible when gas rates in June 2017 and April 2018 are similar at ~6.6 MMScfd; however, BHP is ~400 psi and ~360 psi, respectively. In a stable flow regime, similar gas production should have similar flowing bottom hole pressure. The extra drop in BHP, in this case, is possible due to ineffective liquid unloading that causes additional hydrostatic pressure.

Note that this BHP is calculated from WHP in this case. Assuming frictional pressure is similar for similar gas rates, a decline in WHP (from which we are estimating BHP) can be due to an increase in hydrostatic pressure, which could be caused by additional liquid in the wellbore.

Nodal Analysis

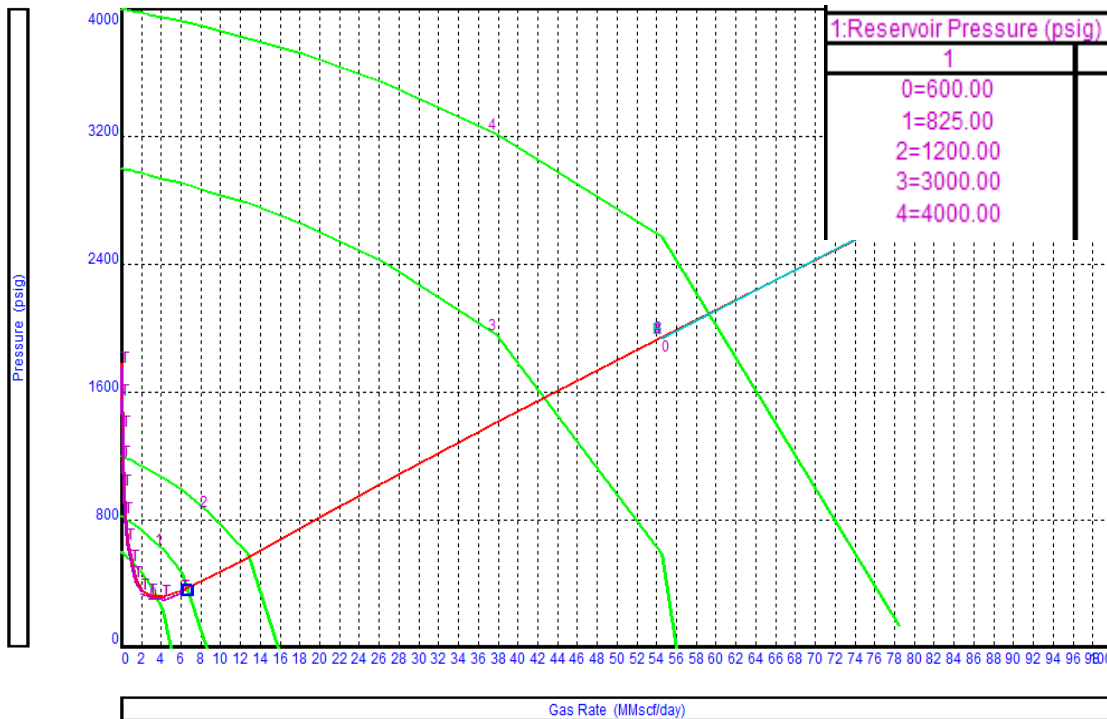


Figure 82 - Well S-1 reservoir pressure sensitivity

Trend analysis of BHP data coupled with critical gas unloading rate suggests possible indications of liquid loading in S-1. However, as current rates are only 13% lower than critical rates, liquid loading is not expected to be severe in this well. Flow stability can also be monitored through a nodal analysis conducted at sand-face (bottom node) and wellhead (top node).

Figure 82 shows the sensitivity of reservoir pressure by changing the IPR curve. Initially, the well produced ~64 MMscfd at virgin reservoir pressure of ~4000 psi (0.433 psi/ft gradient). Reservoir pressure was reduced to ~825 psi to match current flowing conditions.

Although current gas rates are below the critical unloading rate for this wellbore profile, the delta between the two rates is only 13%. Further, due to the relatively high gas rate and low water production (WGR 56), the flow regime is still dominated by gas in the wellbore (mist flow). This suggests stable flow in the wellbore, which is confirmed by the VLP stability plot (Figure 83), where current production is on the right of minimum.

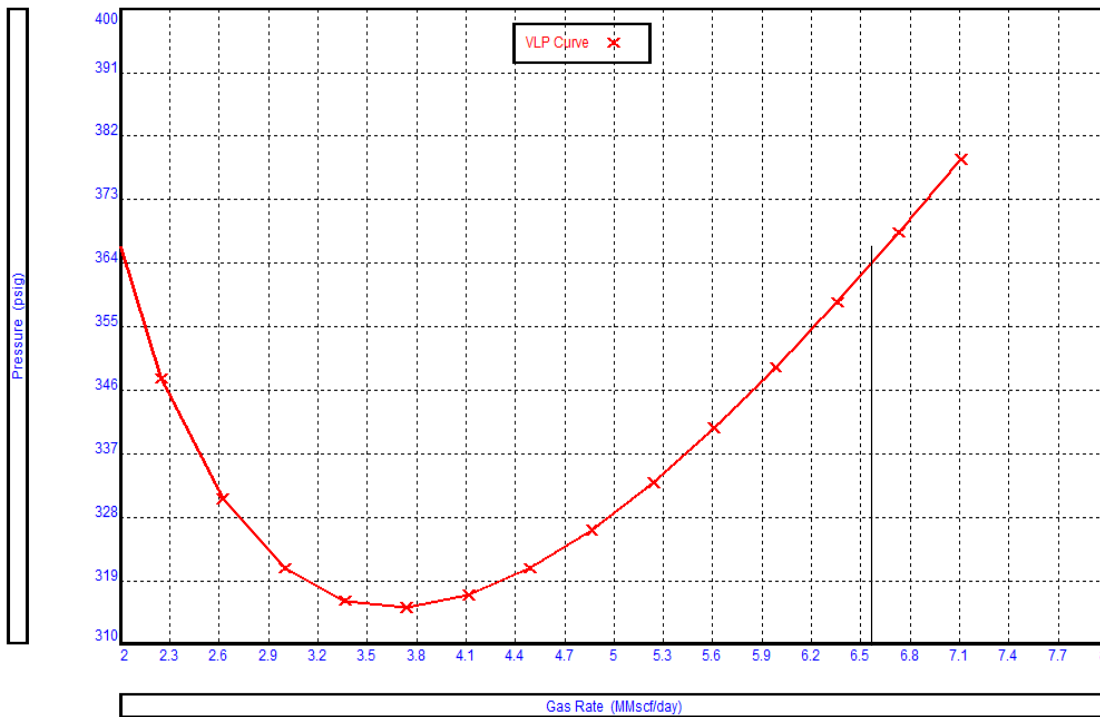


Figure 83 - Well S-1 VLP stability plot

Another way to quantify flow stability is through flow-point analysis (Figure 84). Flow-point is defined as the maximum (apex) of outflow performance curve (OPR) – nodal analysis using wellhead as a solution node. A system cannot flow stably at gas rates lower than the apex gas rate.

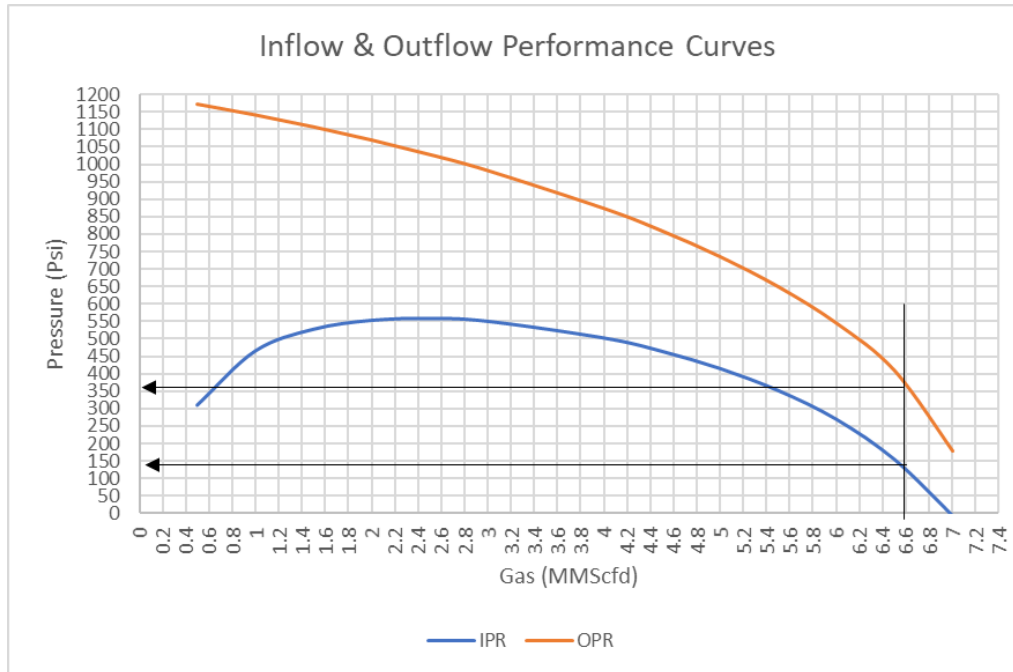


Figure 84 - Well S-1 flow-point analysis

Salinity Analysis

Source of liquid production in the wellbore can also be used to designate the severity of liquid loading. Although any fluid – condensate, formation water and condensed water – can cause an increase in hydrostatic pressure and deteriorate well performance, often formation water is most detrimental to production. This is largely because the liquid is introduced at sand-face from formation and in lower velocities, is not carried towards the surface. The other two sources of fluids are often near the wellbore; therefore, they have to travel a shorter distance.

In the absence of production logs, salinity data from produced water is used to classify condensed water from formation water. Commonly, chloride or sodium chloride content form the basis of salinity classification. Gorrell 1958 suggest the following brackets:

0 to 10,000 ppm NaCl – Fresh/Brackish water

10,000 to 100,000 ppm NaCl – Salty water

Over 100,000 ppm NaCl – Brine

As S-1 water has ~202 ppm salinity, based on the above categories, produced water is most likely condensed in this well and is sourced near the surface.

Artificial Lift Analysis

Production data coupled with nodal analysis for well S-1 suggests liquid loading has recently started in the well as gas rates continue to decline. However, nodal analysis suggests that the flow regime in the wellbore is stable, mist flow. This is expected as current gas rates are only 13% lower than critical rates, and source of water is condensed water. Therefore, the application of artificial lift in this well is not an absolute necessity at this moment in well's life. However, the following systems can be reviewed to evaluate if they provide enough increment in gas production to justify the economics of installation.

Gas Lift

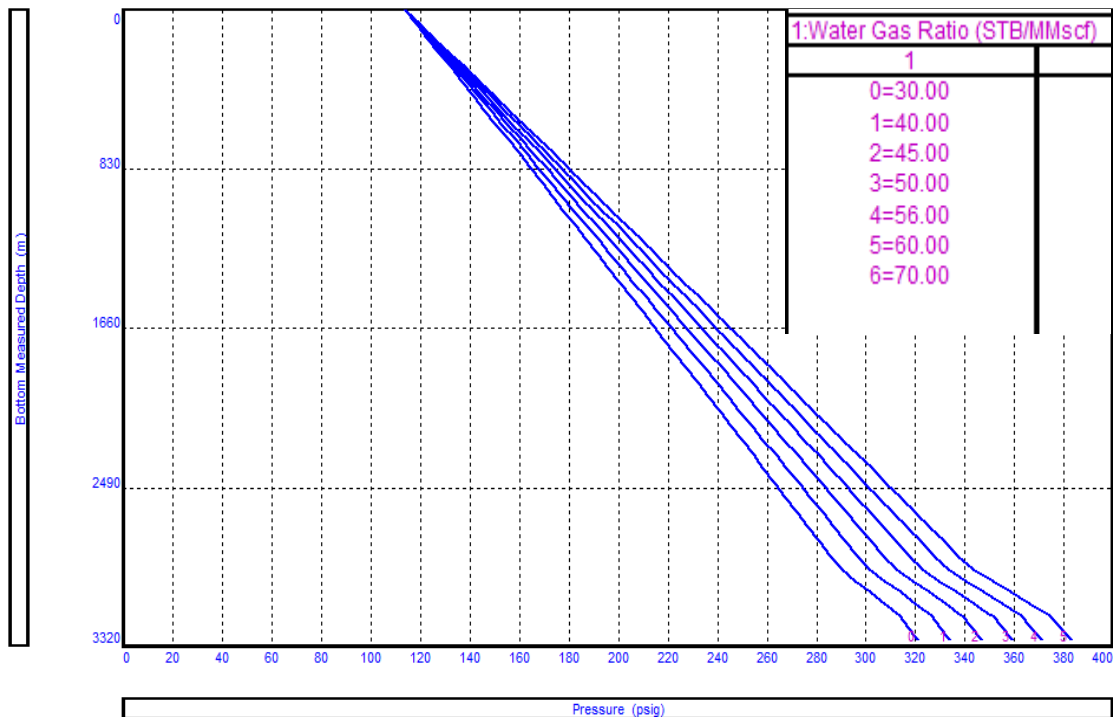


Figure 85 - Well S-1 WGR sensitivity

A sensitivity run is made on bottom hole pressure with changing WGR to evaluate if the application of any artificial lift that requires gas injection (in the wellbore) will aid in improving production. For most conventional reservoirs such as in well S-1, reduction in BHP will generally increase hydrocarbon production.

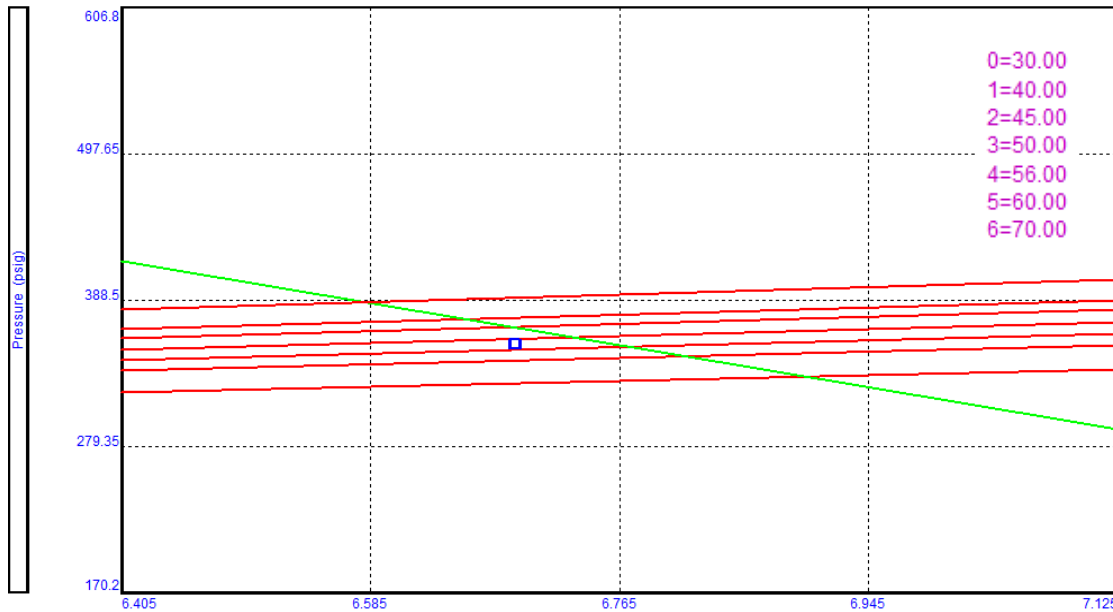


Figure 86 - Well S-1 WGR sensitivity on system plot

As seen in Figure 85, there is a decrease in BHP with decreasing WGR. This suggests that the injection of gas may be beneficial in improving the performance of this well. However, it should be noted that this is a qualitative measure of improvement, as it does not quantify the extent of improvement. That is quantified through system analysis with WGR sensitivities.

Figure 86 shows the effect of decreasing WGR. As WGR decreases from 56 to 45 and further to 30 STB/MMscf (achieving 45 will require a gas injection of 1 MMscfd gas), the resultant increase in hydrocarbon production is negligible - ~0.1 MMScfd. This is an expected result as the flow regime in well is already mist flow. Therefore, the increase in gas content does not improve flow dynamics drastically. It is impractical to conduct gas lift design at this point as incremental gas will not be sufficient to justify gas lift costs.

Velocity String / Smaller ID Tubing

As the well S-1 was completed with large tapered 7" x 5-1/2" tubing combination to produce high initial rates; this may cause slight inefficiencies at this stage of production. Sensitivity analysis is conducted by introducing a 1.5" Coiled Tubing (CT) in the wellbore as a velocity string to improve well dynamics.

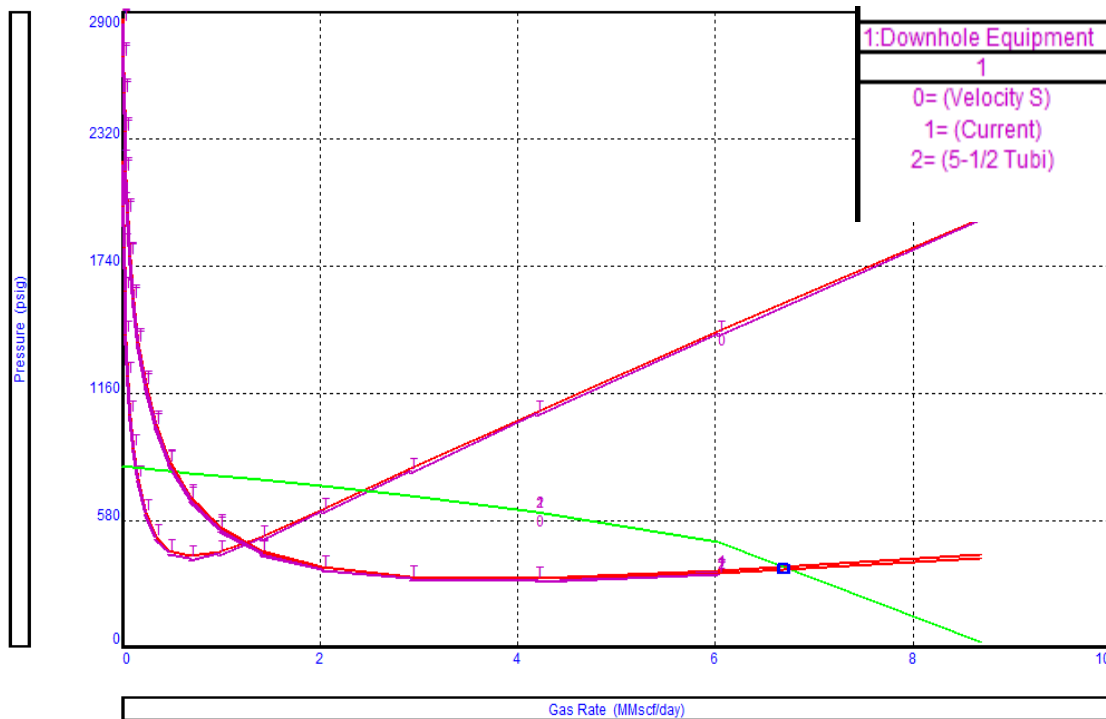


Figure 87 - Well S-1 Lower ID/Velocity string comparison

Similar to gas-lift results, using a smaller ID tubing in the well at this stage reduces the performance of the well by introducing additional friction pressure, which ultimately results in lower gas production. As current configuration consists of tapered tubing that has 4-1/2" at the lower end, using 5-1/2" tubing (ID = 4.892") results in slightly lower frictions and gas rate of ~6.7 MMscfd. This incremental production will again fall short of allowing any intervention in this well due to poor economics, therefore conducting further design will not yield any benefit.

Plunger Assisted Gas Lift

With current 4-1/2" Tubing and 7" Casing (Plunger BHA @ 3170m)

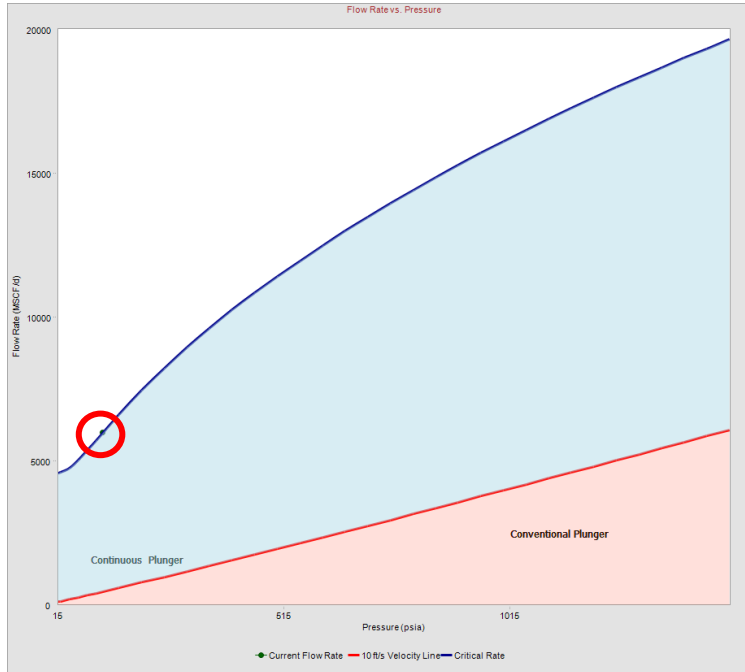


Figure 88 - Well S-1 PAGL type plot

Figure 88 shows the flow rate vs pressure plot to select a plunger type. Current modeled conditions are shown in the red circle in Figure 88. Similar to results predicted by the Weighed Average Critical Rate (WACR) model, current production falls within 25% of the critical rate. Therefore, in this instance, continuous/conventional plunger lift is not required for this well.

As this plot only suggests feasibility regardless of design. To confirm applicability, plunger design is

required.

Plunger Assisted Gas Lift Design		Results	
Well Name	S-1	Required Casing Injection Pressure (psi)	1897
PAGL Type	Continuous	Injection pressure Limited by	Surface
Target Gas Production (Mscf/d)	6000	Calculated WHP (psi)	1877
Target Liquid Production (STB/d)	50	Volume of Liquid Slug (bbl)	0.75
Tubing ID (in)	3.895	Number of Cycles per day	66
Tubing OD (in)	4.5	Gas Velocity at bottom hole (ft/sec)	205.16
Design WHP (psi)	30	Minimum Gas velocity (ft/sec)	54.47
Expected Flowing BHP (psi)		PAGL Possible?	No
Fall Rate in Gas (ft/min)	800		
Fall Rate in Liquid (ft/min)	400		
Rise Rate (ft/min)	700		

Table 19 - Well S-1 PAGL design with current 4-1/2" tubing

Table 19 depicts the design of PAGL with current tubing. Due to the high critical rate in 4-1/2” tubing, installing plunger requires very high surface gas injection pressure to lift fluid and plunger to surface which is impractical. Further, the GLR for this well is ~18 Mscf/STB. As per the GLR cutoff criteria, this well is not a suitable PAGL candidate. With very high current gas rates and a stable flow regime, a plunger lift is not suitable for this well.

Well S-1 Summary

Observations drawn from the analysis conducted suggest the onset of liquid loading has occurred in well S-1. However, its impact is small in current flowrates. Further, system analysis and tubing curves suggest flow in the wellbore is relatively stable, and the addition of any artificial lift technique would not drastically improve gas production. Further, in the current scenario, the most effective technique to improve the performance of well S-1 would be through reservoir stimulation, if such a treatment is required based on well-testing and pressure survey data.

Well S-2

The well S-2 is the appraisal well drilled in S-field. Producing from the sandstone reservoir at ~3400 m TVD, S-2 has produced more than 137.6 BCF gas since 2003. Initial gas production was ~60 MMScfd. Pressure depletion caused rates to decline over the years, and the current gas rate is ~3.7 MMScfd. Water production started in 2016 with increasing WGR. Due to the scarcity of well test data, only annual WGR was available for production and nodal analysis. Figure 89 shows the current wellbore profile of S-2.

Reservoir Pressure	700 psi	Target Interval	3447 m
Current Production	3.7 MMscfd	Following Wellhead Pressure	127 psi

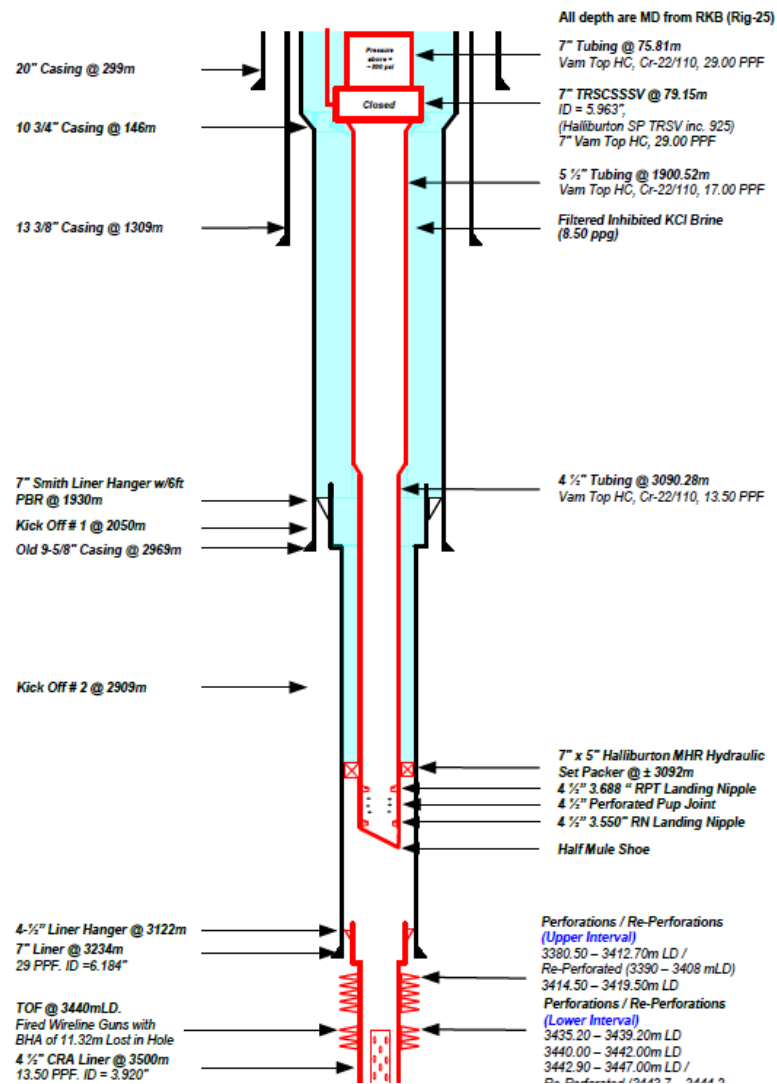


Figure 89 - Well S-2 wellbore profile

Production Plot

Figure 90 below shows gas production and Flowing Wellhead Pressure (FWHP) for S-2 from 2013. Using this data set, we can calculate Bottomhole Pressure (BHP) from measured WHP using VLP correlation. This allows the evaluation of changing sand-face pressure to observe unusual trends and anomalies that may indicate issues like liquid loading.

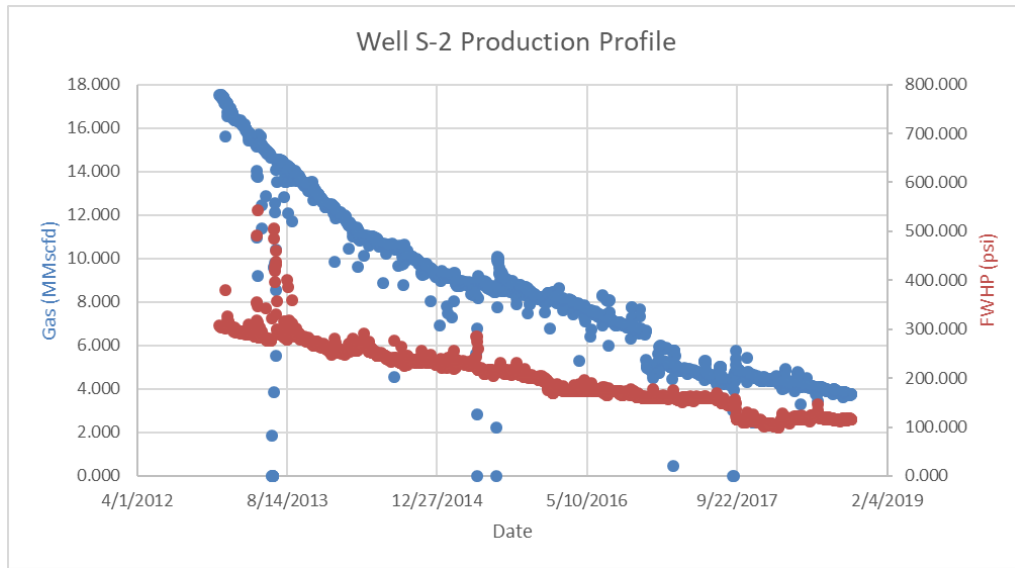


Figure 90 - Well S-2 FWHP plot

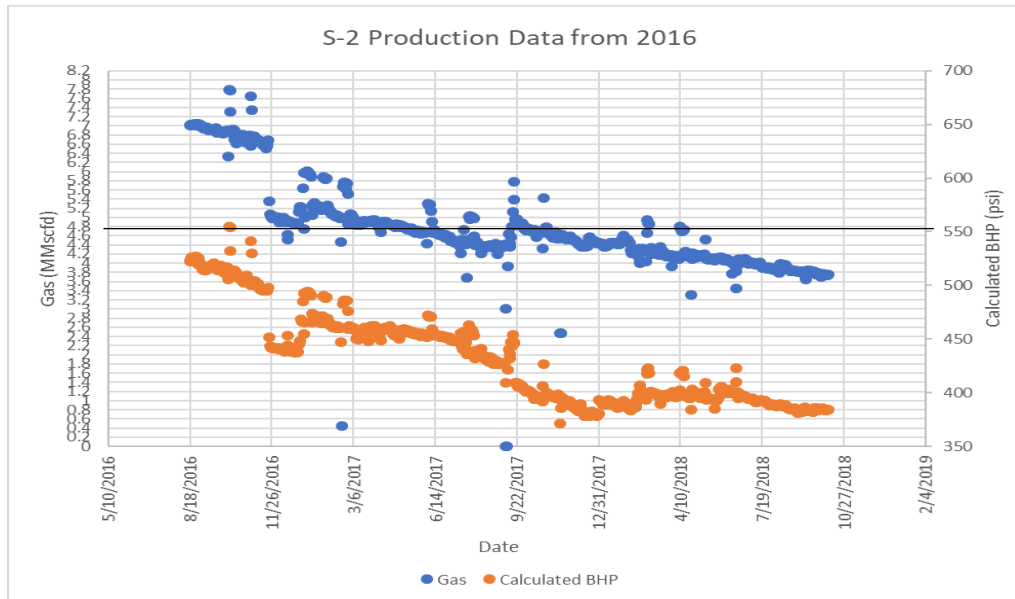


Figure 91 - Well S-2 BHP Plot

Figure 91 shows the gas rates and BHP for S-2 from 2016. The solid black line at gas rate ~4.6 MMScfd in Figure 91 depicts the critical gas unloading rate required to offload all fluids from wellbore effectively. Based on the current production rate of ~3.7 MMScfd, current gas rates are ~24% lower than required critical rates.

An apparent change in trend is observed in BHP data post September 2017. The decline in BHP has changed, which correlates well with the trend in gas rates that have fallen below the critical unloading rate. Moreover, with the loading of water in the wellbore, BHP values had decreased for similar gas rates before and after loading started. This is visible when gas rates in June 2017 and December 2017 are similar at ~4.4 MMScfd; however, BHP is ~450 psi and ~380 psi, respectively. In a stable flow regime, similar gas production should have similar flowing bottom hole pressure. The extra drop in BHP, in this case, is possibly due to ineffective liquid unloading that causes additional hydrostatic pressure.

Nodal Analysis

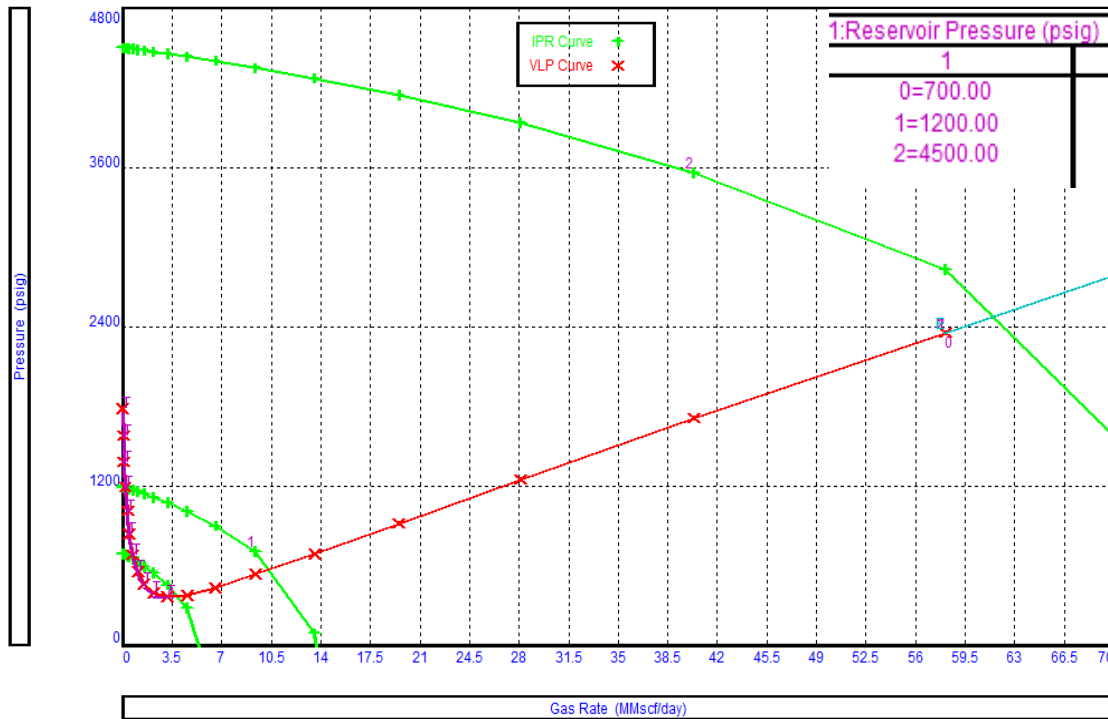


Figure 92 - Well S-2 reservoir pressure sensitivity

Figure 92 shows the sensitivity of reservoir pressure by changing the IPR curve. Initially, the well produced ~60 MMScfd at virgin reservoir pressure of ~4300 psi (0.433 psi/ft gradient). Reservoir pressure is reduced to ~700 psi to match the current flowing conditions.

Similar to well S-1, the small delta between critical gas rate and current gas rate suggest liquid loading is not severe in this well. Further, due to the relatively high gas rate and low water production (WGR 82 STB/MMscf), the flow regime is still dominated by gas in the wellbore (mist flow). This suggests stable flow in the wellbore, which is confirmed by the VLP stability plot (Figure 93), where current production is on the right of minimum.

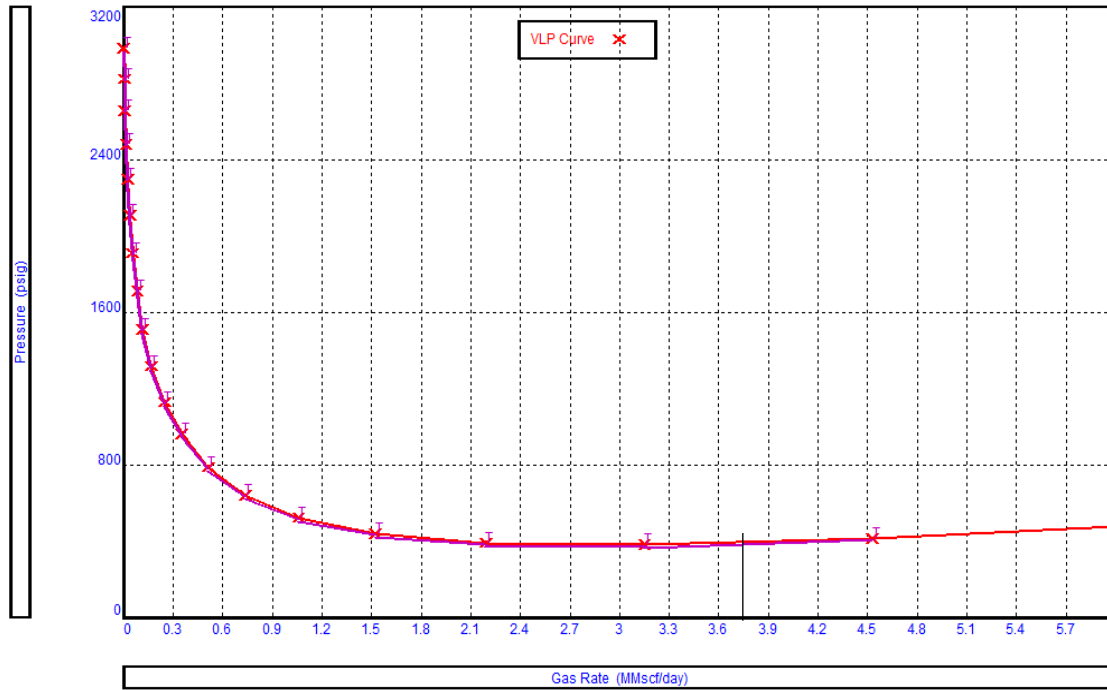


Figure 93 - Well S-2 VLP Stability plot

Note that the current gas rate in well S-2 is very near to the minimum of the VLP curve. If compared with the VLP curve of well S-1, the flow dynamics in well S-2 are significantly more unoptimized. This is expected as wellbore profile of both wells are very similar; however, current gas rates of S-2 are only ~60% of S-1.

Salinity Analysis

Source of liquid production in the wellbore can also be used to designate the severity of liquid loading. Although any fluid – condensate, formation water and condensed water – can cause an increase in hydrostatic pressure and deteriorate well performance, often formation water is most detrimental to production. This is largely because the liquid is introduced at sand-face from

formation and in lower velocities, is not carried towards the surface. The other two sources of fluids are often near the wellbore; therefore, they have to travel a shorter distance.

In the absence of production logs, salinity data from produced water is used to classify condensed water from formation water. Commonly, chloride or sodium chloride content form the basis of salinity classification. Gorrell 1958 suggest the following brackets:

0 to 10,000 ppm NaCl – Fresh/Brackish water

10,000 to 100,000 ppm NaCl – Salty water

Over 100,000 ppm NaCl – Brine

As S-2 water has ~2862 ppm salinity, based on the above categories, produced water is most likely condensed in this well and being sourced near the surface.

Artificial Lift Techniques

Gas Lift

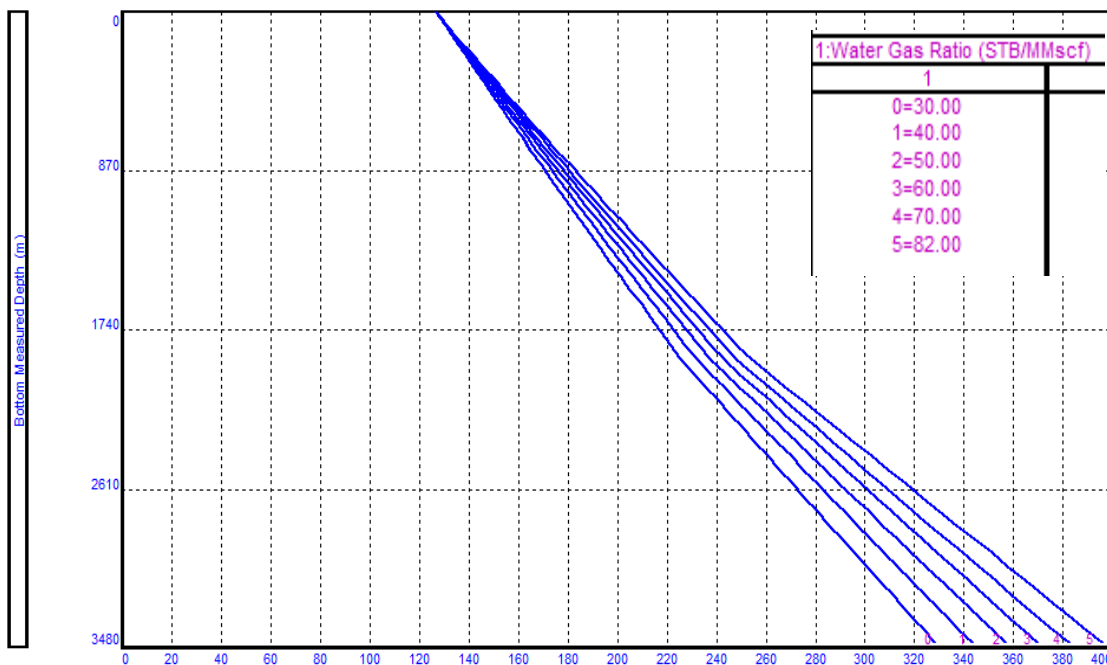


Figure 94 - Well S-2 WGR sensitivity

A sensitivity run is made on bottom hole pressure with changing WGR to evaluate if the application of any artificial lift that requires gas injection (in the wellbore) will aid in improving

production. For most conventional reservoirs, reduction in BHP will generally increase hydrocarbon production.

Similar to S-1, lowering WGR by injecting gas in the system does result in lower bottom hole pressure, as evident in Figure 94. However, as experienced in well S-1, the extent of this reduction coupled with current reservoir parameters are not enough to improve gas production to justify installing a gas lift. WGR sensitivities quantify this in system analysis shown in Figure 95. The increment expected if WGR is reduced from ~82 to ~60 STB/MMscf by the addition of external gas is only ~0.15 MMscfd. Therefore, installing a gas lift in well S-2 at this instance will most likely yield negative economic value.

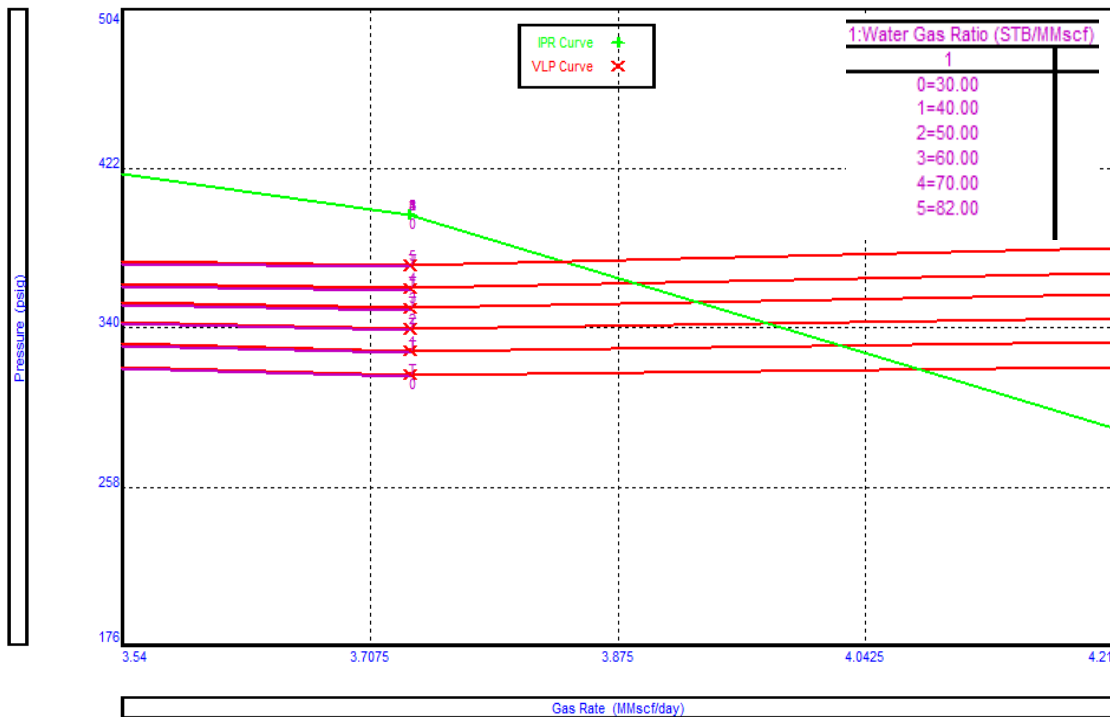


Figure 95 - Well S-2 WGR Sensitivity on system plot

Plunger Assisted Gas Lift

With 5-1/2" x 4-1/2" tubing

Figure 96 shows the flow rate vs pressure plot to select a plunger type. Current modeled conditions are shown in the red circle in Figure 96. Similar to the results predicted by the WACR model, current production falls within 25% of the critical rate. Therefore, in this instance, continuous/conventional plunger lift is not required for this well.

This plot only suggests feasibility regardless of design. To confirm applicability, plunger design is required.

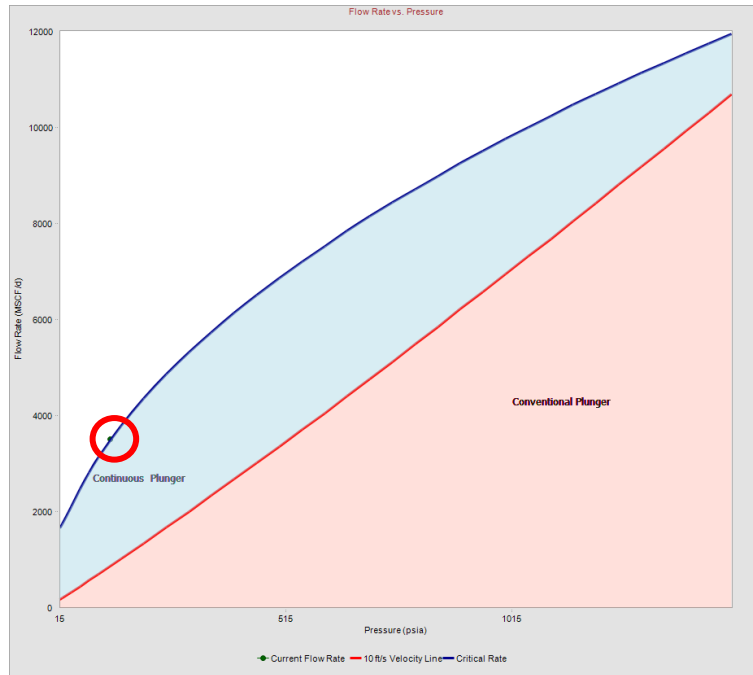


Figure 96 - Well S-2 PAGL type plot

Plunger Assisted Gas Lift Design		Results	
Well Name	S-2	Required Casing Injection Pressure (psi)	2193
PAGL Type	Continuous	Injection pressure Limited by	Surface
Target Gas Production (Mscf/d)	3500	Calculated WHP (psi)	2173
Target Liquid Production (STB/d)	70	Volume of Liquid Slug (bbl)	1.18
Tubing ID (in)	4.895	Number of Cycles per day	59
Tubing OD (in)	5.5	Gas Velocity at bottom hole (ft/sec)	137.7
Design WHP (psi)	30	Minimum Gas velocity (ft/sec)	63.67
Expected Flowing BHP (psi)		PAGL Possible?	No
Fall Rate in Gas (ft/min)	800		
Fall Rate in Liquid (ft/min)	400		
Rise Rate (ft/min)	700		

Table 20 - Well S-2 PAGL design with current 5-1/2" x 4-1/2" tubing

Table 20 depicts the design of PAGL with current tubing. Due to the high critical rate in 5-1/2" tubing, installing plunger requires very high surface gas injection pressure to lift fluid and plunger to surface which is impractical. Further, the GLR for this well is ~12 Mscf/STB. As per the GLR

cutoff criteria, this well is not a suitable PAGL candidate. With very high current gas rates and a stable flow regime, a plunger lift is not suitable for this well.

Velocity String / Smaller ID Tubing

Velocity string or smaller diameter tubing can be used in well S-2 in an attempt to improve production and wellbore hydraulics. Different combinations of strings are evaluated to quantify performance. The sensitivities include:

- Current Profile: 7" x 5-1/2" x 4-1/2" Tubing with ~320m of 7" casing flow
- Smaller diameter tubing: Installing 2-7/8" tubing all the way
- Velocity String: Install 1.5" CT in 7" section of wellbore

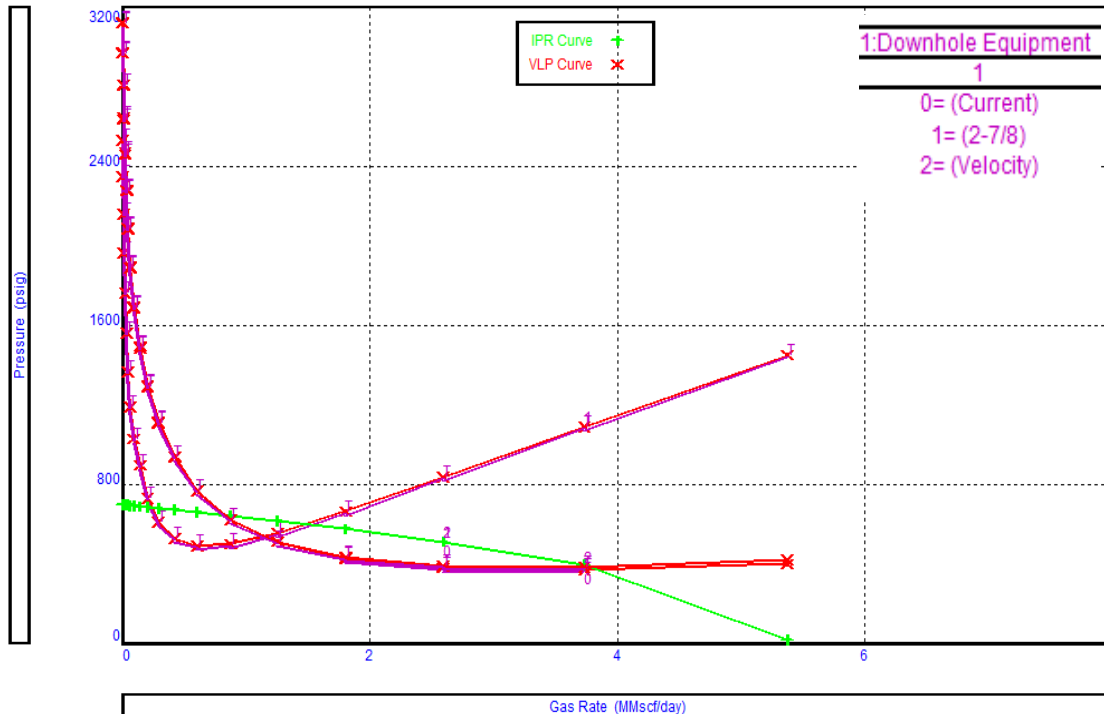


Figure 97 - Well S-2 Lower ID/velocity string comparison

As seen in Figure 97, the use of smaller diameter tubing significantly deteriorates performance due to very high friction pressures, making it an unfeasible option. Application of velocity string in larger tubing sections (7") does yield slight improvement in gas rates (~0.1 MMscfd); however, this would not be adequate to justify the cost of re-completing the well.

Well S-2 Summary

Observations drawn from the analysis conducted suggest the onset of liquid loading has occurred in well S-2; however, its impact is small in the current scenario. Further, system analysis and tubing curves suggest that flow in the wellbore is relatively stable. Stability analysis, coupled with salinity data, suggests produced water is condensed and is not directly causing an increase in the bottom hole pressure. Any addition of artificial lift at this instance would not be economical.

Well S-4

The well S-4 is a development well drilled in S-field. Producing from the sandstone reservoir at ~3260m TVD, S-4 has produced more than 24.5 BCF gas since 2003. Initial gas production was ~12 MMscfd. Pressure depletion caused rates to decline over the years, and the current gas rate is ~3.3 MMscfd. Water production started in 2009, with increasing WGR. Due to the scarcity of well test data, only annual WGR was available for production and nodal analysis. Figure 98 shows the current wellbore profile of S-4.

Reservoir Pressure	1400 psi	Target Interval	3260 m
Current Production	3.3 MMscfd	Following Wellhead Pressure	115 psi

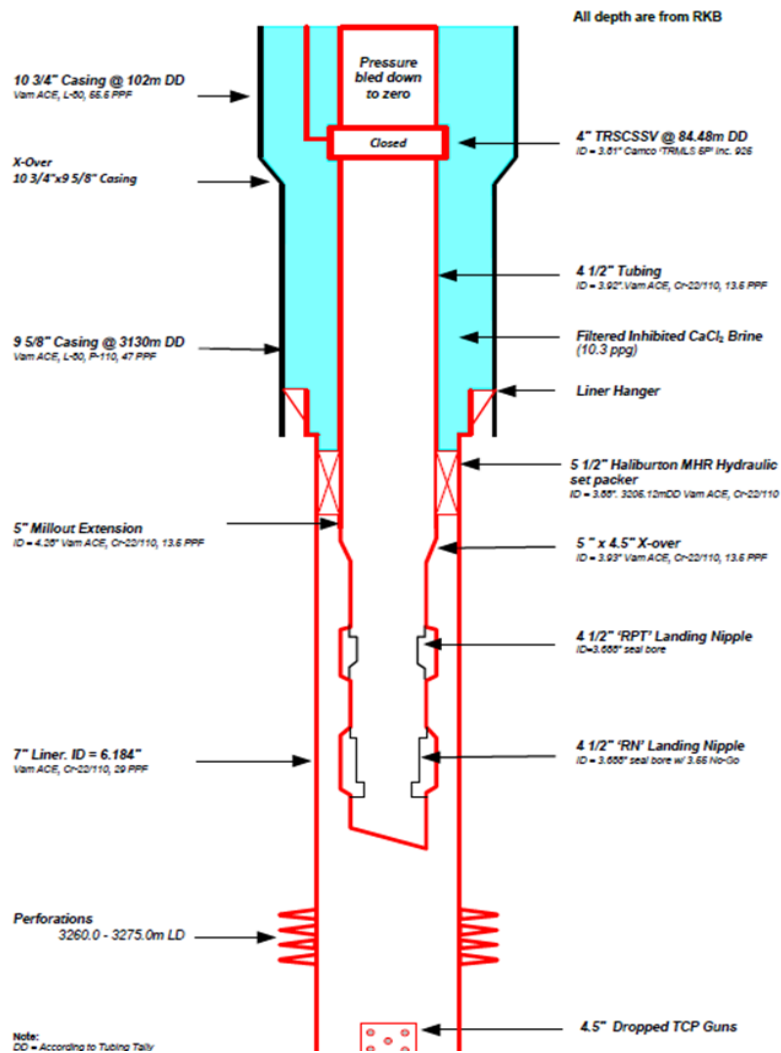


Figure 98 - Well S-4 wellbore profile

Production plot

Figure 99 shows gas production and Flowing Wellhead Pressure (FWHP) for S-4 from 2012. Bottomhole Pressure (BHP) is calculated from measured WHP using the VLP correlation for this data set. This allows the evaluation of changing sand-face pressure to observe unusual trends and anomalies that may indicate issues like liquid loading.

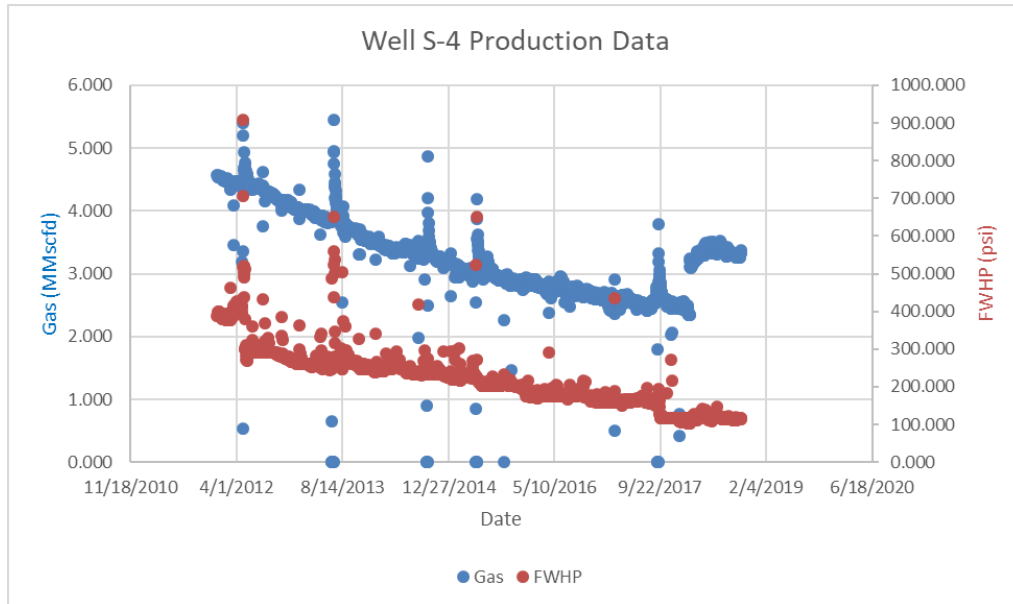


Figure 99 - Well S-4 FWHP plot

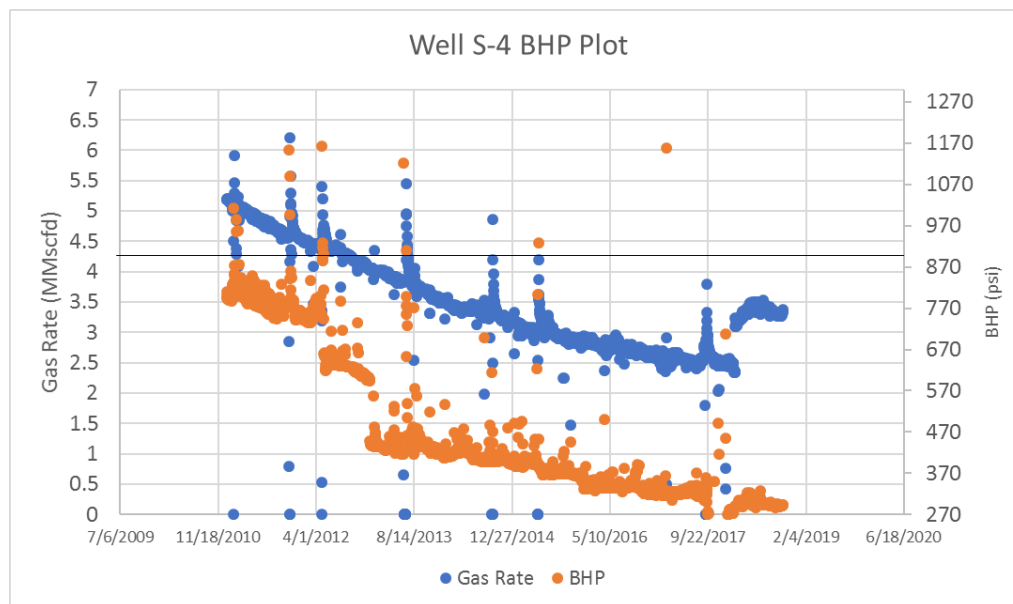


Figure 100 - Well S-4 BHP Plot

Figure 100 shows the gas rates and BHP for S-4 from 2012. The solid black line at gas rate ~4.4 MMScfd in Figure 100 depicts the critical gas unloading rate required to offload all fluids from wellbore effectively. Based on the current production rate of ~3.1 MMScfd, current gas rates are ~26% lower than required critical rates.

The well S-4 has a steady decline in BHP with a relatively similar slope. This suggests that liquid loading has not affected bottom hole pressure significantly. The well S-4 has the lowest initial gas production relative to other S-field wells, and water production is reported since 2009. Despite low gas rates and early water breakthrough, WGR for well S-4 is only 20 STB/MMscf, which suggests that water production issue is not significant. This can be confirmed further with nodal analysis and an attempt to improve gas production through a reduction in WGR.

Nodal Analysis

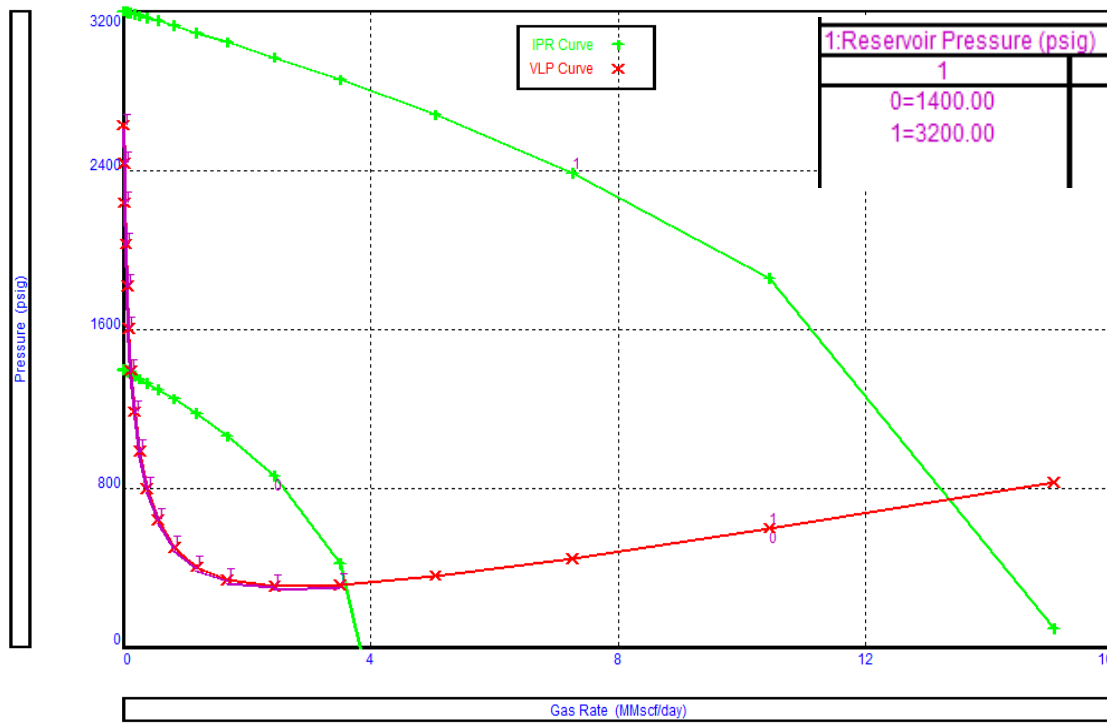


Figure 101 - Well S-4 reservoir pressure sensitivity

Figure 101 shows the sensitivity of reservoir pressure by changing the IPR curve. Initially, the well produced ~12 MMScfd at a depleted reservoir pressure of ~3200 psi. Reservoir pressure is reduced to ~1400 psi to match the current flowing conditions.

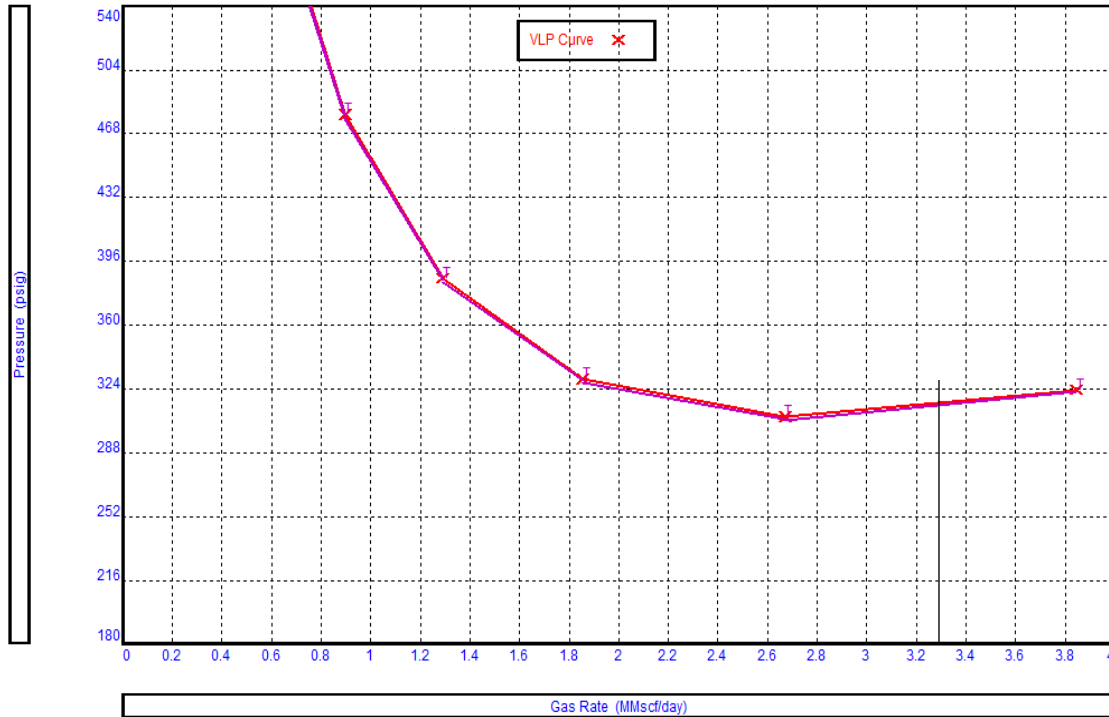


Figure 102 - Well S-4 VLP stability plot

The small delta between critical gas rate and current gas rate suggest liquid loading is not severe in this well. Further, due to the relatively high gas rate and low water production (WGR 20 STB/MMscf), the flow regime is still dominated by gas in the wellbore (mist flow). This suggests stable flow in the wellbore, which is confirmed by the VLP stability plot (Figure 102), where current production is on the right of minimum.

The flow-point analysis shown in Figure 103 suggests a well pressure differential of ~100 psi, which is lower than other wells, suggesting liquid loading is not severe. This supports the findings through VLP stability. As production is on the right of the OPR curve maximum, current flow is stable in the wellbore.

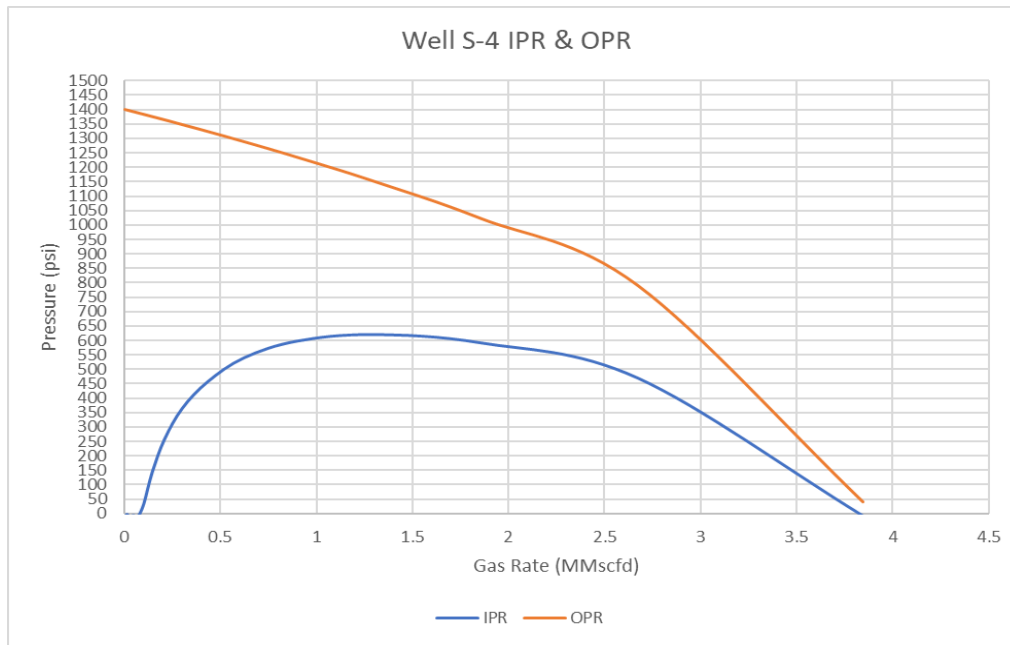


Figure 103 - Well S-4 flow-point analysis plot

Salinity Analysis

Source of liquid production in the wellbore can also be used to designate the severity of liquid loading. Although any fluid – condensate, formation water and condensed water – can cause an increase in hydrostatic pressure and deteriorate well performance, often formation water is most detrimental to production. This is largely because the liquid is introduced at sand-face from formation and in lower velocities, is not carried towards the surface. The other two sources of fluids are often near the wellbore; therefore, they have to travel a shorter distance.

In the absence of production logs, salinity data from produced water is used to classify condensed water from formation water. Commonly, chloride or sodium chloride content form the basis of salinity classification. Gorrell 1958 suggest the following brackets:

0 to 10,000 ppm NaCl – Fresh/Brackish water

10,000 to 100,000 ppm NaCl – Salty water

Over 100,000 ppm NaCl – Brine

As S-4 water has ~32176 ppm salinity, based on the above categories, produced water is likely coming from the formation.

Artificial Lift Techniques

Gas Lift

A sensitivity run is made on bottom hole pressure with changing WGR to evaluate if the application of any artificial lift that requires gas injection (in the wellbore) will aid in improving production. For most conventional reservoirs, reduction in BHP will generally increase hydrocarbon production.

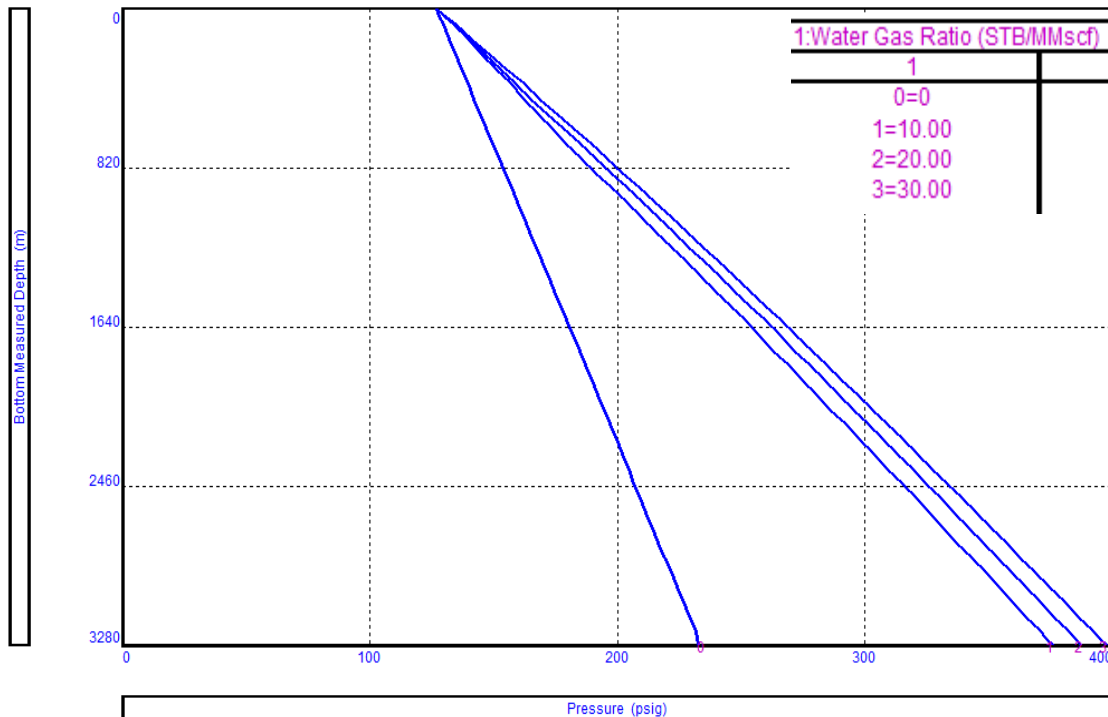


Figure 104 - Well S-4 WGR Sensitivity

The current WGR in well S-4 is ~20 STB/MMscf, which is low compared to other S-field wells. Given the low rate and negligible BHP decline observed in WGR sensitivity on BHP data (Figure 104), a gas lift might not be feasible in improving production from well S-4. This is confirmed by WGR sensitivity on system analysis, as shown in Figure 105, that suggests an increment of only ~0.2 MMScfd with gas lift.

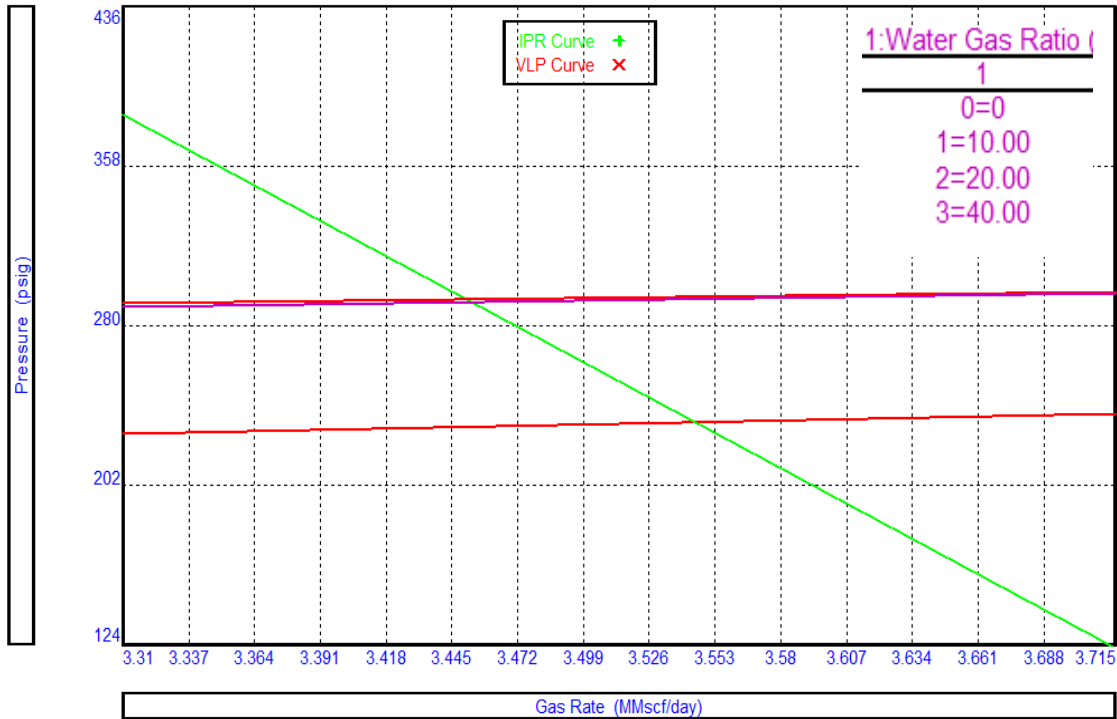


Figure 105 - Well S-4 WGR sensitivity on system plot

Plunger Assisted Gas Lift

With 4-1/2" tubing (Plunger BHA @ 3206m)

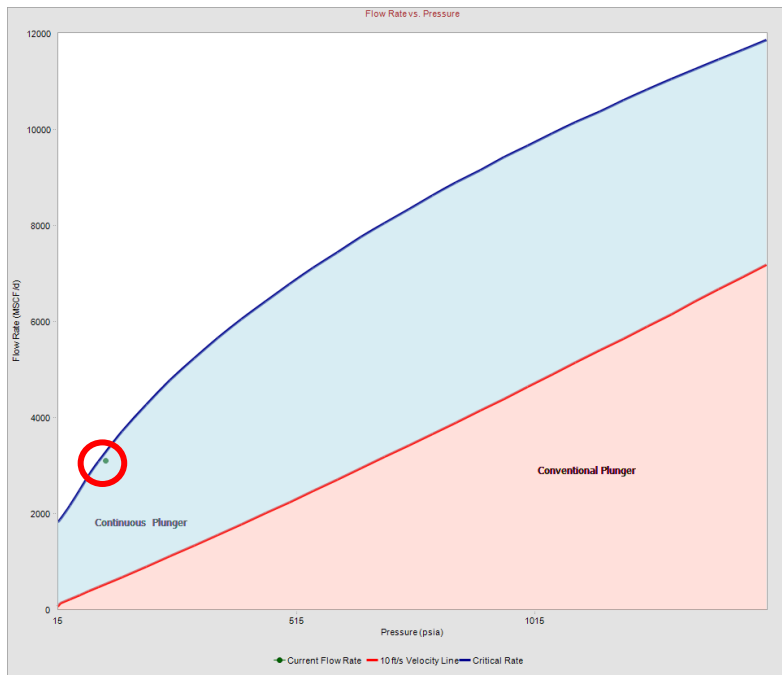


Figure 106 - Well S-4 PAGL type plot

Figure 106 shows the flow rate vs pressure plot to select a plunger type. Current modeled conditions are shown in the red circle in Figure 106. Similar to the results predicted by the WACR model, current production falls within 25% of the critical rate.

As the current production is fairly stable and on borderline for the requirement of a plunger lift, it seems its installation may not add

further value to the well at this instance. Therefore continuous/conventional plunger lift is evaluated for this well.

Velocity String / Smaller ID Tubing

Velocity string or smaller diameter tubing can be used in well S-4 in an attempt to improve production and wellbore hydraulics. Different combinations of strings are evaluated to compare performance. The sensitivities conducted include:

- Current Profile: 7" x 5-1/2" x 4-1/2" Tubing with ~320m of 7" casing flow
- Smaller diameter Tubing: Installing 2-7/8" tubing all the way
- Velocity String: Install 1" CT in 4-1/2" Tubing

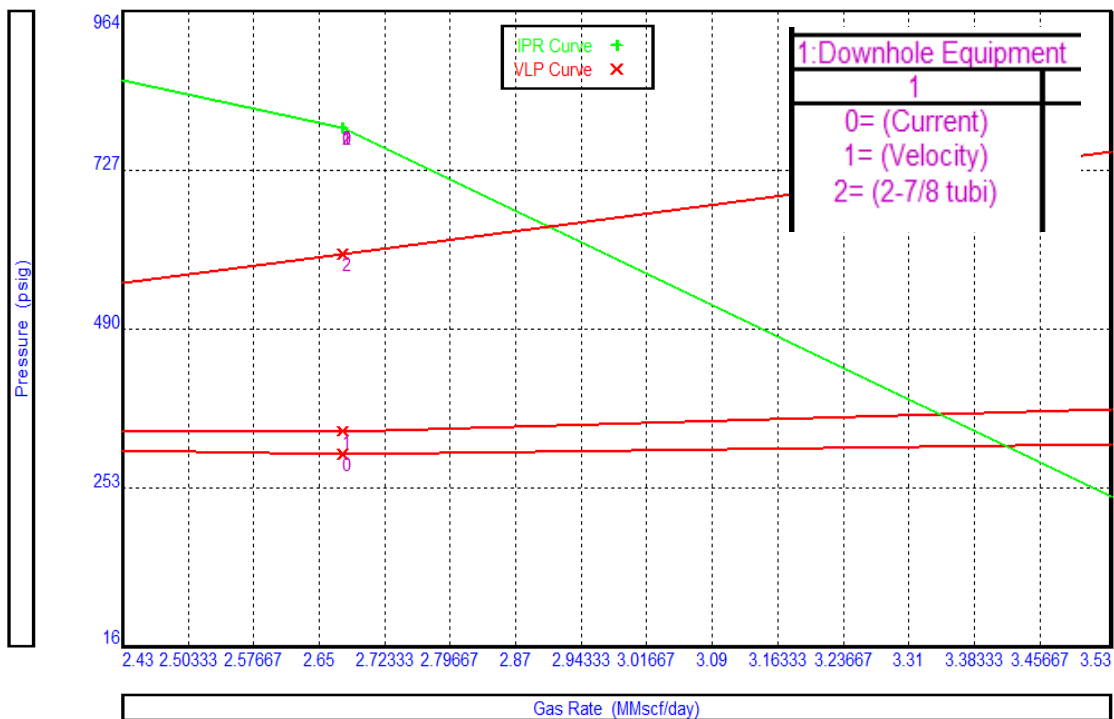


Figure 107 - Well S-4 Lower ID/velocity string comparison

As seen in Figure 107, using smaller diameter tubing significantly deteriorates performance due to very high friction pressures, making that an unfeasible option in the current scenario. Application of velocity string in 4-1/2" tubing yields similar gas rates as current wellbore configuration; therefore, it is not a feasible option.

Well S-4 Summary

Observations drawn from the analysis conducted suggest low WGR and relatively optimized 4-1/2" ID tubing in well S-4 is adequate to create mist-flow in the wellbore. Although the critical gas rate suggests that liquid loading might be an issue in the wellbore, it is manageable at the current WGR value of 20 STB/MMscf. Therefore, the application of artificial lift such as Gas lift and velocity strings does not result in significant gas increment.

Well S-8

The well S-8 is a development well drilled in S-field. Producing from a sandstone reservoir at ~3300 m TVD, S-8 has produced more than 223 BCF gas since September 2003. Initial gas production was ~82 MMscfd. Pressure depletion caused rates to decline over the years, and the current gas rate is ~6.3 MMscfd. Water production started in S-8 from 2016 with increasing WGR. Due to the scarcity of well test data, only annual WGR was available for production and nodal analysis. Figure 108 shows the current wellbore profile of S-8.

Reservoir Pressure	680 psi	Target Interval	3300 m
Current Production	6.3 MMscfd	Following Wellhead Pressure	111 psi

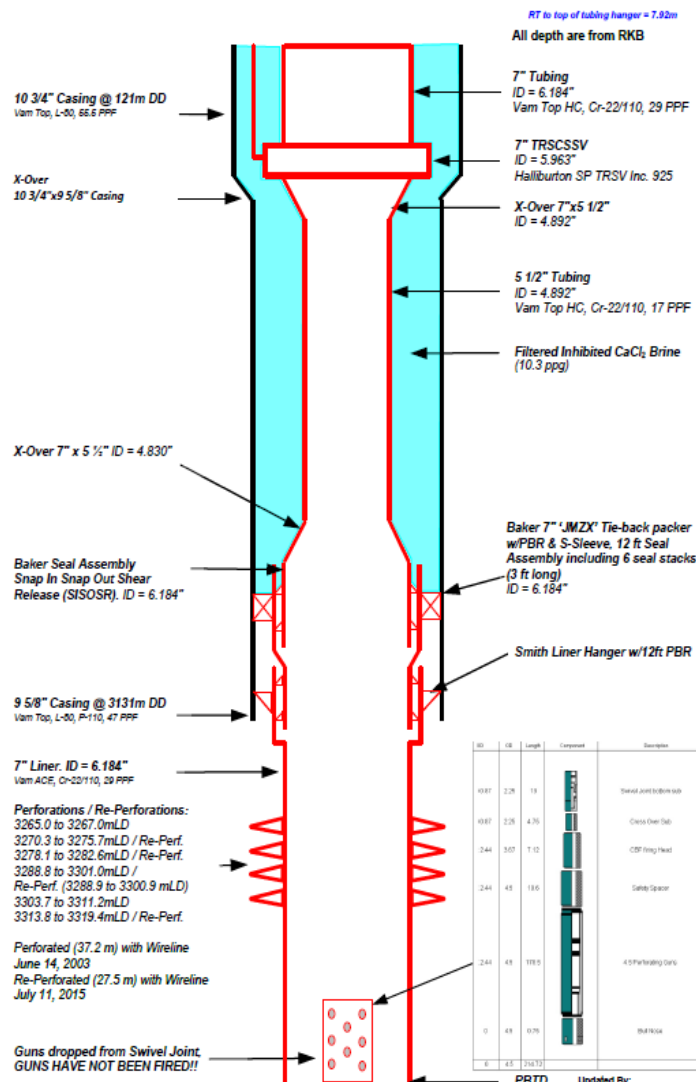


Figure 108 - Well S-8 wellbore profile

Production plot

Figure 109 shows gas production and Flowing Wellhead Pressure (FWHP) for S-8 from 2016. Bottomhole Pressure (BHP) is calculated from measured WHP using the VLP correlation for this dataset. This allows the evaluation of changing sand-face pressure to observe unusual trends and anomalies that may indicate issues like liquid loading.

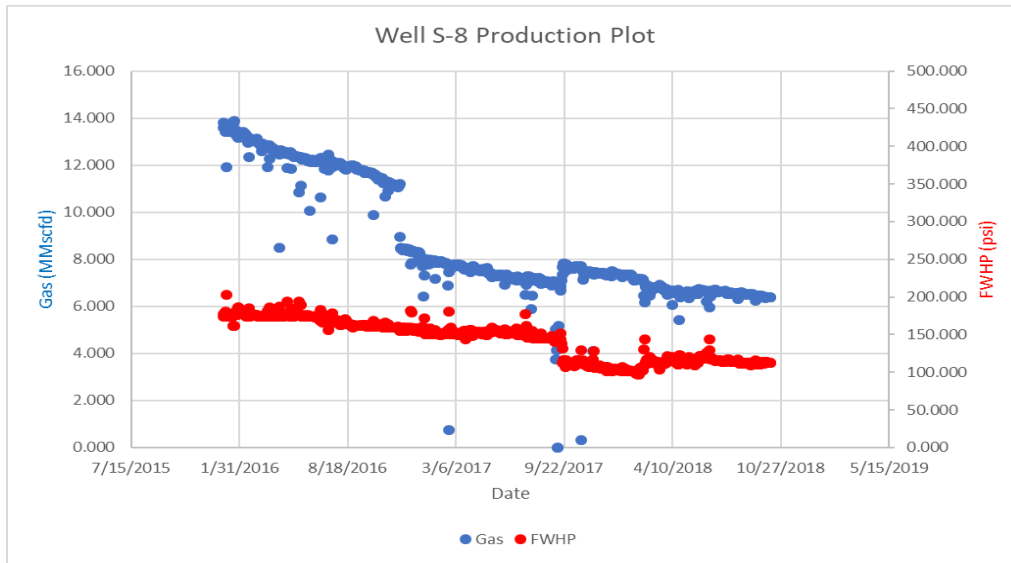


Figure 109 - Well S-8 FWHP plot

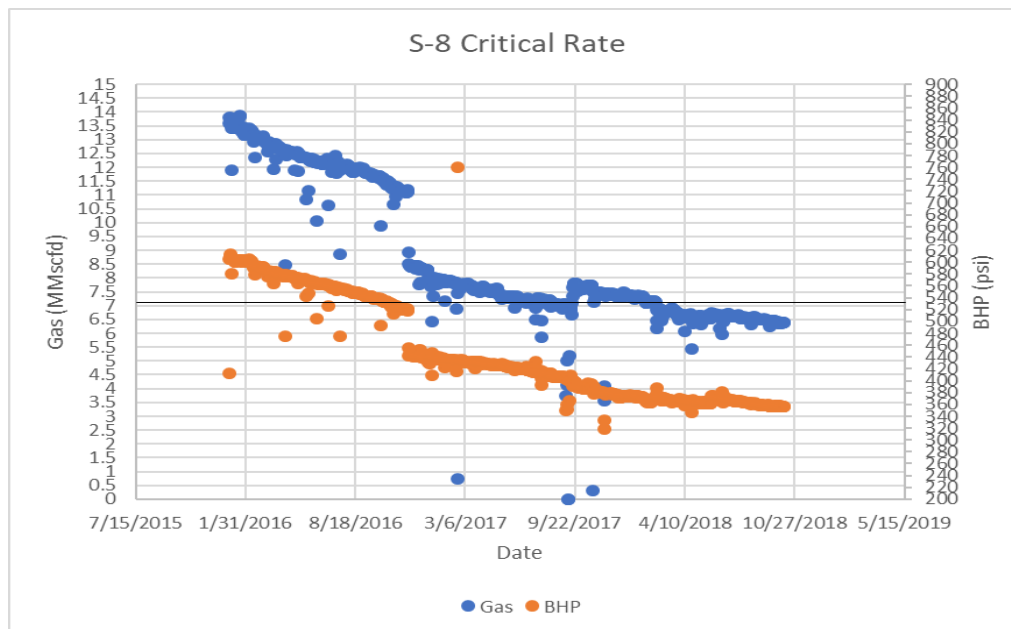


Figure 110 - Well S-8 BHP plot

Figure 110 shows the gas rates and BHP for S-8 from 2016. The solid black line at gas rate ~6.9 MMScfd in Figure 110 depicts the critical gas unloading rate required to offload all fluids from wellbore effectively. Based on the current production rate of ~6.3 MMScfd, current gas rates are only ~8% lower than required critical rates. This suggests that liquid loading is not a significant concern for this well.

The well S-8 has a steady decline in BHP with a relatively similar slope. This supplements the fact that the current gas rates are closer to critical gas rates; therefore, liquid loading has not affected bottom hole pressure significantly. WGR for this well has been relatively constant since 2016. Water production started with a WGR of ~60 STB/MMscf, which increased to ~68 by 2018.

Nodal Analysis

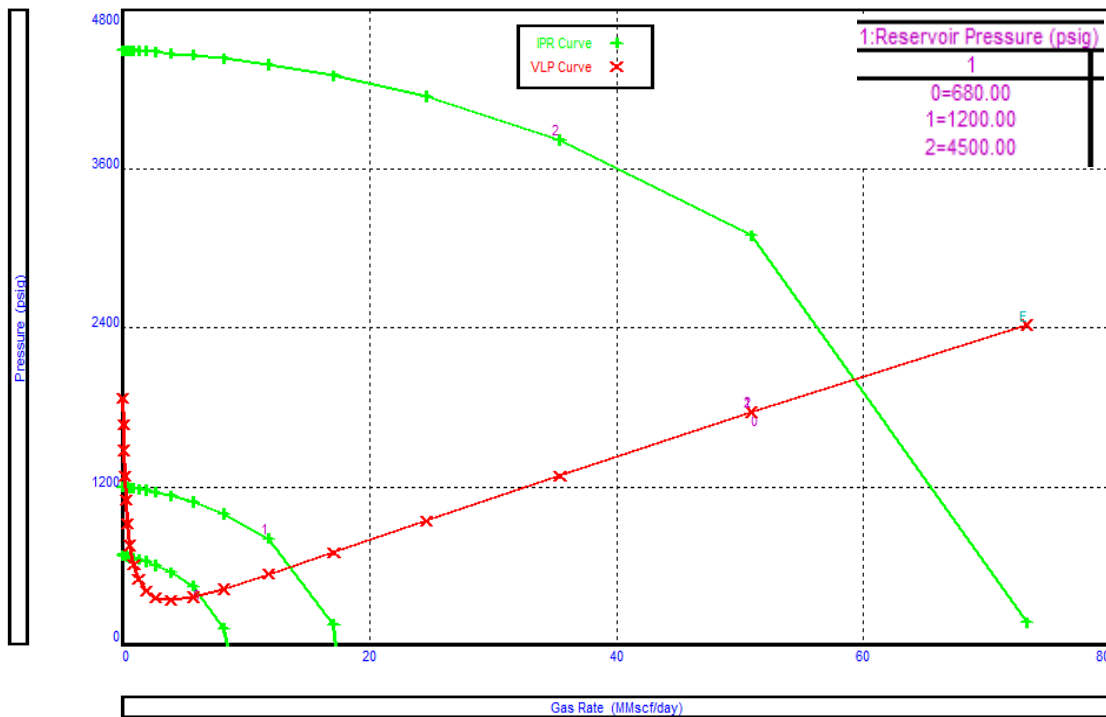


Figure 111 - Well S-8 reservoir pressure sensitivity

Figure 111 shows reservoir pressure sensitivity that is used to match the current production of well S-8 in the nodal analysis. This suggests reservoir pressure has depleted from ~4500 psi (virgin pressure 0.433 psi/ft gradient) to ~680 psi. This is the primary reason behind the drop in production over the years.

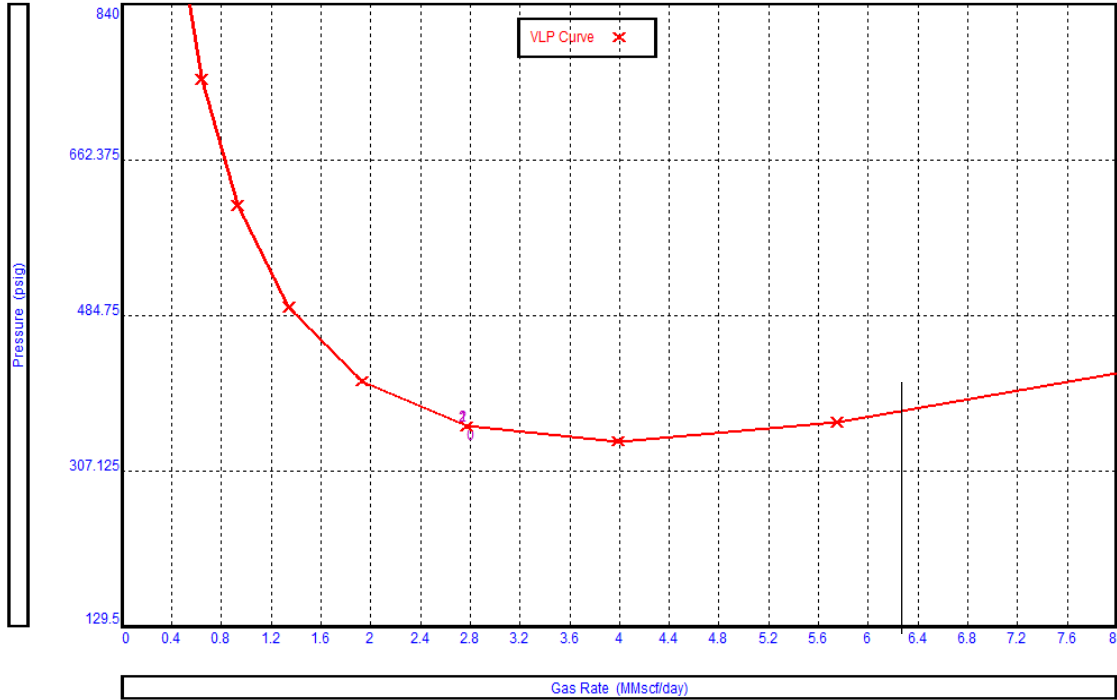


Figure 112 - Well S-8 VLP stability plot

Stability analysis through the VLP curve suggests current production is on the far right of the minimum that denotes stable flow dynamics. This is evident through a consistent gas rate and stable WGR over the years. Figure 112 shows the VLP stability plot.

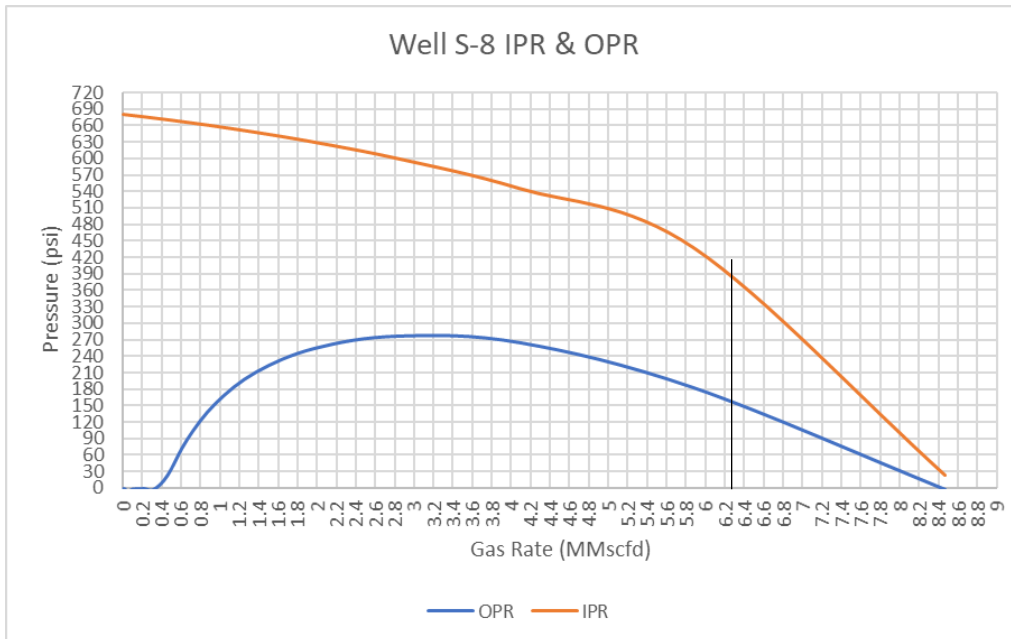


Figure 113 - Well S-8 flow-point analysis plot

Flow-point analysis (Figure 113) suggests that flow in the wellbore is stable, and the effects of liquid loading are not significant. Further, as current production is on the right of the OPR curve apex, this signifies stable wellbore hydraulics as also predicted by VLP stability.

Salinity Analysis

Source of liquid production in the wellbore can also be used to designate the severity of liquid loading. Although any fluid – condensate, formation water and condensed water – can cause an increase in hydrostatic pressure and deteriorate well performance, often formation water is most detrimental to production. This is largely because the liquid is introduced at sand-face from formation and in lower velocities, is not carried towards the surface. The other two sources of fluids are often near the wellbore; therefore, they have to travel a shorter distance.

In the absence of production logs, salinity data from produced water is used to classify condensed water from formation water. Commonly, chloride or sodium chloride content form the basis of salinity classification. Gorrell 1958 suggest the following brackets:

0 to 10,000 ppm NaCl – Fresh/Brackish water

10,000 to 100,000 ppm NaCl – Salty water

Over 100,000 ppm NaCl – Brine

As S-8 water has ~2387 ppm salinity, based on the above categories, produced water is most likely condensed in this well and is sourced near the surface.

Artificial Lift Techniques

Gas Lift

A sensitivity run is made on bottom hole pressure with changing WGR to evaluate if the application of any artificial lift that requires gas injection (in the wellbore) will aid in improving production. For most conventional reservoirs, reduction in BHP will generally increase hydrocarbon production.

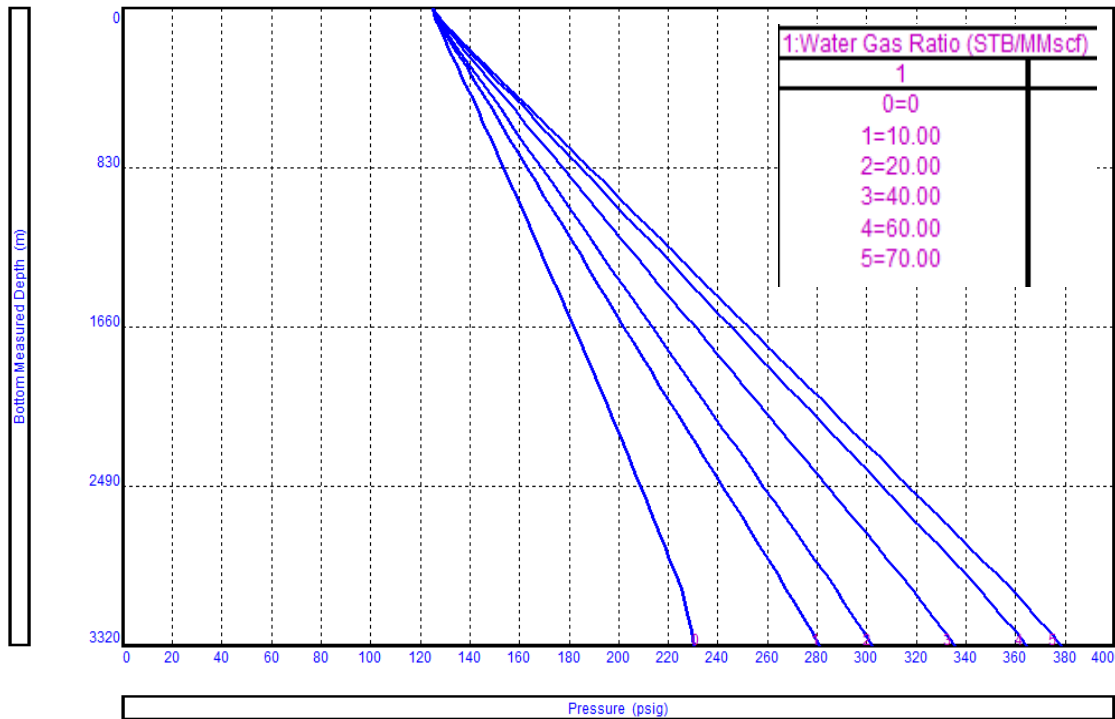


Figure 114 - Well S-8 WGR Sensitivity

The current WGR in well S-8 is ~68 STB/MMscf. Despite high gas rates, we can observe significant bottom hole pressure reduction, as shown in Figure 114, by adding gas in the system (lowering WGR). This would suggest gas increment is possible through a gas lift, which can be confirmed by WGR sensitivity on system analysis.

Figure 115 shows the effect of lowering WGR on system analysis. Significant gas improvement is observed if WGR is lowered to ~20 STB/MMscf or less. Compared to other S-field wells, we see a definite improvement in S-8 with lowering WGR due to the larger tubing in this well (7" x 5-1/2"). The addition of extra gas does not increase friction pressures; therefore, notable improvement is observed.

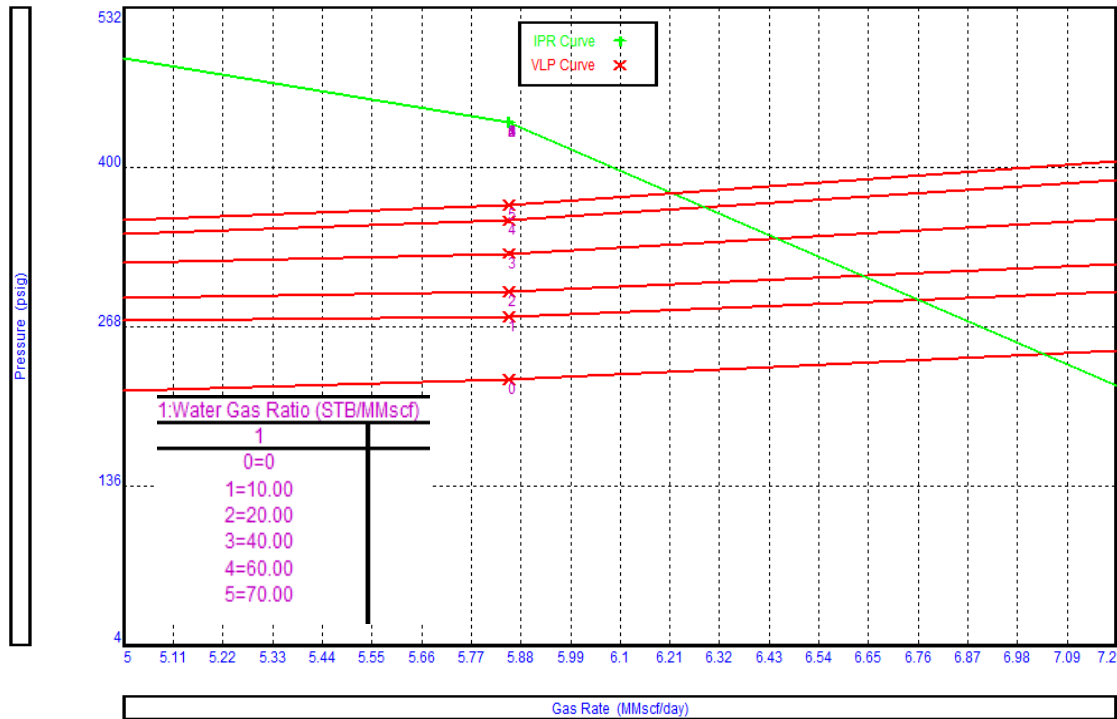


Figure 115 - Well S-8 WGR sensitivity on system plot

Gas lift design is required where the effects of the gas injection are modelled to quantify the actual improvement in production. Most gas lift models are designed for oil reservoirs, therefore as a way around oil IPR with equivalent GOR is used to match the current performance of well S-8. Figure 117 shows the matched model with the same reservoir parameters as Gas IPR with a GLR of ~637744 SCF/STB.

With oil IPR, we can inject gas in the wellbore by two mechanisms, conventional gas lift where gas is injected down the annulus and produced through 5-1/2" tubing. Secondly, gas can also be injected through Coiled Tubing Gas Lift (CTGL), where 1.5" CT is used inside the current 5-1/2" tubing. The performance of both systems is shown in Figure 116 and Figure 118, respectively.

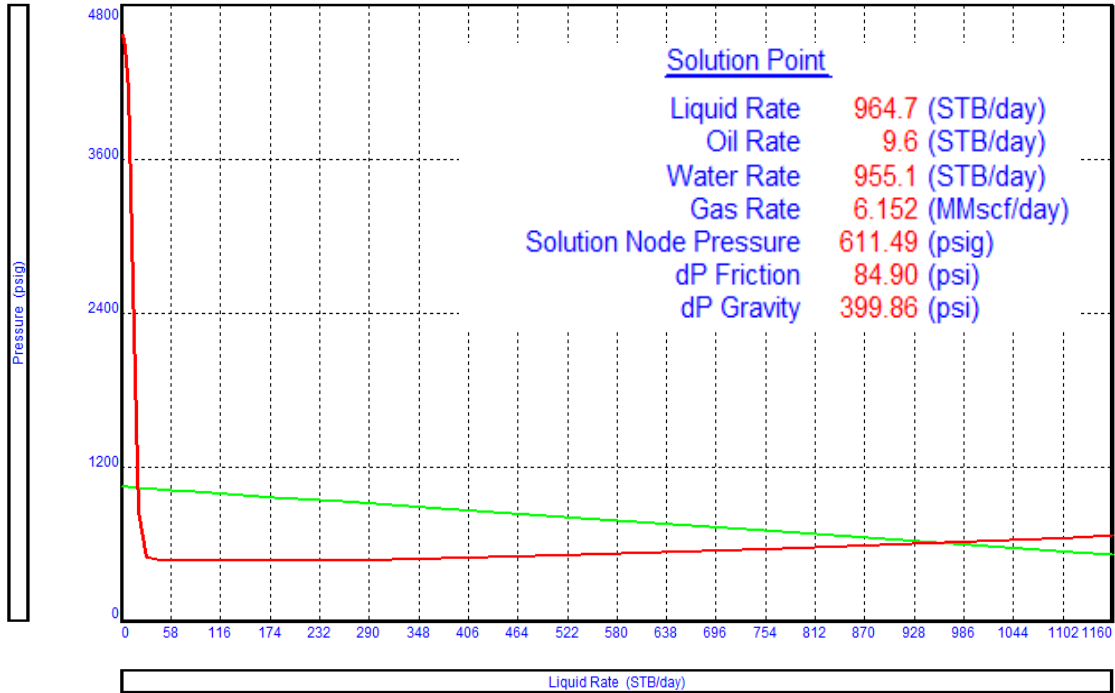


Figure 117 - Well S-8 system analysis using oil IPR

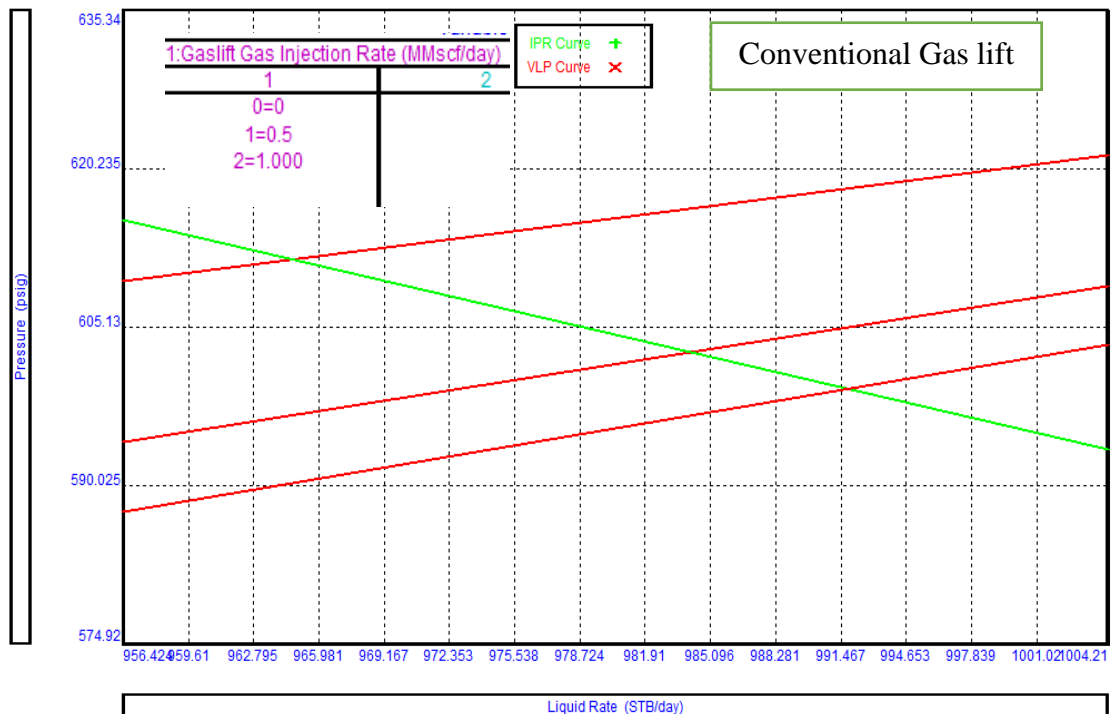


Figure 116 - Well S-8 Conventional gas lift design

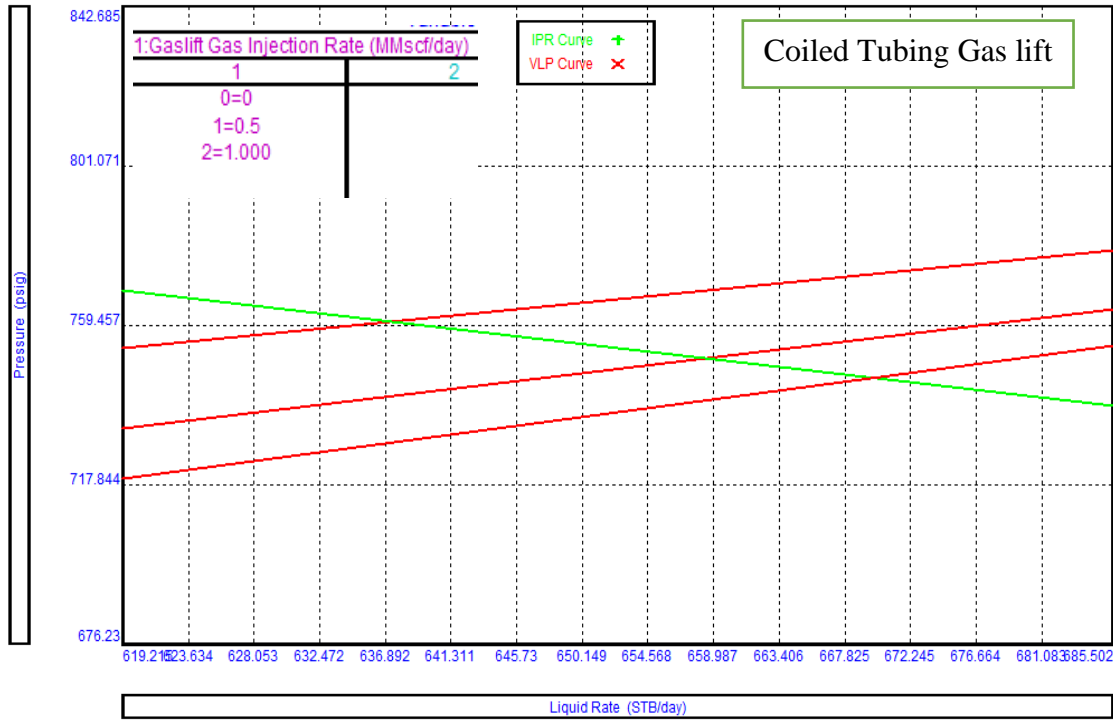


Figure 118 - Well S-8 CT gas lift design

System analysis suggests using CTGL deteriorates performance due to the addition of smaller diameter coiled tubing that creates additional friction pressure. Conventional coiled tubing design suggests ~1 MMscfd gas injection rate (which is a surface constraint) is inadequate to lower BHP substantially. The increment in gas observed when gas injection rate is limited to 1 MMscfd is only ~0.3 MMscfd, which is not adequate to justify the additional cost of installing a gas lift.

Velocity String / Smaller Diameter Tubing

Velocity string or smaller diameter tubing can be used in well S-8 in an attempt to improve production and wellbore hydraulics. Different combinations of strings are evaluated to compare performance. The sensitivities conducted include:

- Current Profile: 7" x 5-1/2" Tubing with ~300m of 7" casing flow
- Velocity String: Install 1" CT in 4-1/2" Tubing
- Smaller diameter tubing in 7" Casing below the packer
- Smaller diameter 2-7/8" tubing inside 5-1/2" tubing

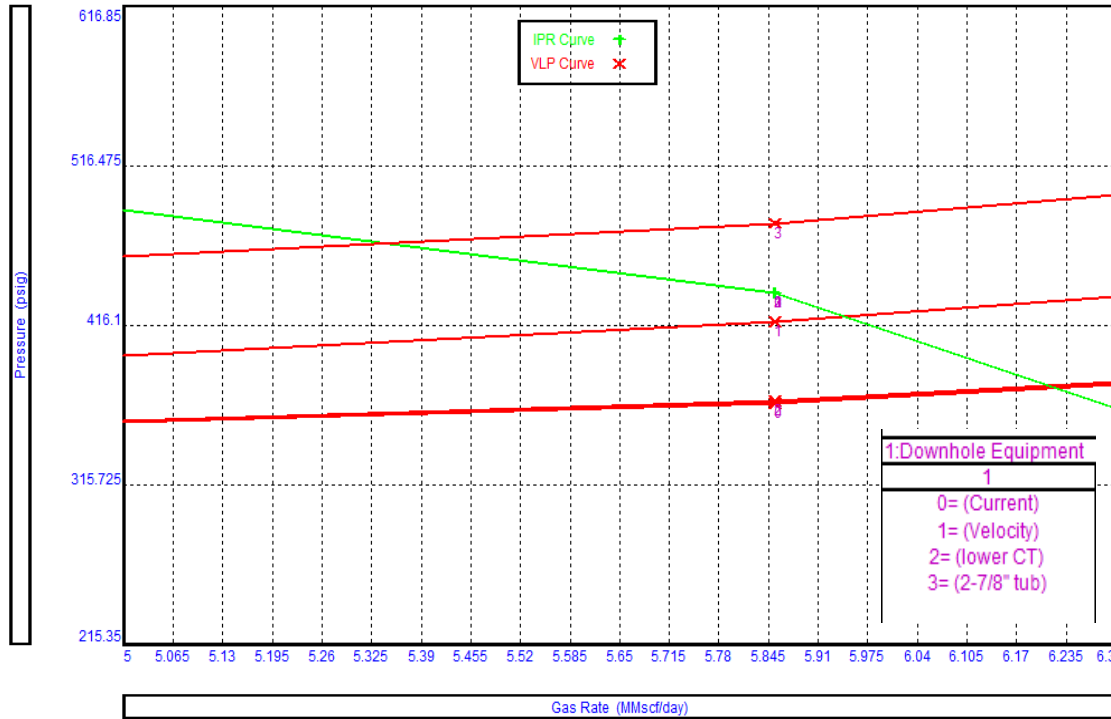


Figure 119 - Well S-8 Lower ID/velocity string comparison

As seen in Figure 119, the use of smaller diameter tubing significantly deteriorates performance due to very high friction pressures, making it an unfeasible option in the current scenario. Application of a velocity string in 5-1/2" tubing yields better gas rates compared to 2-7/8" tubing, however still lower than current performance. Using 1.5" CT in the lower section of 7" casing below packer results in similar gas rates as current production.

Plunger Assisted Gas Lift

With 5-1/2" tubing (Plunger BHA @ 3131m)

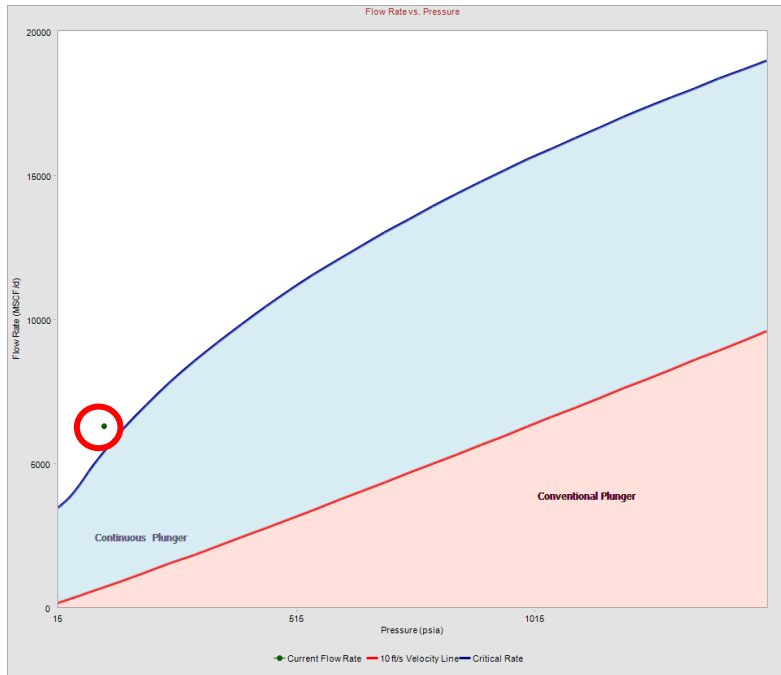


Figure 120 - Well S-8 PAGL type plot

Figure 120 shows the flow rate vs pressure plot to select a plunger type. Current modeled conditions are shown in the red circle in Figure 120. Similar to the results predicted by the WACR model, current production falls within 25% of the critical rate.

As the current production is fairly stable and only slightly below the critical rate, Figure 120 suggests a plunger lift is not required (will not result in any incremental liquid production) due to the sufficient

velocities currently available in the wellbore.

Well S-8 Summary

Observations drawn from analysis conducted suggest the application of gas-lift can result in production improvement if WGR can be lowered significantly. However, detailed design using a conventional gas lift and Coiled Tubing Gas Lift with a surface constraint of ~1 MMscfd injection gas suggest improvement is only limited to ~0.3 MMscfd. Salinity data for this well compared to other S-field wells suggest produced water is condensed water. Therefore, installing a gas lift will not be an effective solution at this instance in the well's life.

Well S-13

The well S-13 is a development well drilled in S-field. Producing from a sandstone reservoir at ~3320 m TVD, S-13 has produced more than 42.2 BCF gas since 2008. Initial gas production was ~28 MMscfd. Pressure depletion caused rates to decline over the years, and the current gas rate is ~3.1 MMscfd. Water production started in S-13 from 2016 with increasing WGR. Due to the scarcity of well test data, only annual WGR was available for production and nodal analysis. Figure 121 shows the current wellbore profile of S-13.

Reservoir Pressure	600 psi	Target Interval	3320 m
Current Production	3.1 MMscfd	Following Wellhead Pressure	143 psi

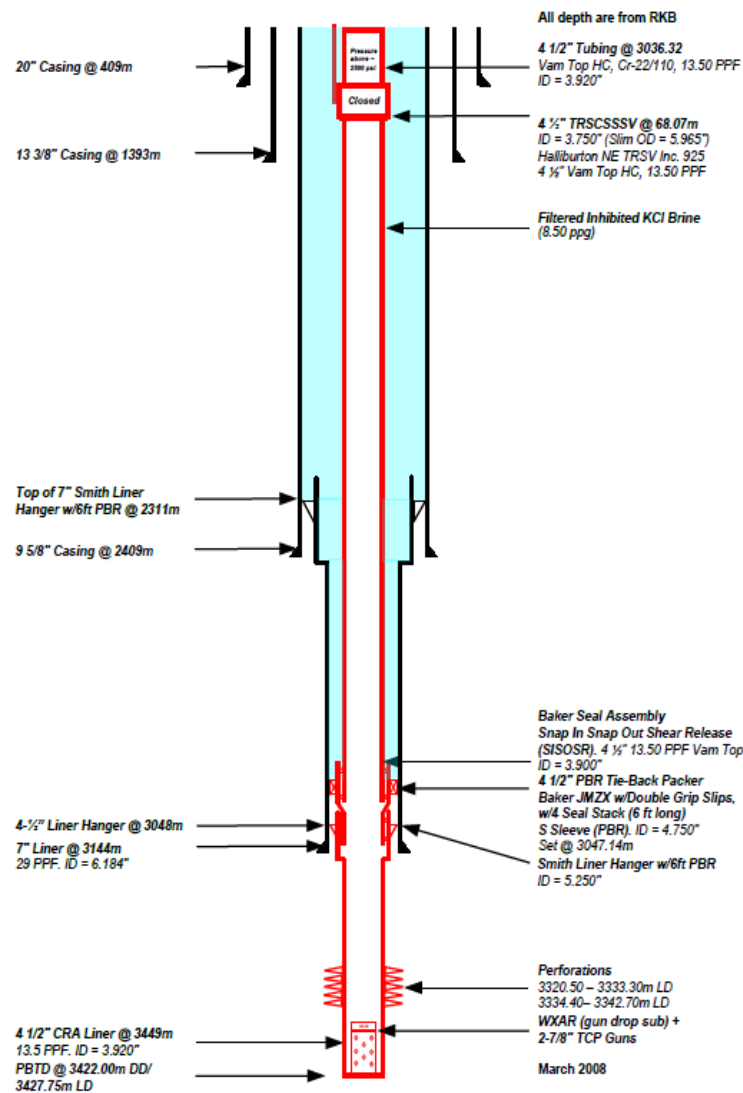


Figure 121 - Well S-13 wellbore profile

Production plot

Figure 122 shows the gas production and Flowing Wellhead Pressure (FWHP) for S-13 from 2016. Bottomhole Pressure (BHP) can be calculated from measured WHP using the VLP correlation for this dataset. This allows the evaluation of changing sand-face pressure to observe unusual trends and anomalies that may indicate issues like liquid loading.

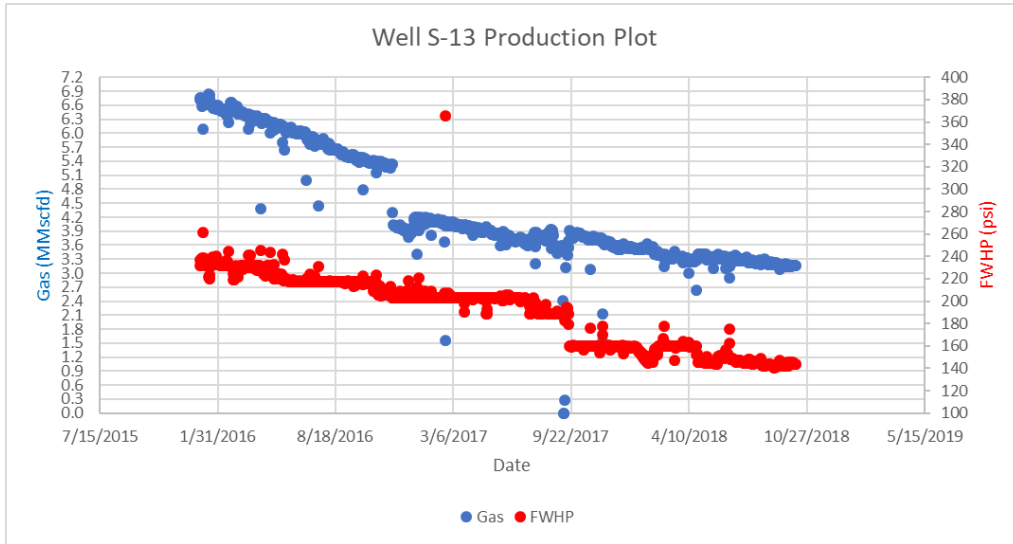


Figure 122 - Well S-13 FWHP plot

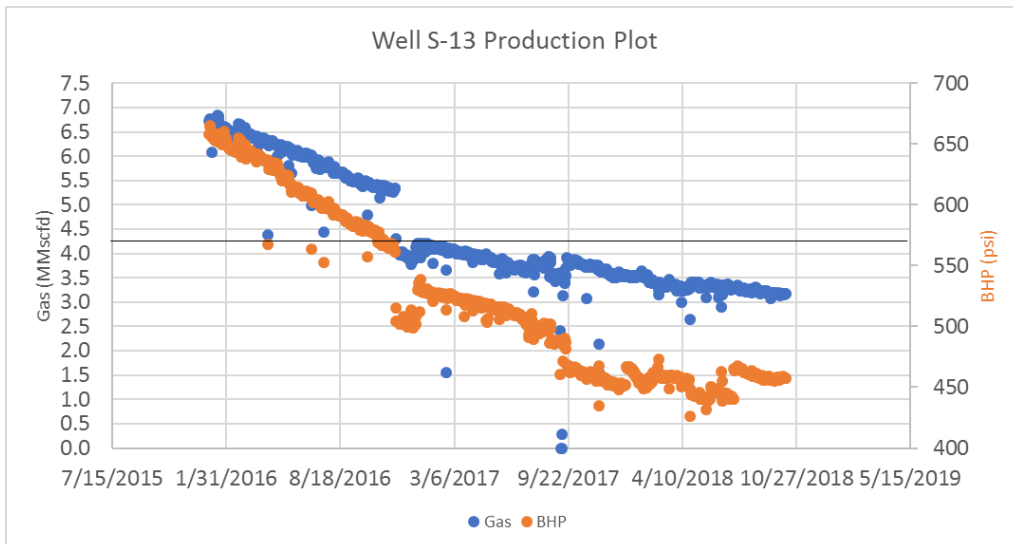


Figure 123 - Well S-13 BHP plot

Figure 123 shows the gas rates and BHP for S-13 from 2016. The solid black line at gas rate ~4.4 MMScfd in Figure 123 depicts the critical gas unloading rate required to offload all fluids from wellbore effectively. Based on the current production rate of ~3.1 MMScfd, current gas rates are ~28% lower than required critical rates.

An apparent change in trend is observed in BHP data post December 2016. The decline in BHP has changed, which correlates well with the trend in gas rates that have fallen below the critical unloading rate. Moreover, with the loading of water in the wellbore, BHP values had decreased for similar gas rates before and after loading started. This is visible when gas rates in June 2017 and September 2017 are similar at ~3.6 MMScfd; however, BHP is ~520 psi and ~460 psi, respectively. In a stable flow regime, similar gas production should have similar flowing bottom hole pressure. The extra drop in BHP, in this case, is possibly due to ineffective liquid unloading that causes additional hydrostatic pressure.

Nodal Analysis

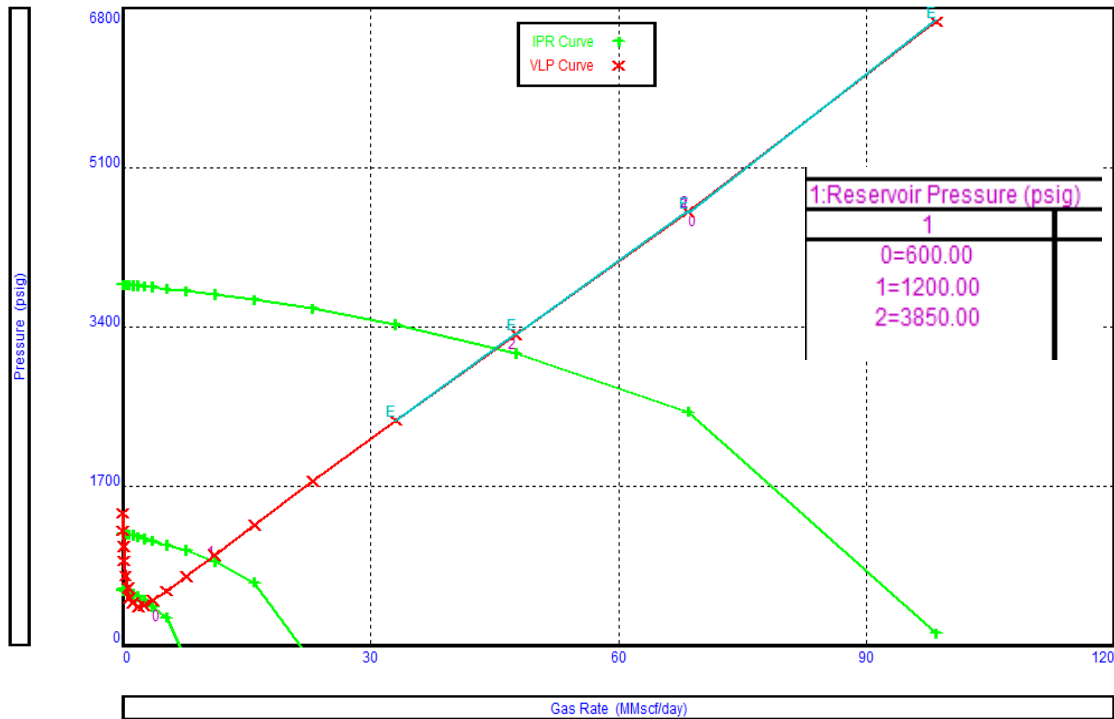


Figure 124 - Well S-13 reservoir pressure sensitivity

Figure 124 shows the sensitivity of reservoir pressure by changing the IPR curve. Initially, the well produced ~28 MMscfd at reservoir pressure of ~3850 psi. Reservoir pressure is reduced to ~600 psi to match current flowing conditions.

Similar to other S-field wells, the small delta between critical gas rate and current gas rate suggest liquid loading is not severe in this well. This is confirmed by stability analysis through the VLP curve, as shown in Figure 125, where current production is on the right of minimum. However, due to higher WGR compared to other wells, the use of artificial lift may significantly improve gas production.

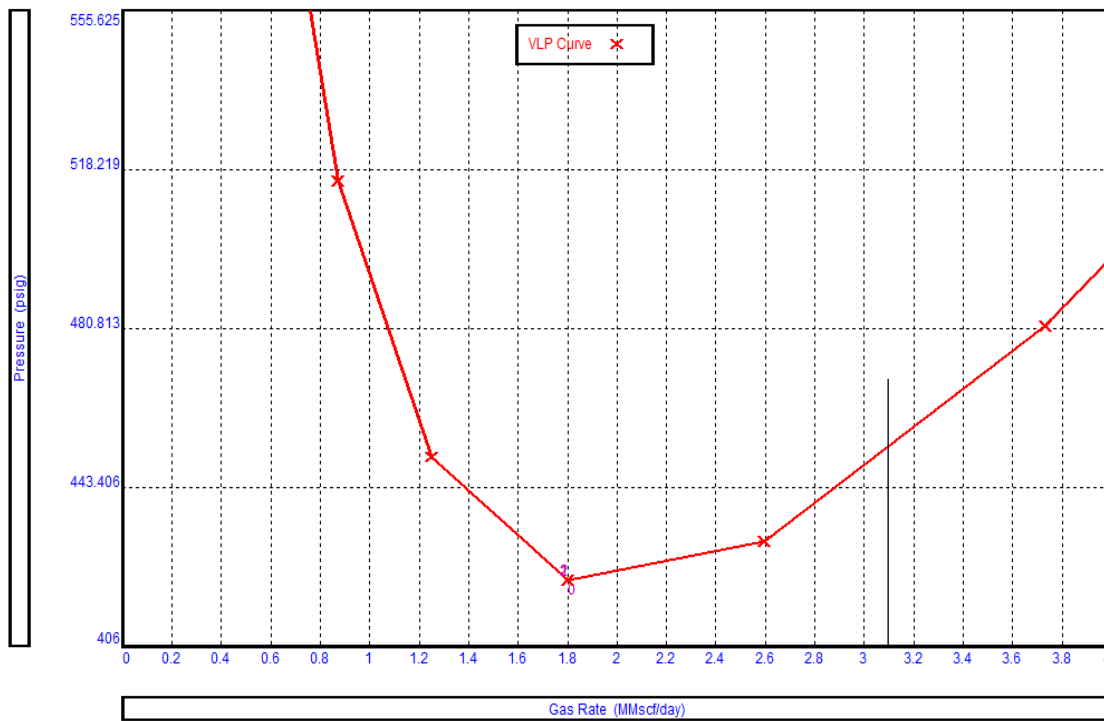


Figure 125 - Well S-13 VLP stability plot

Flow-point analysis (Figure 126) suggests a well pressure difference of ~305 psi, which is higher than other wells. Despite having a high WGR, there is significant pressure available in the wellbore to improve performance. Nevertheless, current production lies on the right of OPR apex that suggests wellbore hydraulics are stable.

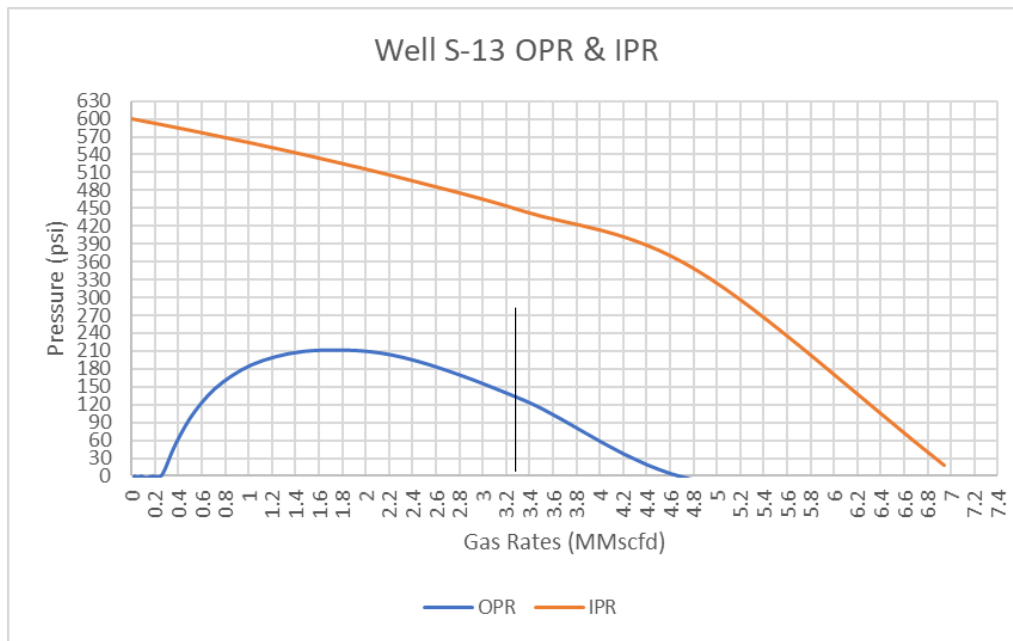


Figure 126 - Well S-13 flowpoint analysis plot

Salinity Analysis

Source of liquid production in the wellbore can also be used to designate the severity of liquid loading. Although any fluid – condensate, formation water and condensed water – can cause an increase in hydrostatic pressure and deteriorate well performance, often formation water is most detrimental to production. This is largely because the liquid is introduced at sand-face from formation and in lower velocities, is not carried towards the surface. The other two sources of fluids are often near the wellbore; therefore, they have to travel a shorter distance.

In the absence of production logs, salinity data from produced water is used to classify condensed water from formation water. Commonly, chloride or sodium chloride content form the basis of salinity classification. Gorrell 1958 suggest the following brackets:

0 to 10,000 ppm NaCl – Fresh/Brackish water

10,000 to 100,000 ppm NaCl – Salty water

Over 100,000 ppm NaCl – Brine

As S-13 water has ~9798 ppm salinity, based on the above categories, it is on the borderline of condensed and formation water. Therefore, this data is not adequate to identify the source.

Artificial Lift Techniques

Gas Lift

A sensitivity run is made on bottom hole pressure with changing WGR to evaluate if the application of any artificial lift that requires gas injection (in the wellbore) will aid in improving production. For most conventional reservoirs, reduction in BHP will generally increase hydrocarbon production.

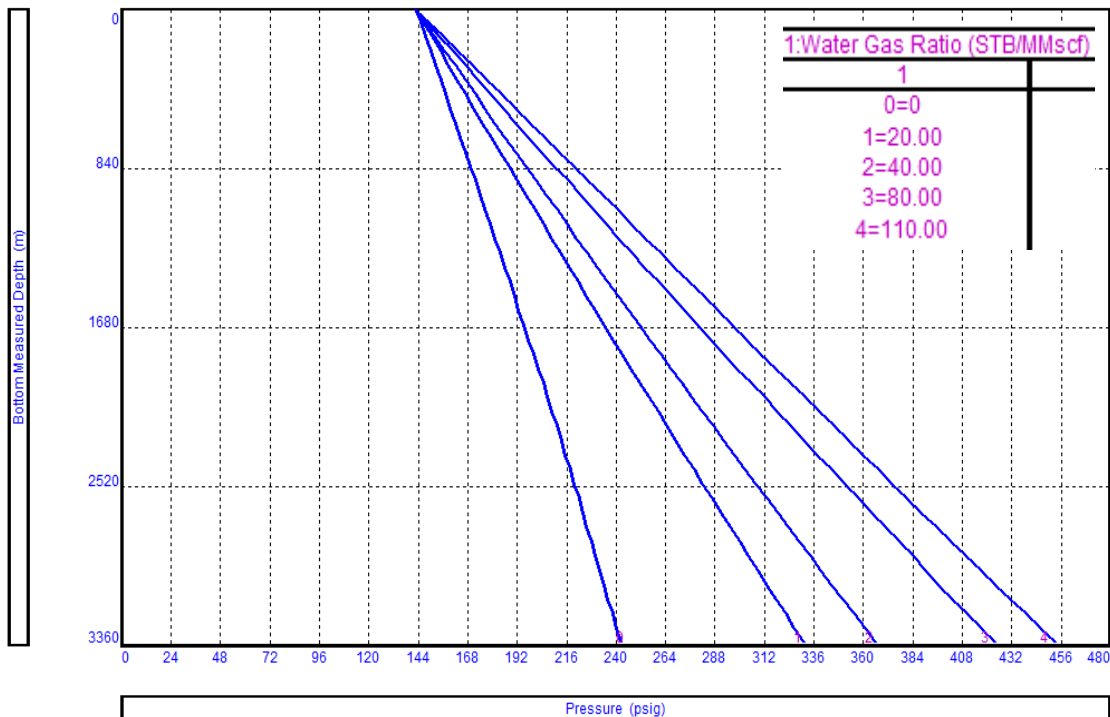


Figure 127 - Well S-13 WGR sensitivity

Lowering WGR by injecting gas in S-13 does result in lower bottom hole pressure, as shown in Figure 127. Although thorough gas lift design is required to quantify the improvement, BHP sensitivity suggests gas lift performance may be beneficial for well S-13, if WGR can be lowered significantly.

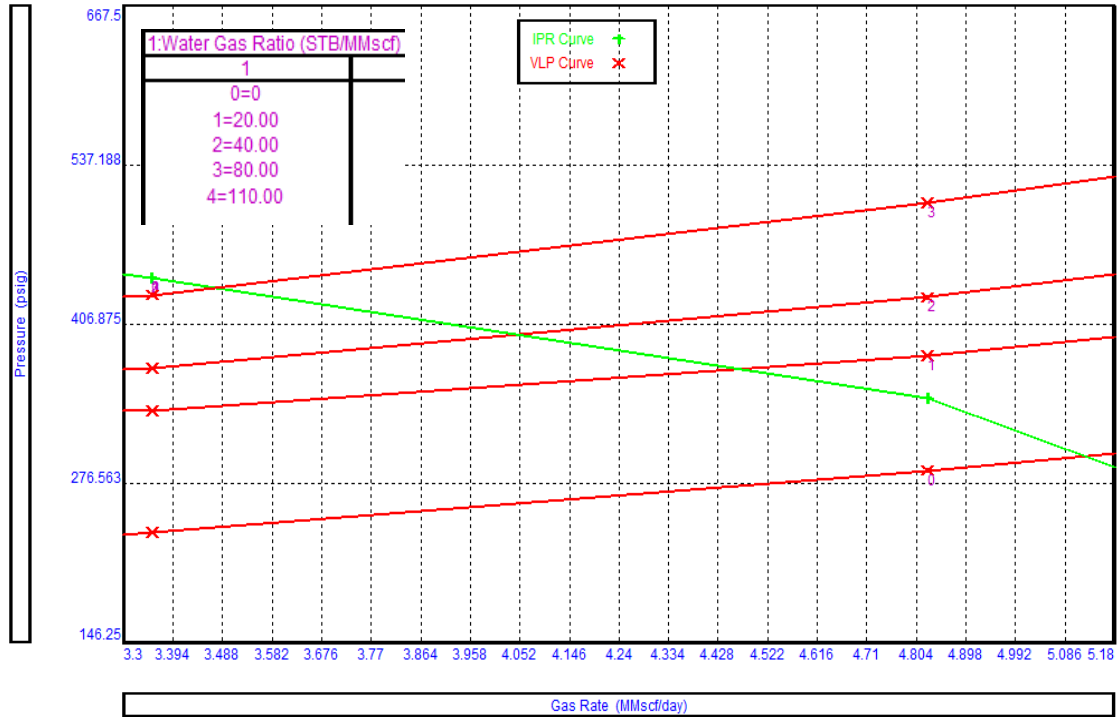


Figure 128 - Well S-13 WGR sensitivity on system plot

Figure 128 shows the effect of lower WGR on system analysis. Running WGR sensitivities on system analysis suggest a significant improvement in gas rates for well S-13, as expected post BHP sensitivities. Gas increments of 1.5 MMscfd and higher are possible if WGR is significantly reduced from the current value of ~110 STB/MMscf.

Given current WGR of 110 STB/MMscf and current gas rates of ~3 MMscfd, daily water production is approximate ~350 bbl/d. As the gas injection rate in S-field is limited to ~1 MMscfd, WGR can only be lowered to ~80 STB/MMscf. This would limit the gas increment to ~0.7 MMscfd, which would be inadequate to justify gas lift expenses.

Velocity String

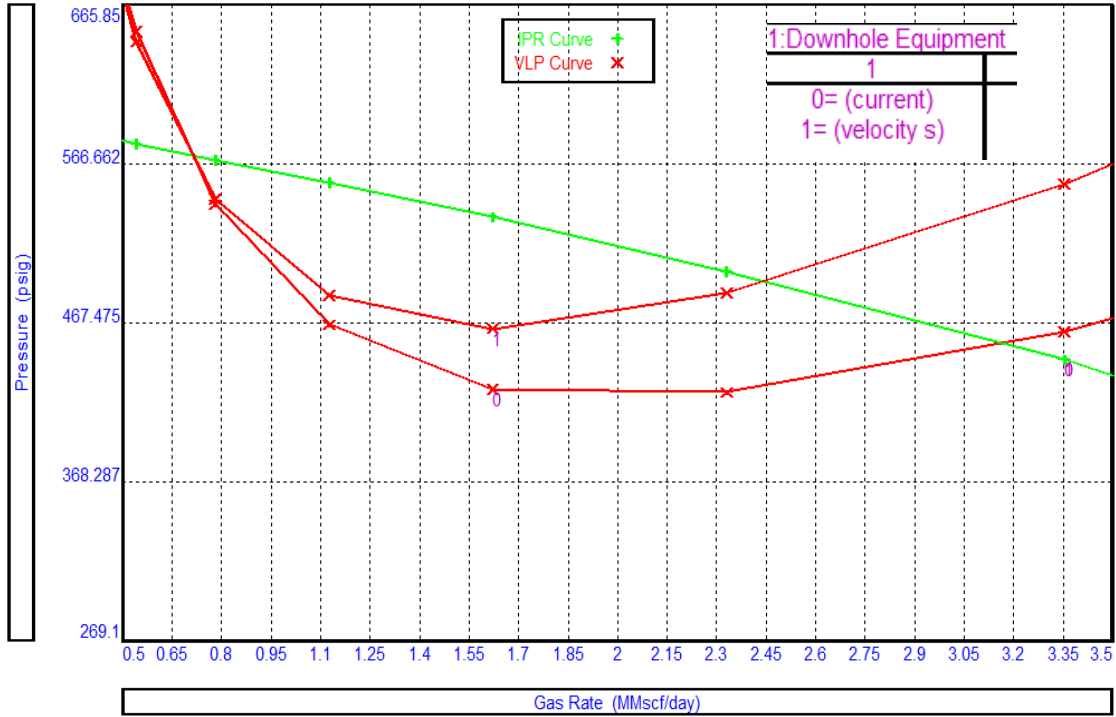


Figure 129 - Well S-13 Velocity string design

Velocity string or smaller diameter tubing can be used in well S-13 in an attempt to improve production and wellbore hydraulics. As the well is completed with 4-1/2” tubing, installing a smaller diameter tubing (which can only be ~2-7/8 flush tubing) will increase friction pressures significantly and, therefore, not considered.

Application of velocity string that is 1” in diameter also deteriorates performance due to added friction pressure. Therefore, at this instance, the velocity string does not seem like a viable option in this well.

Plunger Assisted Gas Lift

With 4-1/2" tubing (Plunger BHA @ 3048m)

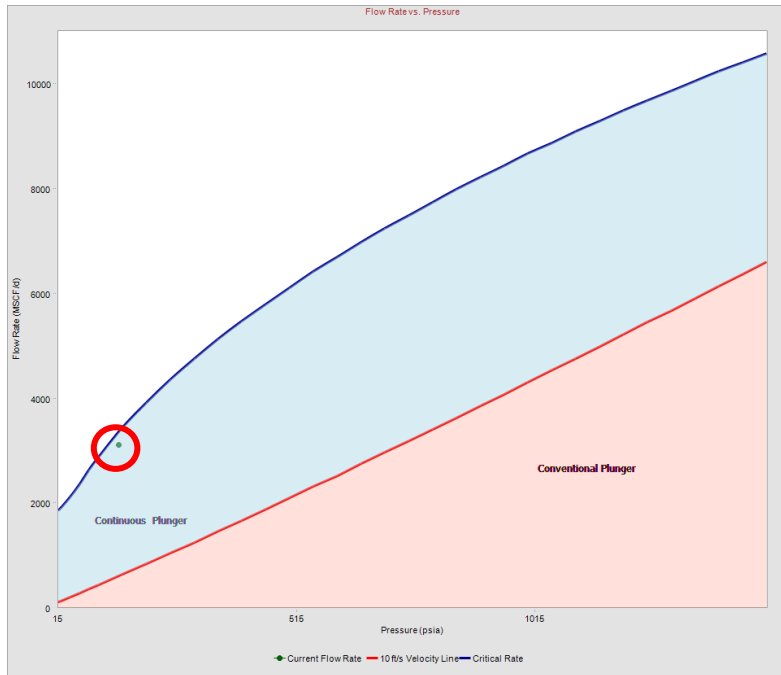


Figure 130 - Well S-13 PAGL type plot

Figure 130 shows the flow rate vs pressure plot to select a plunger type. Current modeled conditions are shown in the red circle in Figure 130. Similar to the results predicted by the WACR model, current production falls within 25% of the critical rate, however within the application range of continuous plunger lift. Plunger lift design is required to ascertain the applicability of a continuous plunger lift on well S-13.

Plunger Assisted Gas Lift Design		Results	
Well Name	S-13	Required Casing Injection Pressure (psi)	1830
PAGL Type	Continuous	Injection pressure Limited by	Surface
Target Gas Production (Mscf/d)	3000	Calculated WHP (psi)	1811
Target Liquid Production (STB/d)	50	Volume of Liquid Slug (bbl)	0.76
Tubing ID (in)	3.92	Number of Cycles per day	66
Tubing OD (in)	4.5	Gas Velocity at bottom hole (ft/sec)	154.28
Design WHP (psi)	30	Minimum Gas velocity (ft/sec)	49.14
Expected Flowing BHP (psi)		PAGL Possible?	No
Fall Rate in Gas (ft/min)	800		
Fall Rate in Liquid (ft/min)	400		
Rise Rate (ft/min)	700		

Table 21 - Well S-13 PAGL design with current 4-1/2" tubing

Table 21 depicts the design of PAGL with current tubing. Due to the high critical rate in 4-1/2” tubing, installing plunger requires very high surface gas injection pressure to lift fluid and plunger to surface which is impractical.

With very high current gas rates and a stable flow regime, a plunger lift is not suitable for this well unless it is re-completed with lower 2-7/8” tubing. Re-completing the well at this instance will lower current production (due to the added frictional pressures in smaller diameter tubing) and well may lose its overall net present value.

Well S-13 Summary

Observations drawn from analysis conducted suggest the application of gas lift can result in improvement if WGR can be lowered significantly. However, detailed design using a conventional gas lift and Coiled Tubing Gas lift with a surface constraint of ~1 MMscfd injection gas suggest improvement is only limited to ~0.7 MMScfd. Further, salinity data is unable to classify produced water as condensed or formation in the absence of production logs. Therefore, based on available data, accurately selecting a suitable artificial lift for this well at this stage is a challenge.

Well S-14

S-14 is a development well drilled in S-field. Producing from the sandstone reservoir at ~3260 m TVD, S-14 has produced more than 35.7 BCF gas since March 2009. Initial gas production was ~25 MMscfd. Pressure depletion caused rates to decline over the years, and the current gas rate is ~2.59 MMscfd. Water production started in 2012 with increasing WGR. Due to the scarcity of well test data, only annual WGR was available for production and nodal analysis. Figure 131 shows the current wellbore profile of S-14.

Reservoir Pressure	650 psi	Target Interval	3260 m
Current Production	2.49 MMscfd	Following Wellhead Pressure	108 psi

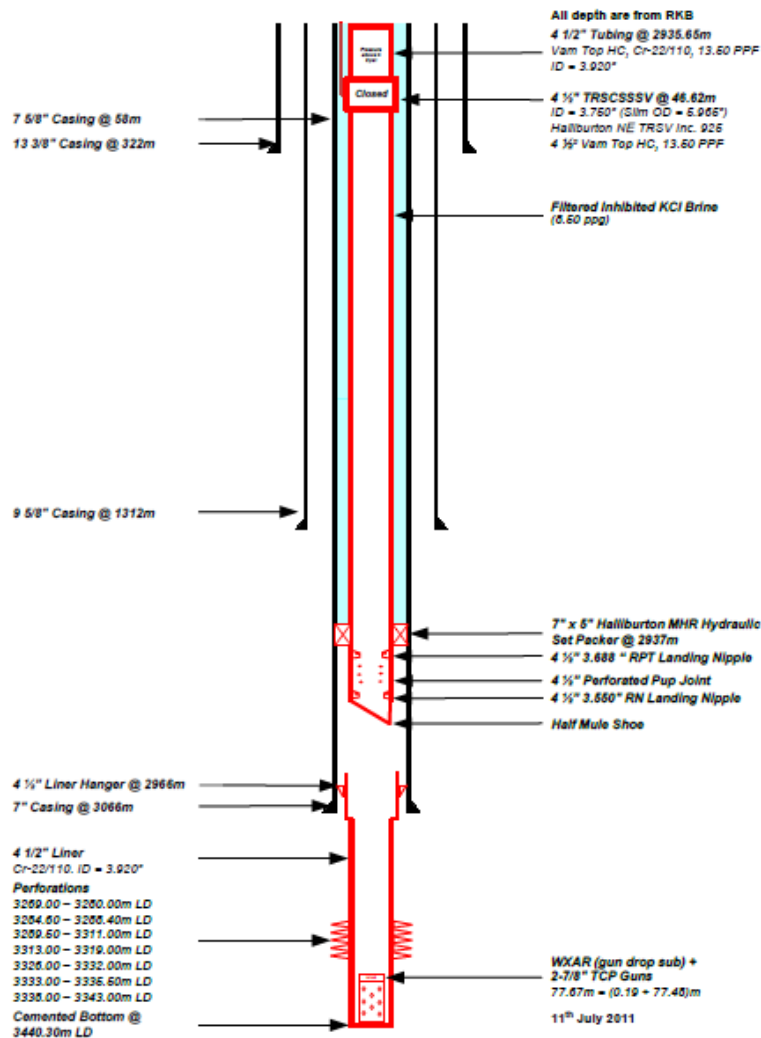


Figure 131 - Well S-14 wellbore profile

Production Plot

Figure 132 shows the gas production and Flowing Wellhead Pressure (FWHP) for S-14 from 2014. Bottomhole Pressure (BHP) can be calculated from measured WHP using the VLP correlation for this dataset. This allows the evaluation of changing sand-face pressure to observe unusual trends and anomalies that may indicate issues like liquid loading.

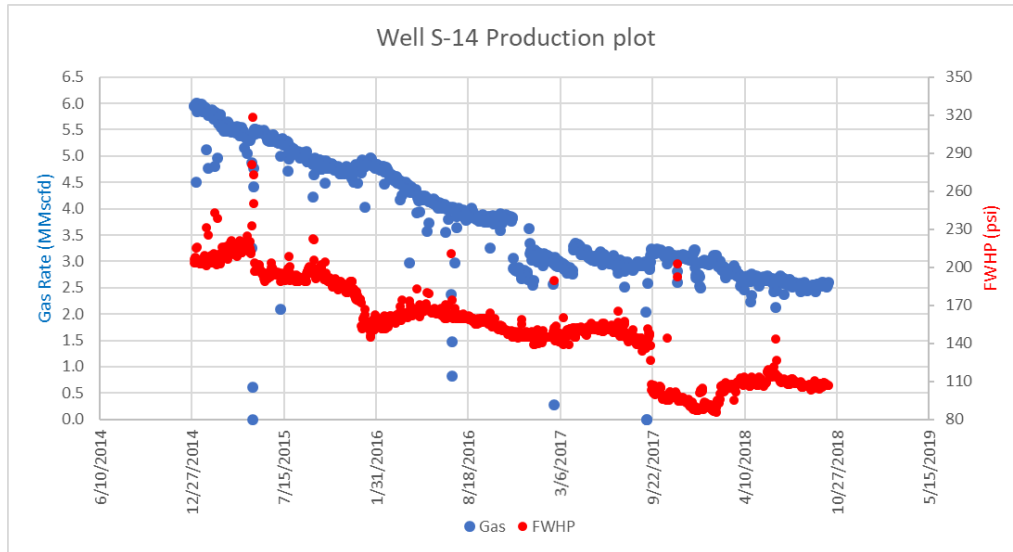


Figure 132 - Well S-14 FWHP plot

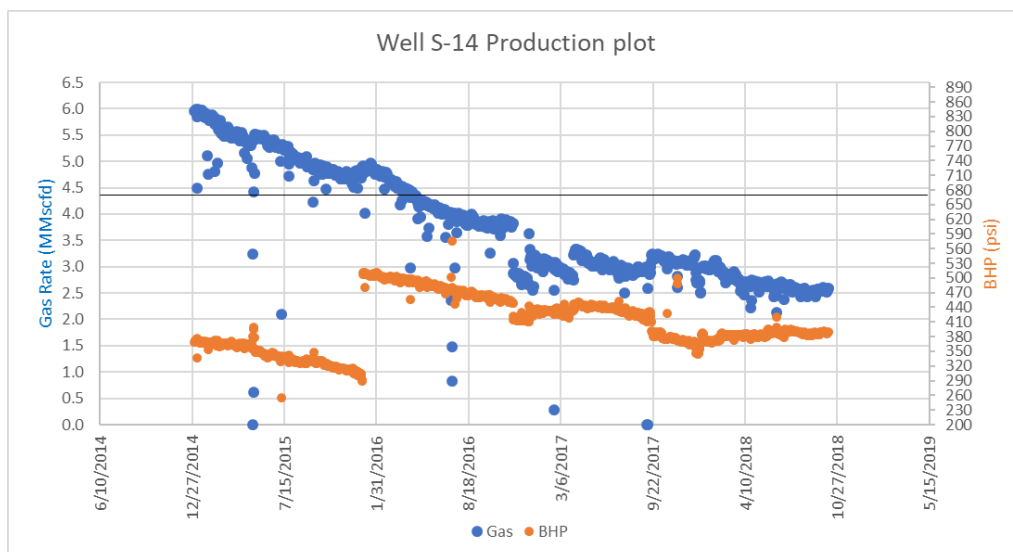


Figure 133 - Well S-14 BHP plot

Figure 133 shows the gas rates and BHP for S-14 from 2014. The solid black line at gas rate ~4.4 MMscfd in Figure 133 depicts the critical gas unloading rate required to offload all fluids from wellbore effectively. Based on the current production rate of ~2.59 MMscfd, current gas rates are ~41% lower than required critical rates.

The well S-14 depicts relatively stable BHP pressure decline with steady gas production decline. Although we can observe regions of stable/constant BHP, overall, the trend between BHP decline and gas rate decline is similar. This suggests, despite the onset of liquid loading, water hold-up is not influencing BHP significantly at this instance.

Nodal Analysis

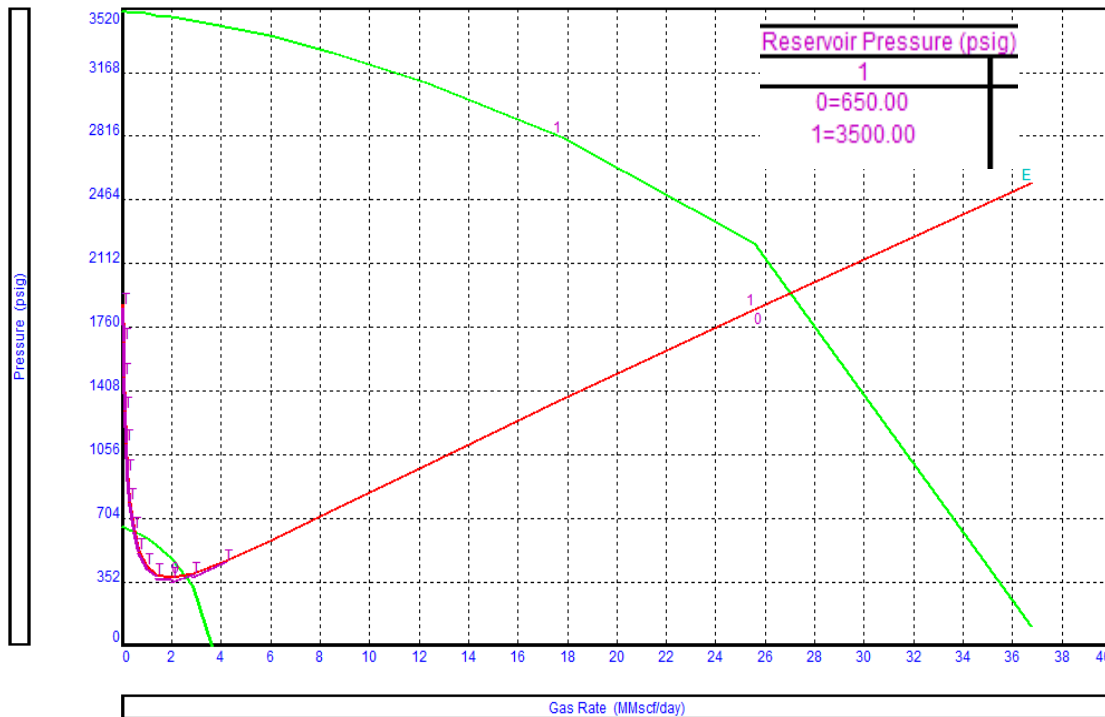


Figure 134 - Well S-14 reservoir pressure sensitivity

Figure 134 depicts the sensitivity of reservoir pressure that is used to match the current production of the well. This suggests reservoir pressure has depleted from ~3500 psi (initial pressure for this well was probably depleted from virgin, due to production from other wells) to ~650 psi. This is the primary reason behind the drop in production over the years.

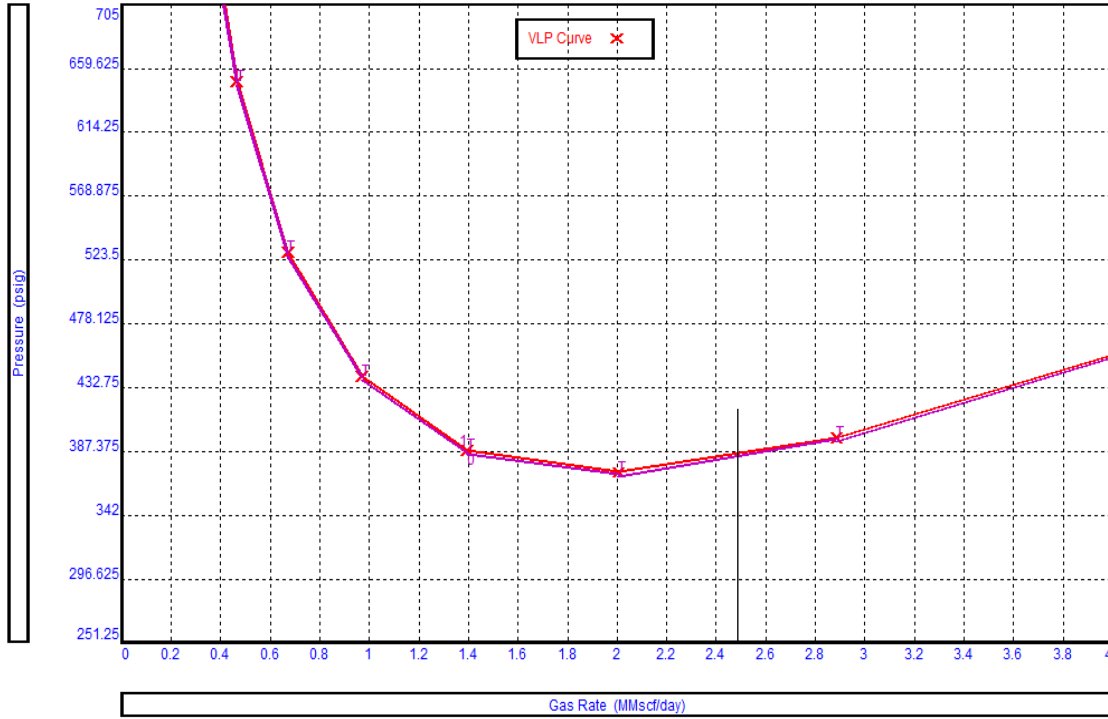


Figure 135 - Well S-14 VLP stability plot

Stability analysis through the VLP curve suggests current production is in the stable region; however, very near to the minimum. Figure 135 suggests the current wellbore profile can support this gas production until production drops below ~2 MMscfd.

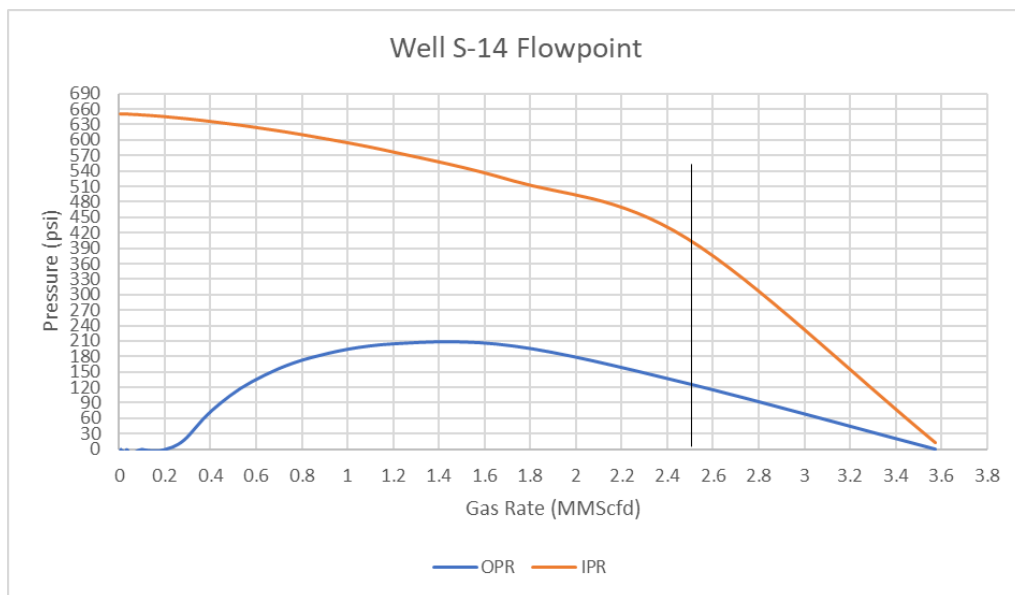


Figure 136 - Well S-14 flow-point analysis plot

Consistent with VLP stability, current production is on the right of the OPR apex, suggesting stable flow, as depicted by Figure 136. Further, flow-point analysis suggests a well pressure difference of ~300 psi. This is consistent with the trend observed in other wells where a higher difference between current production and critical gas rate results in a higher pressure difference between IPR and OPR curves.

Salinity Analysis

Source of liquid production in the wellbore can also be used to designate the severity of liquid loading. Although any fluid – condensate, formation water and condensed water – can cause an increase in hydrostatic pressure and deteriorate well performance, often formation water is most detrimental to production. This is mainly because the liquid is introduced at sand-face from formation and in lower velocities, is not carried towards the surface. The other two sources of fluids are often near the wellbore; therefore, they have to travel a shorter distance.

In the absence of production logs, salinity data from produced water is used to classify condensed water from formation water. Commonly, chloride or sodium chloride content form the basis of salinity classification. Gorrell 1958 suggest the following brackets:

0 to 10,000 ppm NaCl – Fresh/Brackish water

10,000 to 100,000 ppm NaCl – Salty water

Over 100,000 ppm NaCl – Brine

As S-14 water has ~12730 ppm salinity, based on the above categories, produced water is likely coming from the formation.

Artificial Lift Techniques

Gas Lift

A sensitivity run is made on bottom hole pressure with changing WGR to evaluate if the application of any artificial lift that requires gas injection (in the wellbore) will aid in improving production. For most conventional reservoirs, reduction in BHP will generally increase hydrocarbon production.

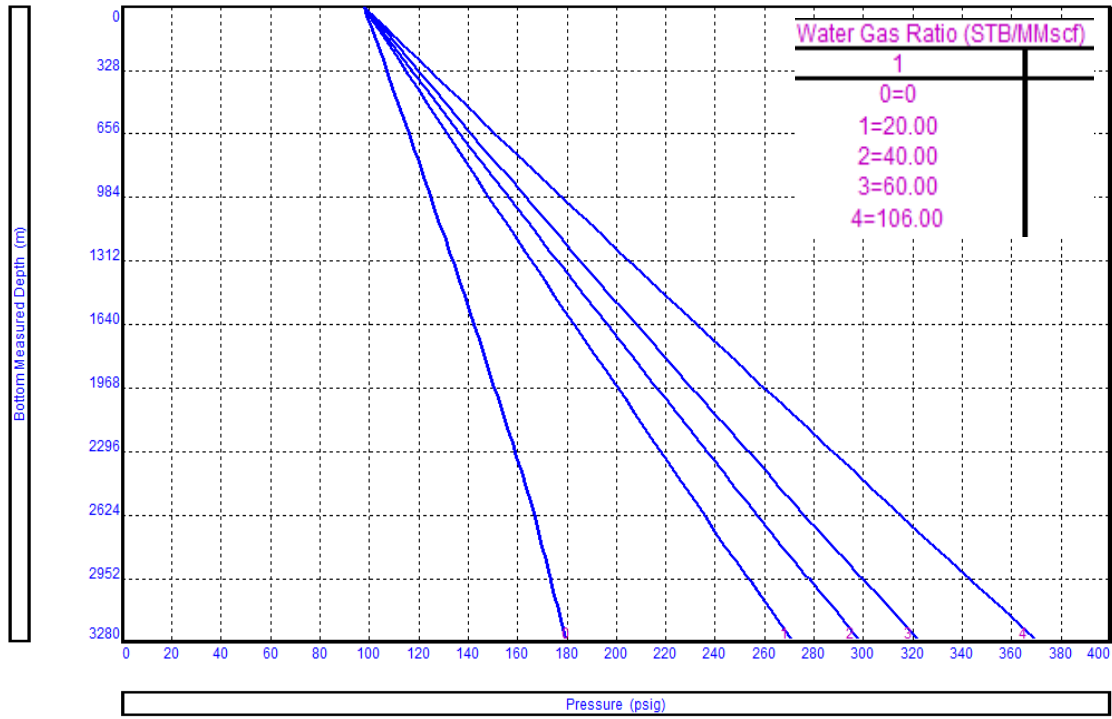


Figure 137 - Well S-14 WGR sensitivity

The current WGR in well S-14 is ~106 STB/MMscf. As evident in Figure 137, by lowering WGR through gas injection, negligible BHP reduction (~100 psi until WGR is ~20 STB/MMscf) is observed. This would suggest a significant gas increment might not be possible with a gas injection technology in this well. However, to quantify the increment, WGR sensitivity on system analysis is required to model the gas injection effects.

Figure 138 shows the effect of lowering WGR on system analysis. Relatively low gas improvement is observed when WGR is lowered to 20 STB/MMscf by injecting gas. The maximum increment observed with the current wellbore configuration is ~0.3 MMscfd. Compared to other S-field wells, a notable increment in gas production is not realized in this well.

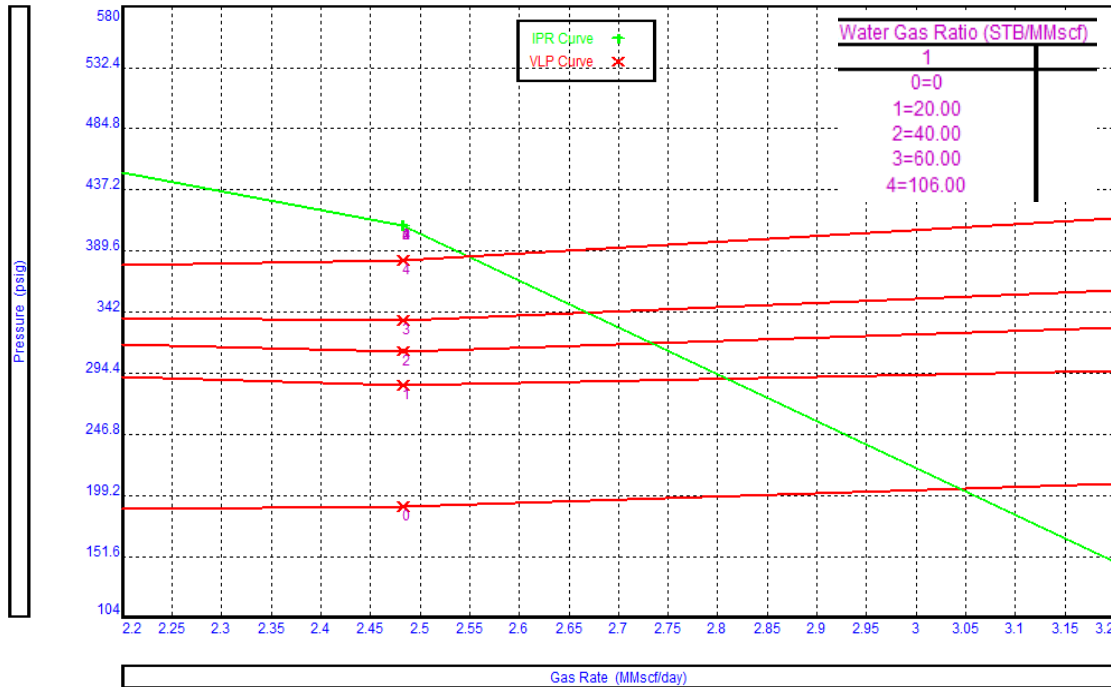


Figure 138 - Well S-14 WGR sensitivity on system plot

A gas lift design is required where the effects of the gas injection are modeled to quantify the actual improvement in production. Most gas lift models are designed for oil reservoirs, therefore as a way around oil IPR with equivalent GOR is used to match the current performance of S-14. Figure 140 shows a matched model with the same reservoir parameters as Gas IPR with a GLR of ~259477 SCF/STB

With oil IPR, we can inject gas in the wellbore through two routes; conventional gas lift where gas is injected down the annulus and produced through 4-1/2" tubing. Secondly, gas can also be injected through Coiled Tubing Gas Lift (CTGL), where 1.5" CT is used inside the current 4-1/2" tubing and gas is injected through it.

Similar to results using gas IPR, conventional gas lift results in an increment of ~0.3 MMscfd with the addition of ~1 MMscfd injection gas. As suggested by VLP stability and flow-point analysis, the flow regime in the wellbore is stable. The addition of any further gas increases friction pressures more than it aids in liquid removal; therefore, the cumulative effect is a modest increase in gas production. Figure 139 shows the conventional gas lift design result for S-14.

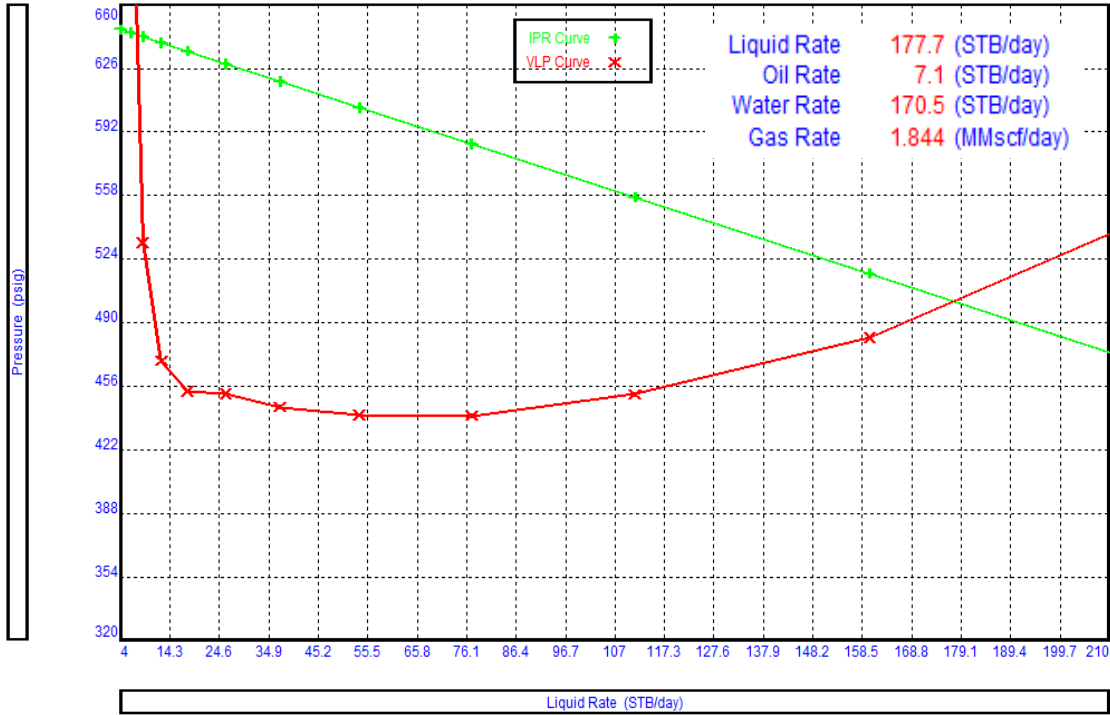


Figure 140 - Well S-14 system plot using oil IPR

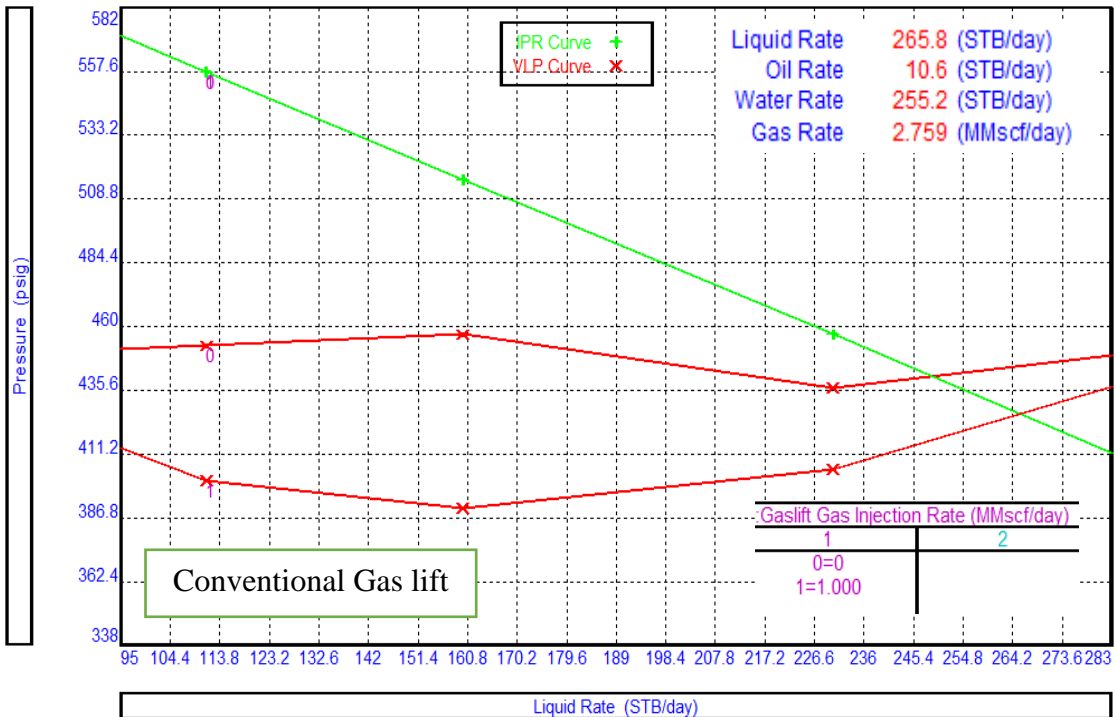


Figure 139 - Well S-14 conventional gas lift design

Similar to the conventional gas lift, using 1.5" CT to inject gas further deteriorates performance as the available flow area for gas is reduced. This results in a significant increase in friction pressures,

resulting in overall lower gas production. Figure 141 depicts the CTGL results.

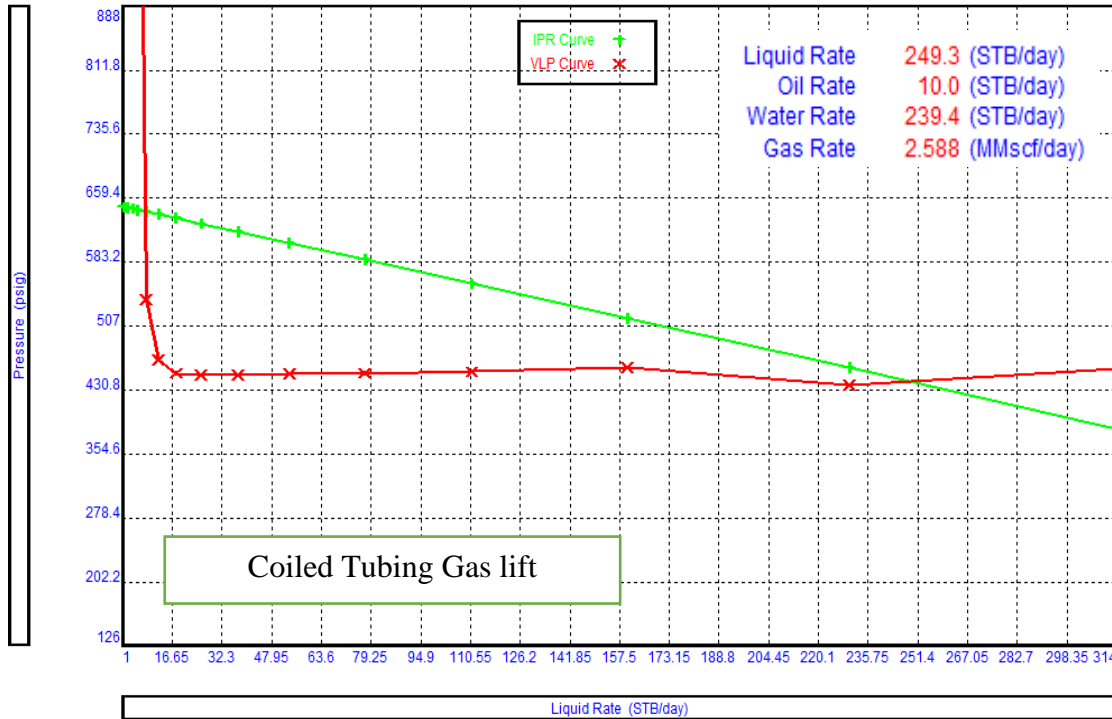


Figure 141 - Well S-14 coiled tubing gas lift design

Plunger Assisted Gas Lift

With 4-1/2" tubing (Plunger BHA @ 2937m)

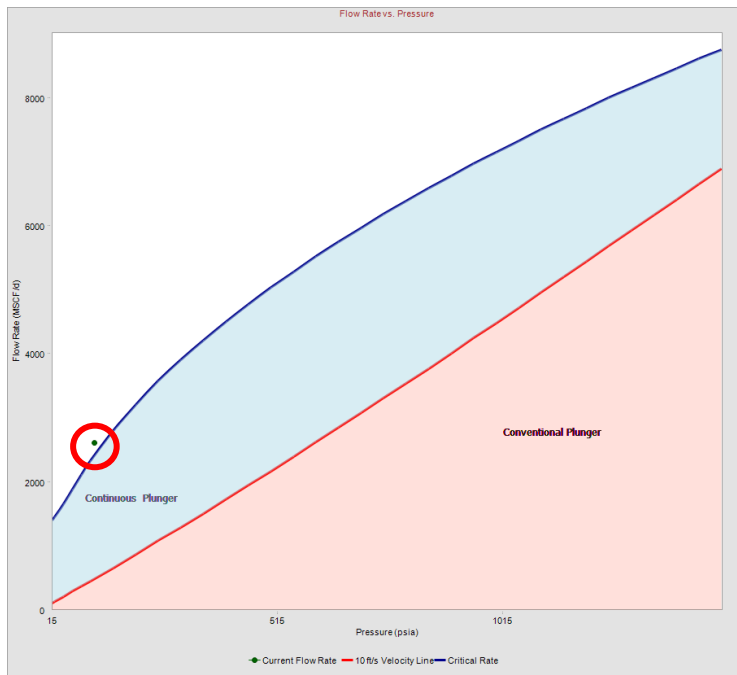


Figure 142 - Well S-14 PAGL type plot

Figure 142 shows the flow rate vs pressure plot to select a plunger type. Current modeled conditions are shown in the red circle in Figure 142. Similar to the results predicted by the WACR model, current production falls within 25% of the critical rate.

As the current production is fairly stable and above the critical rate, Figure 142 suggests a plunger lift is not required (will not result in any incremental liquid production) due to

the sufficient velocities currently available in the wellbore. Therefore, further design for this well is not evaluated.

Velocity String

As expected from the results of CTGL, using coiled tubing or velocity string increases friction pressures in wellbore resulting in higher BHP and lower gas rates. Further, it also deteriorates wellbore hydraulics; therefore, causing the well to load-up earlier than it would in the current configuration. Figure 143 depicts nodal analysis results using 1” velocity string in current 4-1/2” tubing.

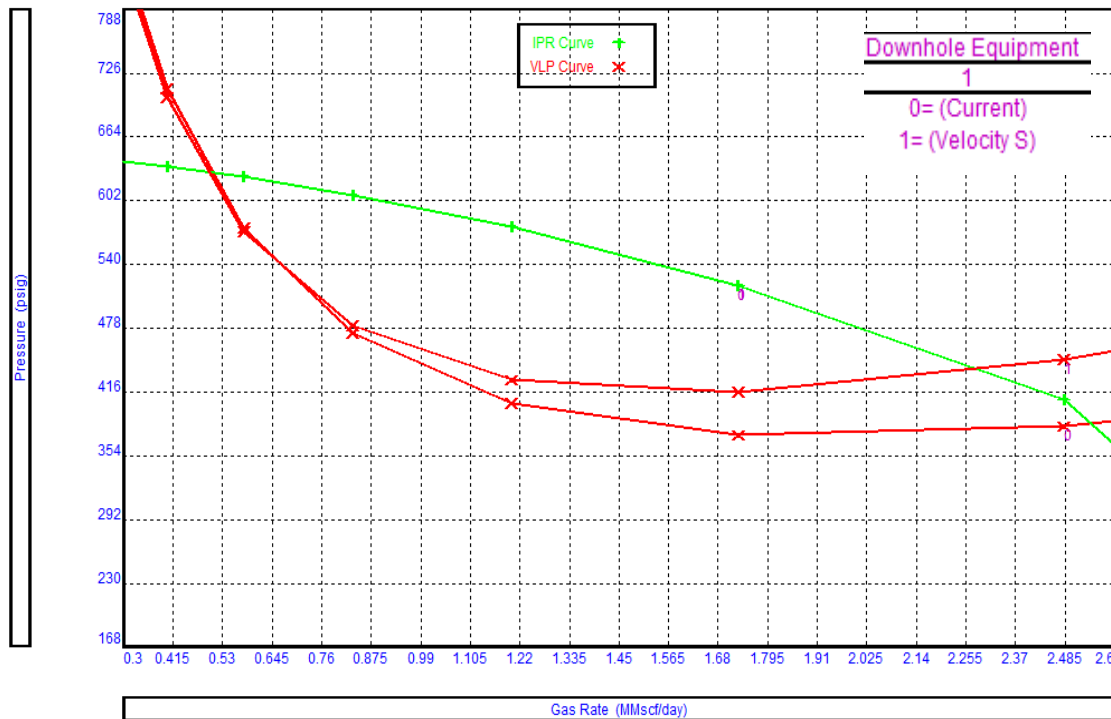


Figure 143 - Well S-14 velocity string design

Well S-14 Summary

Observations drawn from the analysis conducted suggest the application of gas lift through current tubing and coiled tubing results in lower gas production than the current scenario. Further, the use of velocity string increases frictional pressures in the wellbore resulting in lower production. Therefore, in this instance, this well does not require the installation of any artificial lift.

Well S-15

S-15 is a development well drilled in S-field. Producing from a sandstone reservoir at ~3300 m TVD, S-15 has produced more than 30.7 BCF gas since October 2009. Initial gas production was ~26 MMscfd. Pressure depletion caused rates to decline over the years, and the current gas rate is ~2.08 MMscfd. Water production started in 2016 with increasing WGR. Due to the scarcity of well test data, only annual WGR was available for production and nodal analysis. Figure 144 shows the current wellbore profile of S-15.

Reservoir Pressure	525 psi	Target Interval	3300 m
Current Production	2.08 MMscfd	Following Wellhead Pressure	98 psi

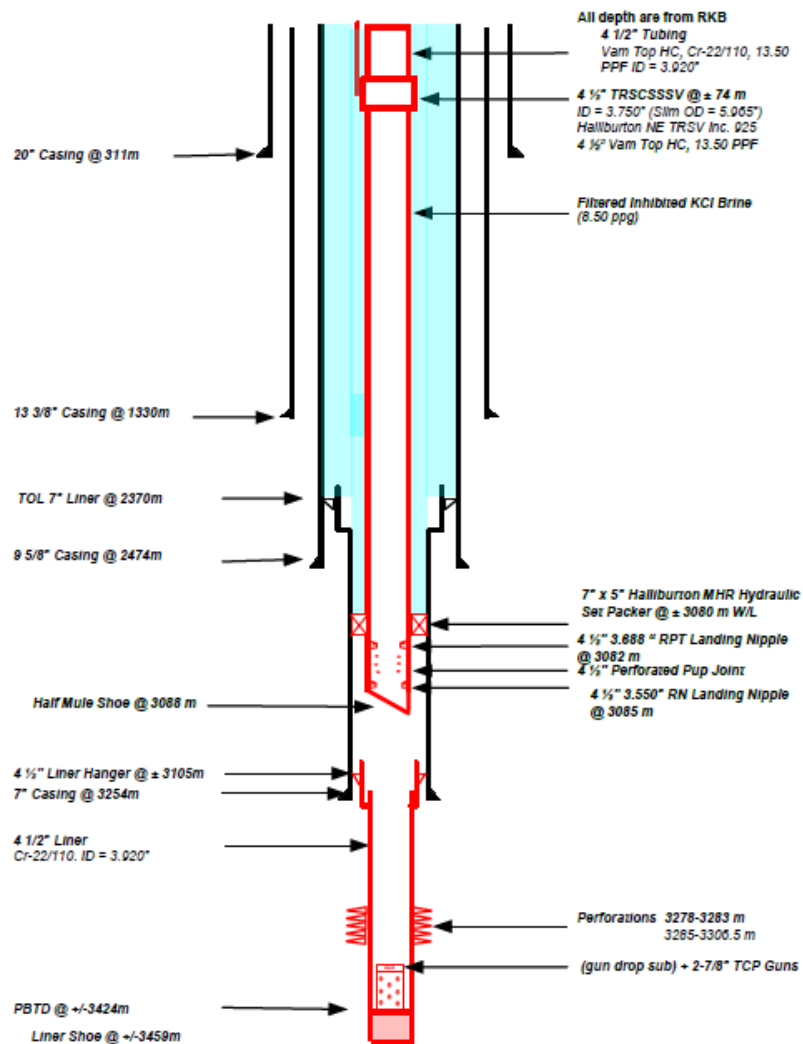


Figure 144 - Well S-15 wellbore profile

Production Plot

Figure 145 shows the gas production and Flowing Wellhead Pressure (FWHP) for S-15 from 2014. Bottomhole Pressure (BHP) can be calculated from measured WHP using the VLP correlation for this dataset. This allows the evaluation of changing sand-face pressure to observe unusual trends and anomalies that may indicate issues like liquid loading.

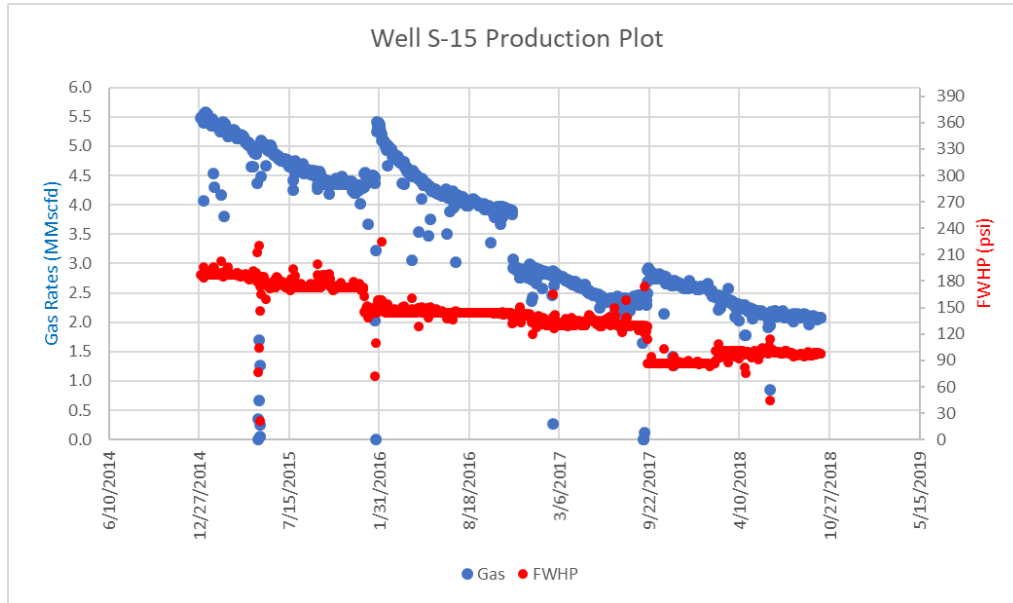


Figure 145 - Well S-15 FWHP plot

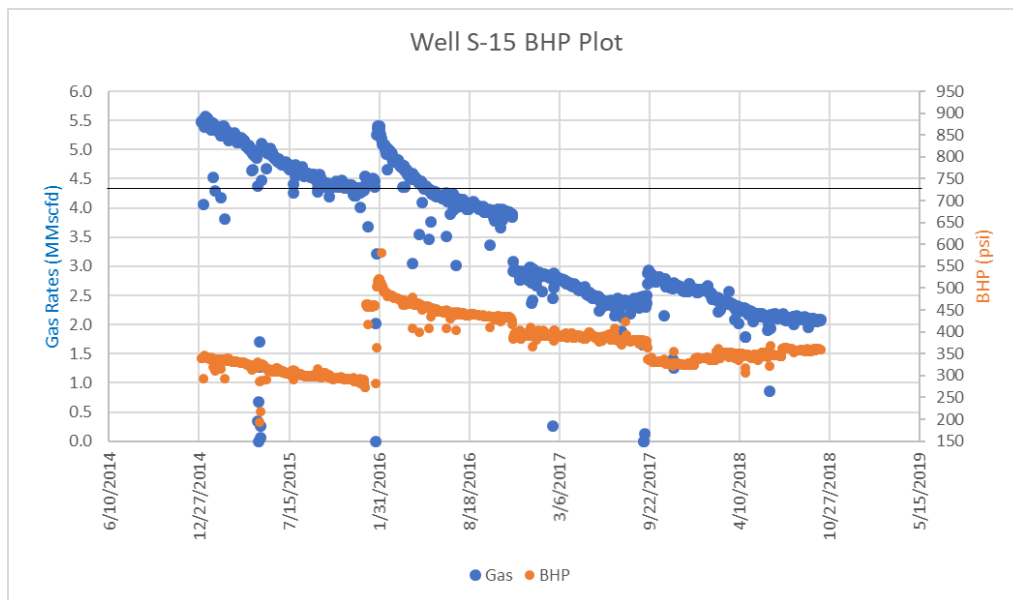


Figure 146 - Well S-15 BHP plot

Figure 146 shows the gas rates and BHP for S-15 from 2014. The solid black line at gas rate ~4.4 MMscfd in Figure 146 depicts the critical gas unloading rate required to offload all fluids from wellbore effectively. Based on the current production rate of ~2.08 MMscfd, current gas rates are ~53% lower than required critical rates.

The well S-15 has a relatively constant BHP with decreasing gas rates. This suggests that the BHP trend is not influenced by the reservoir (else it would have had a similar decline trend as gas rates). Further, an abrupt decline in BHP values is observed at the start of each year, owing to annual WGR values that we use to estimate BHP. Moreover, the WGR for this well has risen drastically from 29 in 2013 to ~105 STB/MMscfd by the end of 2018.

Nodal Analysis

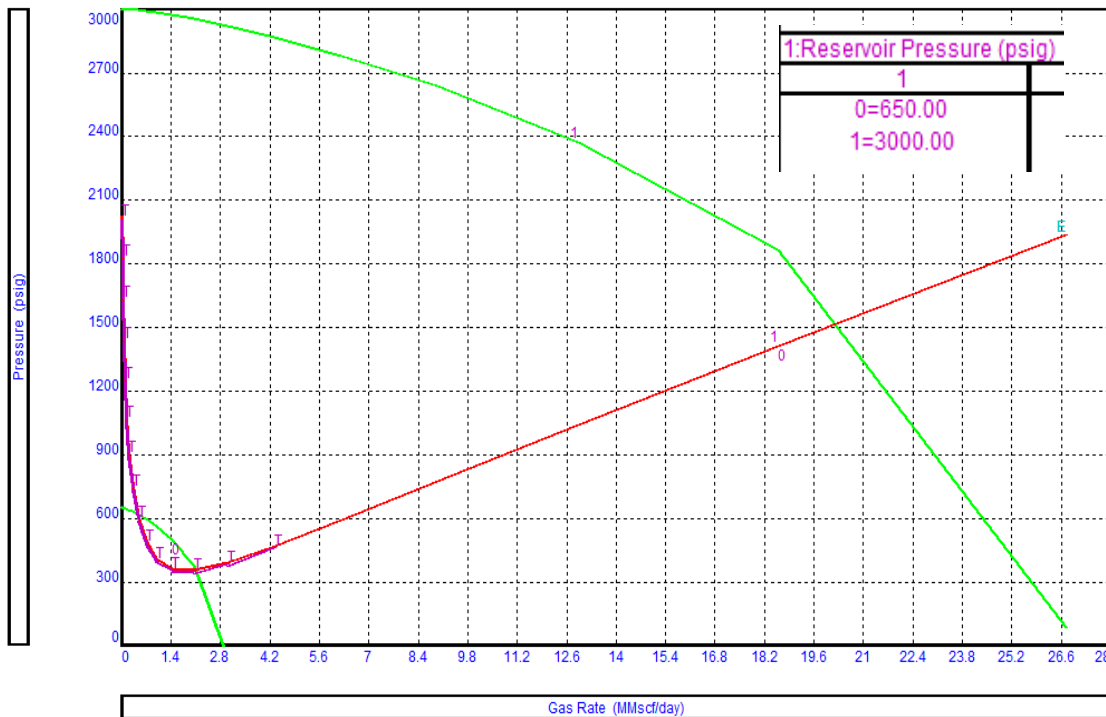


Figure 147 - Well S-15 reservoir pressure sensitivity

Figure 147 depicts the sensitivity of reservoir pressure that is used to match the current production of this well. This suggests reservoir pressure has depleted from ~3000 psi (initial pressure for this well was probably depleted from virgin due to production from other wells) to ~650 psi. This is the primary reason behind the drop in production over the years.

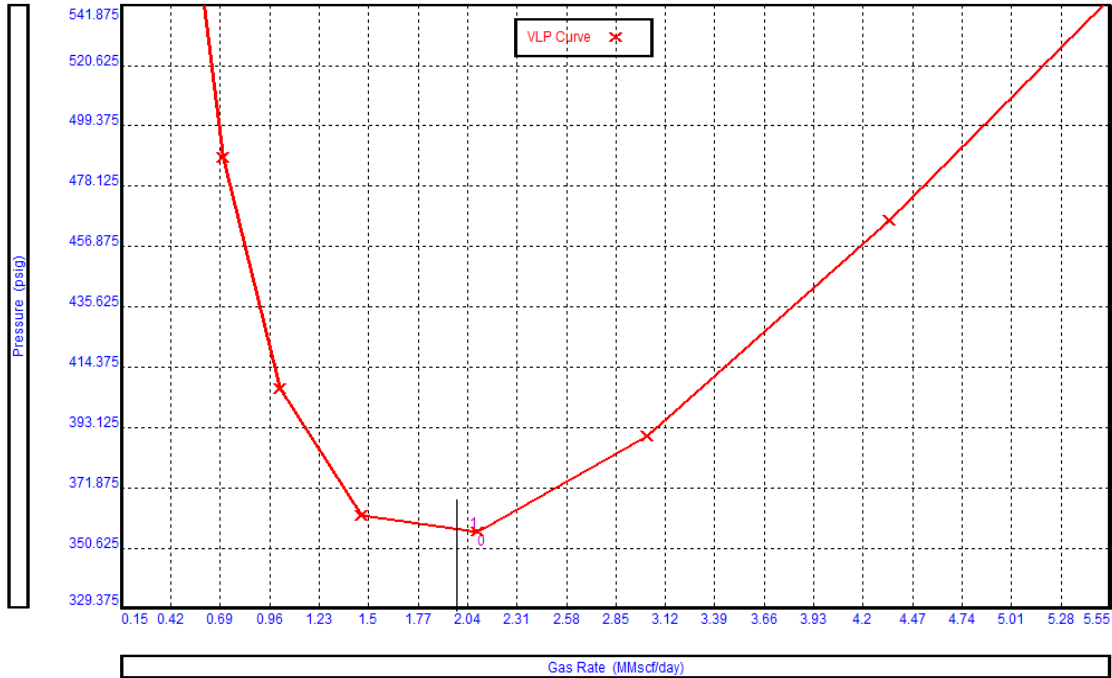


Figure 149 - Well S-15 VLP Stability plot

Stability analysis through the VLP curve (Figure 149) suggests current production is in the unstable region, on the left of the curve minimum. This suggests flow is critical in the wellbore, and any further decrease in gas rates may result in unoptimized flow and possibly a load-up condition.

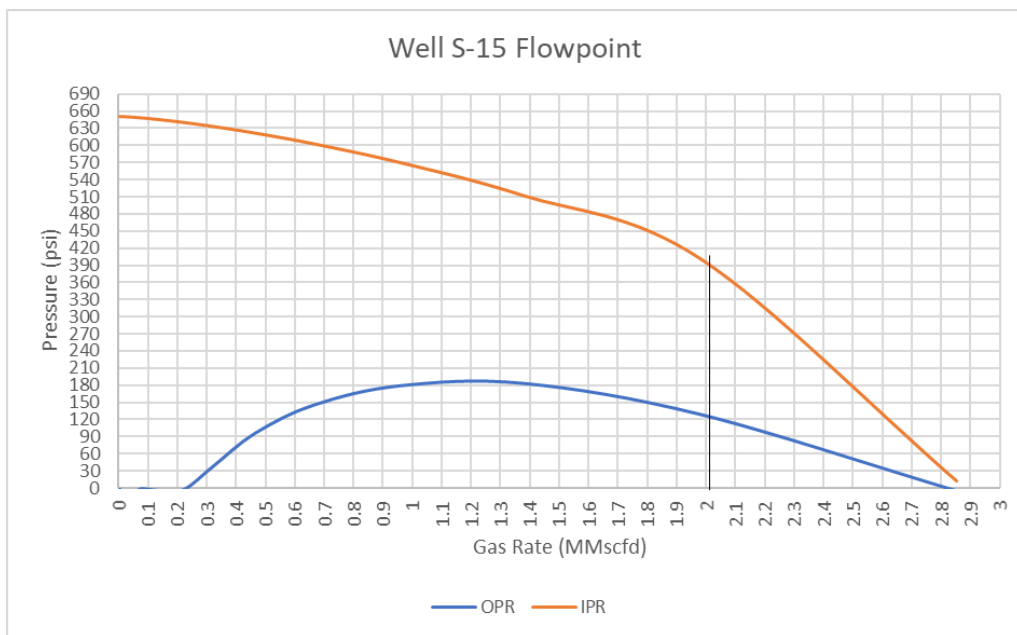


Figure 148 - Well S-15 flow-point analysis plot

Flow-point analysis (Figure 148) and VLP stability (Figure 149) give a contradicting view in this well. The current gas rates are on the left of the VLP curve minimum, suggesting unoptimized flow in the wellbore. However, in flow-point analysis, current gas rates are in the stable region (right to the apex of the OPR curve).

A sensitivity run can be conducted using the nodal analysis to ascertain if liquid loading is a concern in this well. If significant improvement in production is achieved by artificial lift, complete design can be evaluated.

Salinity Analysis

Source of liquid production in the wellbore can also be used to designate the severity of liquid loading. Although any fluid – condensate, formation water and condensed water – can cause an increase in hydrostatic pressure and deteriorate well performance, often formation water is most detrimental to production. This is mainly because the liquid is introduced at sand-face from formation and in lower velocities, is not carried towards the surface. The other two sources of fluids are often near the wellbore; therefore, they have to travel a shorter distance.

In the absence of production logs, salinity data from produced water is used to classify condensed water from formation water. Commonly, chloride or sodium chloride content form the basis of salinity classification. Gorrell 1958 suggest the following brackets:

0 to 10,000 ppm NaCl – Fresh/Brackish water

10,000 to 100,000 ppm NaCl – Salty water

Over 100,000 ppm NaCl – Brine

As S-15 water has ~388 ppm salinity, based on the above categories, produced water is most likely condensed in this well and is sourced near the surface.

Artificial Lift Techniques

Gas Lift

A sensitivity run is made on bottom hole pressure with changing WGR to evaluate if the application of any artificial lift that requires gas injection (in the wellbore) will aid in improving production. For most conventional reservoirs, reduction in BHP will generally increase hydrocarbon production.

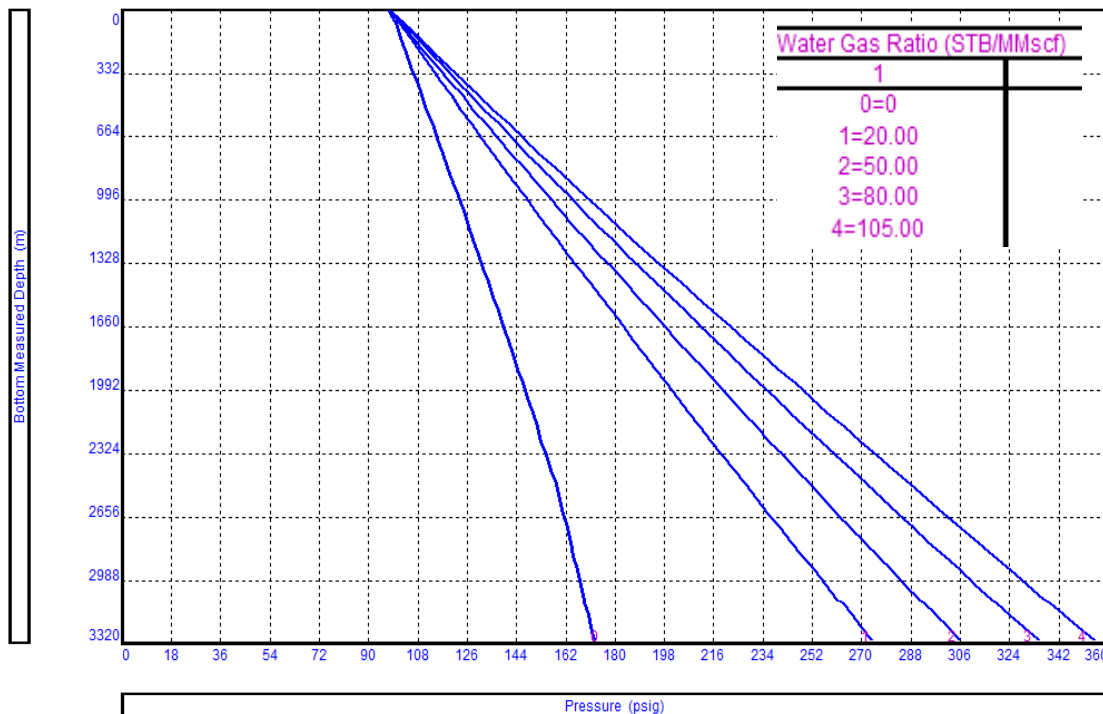


Figure 150 - Well S-15 WGR sensitivity

The current WGR in S-15 is ~105 STB/MMscf. As evident in Figure 150, by lowering WGR through gas injection, a significant reduction in BHP is not observed until WGR is reduced below ~20 STB/MMscf. This suggests a significant increase in gas production is unlikely with the addition of a gas in the wellbore; however, it needs to be confirmed with WGR sensitivity on system analysis.

Figure 151 shows the effect of lowering WGR on system analysis. As suggested by WGR sensitivity, moderate gas improvement of ~0.3 MMscfd is observed when WGR is lowered to ~20 STB/MMscf. Compared to other S-field wells, we do not see adequate improvement in production. This is consistent with wells where current gas rates are higher than ~2 MMscfd and are completed

with 4-1/2" tubing. The low increment is a result of additional frictional pressure in smaller diameter tubing, with the addition of extra gas.

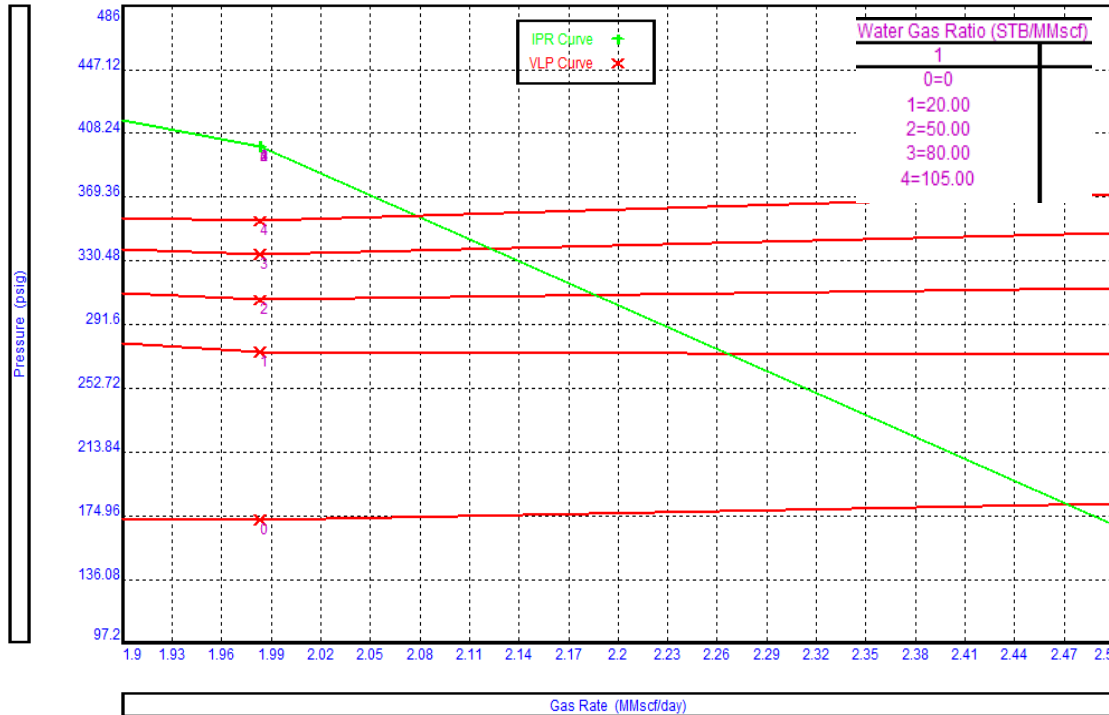


Figure 151 - Well S-15 WGR sensitivity on system plot

A gas lift design is required where the effects of the gas injection are modeled to quantify the actual improvement in production. Most gas lift models are designed for oil reservoirs, therefore as a way around oil IPR with equivalent GOR is used to match the current performance of well S-15. Figure 152 shows a matched model with the same reservoir parameters as Gas IPR with a GLR of ~208137 SCF/STB.

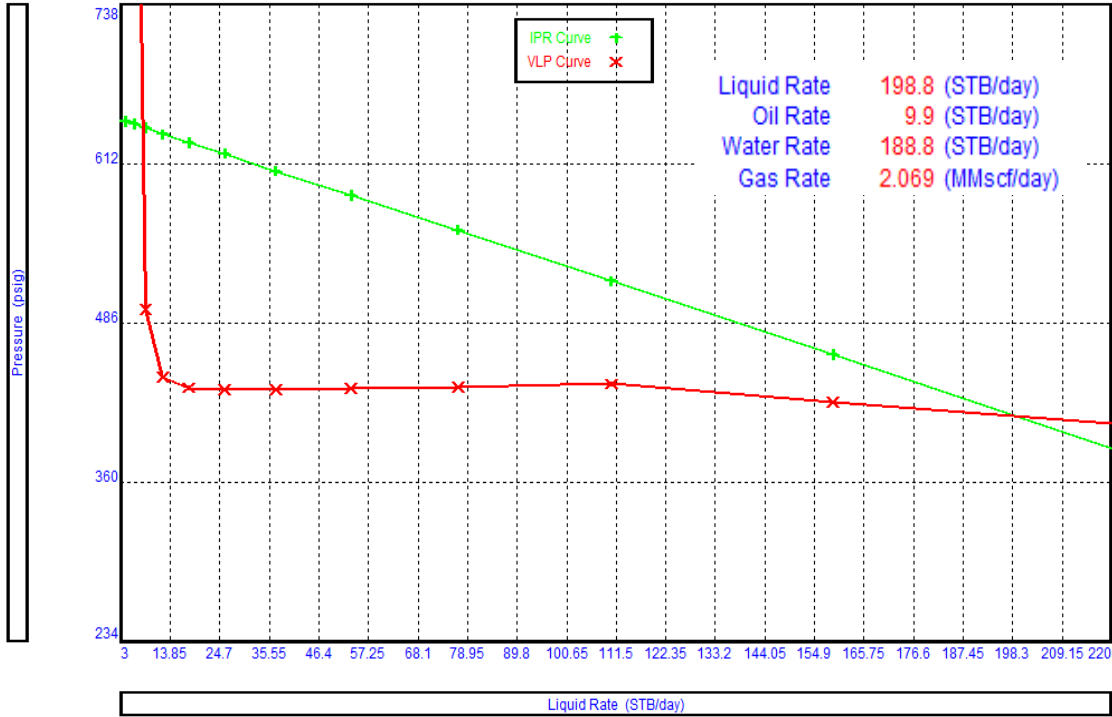


Figure 152 - Well S-15 system plot using oil IPR

Gas can be injected in the wellbore through two routes; conventional gas lift where gas is injected down the annulus and produced through 4-1/2" tubing, and through Coiled Tubing Gas Lift (CTGL) where 1.5" CT is used inside the current 4-1/2" tubing.

Conventional gas lift results in ~0.3 MMscfd increment as predicted by WGR sensitivity in system analysis using gas IPR. Moreover, as the gas increment is insignificant, there is no improvement in recovery by lowering abandonment pressure. Therefore, an increment from the conventional gas lift at this instance in this well would not justify the additional cost of installation. Figure 154 shows the gas lift design on a system plot.

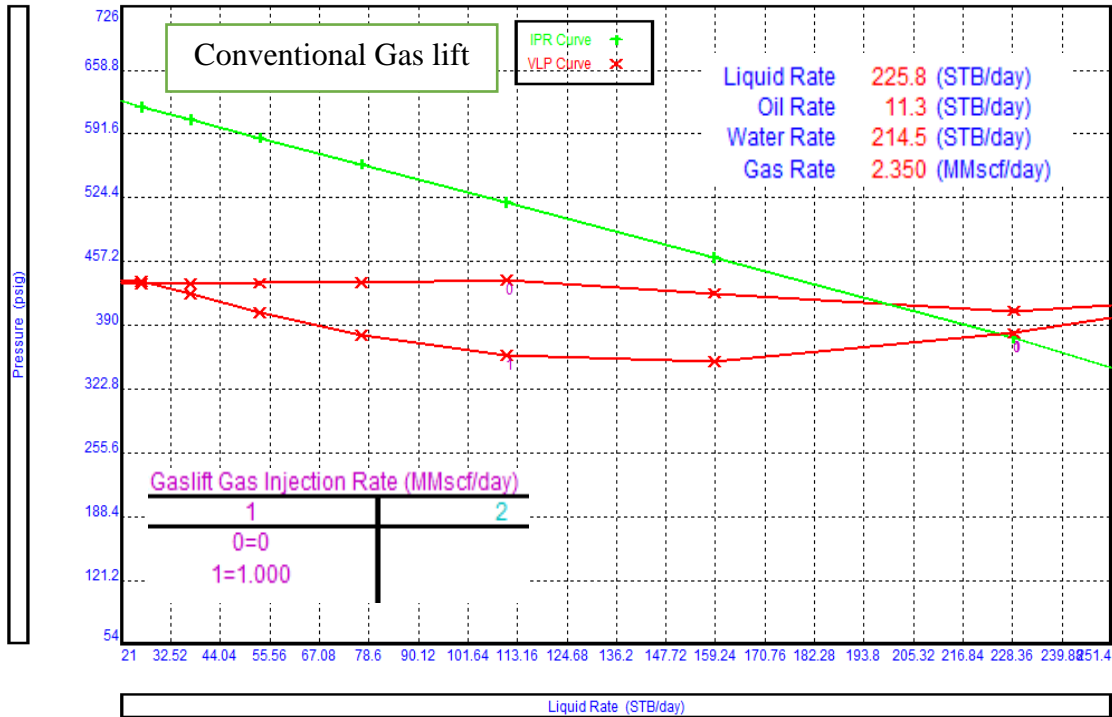


Figure 154 - Well S-15 conventional gas lift design

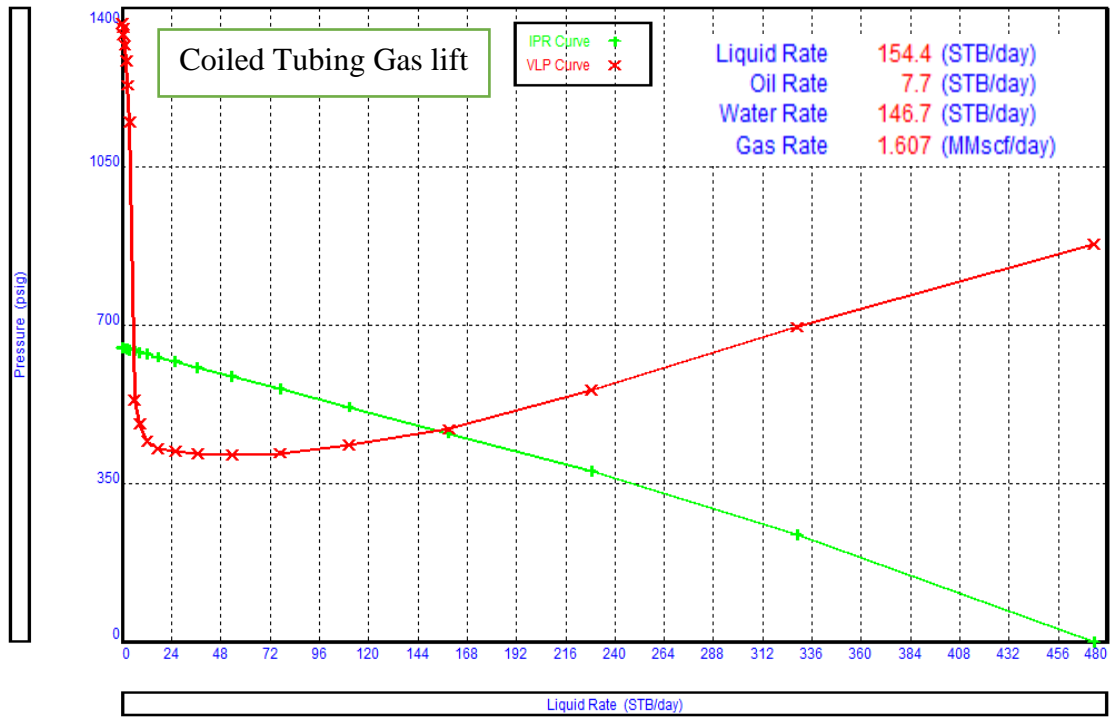


Figure 153 - Well S-15 coiled tubing gas lift design

Similar to the results of the conventional gas lift, where the additional friction pressures due to added gas resulted in low gas increment, Coiled tubing Gas Lift is also not lucrative for this well. System analysis suggests, installing 1.5” CT in 4-1/2” tubing, results in excessive friction pressures. The overall gas production is reduced to ~1.6 MMscfd from the current production of ~2 MMscfd. Figure 155 depicts the system analysis plot using CTGL.

Although CTGL has lower instantaneous rates, due to smaller diameter CT, it can produce the well to a lower abandonment pressure of ~450 psi. On the contrary, conventional gas lift and natural production will only produce the well until reservoir pressure is above ~500 psi. This additional gas might result in higher cumulative recovery with CTGL, due to lower abandonment pressure.

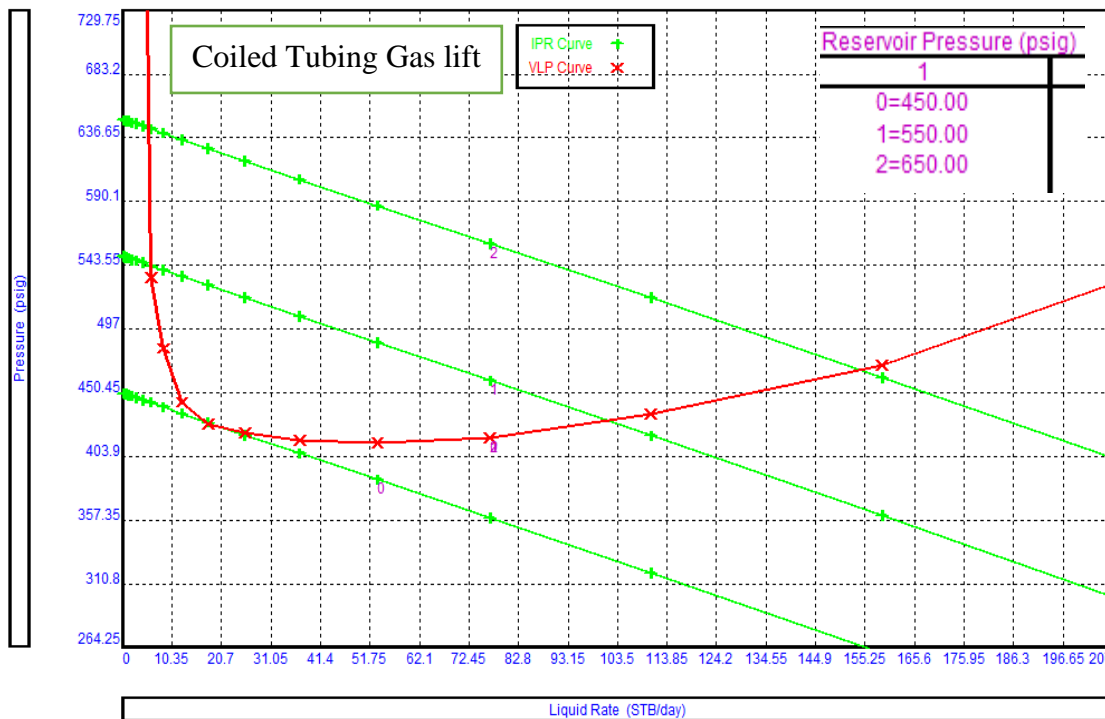


Figure 155 - Well S-15 CTGL abandonment pressure sensitivity

Plunger Assisted Gas Lift

With 4-1/2" tubing (Plunger BHA @ 3085m)

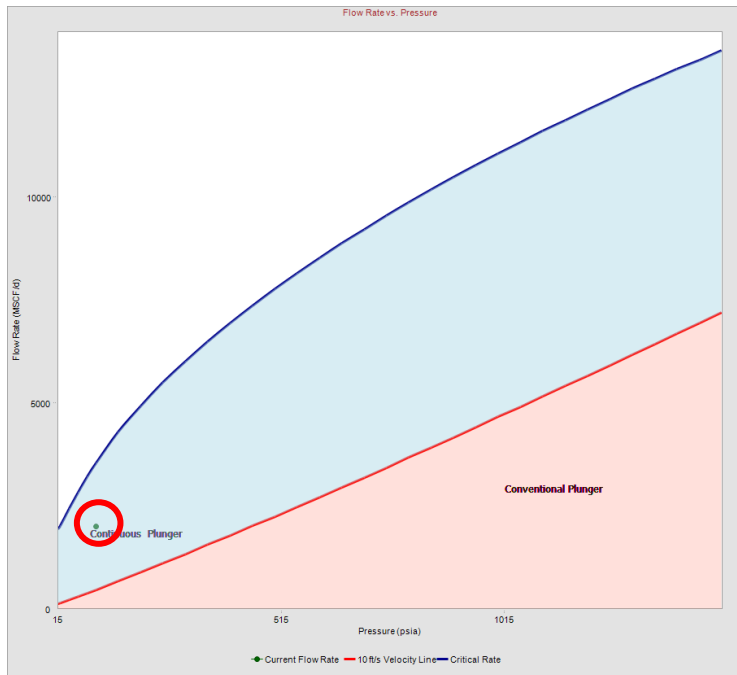


Figure 156 - Well S-15 PAGL type plot

Figure 156 shows the flow rate vs pressure plot to select the plunger type. Current model conditions are shown in the red circle in Figure 156. Based on gas velocity, current conditions fall under continuous plunger lift operating range.

This plot only suggests feasibility regardless of design. To confirm applicability, plunger design is required. Similar to other S-field wells, plunger lift in the current 4-1/2" tubing will not be a feasible option due to the limited surface injection

pressure available. However, similar to well S-11, this can be re-completed with 2-7/8" tubing to improve liquid withdrawals, lower the bottom hole pressures and improve gas production.

Plunger Assisted Gas Lift Design		Results	
Well Name	S-15	Required Casing Injection Pressure (psi)	454
PAGL Type	Continuous	Injection pressure Limited by	FBHP
Target Gas Production (Mscf/d)	1200	Calculated WHP (psi)	325
Target Liquid Production (STB/d)	110	Volume of Liquid Slug (bbl)	1.93
Tubing ID (in)	2.441	Number of Cycles per day	57
Tubing OD (in)	2.875		
Design WHP (psi)	140	Gas Velocity at bottom hole (ft/sec)	44.03
Expected Flowing BHP (psi)	450	Minimum Gas velocity (ft/sec)	19.83
Fall Rate in Gas (ft/min)	800		
Fall Rate in Liquid (ft/min)	400	PAGL Possible?	Yes
Rise Rate (ft/min)	700		

Table 22 - Well S-15 PAGL design using 2-7/8" tubing

Gas production drops to ~1.2 MMscfd if tubing in the well S-15 is switched to 2-7/8". Given the max cycle limit of 60 per day, using a 2-7/8" continuous plunger, well can offload ~110 STB/d liquid with the limited ~450 psi injection pressure from 2-7/8" tubing. To lift this column in every cycle, an injection pressure of ~470 psi is required that is also near the limit of maximum injection pressure.

The addition of a continuous plunger lift, that can offload additional fluid from the wellbore, results in production increase to ~1.6 MMscfd. This increment is estimated through the solution bottom hole pressure that will be achieved if ~100 STB/day fluid is produced by installing a continuous plunger lift. Table 22 shows the PAGL design using 2-7/8" for well S-15.

Figure 157 shows the system plot including sensitivity for plunger lift. The black arrow on the plot depicts incremental production that is achieved by lowering bottom hole pressure. Although incremental production, and possibly additional reserves, are unlocked with plunger lift, these are contingent to the following:

- Well is currently completed with 4-1/2" tubing; workover is required to re-complete well with 2-7/8" tubing and install plunger lift
- Increased production of ~1.6 MMscfd with plunger lift is still lower to the current production of ~2 MMscfd from 4-1/2" tubing

Plunger lift with 2-7/8" tubing is a feasible option to optimize production from well S-15 when current production falls below ~1.6 MMscfd or well loads up due to unoptimized flow in larger 4-1/2" tubing. The scenario for well S-11 and S-15 is almost identical. Plunger lift can be implemented on one of the wells, which can be used as a case study for further applications.

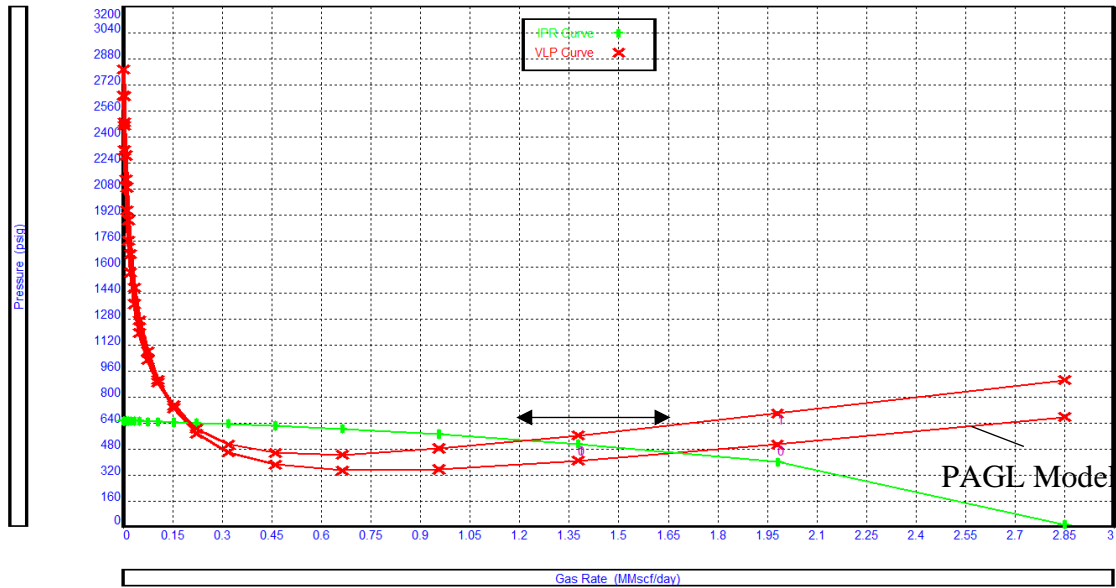


Figure 157 - Well S-15 PAGL system plot

Velocity String

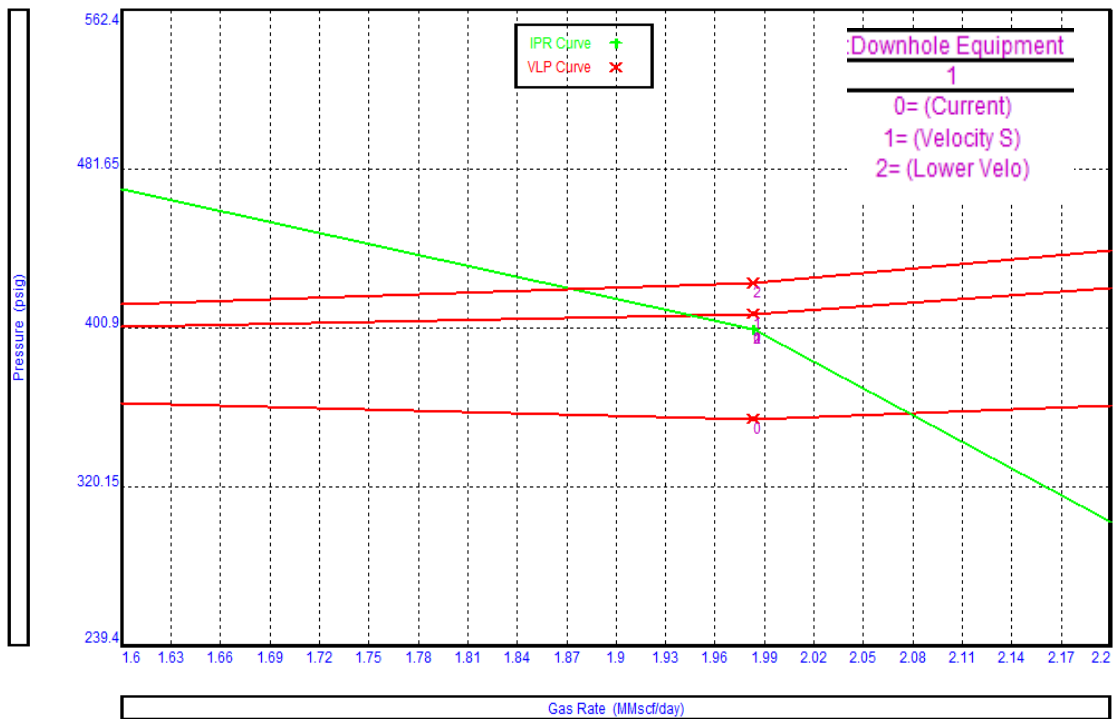


Figure 158 - Well S-15 velocity string design

Velocity string or smaller diameter tubing can be used in well S-15 in an attempt to improve production and wellbore hydraulics. The sensitivities conducted include:

- Current Profile: 4-1/2" Tubing
- Velocity String: Install 1" CT in 4-1/2" Tubing
- Velocity string in 7" Casing section

As depicted in Figure 158, the use of smaller diameter tubing significantly deteriorates performance due to very high friction pressures, making them an unfeasible option in the current scenario. This is similar to the effect in Coiled Tubing Gas Lift. However, production without gas injection in CT is higher than with gas injection. This is expected as additional injected gas further increases friction pressures decreasing overall gas production.

Well S-15 Summary

Observations drawn from the analysis conducted suggest that gas lift or velocity strings do not result in significant improvement of gas production at this instance. However, the use of CTGL allows the production of well until reservoir pressure depletes to ~450 psi, effectively lowering abandonment pressure by ~100 psi, which may unlock additional reserves. A cost-to-benefit and NPV calculation are required to conclude whether additional cumulative gas would result in better economics, supplementing the loss of higher production that is possible through current wellbore configuration. On the contrary, CTGL implementation may be delayed until gas rates decline below the rates predicted by post CTGL installation. In such a scenario, application of PAGL also becomes feasible, when gas rates are lowered to ~1.6 MMscfd. Therefore, economics analysis can be used to select the better option between CTGL and PAGL. However, given low salinity value of produced water, produced water is most likely condensed at the surface, and it is vital to confirm if it is holding up in wellbore before any artificial lift installation is conducted.

Appendix-B: Machine Learning Python Code

```

1  ### Importing libraries required for the workflow
2
3  import os                                     # to set current working
   directory
4  import math                                   # basic calculations like
   square root
5  from sklearn.neighbors import KNeighborsRegressor # for nearest k neighbour
6  from sklearn import metrics                 # measures to check our
   models
7  from sklearn.model_selection import cross_val_score # cross validation method
8  import pandas as pd                         # DataFrames and plotting
9  import pandas.plotting as pd_plot
10 import numpy as np                          # arrays and matrix math
11 import matplotlib.pyplot as plt; plt.rcParams.update({'font.size': 16}) # plottin
12 import seaborn as sns                       # charts
13 from subprocess import check_call
14 from sklearn.model_selection import train_test_split # train and test split
15 from sklearn.ensemble import RandomForestRegressor
16 from sklearn.metrics import mean_absolute_error
17 from sklearn.model_selection import train_test_split
18 from sklearn.tree import DecisionTreeRegressor
19 from sklearn.metrics import mean_squared_error, r2_score # specific measures to
   check our models
20 from sklearn.linear_model import Ridge      # ridge regression
   implemented in scikit learn
21 from sklearn.linear_model import Lasso
22 from sklearn.model_selection import cross_val_score
23
24 ### Importing database file
25 df = pd.read_csv("T_C_A.csv")
26 df.describe()
27
28 ### Ocular inspection of predictor features through histograms to check distribution
29 plt.subplot(231)
30 plt.hist(df['Depth (ft)'])
31 plt.xlabel('Depth (ft)')
32
33 plt.subplot(232)
34 plt.hist(df['WHP (psi)'])
35 plt.xlabel('WHP (psi)')
36
37 plt.subplot(233)
38 plt.hist(df['Tubing\nID\n(inches)'])
39 plt.xlabel('Tubing ID (in)')
40
41 plt.subplot(234)
42 plt.hist(df['Gas SG'])
43 plt.xlabel('Gas SG')
44
45 plt.subplot(235)
46 plt.hist(df['CGR'])
47 plt.xlabel('CGR')
48
49 plt.subplot(236)
50 plt.hist(df['Test\nFlow\nMScf/D'])
51 plt.xlabel('Test\nFlow\nMScf/D')
52
53 plt.subplots_adjust(left=0.0, bottom=0.0, right=2, top=1.5, wspace=0.3, hspace=0.5)
54 plt.show()
55
56 ### mering CGR & WGR feature to form LGR

```

```

57 df['LGR'] = df['CGR'] + df['WGR']
58 df = df.drop(['CGR', 'WGR'], axis=1)
59 df = df[['Depth (ft)', 'WHP (psi)', 'Tubing\nID\n(inches)', 'Gas SG', 'LGR',
60 'Test\nFlow\nMScf/D)']]
61 ### defining partial correlation function, ref: Dr Micheal Pyrcz;
SubsurfaceDataAnalytics_Feature_Ranking; https://git.io/fjm4p
62
63 def partial_corr(C):
64 # Returns the sample linear partial correlation coefficients between pairs of
variables in C, controlling
65 # for the remaining variables in C.
66
67 # Parameters
68 # C : array-like, shape (n, p)
69 # Array with the different variables. Each column of C is taken as a variable
70 # Returns
71 # P : array-like, shape (p, p)
72 # P[i, j] contains the partial correlation of C[:, i] and C[:, j] controlling
73 # for the remaining variables in C.
74
75 C = np.asarray(C)
76 p = C.shape[1]
77 P_corr = np.zeros((p, p), dtype=np.float)
78 for i in range(p):
79     P_corr[i, i] = 1
80     for j in range(i+1, p):
81         idx = np.ones(p, dtype=np.bool)
82         idx[i] = False
83         idx[j] = False
84         beta_i = linalg.lstsq(C[:, idx], C[:, j])[0]
85         beta_j = linalg.lstsq(C[:, idx], C[:, i])[0]
86         res_j = C[:, j] - C[:, idx].dot(beta_i)
87         res_i = C[:, i] - C[:, idx].dot(beta_j)
88         corr = stats.pearsonr(res_i, res_j)[0]
89         P_corr[i, j] = corr
90         P_corr[j, i] = corr
91     return P_corr
92
93 def semipartial_corr(C): # Michael Pyrcz modified the function above by Fabian
Pedregosa-Izquierdo, f@bianp.net for semipartial correlation
94 C = np.asarray(C)
95 p = C.shape[1]
96 P_corr = np.zeros((p, p), dtype=np.float)
97 for i in range(p):
98     P_corr[i, i] = 1
99     for j in range(i+1, p):
100         idx = np.ones(p, dtype=np.bool)
101         idx[i] = False
102         idx[j] = False
103         beta_i = linalg.lstsq(C[:, idx], C[:, j])[0]
104         res_j = C[:, j] - C[:, idx].dot(beta_i)
105         res_i = C[:, i] # just use the value, not a residual
106         corr = stats.pearsonr(res_i, res_j)[0]
107         P_corr[i, j] = corr
108         P_corr[j, i] = corr
109     return P_corr
110
111 ### Test-train split and imputation to fill missing values
112
113 df_x = df.iloc[:, [0,1,2,3,4]] # separate DataFrames for predictor and
response features
114 df_y = df.iloc[:, [5]]
115

```

```

116 from sklearn.impute import SimpleImputer
117 my_imputer = SimpleImputer(strategy = 'most_frequent')
118 x= my_imputer.fit_transform(df_x)
119 df_x = pd.DataFrame({'Depth (ft)':x[:,0], 'WHP
(psi)':x[:,1], 'Tubing\nID\n(inches)':x[:,2], 'Gas SG':x[:,3], 'LGR':x[:,4]})
120 df = pd.concat([df_x, df_y],axis=1)
121
122 # Split into validation and training data
123 df_train_X, df_test_X, df_train_y, df_test_y = train_test_split(df_x,
df_y, test_size=0.1, random_state=10)
124 df_train = pd.concat([df_train_X, df_train_y],axis=1)
125 df_test = pd.concat([df_test_X, df_test_y],axis=1)
126 df_train.describe()
127
128 ##### Feature Engineering
129
130 ### Linearity
131 from scipy.stats.stats import pearsonr
132
133 depth_corr, depth_p = pearsonr(df['Depth (ft)'],df['Test\nFlow\nMScf/D'])
134 print('The p_value of depth with true critical gas rate is '+ str(depth_p) + ', which
is less than significance level of 0.05. We reject null hypothesis.\n')
135
136 WHP_corr, WHP_p = pearsonr(df['WHP (psi)'],df['Test\nFlow\nMScf/D'])
137 print('The p_value of WHP with true critical gas rate is '+ str(WHP_p) + ', which is
less than significance level of 0.05. We reject null hypothesis.\n')
138
139 Tub_corr, Tub_p = pearsonr(df['Tubing\nID\n(inches)'],df['Test\nFlow\nMScf/D'])
140 print('The p_value of Tubing ID with true critical gas rate is '+ str(Tub_p) + ', which
is less than significance level of 0.05. We reject null hypothesis.\n')
141
142 SG_corr, SG_p = pearsonr(df['Gas SG'],df['Test\nFlow\nMScf/D'])
143 print('The p_value of Gas SG with true critical gas rate is '+ str(SG_p) + ', which is
less than significance level of 0.05. We reject null hypothesis.\n')
144
145 LGR_corr, LGR_p = pearsonr(df['LGR'],df['Test\nFlow\nMScf/D'])
146 print('The p_value of LGR with true critical gas rate is '+ str(LGR_p) + ', which is
less than significance level of 0.05. We reject null hypothesis.')
147
148 ### Pearson Moment correlation
149 correlation_matrix = df_train.corr()
150
151 cols = correlation_matrix.index
152 cm = np.corrcoef(df_train.values.T)
153 ht = sns.heatmap(cm,annot=True, annot_kws={'size': 10},fmt='.2f',
154 yticklabels=cols.values, xticklabels=cols.values)
155
156 plt.show()
157
158 ### Partial Correlation Coefficient
159 import geostatpy.GSLIB as GSLIB; import geostatpy.geostats as geostats
160 import numpy as np; import pandas as pd; import os; import matplotlib.pyplot as plt
161 import seaborn as sns; from scipy import stats; import math; import scipy.signal as
signal
162 import random; from scipy import linalg; from sklearn.feature_selection import RFE;
163 from sklearn.linear_model import LinearRegression
164
165 #pearson correlation
166 correlation = df_train.iloc[:,0:8].corr().iloc[:,5]
167 print(correlation)
168
169 #Partial Corelation
170 partial_correlation = partial_corr(df_train.iloc[:,0:8]) # calculate the partial
correlation coefficients

```

```

171 partial_correlation = partial_correlation[:,5][:6] # extract a single row and remove
    production with itself
172 print(partial_correlation)
173
174 ### Feature Importance
175 features = ['Depth','WHP','Tubing ID','Gas SG','LGR','Test Flow']
176 plt.subplot(141)
177 plt.plot(features,correlation,color='black')
178 plt.plot([0.0,0.0,0.0,0.0,0.0,0.0], 'r--',color='red',linewidth = 1.0)
179 plt.xlabel('Predictor Features')
180 plt.ylabel('Correlation Coefficient')
181 t = plt.title('Correlation Coefficient')
182 plt.ylim(-1,1)
183 plt.grid(True)
184
185 plt.subplot(142)
186 plt.plot(features,partial_correlation,color='black')
187 plt.plot([0.0,0.0,0.0,0.0,0.0,0.0], 'r--',color='red',linewidth = 1.0)
188 plt.xlabel('Predictor Features')
189 plt.ylabel('Partial Correlation Coefficient')
190 t = plt.title('Partial Correlation Coefficient')
191 plt.ylim(-1,1)
192 plt.grid(True)
193
194 from sklearn.feature_selection import mutual_info_regression
195
196 x = df_train.iloc[:,[0,1,2,3,4]] # separate DataFrames for predictor and
    response features
197 y = df_train.iloc[:,[5]]
198
199 mi = mutual_info_regression(x,np.ravel(y)) # calculate mutual information
200 mi /= np.max(mi) # calculate relative mutual information
201
202 indices = np.argsort(mi)[::-1] # find indicies for descending order
203
204 print("Feature ranking:") # write out the feature importances
205 for f in range(x.shape[1]):
206     print("%d. feature %d (%f)" % (f + 1, indices[f], mi[indices[f]]))
207
208 plt.subplot(143) # plot the relative mutual information
209 plt.title("Mutual Information")
210 plt.bar(range(x.shape[1]), mi[indices],
211         color="g", align="center")
212 plt.xticks(range(x.shape[1]), x.columns[indices],rotation=90)
213 plt.xlim([-1, x.shape[1]])
214 plt.grid(True)
215
216
217 # Code modified from https://www.kaggle.com/kanncaa1/feature-selection-and-data-
    visualization
218 from sklearn.ensemble import RandomForestRegressor
219 from sklearn import preprocessing
220 import warnings # silence warnings that commonly occur with
    random forest
221 warnings.filterwarnings('ignore')
222
223 lab_enc = preprocessing.LabelEncoder(); y_encoded = lab_enc.fit_transform(y) # this
    removes an encoding error
224
225 random_forest = RandomForestRegressor(max_depth=100) # instantiate the random forest
226 random_forest = random_forest.fit(x,np.ravel(y_encoded)) # fit the random forest
227 importances = random_forest.feature_importances_ # extract the expected feature
    importances
228 std = np.std([tree.feature_importances_ for tree in random_forest.estimators_],axis=0)

```

```

# calculate stdev over trees
229 indices = np.argsort(importances[::-1]) # find indicies for descending order
230
231 print("Feature Importances:") # write out the feature importances
232 for f in range(x.shape[1]):
233     print("%d. feature %d (%f)" % (f + 1, indices[f], importances[indices[f]]))
234
235 plt.subplot(144) # plot the feature importance
236 plt.title("Feature importances")
237 plt.bar(range(x.shape[1]), importances[indices],
238         color="g", yerr=std[indices], align="center")
239 plt.xticks(range(x.shape[1]), x.columns[indices],rotation=90)
240 plt.xlim([-1, x.shape[1]])
241 plt.grid(True)
242
243 plt.subplots_adjust(left=0.0, bottom=0.0, right=3.2, top=1.2, wspace=0.3, hspace=0.2)
244 plt.show()
245
246 ### RFE
247 rfe = RFE(LinearRegression(), 1,verbose=0) # set up RFE linear regression model
248 #df_train['const'] = np.ones(len(df_train)) # let's add one's for the
constant term
249 rfe = rfe.fit(x,y) # recursive elimination
250 #dfS = df_train.drop('const',axis = 1) # remove the ones
251 print(rfe.ranking_) # print the variable ranks
252
253 ### SVM optimum feature count
254 from sklearn.svm import SVR
255 from sklearn.datasets import make_classification
256
257 from yellowbrick.model_selection import RFECV
258
259 # Instantiate RFECV visualizer with a linear SVM classifier
260 visualizer = RFECV(SVR(kernel='linear'))
261
262 visualizer.fit(x, y) # Fit the data to the visualizer
263 visualizer.show() # Finalize and render the figure
264
265 ##### Prediction Model
266
267 ### First model data subset
268 df_test_X = df_test_X.iloc[:, [1,2,3,4]]
269 x = df_train.iloc[:, [1,2,3,4]] # separate DataFrames for predictor and
response features
270 y = df_train.iloc[:, [5]]
271
272 # Split into validation and training data
273 train_X, val_X, train_y, val_y = train_test_split(x, y,test_size=0.2, random_state=10)
274
275 df_test_X.describe()
276 df_train_X.describe()
277
278 ### Instantiate first machine learning model
279 from xgboost import XGBRegressor
280 #Define XGB
281 XGBmodel = XGBRegressor(learning_rate=0.01, n_estimators=10,
282                          max_depth=3, silent=1)
283
284 rf_model = RandomForestRegressor(n_estimators = 10,max_depth = 3, random_state=1)
285 rf_model.fit(train_X, train_y)
286 rf_val_predictions = rf_model.predict(val_X)
287 rf_val_mae = mean_absolute_error(rf_val_predictions, val_y)
288 print("Validation MAE for Random Forest Model: {:, .0f} Mscfd".format(rf_val_mae))
289

```

```

290 # Fit the XGB model
291 XGBmodel.fit(train_X, train_y, verbose=False)
292 xgb_val_predictions = XGBmodel.predict(val_X)
293 val_mae = mean_absolute_error(xgb_val_predictions, val_y)
294 print("Validation MAE for best value of XGB: {:.0f} Mscfd".format(val_mae))
295
296 ### Tuning hyper parameters
297 from sklearn.model_selection import cross_val_score
298 from sklearn.pipeline import Pipeline
299
300 cv_train_X = val_X
301 cv_train_y = val_y
302
303 #Cross Validation on Number of Trees
304 def get_score_tree(n_estimators):
305     my_pipeline = Pipeline(steps=[
306         ('model', RandomForestRegressor(n_estimators = n_estimators,max_depth = 4,
307         random_state=1))])
308     scores = -1 * cross_val_score(my_pipeline, cv_train_X, cv_train_y,
309     cv=5,
310     scoring='neg_mean_absolute_error')
311     return scores.mean()
312
313 results_tree = {}
314 for i in range(1,20):
315     results_tree[100*i] = get_score_tree(100*i)
316
317 #Cross validation on Maximum depth given optimum trees
318 def get_score_depth(n_depth):
319     my_pipeline = Pipeline(steps=[
320         ('model', RandomForestRegressor(n_estimators = 50,max_depth = n_depth,
321         random_state=1))])
322     scores = -1 * cross_val_score(my_pipeline, cv_train_X, cv_train_y,
323     cv=5,
324     scoring='neg_mean_absolute_error')
325     return scores.mean()
326
327 results_depth = {}
328 for i in range(1,10):
329     results_depth[1*i] = get_score_depth(1*i)
330
331 import matplotlib.font_manager as font_manager
332
333 # Set the font dictionaries (for plot title and axis titles)
334 title_font = {'fontname':'Arial', 'size':'28', 'color':'black', 'weight':'normal',
335     'verticalalignment':'bottom'} # Bottom vertical alignment for more space
336 axis_font = {'fontname':'Arial', 'size':'26'}
337
338 #%matplotlib inline
339 plt.subplot(121)
340 plt.plot(list(results_tree.keys()), list(results_tree.values()))
341 plt.ylabel("MAE (Mscf/d)", **axis_font)
342 plt.xlabel("Number of Trees", **axis_font)
343 plt.rc('xtick', labels=24)
344 plt.rc('ytick', labels=24)
345 plt.title("Random Forest Tree Sensitivity", **title_font)
346
347
348 plt.subplot(122)
349 plt.plot(list(results_depth.keys()), list(results_depth.values()))
350 plt.ylabel("MAE (Mscf/d)", **axis_font)
351 plt.xlabel("Maximum Depth", **axis_font)

```

```

352 plt.rc('xtick', labelsizes=24)
353 plt.rc('ytick', labelsizes=24)
354 plt.title("Random Forest Tree Sensitivity", **title_font)
355
356 plt.subplots_adjust(left=0.0, bottom=0.0, right=3, top=1.5, wspace=0.1, hspace=0.1)
357 plt.rcParams.update({'font.size': 22})
358 plt.show()
359
360 #Cross Validation on Number of Trees - XGB
361 def get_score_tree(n_estimators):
362     my_pipeline = Pipeline(steps=[
363         ('model', XGBRegressor(n_estimators = n_estimators,max_depth = 6, random_state=1,
364             silent=1))])
365     scores = -1 * cross_val_score(my_pipeline, cv_train_X, cv_train_y,
366                                 cv=5,
367                                 scoring='neg_mean_absolute_error')
368     return scores.mean()
369 results_tree = {}
370 for i in range(1,20):
371     results_tree[5*i] = get_score_tree(5*i)
372
373
374 #Cross validation on Maximum depth given optimum trees
375 def get_score_depth(n_depth):
376     my_pipeline = Pipeline(steps=[
377         ('model', XGBRegressor(n_estimators = 40,max_depth = n_depth, random_state=1,
378             silent=1))])
379     scores = -1 * cross_val_score(my_pipeline, cv_train_X, cv_train_y,
380                                 cv=5,
381                                 scoring='neg_mean_absolute_error')
382     return scores.mean()
383 results_depth = {}
384 for i in range(1,10):
385     results_depth[1*i] = get_score_depth(1*i)
386
387 import matplotlib.font_manager as font_manager
388
389 # Set the font dictionaries (for plot title and axis titles)
390 title_font = {'fontname':'Arial', 'size':'28', 'color':'black', 'weight':'normal',
391             'verticalalignment':'bottom'} # Bottom vertical alignment for more space
392 axis_font = {'fontname':'Arial', 'size':'26'}
393
394
395 #%matplotlib inline
396 plt.rcParams.update({'font.size': 22})
397 plt.subplot(121)
398 plt.plot(list(results_tree.keys()), list(results_tree.values()))
399 plt.ylabel("MAE (Mscf/d)", **axis_font)
400 plt.xlabel("Number of Trees", **axis_font)
401 plt.rc('xtick', labelsizes=24)
402 plt.rc('ytick', labelsizes=24)
403 plt.title("Gradient Boosting Tree Sensitivity", **title_font)
404
405 plt.subplot(122)
406 plt.plot(list(results_depth.keys()), list(results_depth.values()))
407 plt.ylabel("MAE (Mscf/d)", **axis_font)
408 plt.xlabel("Maximum Depth", **axis_font)
409 plt.rc('xtick', labelsizes=24)
410 plt.rc('ytick', labelsizes=24)
411 plt.title("Gradient Boosting Tree Sensitivity", **title_font)
412
413 plt.subplots_adjust(left=0.0, bottom=0.0, right=3, top=1.5, wspace=0.1, hspace=0.1)

```

```

414 plt.show()
415
416 ### Validating model with optimized hyper parameters
417 #Define XGB
418
419 XGBmodel = XGBRegressor(n_estimators=30,max_depth=3, silent=1, random_state=1)
420 rf_model = RandomForestRegressor(n_estimators = 250,max_depth = 4, random_state=1)
421
422
423 rf_model.fit(train_X, train_y)
424 rf_val_predictions = rf_model.predict(val_X)
425 rf_val_mae = mean_absolute_error(rf_val_predictions, val_y)
426 print("Validation MAE for Random Forest Model: {:,.0f}".format(rf_val_mae))
427
428 # Fit the XGB model
429 XGBmodel.fit(train_X, train_y)
430 xgb_val_predictions = XGBmodel.predict(val_X)
431 val_mae = mean_absolute_error(xgb_val_predictions, val_y)
432 print("Validation MAE for best value of XGB: {:,.0f}".format(val_mae))
433
434 ### Model Test
435 df_x = df_train_X.iloc[:, [1,2,3,4]]
436 #df_y = df.iloc[:, [5]]
437 df_test_X = df_test_X.iloc[:, [0,1,2,3]]
438
439 #training with full dataset
440 XGBmodel.fit(df_x, df_train_y)
441
442 #model check
443 model_predict = XGBmodel.predict(df_x)
444
445 #final predictions
446 final_predictions = XGBmodel.predict(df_test_X)
447 final_mae = mean_absolute_error(final_predictions, df_test_y)
448 print("Validation MAE for TEST DATA DecisionTree: {:,.0f} Mscfd".format(final_mae))
449
450 plt.subplot(121)
451 plt.scatter(model_predict,df_train_y,s=None, c='red',marker=None, cmap=None, norm=None,
vmin=None, vmax=None, alpha=1, linewidths=0.3, verts=None, edgecolors="black")
452 plt.arrow(0,0,4000,4000,width=0.02,color='black',head_length=0.0,head_width=0.0)
453 plt.xlim(0,4000); plt.ylim(0,4000)
454 plt.xlabel('Estimated Critical Rate (MCFPD)', **axis_font); plt.ylabel('True Critical
Rate (MCFPD)', **axis_font)
455 plt.title('TRAINING Data on the Final Model', **title_font)
456
457 plt.subplot(122)
458 plt.scatter(final_predictions,df_test_y,s=None, c='blue',marker=None, cmap=None,
norm=None, vmin=None, vmax=None, alpha=1, linewidths=0.3, verts=None,
edgecolors="black")
459 plt.arrow(0,0,4000,4000,width=0.02,color='black',head_length=0.0,head_width=0.0)
460 plt.xlim(0,4000); plt.ylim(0,4000)
461 plt.xlabel('Estimated Critical Rate (MCFPD)', **axis_font); plt.ylabel('True Critical
Rate (MCFPD)', **axis_font)
462 plt.title('TESTING Data on the Final Model', **title_font)
463
464 plt.subplots_adjust(left=0.0, bottom=0.0, right=2, top=1.5, wspace=0.3, hspace=0.2)
465 plt.show()
466
467 ### Model Improvement using outliers and Skewness
468
469 df_skew = pd.read_csv("T_C_A_corr.csv")
470 df_skew['LGR'] = df_skew['CGR'] + df_skew['WGR']
471 df_skew = df_skew.drop(['CGR', 'WGR'], axis=1)
472 df_skew = df_skew[['Depth (ft)', 'WHP (psi)', 'Tubing\nID\n(inches)', 'Gas SG', 'LGR',

```

```

    'Test']]
473 df_skew.describe()
474
475 import seaborn as sns
476 from scipy import stats
477 from scipy.stats import norm
478
479 #['Depth (ft)', 'WHP (psi)', 'Tubing\nID\n(inches)', 'Gas SG', 'LGR',
    'Test\nFlow\nMScf/D)']
480
481 print ('Skewness in Depth is', df_skew['Depth (ft)'].skew())
482 print ('Skewness in WHP is', df_skew['WHP (psi)'].skew())
483 print ('Skewness in TID is', df_skew['Tubing\nID\n(inches)'].skew())
484 print ('Skewness in GSG is', df_skew['Gas SG'].skew())
485 print ('Skewness in LGR is', df_skew['LGR'].skew())
486 print ('Skewness in critical rate is', df_skew['Test'].skew())
487
488 df_skew = df_skew.iloc[:, [1,2,3,4,5]]
489
490 ## Log transform target variable
491 WHP = df_skew['WHP (psi)']
492 #WHP = np.log(df_skew['WHP (psi)'])
493 TID = df_skew.iloc[:, [1]]
494 #ID = np.log(df_skew['Tubing\nID\n(inches)'])
495 Gas_SG = df_skew.iloc[:, [2]]
496 #as_SG = np.log(df_skew['Gas SG'])
497 LGR = df_skew.iloc[:, [3]]
498 Tflow = np.log(df_skew['Test'])
499
500
501 df_final = pd.concat([WHP, TID, Gas_SG, LGR, Tflow], axis=1)
502 #df_final = df_skew
503 df_final.describe()
504
505 ### deleting outliers
506 from scipy import stats
507 import numpy as np
508 z = np.abs(stats.zscore(df_final))
509 df_final = df_final[(z < 2.5).all(axis=1)]
510
511 df_final = df_skew[df_skew.Test < 2500]
512 df_final.reset_index(drop=True, inplace=True)
513 df_final.describe()
514
515 # Testing final optimized model with subset of dataset (deleted outliers and corrected
    skewness)
516 df_x = df_final.iloc[:, [0,1,2,3]]
517 df_y = df_final.iloc[:, [4]]
518
519 final_train_X, final_test_X, final_train_y, final_test_y = train_test_split(df_x,
    df_y, test_size=0.2, random_state=10)
520
521 #training with full dataset
522 XGBmodel.fit(final_train_X, final_train_y)
523
524 #model check
525 model_predict = XGBmodel.predict(final_train_X)
526
527
528 #final predictions
529 final_predictions = XGBmodel.predict(final_test_X)
530
531
532 final_mae = mean_absolute_error(final_predictions, final_test_y)

```

```

533 print("Final MAE for XGB model corrected for Outlier & Skewness: {:.0f}
      Mscfd".format(final_mae))
534
535 plt.subplot(121)
536 plt.scatter(model_predict,final_train_y,s=None, c='red',marker=None, cmap=None,
      norm=None, vmin=None, vmax=None, alpha=1, linewidths=0.3, verts=None,
      edgecolors="black")
537 plt.arrow(0,0,2500,2500,width=0.02,color='black',head_length=0.0,head_width=0.0)
538 plt.xlim(0,2500); plt.ylim(0,2500)
539 plt.xlabel('Estimated Critical Rate (MCFPD)', **axis_font); plt.ylabel('True Critical
      Rate (MCFPD)', **axis_font)
540 plt.title('TRAINING Data on the Final Model', **title_font)
541
542 plt.subplot(122)
543 plt.scatter(final_predictions,final_test_y,s=None, c='blue',marker=None, cmap=None,
      norm=None, vmin=None, vmax=None, alpha=1, linewidths=0.3, verts=None,
      edgecolors="black")
544 plt.arrow(0,0,4000,4000,width=0.02,color='black',head_length=0.0,head_width=0.0)
545 plt.xlim(0,2500); plt.ylim(0,2500)
546 plt.xlabel('Estimated Critical Rate (MCFPD)', **axis_font); plt.ylabel('True Critical
      Rate (MCFPD)', **axis_font)
547 plt.title('TESTING Data on the Final Model', **title_font)
548
549 plt.subplots_adjust(left=0.0, bottom=0.0, right=2, top=1.5, wspace=0.3, hspace=0.2)
550 plt.show()
551
552 ##### End of Code

```

References

- Albon C. (2017) Article: Feature Selection Using Random Forest. https://chrisalbon.com/machine_learning/trees_and_forests/feature_selection_using_random_forest/. Accessed 11 Mar 2020
- Awolusi O. (2005) Resolving Discrepancies in Predicting Critical Rates in Low Pressure Stripper Gas Wells. Texas Tech University
- Brownlee J. (2016) A Gentle Introduction to the Gradient Boosting Algorithm for Machine Learning. <https://machinelearningmastery.com/gentle-introduction-gradient-boosting-algorithm-machine-learning/>. Accessed 11 Mar 2020
- Burns M. (2018) Plunger-assisted gas lift and gas-assisted plunger lift. In: Society of Petroleum Engineers - SPE Artificial Lift Conference and Exhibition - Americas 2018. Society of Petroleum Engineers
- Coleman S. B., Clay H. B., Mccurdy D. G., Norris H. I. (1991) New look at predicting gas-well load-up. *Journal Petroleum Technology* 43:329–333. <https://doi.org/10.2118/20280-pa>
- Dangeti P. (2017) *Statistics for Machine Learning*. Packt Publishing
- Espin D. A., Gasbarri S, Chacin J. E. (1994) SPE 26967 Expert System for Selection of Optimum Artificial Lift Method. SPE Latin America/Caribbean Petroleum Engineering Conference.
- Gorrell H. A. (1958) Classification Of Formation Waters Based On Sodium Chloride Content. *American Assoc Petroleum Geologist* 42:2513–2522
- Gray H. (1978) Vertical Flow Correlation in Gas Wells. 2nd Ed American Petroleum Institute
- Greene W. R. (1983) Analyzing the Performance of Gas Wells. *Journal of Petroleum Technology*. <https://doi.org/10.2118/10743-PA>
- Hashmi G. M., Hasan A. R., Kabir C. S. (2016) Design of plunger lift for gas wells. SPE - SPE North American Artificial Lift Conference Exhibition 2016 25–27
- Hinze J. (1955) Fundamentals of the hydrodynamic mechanism of splitting in dispersion processes. *AIChE J* 1:289–295. <https://doi.org/10.1002/aic.690010303>
- Iglewicz B., Hoaglin D. (1993) *How to Detect and Handle Outliers*. ASQC Quality Press
- Joshi A. (2020) *Machine Learning and Artificial Intelligence*. Springer International Publishing, Cham
- Koehrsen W. (2018) An Implementation and Explanation of the Random Forest in Python. <https://towardsdatascience.com/an-implementation-and-explanation-of-the-random-forest-in-python-77bf308a9b76>. Accessed 11 Mar 2020
- Lea J., Nickens H., Wells M. (2008) *Gas Well Deliquification*, Elsevier
- Li M., Lei S., Li S. (2001) New View on Continuous-removal Liquids from Gas Wells. In: SPE

Permian Basin Oil and Gas Recovery Conference. Society of Petroleum Engineers

Luan G., He S. (2012) A New Model for the Accurate Prediction of Liquid Loading in Low-Pressure Gas Wells. *J Canadian Petroleum Technology* 51:493–498.

<https://doi.org/10.2118/158385-PA>

Nosseir M., Darwich T., Sayyoub M., El Sallaly M. (2000) A new approach for accurate prediction of loading in gas wells under different flowing conditions. *SPE Production Facilities* 15:241–246. <https://doi.org/10.2118/66540-PA>

Ounsakul T., Sirirattanachatchawan T., Pattarachupong W., Yokrat Y. (2019) IPTC-19423-MS Artificial Lift Selection Using Machine Learning. International Petroleum Technology Conference

Oyewole P., Lea J. (2008) SPE 115950 Artificial Lift Selection Strategy for the Life of a Gas Well with some Liquid Production. SPE Annual Technical Conference and Exhibition

Scikit-Learn-Developers (2019) Recursive Feature Elimination — Yellowbrick v1.1 documentation. https://www.scikit-yb.org/en/latest/api/model_selection/rfecv.html. Accessed 11 Mar 2020

Sullivan W. (2018) *Decision Tree and Random Forest - Machine Learning and Algorithms: The Future Is Here!* CreateSpace Independent Publishing Platform

Turner R., Hubbard M., Dukler A. (1969) Analysis And Prediction Of Minimum Flow Rate For The Continuous Removal Of Liquids From Gas Wells. *J Petroleum Technology* 21:1475–1482. <https://doi.org/10.2118/2198-pa>

Valentin E., Hoffmann F. (1988) SPE 18184 OPUS: An Expert Advisor for Artificial Lift. SPE Annual Technical Conference and Exhibition

Zheng A., Casari A. (2018) *Feature Engineering for Machine Learning: Principles and Techniques for Data Scientists*. O'Reilly Media